universität wien

DISSERTATION / DOCTORAL THESIS

Titel der Dissertation /Title of the Doctoral Thesis

„Synthesis of novel PET tracers for the Translocator Protein“

verfasst von / submitted by

Neydher Jesus Enrique Berroteran Infante

angestrebter akademischer Grad / in partial fulfilment of the requirements for the degree of

Doktor der Naturwissenschaften (Dr. rer. nat)

Wien, 2019 / Vienna, 2019

Studienkennzahl lt. Studienblatt / degree programme code as it appears on the student record sheet:	A 796 605 419
Dissertationsgebiet lt. Studienblatt / field of study as it appears on the student record sheet:	Chemistry
Betreut von / Supervisor:	Assoc. Prof. Mag. Dr. Wolfgang Wadsak

AUTHOR DECLARATION

I hereby declare that this doctoral thesis has been composed by myself and it has not been submitted, in whole or in part, for the award of any other academic degree. Therefore, I confirm that the work is my own and it was performed following good scientific practices. I significantly contributed to all peer-reviews publications comprised in this dissertation and the nature of those contributions are stated for each article. All included publications are in the corresponding journal's format, either as submitted or printed versions, respecting the citation style of the respective journal.

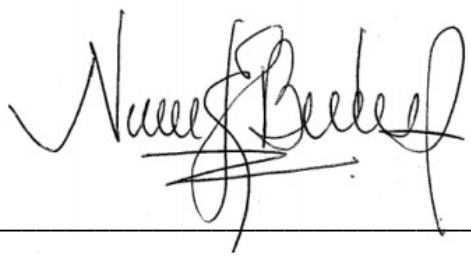

Lic. Neydher Jesús Enrique Berroterán Infante

“Your intuition knows what to write, so get out of the way”

– Ray Bradburry

“Ideas do not always come in a flash but by diligent trial-and-error experiments that take time and thought”

– Charles. K Kao

“Facts are the air of scientists. Without them you can never fly”

– Linus Pauling

Dedicado a todos los hombres y mujeres de ciencia en Venezuela, y en general a todos los ciudadanos venezolanos, quienes a pesar de tantas adversidades, trabajan incansablemente por el país que todos queremos.

Dedicated to all researchers in Venezuela, and in general to all Venezuelan citizens, who despite all adversities, work untiringly for the country we all want.

Für alle ForscherInnen in Venezuela, und generell für alle venezolanischen BürgerInnen, die trotz aller Widrigkeiten unermüdlich für unseres Land arbeiten.

"Para el logro del triunfo siempre ha sido indispensable pasar por la senda de los sacrificios"

"For the achievement of victory, it has been always necessary going through the path of sacrifices"

„Um den Sieg zu erringen, war es immer unerlässlich, den Weg der Opfer zu gehen"

– Simón Bolívar

ACKNOWLEDGMENTS

"Those who are truly grateful are deeply moved by the privilege of living"

– Auliq-Ice

I would like to sincerely acknowledge my mentor Wolfgang Wadsak for his supervision and support during the last years. His enthusiastic discussions and his trust in me and in my research skills paved the way for my growth as a scientist. He allowed me to take my own decisions and to follow the path into this (most of the time) marvelous work. I am in great debt to him and to Markus Mitterhauser, who is also an integral part of this doctoral thesis, for welcoming me in their research group at the Division of Nuclear Medicine at the Medical University of Vienna, first as an intern and then as PhD student. This was not just the entrance to a new job, but rather the entrance to a life change for which I am truly excited. *Vielen Dank Euch beide!*

It would be selfish not to thank Christina Rami-Mark and Katharina Pallitsch for their significant guidance and patience through this work. I have learned so much from you and I am really proud of both of you and our friendship. I wish you all the success you truly deserve. *Danke Christina, Danke Kathi für Eure Unterstützung!*

Moreover, I would like to thank Rupert Lanzenberger for his funding through his research projects. Being a part of them gave me not only financial flexibility during the last years but also allowed me to learn a lot about neuroimaging. *Danke Rupert!* On this matter, I would also like to thank the Austrian Academy of Sciences for its funding through the *Monatshefte für Chemie Stipendium* for the finalization of this doctoral thesis.

Teaching is certainly the best way to learn, by doing so I had the privilege to supervise four students during their master theses, who contributed to this work: Petra, Stefan, Victoria, and Monika. I thank you for trusting in me, for your motivation and for your help to develop this work. *Danke liebe Studenten!*

Thanks to Thomas Kalina and Judit Fazekas who assisted me with their knowledge in organic chemistry and biology, respectively. Thomas performed the organic synthesis and characterization of several compounds here described, while Judit taught me everything I know about genotyping and PCR. Thanks also to all volunteers who donated blood for the genotyping experiments and subsequent binding affinity assays, especially to Karsten Bamminger; whose TSPO genotype is

particularly special. My gratitude goes also to all members of the Preclinical Imaging Laboratory (PIL) of the Medical University of Vienna: Lukas, Max, Stefanie, Elena, Anna Z. and Anna P.; for their support in animal experiments as well as image processing.

My deepest acknowledge goes to all the workers of the Division of Nuclear Medicine, especially to the members and some ex-members of the Medicinal Radiochemistry & Biomarker Development and Radiopharmacy & Experimental Nuclear Medicine Groups: Marius, Eva-Maria, Verena, Florian, Theresa, Sarah, Moni, Chrysoula, Markus, Cécile and Lukas who accompanied me with their thoughts, fruitful discussions, infinite cooperation, charisma and friendship through so diverse situations, including a lot of laughs and a little bit of drama. You welcomed me since the very beginning. It is an honor and a blast to work with all of you. Thank you very much! *Vielen Dank, ich wünsche Euch nur viel Erfolg!*

I am also grateful to my family and their unlimited support and for being all the time beside me, despite the physical distance between us. You are for sure the greatest gift I have ever received. *¡Muchas Gracias!*

Last but not least, I am really thankful for the city of Vienna, for giving me the ideal atmosphere for living during the last years. In this city, which I now call home, I have met wonderful people, who are my friends.

¡GRACIAS POR TANTO Y POR TODO!

TABLE OF CONTENTS

LIST OF FIGURES

ABSTRACT

The 18 kDa Translocator Protein (TSPO), first described as the peripheral benzodiazepine receptor, is suggested to be dysregulated in a variety of pathologies, such as neurodegenerative disorders, heart failure and several types of cancer, which underlines TSPO as an interesting target for treatment and diagnosis of the aforementioned diseases. In this regard, positron emission tomography (PET) has become the lead strategy for the *in vivo* quantification and distribution of TSPO, by using radiolabeled ligands (tracers) with high affinity toward this target. Although several TSPO PET tracers have been introduced, a single nucleotide polymorphism in the *TSPO* gene has hampered the occurrence of the ideal radioligand, so far. In detail, this polymorphism causes a heterogeneous binding affinity of the tracers to the TSPO in subjects with different genotype, ultimately leading in a genotype classification of subjects with high-affinity (HAB), medium-affinity (MAB) and low-affinity (LAB) binding properties. Even though a couple of TSPO PET tracers seem to exhibit low sensitivity towards the polymorphism (i.e. they exhibit a homogeneous binding affinity towards the TSPO), on the other hand, they lack of adequate pharmacokinetic properties, e.g. displaying high non-specific binding and slow brain kinetics, which hinder their use.

Accordingly, in this doctoral thesis several compounds were designed as potentially ideal TSPO PET ligands, overcoming these challenges. Consequently, the syntheses of the reference standards as well as the radiolabelling precursors were planned and carried out with satisfactory yields. Moreover, the binding affinities toward the TSPO of the newly developed substances were determined in competition experiments, using platelets membranes of subjects previously genotyped. On the basis of these results, two compounds were identified as TSPO PET tracers, with potential for further *in vivo* application, since they exhibit a high affinity and no sensitivity toward the TSPO polymorphism. Therefore, two TSPO PET tracers were developed and evaluated in this dissertation: (*R*)-[^{11}C]Me@NEBIQUINIDE and its fluorinated analogue (*R*)-[^{18}F]NEBIFQUINIDE. Briefly, (*R*)-[^{11}C]Me@NEBIQUINIDE was synthesised *via* [^{11}C]methyl triflate, whereas the radiosynthesis of [^{18}F]NEBIFQUINIDE was only possible *via* ^{18}F-fluorination with assisted microwave heating. Both tracers were synthesized in a reliable and feasible manner. Preclinical *in vitro* evaluation included, stability testing, determination of log*P* and binding to plasma protein (α1-AGP). In both cases, promising results were achieved, which suggested a further evaluation *in vivo*. Due to its more advantageous half-life, only (*R*)-[^{18}F]NEBIFQUINIDE was evaluated in *in vivo* settings in mice, showing outstanding results which encourage its use in animal models and in vivo application in humans. As a secondary finding of this thesis, radioligand binding

assays using already known TSPO ligands allowed a further characterization of this molecular target in colorectal cancer as well as regarding the genetic polymorphism.

ZUSAMMENFASSUNG

Die *in vivo* Bildgebung des Translokator Proteins (TSPO) wird intensiv diskutiert als Anwendung für einige wesentliche Erkrankungen, wie diverse Krebsarten, Herzinsuffizienz, und besonders für neurodegenerative Krankheiten. In dieser Hinsicht wurde die Positronen-Emissions-Tomographie (PET) zur wesentlichsten Methodik für die *in vivo* Quantifizierung und Verteilung von TSPO, indem radioaktiv markierte Liganden mit hoher Affinität zu TSPO benutzt. Dessen ungeachtet ist die TSPO PET Bildgebung immer noch eine Herausforderung, da adäquate Radiopharmaka fehlen. Bislang existiert kein einzelner TSPO PET Tracer, der alle gewünschten und nötigen pharmakokinetischen und pharmakodynamischen Eigenschaften aufweist. Hier steht man unter der Herausforderung einer oftmals hohen unspezifischen Bindung und einer heterogene Bindungsaffinität in Abhängigkeit eines Einzelnukleotid-Polymorphismus. Im Detail bewirkt dieser Polymorphismus unterschiedliche Bindungsaffinität der Tracer an TSPO bei Personen mit unterschiedlichem Genotyp, was letztendlich zu einer Genotypklassifizierung in Personen mit hoher Affinität (HAB), mit mittlerer Affinität (MAB) und mit niedriger Affinität (LAB) führt. Obwohl einige TSPO-PET-Tracer scheinbar eine geringe Empfindlichkeit zu diesem Polymorphismus aufweisen (d.h. sie zeigen eine homogene Bindungsaffinität zu TSPO in allen Personen), zeigen diese eine für TSPO-PET-Tracer unzureichend hohe, unspezifische Bindung und langsame Hirnkinetik aufweisen, was ihre Verwendbarkeit einschränkt.

Dementsprechend wurden in dieser Doktorarbeit mehrere neue Verbindungen als TSPO PET Liganden entwickelt, um den einen potentiell „idealen“ TSPO PET Tracer zu erhalten. Daher wurden die Synthesen der Referenzstandards sowie der Vorläuferverbindungen geplant und mit ausreichenden Ausbeuten durchgeführt. Darüber hinaus wurden die Bindungsaffinitäten der neu entwickelten Substanzen zu TSPO in Versuchen unter Verwendung von Thrombozyten von zuvor genotypisierten Personen bestimmt. Aufgrund dieser Ergebnisse wurden zwei Verbindungen als potentielle TSPO PET Substanzen identifiziert, da sie eine hohe Affinität und keine Polymorphismusempfindlichkeit zu TSPO aufwiesen. In der Folge wurden in dieser Dissertation zwei radiomarkierte TSPO PET Tracer entwickelt und getestet: (*R*)-[^{11}C]Me@NEBIQUINIDE und sein fluoriertes Analogon (*R*)-[^{18}F]NEBIFQUINIDE. (*R*)-[^{11}C]Me@NEBIQUINIDE wurde über [^{11}C]Methyltriflat gemäß Standardvorschriften synthetisiert, während die Radiosynthese von (*R*)-[^{18}F]NEBIFQUINIDE nur über die ^{18}F-Fluorierung mit Mikrowellenunterstützung möglich war. Beide Tracer wurden zuverlässig und reproduzierter synthetisiert. Die präklinische in *vitro* Evaluierung umfasste Stabilitätsuntersuchungen, die Bestimmung von log*P* und die Bindung an Plasmaprotein α1-AGP. Für beide Substanzen wurden vielversprechende Ergebnisse erzielt, die eine weitere

Analyse des *in vivo* Verhaltens nahelegten. Aufgrund seiner vorteilhaften physikalischen Halbwertszeit wurde zunächst nur (*R*)-[^{18}F]NEBIFQUINIDE in Mäusen getestet, was hervorragende Ergebnisse zeigte, die seine Verwendung in Tiermodellen und der *in vivo* Anwendung beim Menschen nahelegten. Außerdem ermöglichten Radioliganden-Bindungsassays unter Verwendung bereits bekannter TSPO Liganden eine weitere Charakterisierung dieser molekularen Zielstruktur bei Darmkrebs sowie hinsichtlich des genetischen Profils.

RESUMEN

La proteína translocadora con un peso molecular de 18 kDa (TSPO), la cual ha sido descrita inicialmente como el receptor periférico de benzodiacepinas, presenta diferentes niveles de expresión en una variedad de enfermedades, como trastornos neurodegenerativos, insuficiencia cardíaca y varios tipos de cáncer, lo que resalta a dicha proteína como un biomarcador interesante para el tratamiento y diagnóstico de las enfermedades antes mencionadas. En este sentido, la tomografía por emisión de positrones (TEP) se ha convertido en la estrategia principal para la cuantificación y distribución *in vivo* de la TSPO, mediante el uso de radiotrazadores con alta afinidad. Aunque se han introducido varios trazadores, un polimorfismo en el gen *TSPO* ha impedido el desarrollo del radiofármaco ideal. En detalle, este polimorfismo causa una diferencia en la afinidad de los radiofármacos en sujetos con diferentes genotipos, lo que finalmente lleva a una clasificación de sujetos con alta afinidad (HAB), afinidad media (MAB) y baja afinidad (LAB). A pesar de que algunos radiofármacos exhiben una baja sensibilidad hacia este polimorfismo (es decir, exhiben una afinidad similar hacia la TSPO, independiente del genotipo), carecen de propiedades farmacocinéticas adecuadas que dificultan su uso. Por consiguiente, en esta tesis doctoral, varios compuestos fueron diseñados como ligandos de la TSPO para lograr el tan requerido radiofármaco para imágenes TEP de la TSPO.

En consecuencia, las síntesis de estos compuestos así como de los precursores para el radiomarcaje fueron planificadas y ejecutadas con rendimientos satisfactorios. Además, las afinidades hacia la TSPO de dichas sustancias fueron determinadas en experimentos competitivos, utilizando membranas de trombocitos de sujetos previamente genotipificados. Sobre la base de estos resultados, se identificaron dos compuestos con alto potencial como radiotrazadores de la TSPO, ya que exhiben una alta afinidad y ninguna sensibilidad respecto al polimorfismo. Por lo tanto, se desarrollaron y evaluaron dos radiofármacos en esta tesis doctoral: (*R*)-[^{11}C]Me@NEBIQUINIDE y su análogo fluorado (*R*)-[^{18}F]NEBIFQUINIDE. Para ello, se sintetizó (*R*)-[^{11}C]Me@NEBIQUINIDE a través del [^{11}C]triflato de metilo, mientras que la radiosíntesis de (*R*)-[^{18}F]NEBIFQUINIDE solo fue posible mediante ^{18}F-fluoración asistida con radiación microondas. Ambos radiofármacos se sintetizaron de una manera confiable y factible. La evaluación preclínica *in vitro* incluyó pruebas de estabilidad, determinación de log*P* y unión a proteínas plasmáticas (α1-AGP). En ambos casos, se lograron resultados prometedores, que sugirieron una evaluación adicional *in vivo*. En consecuencia, debido a su período de semidesintegración más apropiado, solamente (*R*)-[^{18}F]NEBIFQUINIDE fue evaluado en roedores, mostrando resultados sobresalientes que promueven su uso en modelos animales y la aplicación *in vivo* en humanos. Además,

experimentos para la determinación de constantes de afinidad utilizando ligandos de la TSPO previamente conocidos permitieron una caracterización adicional de la misma en cáncer colorrectal, así como en relación con el polimorfismo genético.

CHAPTER I
INTRODUCTION

1. MOLECULAR IMAGING

According to the Society of Nuclear Medicine and Molecular Imaging (SNMMI) and its Molecular Imaging Center of Excellence (MICoE, currently known as the Center for Molecular Imaging Innovation and Translation), "*molecular imaging is the visualization, characterization and measurement of biological processes at the molecular and cellular levels in humans and other living systems*."[1] A variety of processes can be studied with molecular imaging modalities, e.g. organ function, metabolic rates and changes, enzyme activity, blood flow, gene and receptor expression, and neurotransmitter synthesis and release.[2,3] Such biological processes are often altered during disease development and therefore constitute an important monitoring point for disease assessment.[4] Hence, molecular imaging is a type of medical imaging able to provide information regarding those alterations beyond the physical structure and localization of the disease, as offered by other diagnostic imaging procedures, such as x-rays and classical computed tomography (CT).[5,6] Moreover, molecular imaging techniques are minimal invasive and promote an early disease diagnosis, a personalized patient management, an appropriate therapy selection, and a more accurate assessment of a treatment's effectiveness.[7–10] As a field, molecular imaging includes several modalities where diverse disciplines converge, e.g. biology, chemistry, medicine, pharmacology, medical physics, bioinformatics, engineering, mathematics, among others.[11,12] Each modality requires high resolution and high sensitive instruments to detect endogenous or exogenous specific probes, known as molecular imaging agents, which are associated to the molecular process of interest.[13,14] In general, five modalities are identified within the molecular imaging's scope, namely specific-contrast CT imaging, optical imaging (OI), ultrasound (US), magnetic resonance imaging (MRI), and radionuclide imaging, as the most performed procedure within this area.[15] Each modality possesses its own benefits and limitations.[16]

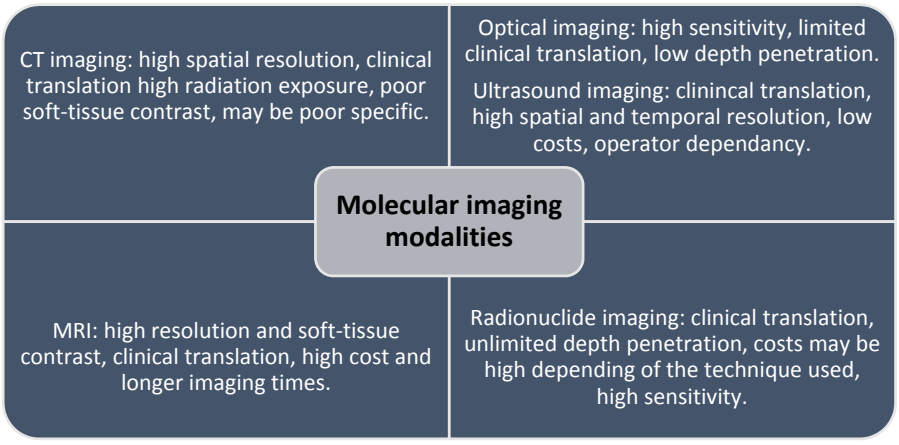

Figure 1. An overview of molecular imaging modalities: Some advantages and disadvantages

1.1. NUCLEAR MEDICINE AND RADIONUCLIDE IMAGING

Nuclear medicine is a branch of medicine which uses radioactive substances for the treatment and, more regularly, the diagnosis of diseases. Such diagnosis is achieved through the administration (normally intravenously, although oral and inhaled administrations are also possible) of radioactive substances (commonly known as radiopharmaceuticals, radiotracers and/or radioligands) capable to *in vivo* target a probe of interest in a specific fashion and subsequent detection of the intrinsic radioactive decay emitted by those substances using dedicated medical devices. After an adequate processing, this provides an image of the biodistribution density of the radiopharmaceutical, thus reporting a particular molecular event.[17,18]

Radiopharmaceuticals are, as a result, molecular imaging agents consisting in a molecule with high affinity to the target of interest containing a radioactive atom in its chemical structure. Accordingly, a broad range of radiotracers are devisable, considering different types of molecules, e.g. small molecules, peptides, antibodies, nanoparticles; and the type of radionuclide used. Two types of radionuclide imaging are available, depending on the used isotope, which undoubtedly determines the type of decay and consequently the required detection system: positron emission tomography (PET) and scintigraphy. The former utilizes radiopharmaceuticals, whereby the nuclear disintegration is defined by a positron-emitter radionuclide, whereas the latter demands radiotracers containing gamma-emitters and it is subcategorized in planar (two-dimensional) scintigraphy and single-photon emission computed tomography (SPECT), which is able to delivery three-dimensional information. Due to the main focus of this doctoral thesis, more information regarding PET will provided in the following sections.[19,20]

Both techniques are quantitative, high sensitive, offer good temporal resolution, unlimited depth penetration, and whole-body imaging. Some disadvantages include the obvious radiation exposure, in some cases long acquisition times and particularly low spatial resolution, due to the complex determination of the exact origin of emission in the tissue.

1.1.1. POSITRON EMISSION TOMOGRAPHY

This molecular imaging technique is based on the coincidence detection of two oppositely directed gamma-rays (γ-rays) resulted from the mutual annihilation of positron (β^+) and an electron (β^-). In detail, the neutron-deficient nucleus of the radioisotope contained in the radiopharmaceutical

decays spontaneously by converting a proton into a neutron leading to a simultaneous emission of a positron. The emitted positron travels a very short distance, known as positron range, while completely dissipates its kinetic energy until collides with an electron. Since positrons and electrons are mutually antiparticles, this interaction rises its combination into an extremely unstable composition, called positronium, which is instantly annihilated to produce two photons (γ-rays). Considering the resting energy of each colliding particle, as well as the energy and momentum conservation principles, the produced photons are ejected in opposite directions (180° angle) with an energy of 511 keV each and captured by a series of detectors incorporated in PET scanners. The circular arrangement of those detectors and the opposite directions of the photon pair enables to localize the annihilation event along a straight line (line of response, LOR), therefore providing information about the position and concentration of the positron emitter within the living subject. As mentioned before, only true coincidence detections, i.e. corrected for random and scattered coincidences, are considered in the algorithms for image reconstruction.[21–24]

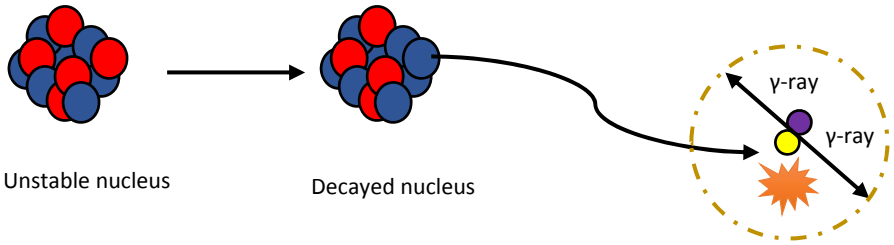

Figure 2. Positron emission and PET detection: The unstable neutron-deficient nucleus decays by converting a proton (red) in a neutron (blue), which leads to the simultaneous emission of a positron. The positron (yellow) is then annihilated by an electron (purple) after traveling a short distance. As a result, two γ-rays (511 keV each) are emitted in opposite directions and detected by a PET camera.

PET imaging was first introduced in 1975 and although it was mainly used within a research framework during its beginning, it escalated rapidly into clinical practice in the 1990s. Currently, it is seen as a powerful imaging technique with valuable clinical applications in oncology, neurology, and cardiology, to name a few.[25,26] Moreover, the impact of PET imaging in modern medicine has considerably raised since the introduction of multimodality imaging as PET/CT and PET/MRI, which provide the functional information of PET as well as the anatomical reference delivered by CT or MRI.[27,28] Additional technical upgrades in PET instrumentation have resulted in major progresses in image quality for patient studies.[29]

Unsurprisingly, the present clinical applications of PET have not superseded its research value. Indeed, a growing number of evidence points out the use of PET imaging for instance in drug discovery and development.[30,31] Moreover, PET and its combined techniques are also available for animal imaging (called µPET for small animals), enabling their use in pre-clinical settings. The wide availability of mice disease models as well as genetically engineered mice turns µPET imaging into a robust method for a better understanding of pathophysiological processes.[32]

1.1.1.1. PET RADIOCHEMISTRY

As already mentioned, positron emitters are incorporated into relevant ligands to obtain the radioactive probes known as radiopharmaceuticals. Consequently, this enables an *in vivo* tracing of biological processes by customizing appropriate probes for each application. Therefore, introducing such positron emitters generally involves the replacement of an atom in the molecular structure of the ligand by its radioactive counterpart. In general, a considerable number of biomolecules contain carbon, fluorine, nitrogen or oxygen, which allows an isotopic substitution to achieve chemically identical compounds. In these circumstances, the radiopharmaceuticals retain the main biochemical and physicochemical properties of the non-radioactive ligands, despite a minor isotopic effect. In other cases, some positron emitters may substitute other atoms or functional groups with minimal perturbation and even improving the binding properties.[33,34] In practice, the inclusion of positron emitters in such molecules represent an enormous challenge due to the intrinsic molecular properties and available radiolabeling methods.

Since several PET radionuclides are available, it seems logical to follow a rational approach for the selection of the radiolabeling precursor, i.e. the compound to which the radionuclide will be incorporated, and the appropriate radionuclide. Moreover, the choice of the suitable radionuclide must consider its half-life in relationship with the pharmacokinetics of the radioligand, as well the chemical authenticity. In general, PET radionuclides are divided in metallic and covalent radionuclides and produced in cyclotrons or, less frequently, extracted from devices known as generators. As a result, radiopharmaceutical molecular structures consist in the motif responsible for target interactions, the radionuclide itself and, in the case of metallic radionuclides, a chelator for metal complexation. Some characteristics of common PET radionuclides are shown in table 1.

Table 1. Physical properties of some PET radionuclides[33]

Nuclide	Half-life (min)	Maximum energy (MeV)	Mode of decay (%)	Production Method
^{18}F	109.77	0.64	β^+ (97%) EC (3%)	Cyclotron
^{11}C	20.33	0.97	β^+ (99%)	Cyclotron
^{13}N	9.96	1.20	β^+ (100%)	Cyclotron
^{15}O	2.03	1.74	β^+ (100%)	Cyclotron
^{68}Ga	67.71	1.90	β^+ (89%) EC (11%)	Generator
^{64}Cu	762.06	0.66	β^+ (19%) EC (41%) β^- (40%)	Cyclotron
^{44}Sc	238.20	0.63	β^+ (94%) EC (56%)	Generator

As inferred from the half-lives outlined in table 1, radiosynthetical approaches for delivering radiopharmaceuticals should be fast. As a general rule, radiosynthesis should not take more than three half-lives of the used radionuclide.[33] Fortunately, reaction kinetics in PET radiochemistry situations are described by pseudo-first order kinetics, due to the higher concentration of the radiolabeling precursor compared to the radionuclide (at least a 100-fold excess), which drives the reaction toward the formation of products within minutes. Nevertheless, radiochemical routes should avoid multi-step reactions and when possible they should incorporate the radionuclide as late as possible.[33] Similarly, purification and quality control times should be reduced as much as viable.

Generally, those radiosyntheses are carried out in modules, i.e. automated synthesizers which provide a reliable a manner to deliver clinical relevant as well as novel radiopharmaceuticals in PET production centers around the globe. These modules are versatile and robust systems which include a variety of components to reduce the manual intervention in order to produce radiopharmaceuticals, including purification systems as HPLC. As a consequence, PET tracers are obtained in a fast, reproducible and particularly in a safe way, which means the minimization of potential human faults and a minimum radiation exposure to production personnel.[35–38]

Since PET radiopharmaceuticals are ultimately applied in living systems, i.e. animals or humans, they must be tested to guarantee acceptable quality prior to administration of each produced batch. The criteria for quality must be carefully defined for each radiopharmaceutical and appropriate tests must be validated prior to implementation, following relevant guidelines for each country, e.g. USP, FDA and European Pharmacopoeia.[39] Regular tests are summarized in table 2 and include an examination for determining the sterility and the absence of endotoxins in the produced radiopharmaceutical batch. Nevertheless, the timeframe for those tests exceed the half-life of most PET radionuclides. Hence, the microbiological safety is exceptionally confirmed after administration of the radiopharmaceutical.

Table 2. Regular quality control criteria for PET radiopharmaceutical preparations

Criteria	Typical test method	Typical acceptance criteria
Clearness	Visual inspection	Clear, colorless, free of particles
Radiochemical purity	Radio-HPLC and radio-TLC	≥95%
Radiochemical identity	Radio-HPLC and radio-TLC	Same t_R and R_f as authentic non-radioactive samples
Chemical purity	HPLC	No side-products, low precursor amounts.
pH	pH measure	4.5 – 8.5
Osmolality	Osmometer	200 – 400 mosm/kg
Radionuclide identity and purity	γ-spectroscopy; half-life determination	γ-spectrum peak 430 – 520 keV; half-life ±10%
Residual solvents	GC	Different thresholds according to the solvent used
Sterility and absence of endotoxins	Sterility test; LAL-test	Sterile and endotoxins < 1 EU/mL

Although not outlined in table 2, an important parameter to assess in some radiopharmaceutical productions is the specific and molar activity. This concept denotes the proportion of radiotracer to the total amount of compound (both labeled and unlabeled) in mass (specific activity) or in moles (molar activity). Since amounts of the non-radioactive ligand are usually present in the radiopharmaceutical preparation, it reflects the dilution of the radiolabeled compound related to the non-radioactive compound.[40,41] This is of high importance considering the pharmacological equivalence of both compounds, which might bring a poor signal in the PET image due to the high occupancy of the target with non-radioactive compound. Moreover, an undesired pharmacological side effect, due to the administration of high quantities of non-radiolabeled compound, should be considered.

Due to the major focus of this doctoral thesis on carbon-11 and fluorine-18 radiopharmaceuticals, an overview of the chemistry of the chemistry of these both radionuclides will be given below.

1.1.1.1.1. CARBON-11

In 1934, carbon-11 was produced by Crane and Lauritsen for the first time. At that moment, they determined its half-life of 20.33 min and its decay characteristics to the stable isotope boron-11: 99.81% by positron emission and 0.19% by electron capture.[42] Carbon-11 became rapidly an important radioactive isotope suitable for biological research, due to the presence of carbon in all organic molecules. In fact, radiolabeling of a molecule with this isotope gives a radioactive copy of such molecule.[43]

Carbon-11 radiolabeling methods include a multitude of reactions, which in addition to the radioactive copy characteristics and clean positron decay, highlights the use of this nuclide in positron emission tomography.[43] However, its short half-life requires production of the radiopharmaceutical at the same place of the PET scan, as well as a minimum amount and fast reaction times. For PET, carbon-11 is produced within a cyclotron by bombardment of a target filled with $^{14}N_2$ with accelerated protons. The nitrogen used for filling the target is generally mixed with traces of oxygen (O2, <2%) or hydrogen (H_2, 5-10%), to obtain gaseous [^{11}C]carbon dioxide {[^{11}C]CO_2} or [^{11}C]methane {[^{11}C]CH_4}, respectively.[33,44]

Afterwards, [^{11}C]CO_2 or [^{11}C]CH_4, are further processed to yield a variety of ^{11}C-synthons, which allow the incorporation of carbon-11 in the molecule (Figure 3).

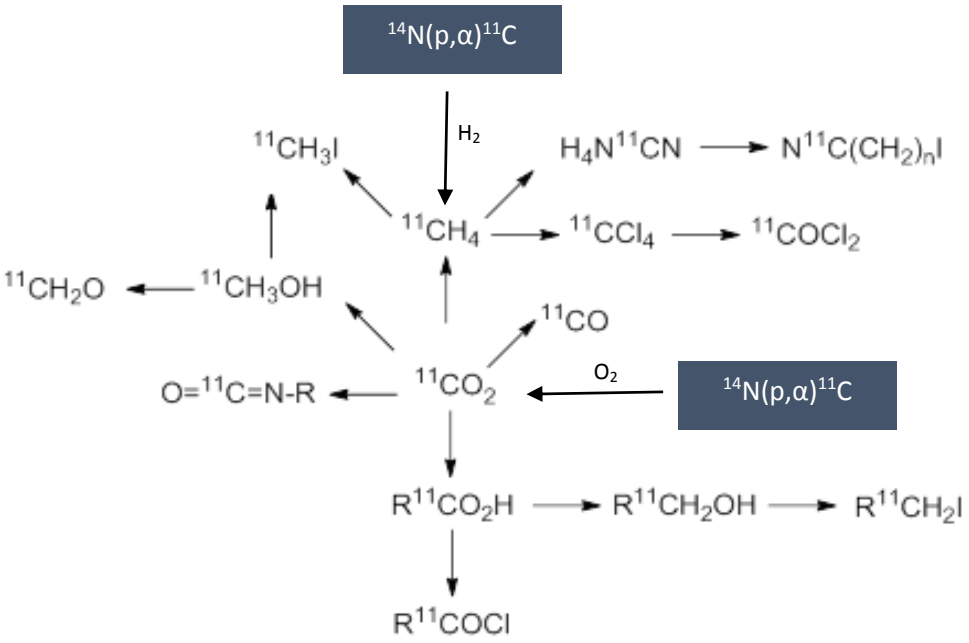

Figure 3. Different strategies to obtain ^{11}C-labeled synthons

In particular, nucleophilic ^{11}C-methylations constitute the majority of ^{11}C-labeling reactions, for which [^{11}C]methyl iodide {[^{11}C]CH_3I} has become the most important labeling moiety. As shown in Figure 4, two methods are used to produce [^{11}C]CH_3I, commonly known as the wet and dry methods. The wet method involves the reduction of [^{11}C]CO_2 to [^{11}C]methanol {[^{11}C] CH_3OH} by treatment with lithium aluminum hydride. Subsequently, [^{11}C] CH_3OH is converted to [^{11}C]CH_3I after reaction with hydroiodic acid.[43,45] The dry method requires elemental iodine for a free radical iodination of [^{11}C]CH_4 (obtained from reduction of [^{11}C]CO_2 through a nickel-catalyzed hydrogenation on a molecular sieve or directly from the cyclotron target as described previously).[46] Moreover, further processing of [^{11}C]CH_3I provides additional labeling synthons for reactions with less reactive nucleophiles. For instance, by passing the produced [^{11}C]CH_3I through a column impregnated with silver triflate, the new radiomethylation agent [^{11}C]methyl triflate {[^{11}C]$CH_3OSO_2CF_3$} is obtained.[47]

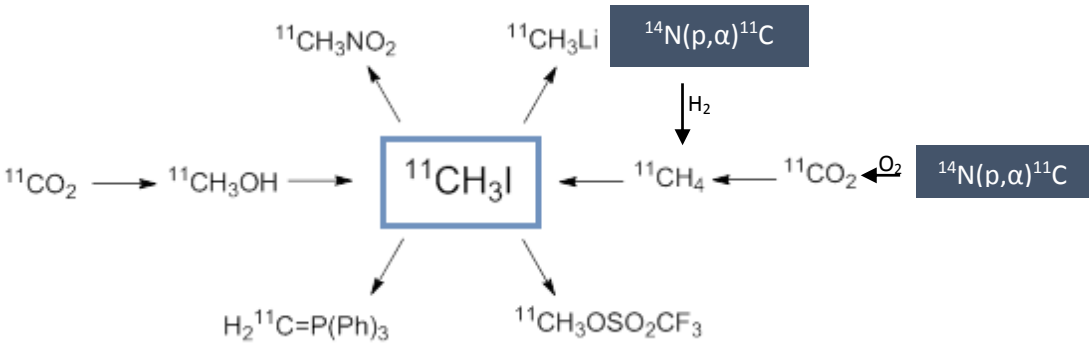

Figure 4. Wet and dry methods to produce [^{11}C]CH_3I

1.1.1.1.2. FLUORINE-18

The nucleus of fluorine-18 consists of nine protons and nine neutrons. It is usually considered as a very ideal radionuclide for PET, due to its advantageous half-life of 109.77 min and clean positron emission profile (97% by positron emission and 3% electron by electron capture) to yield stable oxygen-18.[40] These favorable characteristics have promoted several efforts for the synthesis of several ^{18}F-radiopharmaceuticals. Remarkably, the benefits of fluorine substitution on ADME profiling (absorption, distribution, metabolism, excretion) are well described for several class of molecules, including agrochemicals and (radio)pharmaceutical drugs. It serves as modulator of conformational and stereo electronic properties, as well as influencer on polarity, lipophilicity, and pKa values of neighboring Brønsted acid/base centers. Hence, ^{18}F-labeling permits not only the incorporation of a radioactive tag for PET detection, but also the improvement of the radiotracer performance.[48]

Production of fluorine-18 for PET is carried out in a cyclotron by irradiation with accelerated protons of a target filled with oxygen-18 enriched water {[^{18}O]H_2O} to yield [^{18}F]fluoride {[^{18}F]F^-}. Moreover, a second method for fluorine-18 production utilizes accelerated deuterons to bombard a target filled with neon-20 to yield gaseous [^{18}F]F_2 (^{18}F-^{19}F).[40]

Figure 5. Nuclear reactions for the production of fluorine-18

Hence, diverse radiochemical transformations, allowing the introduction of fluorine-18, have been developed in line to the produced ^{18}F-labeling motif {[^{18}F]F_2 or [^{18}F]F^-}. Accordingly, two general methods for ^{18}F-labeling are generally described: nucleophilic and electrophilic, whereby nucleophilic radiofluorinations are predominant due to the poor molar activity achieved with [^{18}F]F_2.

A plethora of methods are available to introduce fluorine-18 *via* nucleophilic reactions.[48–50] Nevertheless, the removal of target water is normally mandatory due to the poor nucleophilicity of fluoride in aqueous media as well as the hampering of the reaction due to moisture traces. This is commonly achieved by retention of [^{18}F]F^- in a anion exchange cartridge, subsequent elution with alkali metals or quaternary ammonium carbonates or bicarbonates and simultaneous activation with amino polyethers as Kryptofix K2.2.2. (4,7,13,16,21,24-hexaoxa-1,10-diazabicyclo[8.8.8]hexacosane). Likewise, tetra-alkyl ammonium salts are also used as phase transfer catalysts for the elution and activation of [^{18}F]F^-. Normally these steps are followed by azeotropic distillation to remove last traces of water. In the last years, "minimalistic methods" have been developed to circumvent the use of bases, additives or azeotropic distillation to yield dried [^{18}F]F^-.[40,51,52]

1.1.1.2. PET Radiopharmaceutical Development

The development of PET radiopharmaceuticals is a multidisciplinary process encompassing several complex, and often iterative, steps. Such process begins with a biomedical question arose from the necessity to accomplish appropriate diagnosis and/or treatment of patients.[53–55] Afterwards, a suitable molecular target is carefully chosen, especially considering its expression and localization. Once the target has been identified, screening and scrutiny of lead compounds is performed to determine hit molecules. This step can be achieved by revising compound libraries,

conducting structure-activity relationship (SAR) studies, and by modifying endogenous or existing synthetic ligands.[56–58] In this phase, compounds are evaluated and, if needed, optimized regarding to their physicochemical properties, binding affinity and selectivity. With a promising candidate in hand, radiolabeling approaches to deliver the radiotracer in acceptable quality are carried out. These strategies must include the selection of a suitable radionuclide, synthesis of a suitable radiolabeling precursor, a chemical route for the radiolabeling itself, purification and quality control. To complete the process, *in vitro* and *in vivo* animal investigations are conducted using the newly developed radiopharmaceutical. With these investigations, a comprehensive overview of the binding characteristics, stability, and pharmacokinetic profile of the radiotracer are obtained. In the long run, if all investigations and regulatory issues are met, a clinical study of the novel PET radiopharmaceutical may be granted. [59–63]

Regarding the *in vitro* and *in vivo* investigations, the criteria to be met for developing useful PET radiotracers include: high affinity and target selectivity, low non-specific binding, metabolic stability, suitable pharmacokinetics particularly in relationship with the radionuclide half-life, preferably accessibility to radiolabeling at high molar activities, and in case of cerebral applications, ability to penetrate the blood-brain-barrier (BBB).[64,65] Such criteria are synopsized below.

1.1.1.2.1. Affinity and Selectivity

The binding affinity reflects the strength of the interactions between a ligand and a binding site. This binding site may refer to the desired target or an adjacent target. These interactions are often described by the dissociation or inhibition constants, K_d and K_i, respectively. Ideally, a radioligand should exhibit small values of K_d or K_i toward the target of interest (high affinity, usually in the nanomolar range) and high values toward adjacent or unrelated targets (high selectivity), i.e. ligand-binding site interactions are stronger for the relevant binding site than for irrelevant targets.

The determination of these binding parameters are based on the law of mass action, which explains the formation of ligand-receptor complex under reversible conditions. Accordingly, the rate at which the complex is formed equals to the rate at which the complex is dissociated.

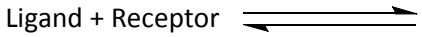

$$[Ligand] \cdot [Receptor] \cdot k_{on} = [Ligand \cdot Receptor] \cdot k_{off}$$

$$\frac{[Ligand] \cdot [Receptor]}{[Ligand \cdot Receptor]} = \frac{k_{off}}{k_{on}} = K_d$$

Per definition, the K_d value is the concentration of the ligand which occupies 50% of the target population and can be determined in saturation binding assays.[66]

Similarly, K_i can be obtained through competitive binding assays, where previously a half maximal inhibitory concentration value, IC_{50}, is gained. In these kind of experiments, the binding of a ligand with known K_d and fixed concentration, [L], is challenged against different concentrations of another ligand candidate, which produces an inhibitory effect. Thus, a dose-response curve is examined and the K_i value is achievable through the Cheng-Prusoff equation.[67]

$$K_i = \frac{IC_{50}}{1 + \frac{[L]}{K_d}}$$

Besides saturation and competitive assays for obtaining K_d and K_i values, respectively, additional class of experiments can be performed to determine affinity and selectivity. For instance, autoradiography serves as *in vitro* imaging technique to characterize binding behavior of radioligands. The method uses cryo-slices of relevant organs which are incubated with the radiotracer in physiological buffer. After incubation time, the slices are placed on phosphor screens until complete decay of the radioactivity.[68] Processing of the screens with dedicated devices offers a qualitative and quantitative image. The results can be used to assess affinity and selectivity if the slices are co-incubated with known non-radioactive ligands of the relevant target.[69]

1.1.1.2.2. Non-specific and Plasma Protein Binding

High non-specific binding is largely responsible for the high discarding rate of PET radiopharmaceutical candidates in preliminary rounds of preclinical imaging experiments, causing PET images to have poor contrast. Therefore, it represents an important determinant for the success or failure of PET radiotracer candidates. Apparently, non-specific binding results from binding of the tracer to cell membranes and moieties other than their desired target. In this regard, although no absolute parameter has been identified to predict non-specific binding of PET radiopharmaceuticals, several properties have been somehow correlated to the outcome of the

radiotracer's *in vivo* behavior. Despite its consideration as poor predictive parameter of non-specific binding, and moreover BBB penetration, the lipophilicity or more properly the log*P* value, is still used as reference to judge and compare different PET radiotracers, due to the lack of real predictive parameters. In this regard, although not yet conclusive, several *in silico* methods have been proposed as prediction models. In *in vivo* settings, non-specific binding is measured by fitting the curve of the radioactivity concentration as a function of time in the regions of interest to a model that incorporates a non-specific binding compartment.[53,70–72]

Likewise, the plasma protein binding plays a major role in the pharmacokinetic profile of PET radiopharmaceuticals. In fact, it is considered that only the free drug concentration in plasma is responsible for binding at the desired target. Thus, determination of plasma protein binding of PET tracers constitutes another evaluation point to predict the targeting of the radioligand candidate.[73–76]

1.1.1.2.3. STABILITY

In vitro evaluation of the metabolism of a PET radiotracer is mandatory prior to *in vivo* testing. Even highly affine and selective candidates might not offer the sufficient stability to reach the target in an intact fashion. In addition, a further metabolism can be expected after reaching the desired organ, for instance cleavage reactions in the brain. The metabolic fate of a radiotracer plays a pivotal role in the assessment of its pharmacokinetics.[65] Firstly, a fast degradation of the radiopharmaceutical impedes the reaching of the target, leading to an accumulation of the radioactivity in emunctory organs or in tissues of no interest. Secondly, the signal emitted from possible emerged of radioactive metabolites is not discriminated from the signal of the intact radioligand, which ultimately leads to a false registration of the tracer biodistribution. Several enzymes and multi-enzymes complexes may be responsible for the metabolic degradation of the radiotracer. Noteworthy, the majority of enzymes implicated of such degradation are part of the cytochromes P450 proteins mainly present in liver microsomes and account for 75% of the total metabolism. Fortunately, these and other important enzymes are available for metabolism screening. [77]

Although *in vitro* assessment of the metabolism does not fully represent the complex *in vivo* situation,[78] it constitutes an important first approach to determine the stability of the radiotracer.

Nevertheless, the evaluation of the metabolic fate of radiotracer candidates must continue in the *in vivo* experiments to fully guarantee a considerable amount of intact tracer in organs of interest.

1.1.1.2.4. *IN VIVO* PHARMACOKINETICS

Pharmacokinetic excretion and distribution in organs of interest of the PET radiopharmaceutical can be assessed by measurement of the amount of radioactivity present in relevant tissues and fluids of animals after administration of the radiotracer, followed by sacrifice after defined time points and subsequent removal of relevant tissues and fluids. For this class of measurements, the measured radioactivity is related to the amount of radioactivity injected as well as the weight of the respective organ.[79–81]

Analogously, administration of a PET radiopharmaceutical in animals can be followed by µPET (for small animals) and PET (large animals). Therefore, a picture of the tracer biodistribution and therefore the density of the target of interest is obtained, providing additionally a vision of the tracer binding kinetics and excretion. µPET/CT and µPET/MRI devices are also available to correlate the tracer biodistribution and anatomical information. These animal experiments allow a relative rapid screening of several compounds as well as the performance of the radiopharmaceuticals in different groups of animals, e.g. control and sick animals. Nevertheless, inter-species differences should be considered to guarantee complete and appropriate translation to humans.[82–84]

2. BENZODIAZEPINES AND BENZODIAZEPINE BINDING SITE

Benzodiazepines are a class of chemical compounds bearing a diazepine fused to a benzene ring with different side chains (Figure 3). The first benzodiazepine, chlordiazepoxide, was synthetized in 1955 by Leo Sternbach while presumably working on the synthesis of heptoxdiazines.[85] Subsequent trials in animals demonstrated hypnotic, anxiolytic, and muscle relaxant effects exerted by chlordiazepoxide, [86,87] which was later tested in humans, exhibiting almost no side effects without significant influence on the state of consciousness.[88] The new drug was finally traded in 1960 as Librium® and a wider study identified the role of different side chains (in the benzodiazepine core structure) in the pharmacokinetic profile of diverse benzodiazepines. [89] Accordingly, alternative benzodiazepines with more potent properties were identified and likewise marketed by several pharmaceutical companies. Among these, diazepam (commercialized as Valium®) arose as a highly potent compound and became the most prescribed benzodiazepine and medical treatment worldwide in the 1970s. Despite the significant lack of knowledge of the action mechanism of benzodiazepines at the time of their development, they were prescribed for the treatment of several diseases, including epilepsy, muscle spasms, alcohol withdrawal, and mostly anxiety and neurotic disorders.[90]

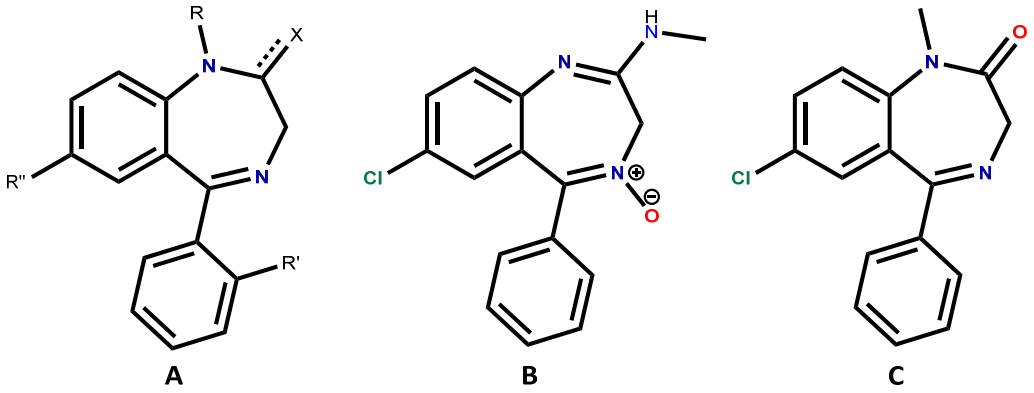

Figure 6. (A) General structure of benzodiazepines; (B) Librium®; (C) Valium®

In fact, the development of benzodiazepines contributed to the field of neurotransmission,[91] since it became later clear the relationship between the effects of these drugs and the pharmacological effect of gamma-aminobutyric acid (GABA), the major inhibitory neurotransmitter in the brain.[92] Several investigations led to conclude a binding enhancement of GABA on its post-synaptic receptor (the $GABA_A$ receptor).[93–95] This phenomenon, known as positive allosteric modulation, inevitably produces a superior inhibitory effect of each GABA molecule and it is only possible due to the different binding sites of GABA and benzodiazepines: GABA binds to the $GABA_A$ receptor between the α- and β-subunits, whereas benzodiazepines bind to the $GABA_A$ receptor at the

interface between the α- and γ-subunits, commonly called central benzodiazepine receptor (CBR), although properly known as benzodiazepine site.[96]

2.1. PERIPHERAL BENZODIAZEPINE RECEPTOR AND TRANSLOCATOR PROTEIN

Additional investigations on benzodiazepines led to conclude an additional binding site of this class of compounds outside the brain,[97] which was accordingly called peripheral benzodiazepine receptor (PBR), to distinguish it from the CBR, from which differs pharmacologically and structurally.[98–100] Although several names were proposed to properly designate the PBR, it is currently known as the 18 kDa translocator protein (TSPO), in accordance to its transport functions (see following section) instead of a proper receptor.[101]

As part of the tryptophan-rich sensory proteins, the TSPO is topologically and functionally well conserved from bacteria to humans with five transmembrane domains, although important dissimilarities have been also reported at the amino acid sequence level.[102] Bacterial and mouse TSPO's structures have been reported, whereas no 3D structure for the human TSPO is available.[103] The human TSPO consists of 169 amino acid residues and is ubiquitously expressed throughout several organs in the body. In detail, the TSPO is localized in a subcellular level at the outer mitochondrial membrane (OMM) and abundantly found in tissues such as lungs, kidneys, heart, adipose tissue, testis, and adrenal cortex, whereas it is poorly expressed in the healthy brain.[104,105] Moreover, its interactions with other proteins at the OMM and inner mitochondrial membrane (IMM) to form a multiprotein complex have been extensively suggested.[106–108]

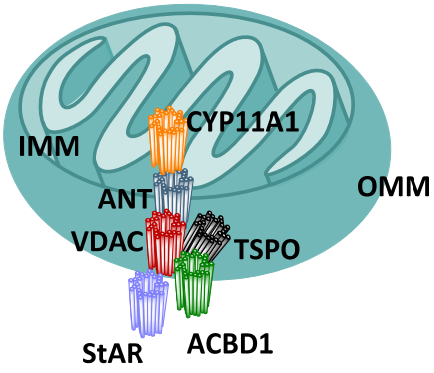

Figure 7. Figure 4. TSPO forming the transduceosome complex with other proteins at the outer and inner mitochondrial membranes (OMM and IMM): the voltage-dependent anion channel (VDAC), the adenine nucleotide translocator (ANT), the steroid acute regulatory protein (StAR), the cytochrome P450 family 11 subfamily A member 1 (CYP11A1) and acyl-CoA binding protein (ACBD1).

2.1.1. rs6971 SINGLE NUCLEOTIDE POLYMORPHISM

Several reports have mapped the *TSPO* gene to the human chromosome 22, band 22q13.31; as a single copy having 169-amino acid residues.[104,109–111] Within these amino acid residues, at least two single nucleotide polymorphisms (SNPs) have been found: rs6971 and rs6972, which result in a non-conservative amino acid substitution at positions 147 and 162, respectively. In the first case, alanine is spontaneously replaced by threonine (Ala147Thr); whereas in the second case, histidine is substituted by arginine (His162Arg).[112,113]

The rs6971 SNP is located in the exon 4 of the *TSPO* gene and has been linked to altered steroidogenesis and incidence of anxiety-related conditions.[114–118] Moreover, this substitution apparently facilitates a lower-affinity conformation, which modifies a potential ligand binding site in the fifth transmembrane domain.[119] This mutation significantly varies the flexibility and stability of the protein.[103] The ultimate consequence of such SNP is a genotype-dependent heterogeneity of several TSPO ligands, i.e. numerous TPSO ligands exhibit distinctive binding affinities toward subjects with different genotypes. In this regard, three affinity patters related to the amino acid residue can be distinguished as follows: high-affinity-binders (HAB, homozygotes, alanine in position 147 on both alleles), low-affinity-binders (LAB, homozygotes, threonine in position 147 on both alleles), mixed-affinity-binders (MAB, heterozygotes, expressing both versions of the protein).[120–122] The relative incidence of such groups is the special importance in the Caucasian population, in which the rs6971 SNP is present in about 30%; whereas minor differences have been found in Japanese, African American and Han Chinese people.[123]

The origin of these denominations resides in the first observations of the heterogeneity of TSPO ligands. In fact, the effects of the rs6971 SNP on the binding affinity of TSPO ligands was first observed by using TSPO radiopharmaceuticals, which inexplicably did not bind to certain subjects (LAB), despite of the TSPO expression.[122,124] These findings promoted additional investigation until the rs6971 polymorphism was attributed as the reason for such inhomogeneous binding affinity.[121] Thus, the rs6971 SNP plays until now an essential role in the development of TSPO radioligands and it constitutes an additional point of evaluation for novel TSPO radiopharmaceuticals.

2.1.2. TSPO PHYSIOLOGY

The absolute functions of the TSPO as well as its operation mode are a major debate around different research groups around the world.[125–127] Thus, its involvement in numerous cellular processes has been largely reported and discussed, including apoptosis, cell proliferation and differentiation, immunomodulation, mitochondrial respiration, permeability transition pore opening, and steroid synthesis.[128–133] The latter being perhaps the most studied function attributed to TSPO.[134]

On this matter, the enriched TSPO expression in steroid-producing tissues as adrenal cortex and adipose tissue,[135] pointed out a role of TSPO in the steroid synthesis, which has been investigated using cell lines and animal models.[63] As a result, the evidence suggests the involvement of TSPO in the transport of cholesterol into the mitochondrion, which acts as the rate-determining step in steroidogenesis.[106–108,137,138] Moreover, several TSPO ligands demonstrated to enhance steroid production, meanwhile TSPO inhibitors blocked the hormone-induced steroid synthesis.[139–144] On the contrary, some controversial results have been achieved by genetic deletion of the *TSPO* gene in *in vitro* and *in vivo* contexts, through which TSPO exerts a significant role or no role at all in steroidogenesis.[145–151] In human settings, some investigations indicate an influence of the rs6971 polymorphism on the synthesis of pregnenolone, the major steroid in the human body.[114]

As a constituent protein of the OMM, the TSPO functions are also reflected in the essential mitochondrial role inside the cell.[152] Hence, a substantial number of research associates TSPO with core mitochondrial tasks, such as intracellular calcium signaling, apoptosis, glucose homeostasis, cellular energy production, reactive oxygen species generation, respiration, and tetrapyrrole transport into the mitochondrion.[153–155] Apparently, the modulation of nuclear gene expression *via* the mitochondria-nucleus signaling pathway is responsible for the astonishing amount of functions, which TSPO seemingly regulates.[156]

2.1.3. TSPO PATHOLOGY

As a consequence of its involvement in numerous biological processes, the TSPO has also been related to a plethora of pathological conditions. Exhaustively, dysregulation in TSPO expression levels has been reported in multiple diseases, including cancer, heart insufficiency, endocrine syndromes, as well as psychiatric and neurological disorders. Once again, its specific location at the OMM represents an utmost important characteristic, considering the participation of mitochondrial dysfunctions in a number of clinical affections, as well as the role of the mitochondrion in cell survival. [128]

The engagement of TSPO in immunomodulation seems to be an important hallmark for TSPO pathology. As TSPO is expressed in immune cells and they become reactive during the inflammation processes, different levels of TSPO have been reported during inflammation and healthy conditions. This is of particular importance for neuroinflammation where microglia, and in less extent astrocytes, respond to injuries leading to high TSPO levels. Likewise, its role in cell proliferation and apoptosis accounts for the elevated levels of TSPO in tumor cells.

2.1.4. TSPO LIGANDS AND RADIOPHARMACEUTICALS

Numerous substances have been proposed as TSPO ligands. An important characteristic is the variety of binding sites which TSPO seems to own, according to the nature of the ligand. Furthermore, the role of these ligands, regarding an agonistic or antagonistic behavior, has been evaluated in the basis of the observed effects on steroid production. As already mentioned, TSPO ligands (endogenous and synthetic) exhibit different profiles in their binding affinities regarding the rs6871 SNP.

2.1.4.1. ENDOGENOUS LIGANDS

Identification and following investigations of endogenous TSPO ligands represent important stages to its complete characterization as well as the elucidation of its physiological function.[157]

2.1.4.1.1. CHOLESTEROL

Cholesterol is an essential structural element of cellular membranes biosynthesized in all animal cells. In addition, it is a precursor for steroid hormones. Hence, it is ubiquitously found in the body

and binds to numerous receptors and ion channels. Along with its controversial role in steroidogenesis, cholesterol has been naturally suggested as an endogenous ligand of the TSPO.[118] The presence of the cholesterol recognition amino acid consensus (CRAC, and possibly also its reverse motif CARC) on the fifth transmembrane α-helix of the TSPO determines the affinity of cholesterol towards TSPO. On this matter, results clearly point out the binding of cholesterol to the CRAC motif, whereas it is unknown for the CARC motif.[158–160]

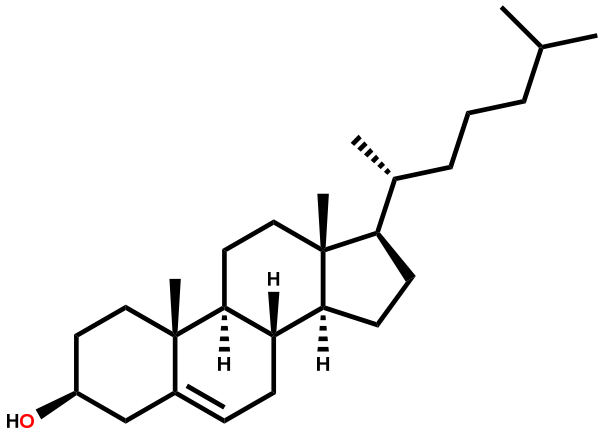

Figure 8. Cholesterol as endogenous TSPO ligand

2.1.4.1.2. PORPHYRINS

This class of tetrapyrroles, particularly protoporphyrin IX and its iron-containing derivative heme, have demonstrated to act as endogenous TSPO ligands with a high affinity and selectivity (against the CBR).[161] Since porphyrin biosynthesis takes place in the mitochondria, protoporphyrin IX and heme must pass through the outer mitochondrial membrane and therefore interact with the TSPO, suggesting a role of TSPO in heme biosynthesis. Nevertheless, the mechanisms involved in this interaction are not fully understood.[162,163] Moreover, controversial results with genetic-modified mice have questioned the premise of TSPO physiological role in heme biosynthesis.[164]

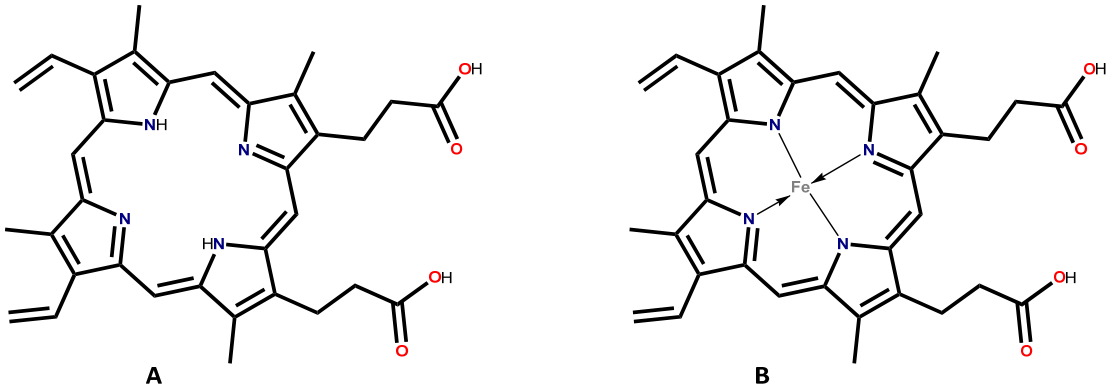

Figure 9. Protoporphyrin IX (A) and heme (B) as endogenous TSPO ligands

2.1.4.1.3. DIAZEPAM BINDING INHIBITOR

Other endogenous TSPO ligands include the diazepam binding inhibitor (DBI) and its proteolytic endozepines derivatives, DBI33-50 (ODN) and DBI17-50 (TTN). DBI is an 11 kDa polypeptide ubiquitously distributed in the CNS and steroidogenic cells and it was first discovered for its capability to interact with the CBR and regulate GABAergic transmission.[165,166] Its expression in steroidogenic cells suggests a role in steroid synthesis, which has been strongly proposed due to the evidence of its ability to bind TSPO as well as the promoting effect in transporting cholesterol into the mitochondria.[167–169]

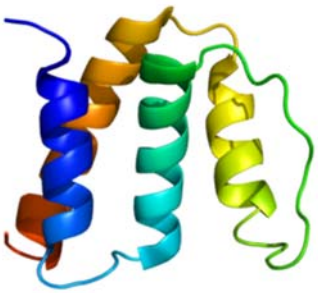

Figure 10. Diazepam binding inhibitor (DBI) as TSPO ligand

2.1.4.2. SYNTHETIC LIGANDS

A vast amount of synthetic compounds has been depicted as TSPO ligands over the last decades. Some common characteristics include:

- Bi- and tri-cyclic ring-based structures.
- An aryl or heteroaryl substituent.
- Different halogen substitution may influence the affinity of the ligands.
- Different behavior in binding affinity regarding the rs6971 SNP
- Anxiolytic effects.

A large number of SAR investigations have been performed to determine leading scaffolds to achieve high-affine TSPO ligands. The extent number of TSPO ligands share the following structural characteristics: a planar aromatic (hetero)cycle (PAH) as a core (substituted or not) with an amide group with lipophilic substituents (LS). In particular, the carbonyl moiety (CG) of the amide group has been identified as a key element to show TSPO affinity.[170–172]

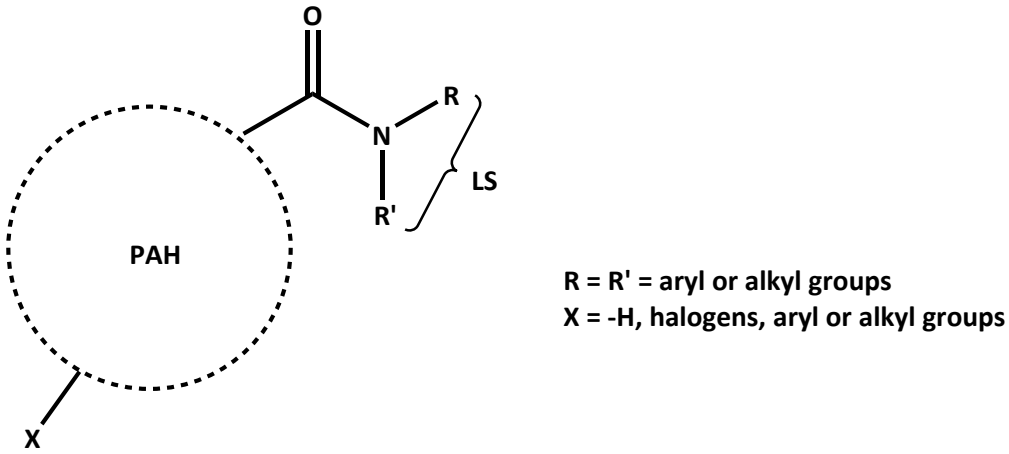

Figure 11. General structural requirements for TSPO ligand binding: An amide linked to a substituted or not planar aromatic (hetero)cycle (PAH), as well as to lipophilic substituents R and R' (LS)

2.1.4.2.1. Benzodiazepines, Benzothiazepines and Benzoxazepines

As previously discussed, benzodiazepines were the first class of compounds known to bind the TSPO. Indeed, it was the diazepam boom which allowed the discovery of this protein. Nevertheless, diazepam shows poor selectivity toward the TSPO, due to its potent binding to the CBR, which impedes the use of this ligand to characterize the cerebral TSPO. As a result, major efforts were made to distinguish the difference in both classes of benzodiazepine receptors. For instance, clonazepam exhibits high affinity toward the CBR and mild affinity toward the TSPO. In opposition, Ro5-4864 (4'-chlorodiazepam), a clinically inactive benzodiazepine, displays high affinity and selectivity toward TSPO, i.e. poor affinity toward the CBR, which undoubtedly allows a distinctive characterization of the TSPO in the brain.[173,174]

Ro5-4864 has been utilized as a specific ligand for the TSPO in several studies. However, species dependency has been reported, e.g. different results between rats and humans, which restricts its suitability as a TSPO ligand.[175]

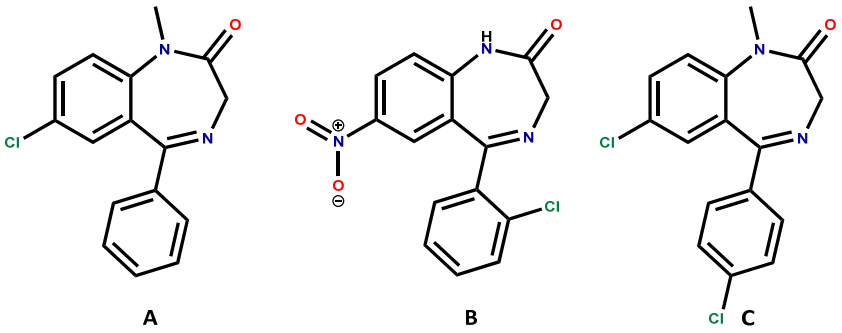

Figure 12.Benzodiazepines as TSPO ligands: (A) Diazepam; (B) Clonazepam; (C) Ro5-4864

Interestingly, the poor selectivity of some benzodiazepines, as midazolam, to distinguish the CBR and the TSPO, has raised the uncertainty if some of the exerted amnestic effect is TSPO-mediated,[176] although a low TSPO occupancy of such compound has been reported in humans.[177]

Other related structures to benzodiazepines, as benzothiazepines and benzoxazepines, exhibit also high affinity and selectivity toward the TSPO. Actually, several SAR studies were conducted to further elucidate the relevant moieties for TSPO binding and consequently obtain ligands with very high affinity. Furthermore, some benzoxapines were used to gain more information about the binding pockets on the TSPO.[178–180] While these ligands have proved to be useful probes for *in vitro* studies, their *in vivo* pharmacological profile is still missing.[157]

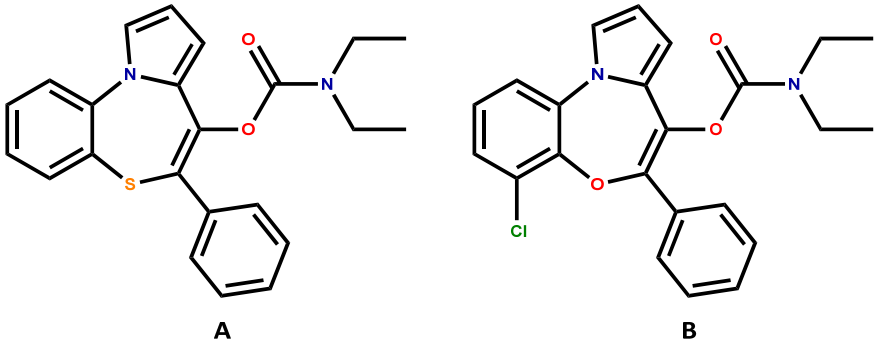

Figure 13. (A) THIA-4i a benzothiazepine and (B) OXA-17f a benzoxapine as TSPO ligands

2.1.4.2.2. Isoquinoline-, Quinoline- and Quinazoline-Carboxamides

The isoquinolinecarboxamide derivative PK11195 was the first non-benzodiazepine compound identified as a TSPO ligand. Indeed, PK11195, and in particular the *R*-enantiomer, remains until now as the prototypical TSPO ligand, exhibiting superior binding affinity than Ro5-4864 as well as a high selectivity toward several targets.[170,181,182] Moreover, it was rapidly revealed a higher abundance of isoquinolinecarboxamide binding sites compared to the benzodiazepine binding sites at the TSPO, which obviously highlights the former over the latter as TSPO ligands.[183] Despite the extended use of PK11195 in countless studies, a high lipophilicity and a low bioavailability have been reported, which limits the sensitivity of PK11195 for an accurate assessment of the TSPO.[184] In order to overcome the challenges associated to the use of PK11195 and in view of its high lipophilicity other isoquinolinecarboxamides, as PK14105 and PK11211, as well as other analogues as quinoline- and quinazolinecarboxamides with professed less lipophilicity were developed. Several of those analogues have shown not only a superior appropriateness regarding the lipophilicity aspect but also a higher affinity. Moreover, these substances share a low sensitivity

toward the rs6971 polymorphism, i.e. they do not exhibit different binding affinities in subjects with different genotype.[185–193]

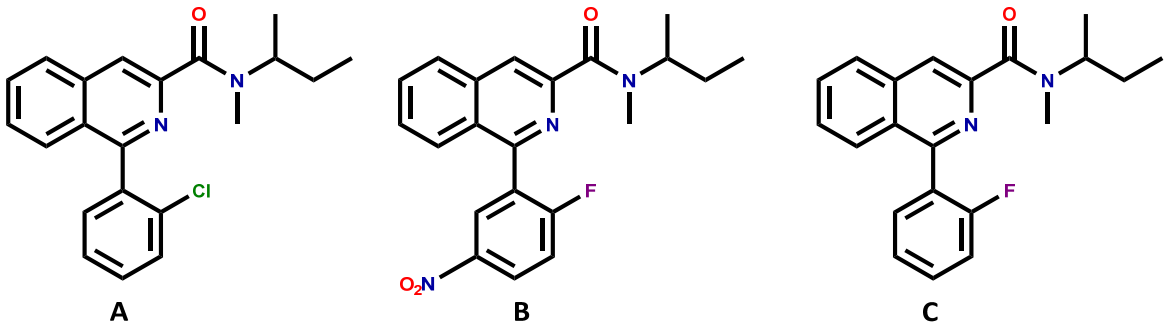

Figure 14. Isoquinolinecarboxamides as TSPO ligands: (A) PK11195, (B) PK14105 and (C) PK11211

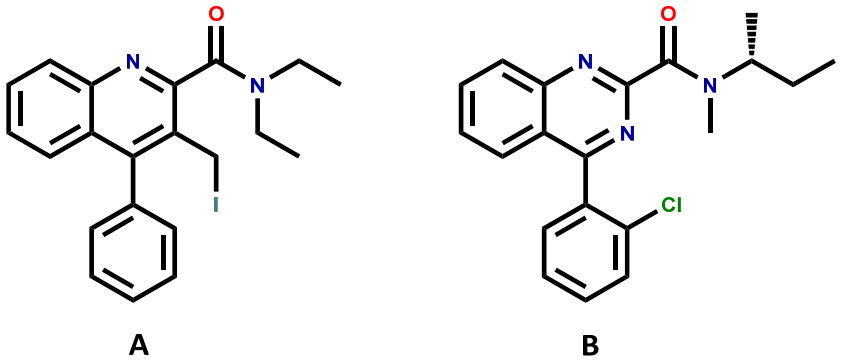

Figure 15. (A) N,N-Diethyl-3-iodomethyl-4-phenylquinoline-2-carboxamide, a quinolinecarboxamide and (B) (R)-ER-176, an isoquinoline carboxamide as TSPO ligands

2.1.4.2.3. PHENOXYACETAMIDES

Core ring opening of Ro5-4864 leads to a phenoxyacetamide structure, which resulted in a highly affine and selective motif to the TSPO. In fact, various ligands containing this moiety have been developed since its introduction in 1999.[194] A further development of other phenoxyacetamide-based ligands was mainly based on the development of radiopharmaceuticals to image TSPO (see also radiopharmaceuticals section below). In fact, the discovery of the rs6971 polymorphism effect on the binding affinity of TSPO ligands was first observed with the carbon-11 labeled phenoxyacetamide PBR28,[124] and soon after with other radiolabeled analogues.[195,196] A major breakthrough of this group of ligands was also supported by suggested interactions of some compounds, as DAA1097 and DAA1106, with additional TSPO binding sites, beyond the PK11195 binding site.[197] In this regard, the majority of phenoxyacetamide derivatives shows higher affinity

compared to PK11195. Likewise, lipophilicity and pharmacokinetics were improved through the development of different analogues.

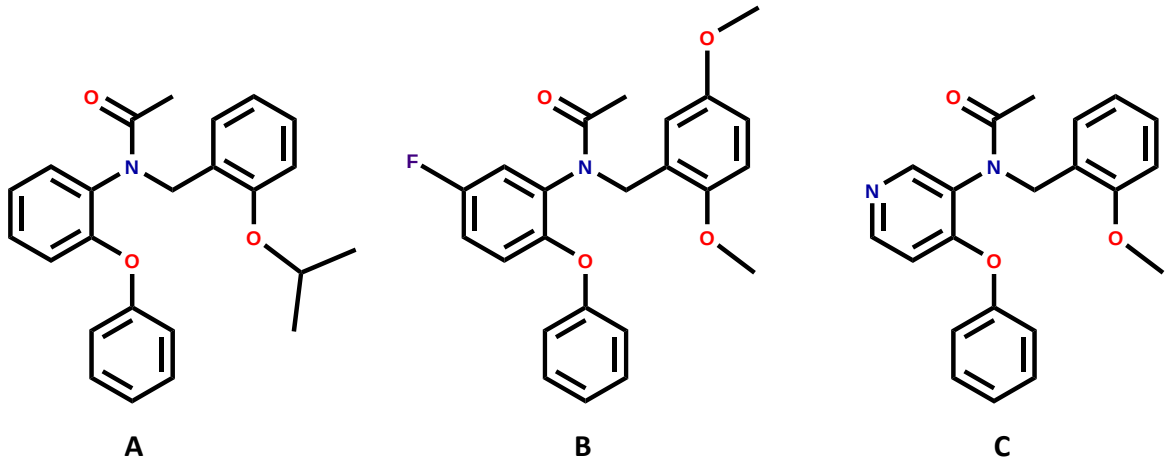

Figure 16. Phenoxyacetamides as TSPO ligands: (A) DAA1097; (B) DAA1106; (C) PBR28

2.1.4.2.4. IMIDAZOPYRIDINES, PYRAZOLOPYRIMIDINES AND INDOLEACETAMIDES

The imidazopyridine alpidem was first identified as a high affinity ligand for both CBR and TSPO.[198,199] Although its poor selectivity, and later discovered hepatotoxicity, limited its potential as a TSPO ligand; several studies based on alpidem molecular structure allowed the development of additional imidazopyridines. In this context, SAR examinations revealed the influence of several replacements to achieve higher TSPO selectivity, such as different alkyl chains on the acetamide moiety, different substituents in position 6 and 8 of the imidazopyridine ring as well as in *para* position to the phenyl ring at carbon atom 2 of the heterocycle system. [200–206] Those investigations uncovered the imidazopyridine compound CB34 as a highly affine and selective ligand for the TSPO.

Additional SAR analyses, exclusively targeting the imidazopyridine nucleus of alpidem, guided the synthesis of the pyrazolopyrimidines. These bioisosteres, and particularly the compound DPA-713, emerged as highly potent TSPO ligands.[207]

Furthermore, taking into account electronic considerations, it seemed convenient to research the affinity and selectivity of other alpidem derivatives bearing a carbon atom instead of a nitrogen one at the ring fusion position. This structural change pinpointed the indoleacetamide scaffold as a remarkable structure to yield relevant TSPO ligands, as FGIN-1-27. [208]

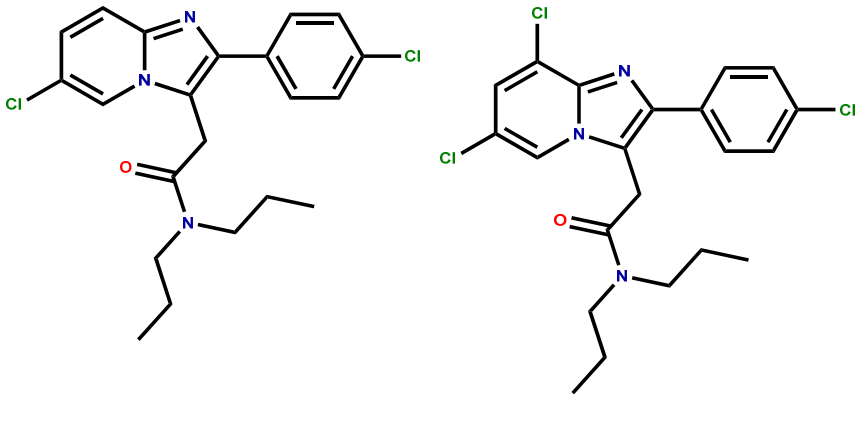

Figure 17. Imidazopyridines as TSPO ligands: (A) Alpidem; (B) CB-34

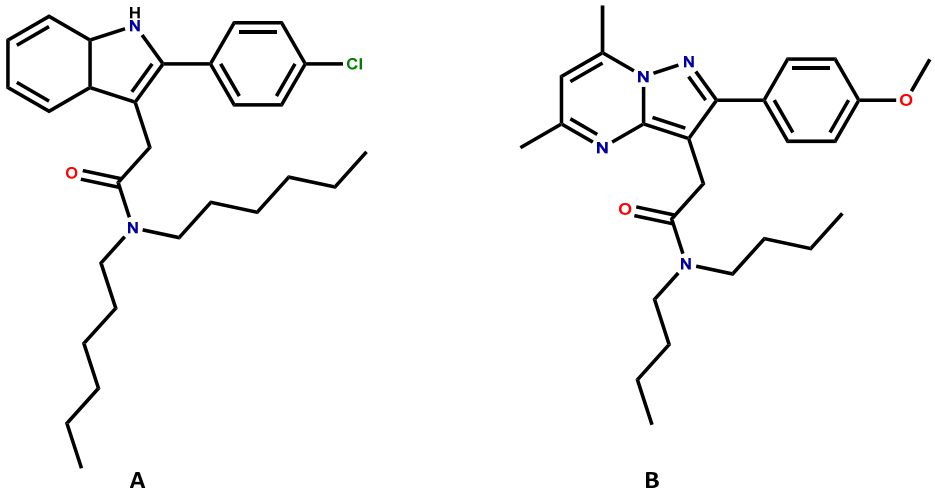

Figure 18. (A) FGIN-1-27 an indoleacetamide and (B) DPA-713 a pyrazolopyrimidine as TSPO ligands

2.1.4.3. TSPO PET RADIOPHARMACEUTICALS

The involvement of TSPO in several diseases offers an extraordinary characteristic to use it as a disease biomarker. As previously mentioned, different TSPO expression levels are found under normal and pathological conditions. Hence, the beauty on assessing such changes through PET imaging lies in assisting the diagnosis of such disorders. In particular, the clinical interest in TSPO PET imaging is the much diminished expression of TSPO in healthy brain compared to the increased expression levels found under neuroinflammation conditions and glioblastomas. For instance, a difference of 15-fold has been reported in glioblastomas cells. This difference is astonishing, if the high sensitivity of PET imaging is taken into account. Moreover, several studies have correlated the TSPO expression levels with severity and clinical outcome.[104,128,209–212]

Therefore, a great interest has been placed to develop suitable TSPO PET radiopharmaceuticals. In fact, many developed radiotracers have reached clinical stage and are used in investigations concerning TSPO-related diseases. Unsurprisingly, available TSPO PET radiopharmaceuticals are the radioactive counterparts of many of the non-radioactive ligands listed in the previous subsections and are classified regarding their pharmacokinetics and their sensitivity toward the rs6971 SNP: first-, second- and third-generation. The radiotracers presented below are only a small part of a large number of available PET radiopharmaceuticals.

Table 3: Summary of TSPO PET radiopharmaceuticals[213,214]

Common name	IUPAC name	Structure	Generation	Class	Status
(*R*)-[^{11}C]PK11195	(*R*)-[^{11}C]*N*-(sec-butyl)-1-(2-chlorophenyl)-*N*-methylisoquinoline-3-carboxamide	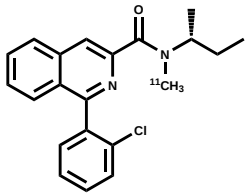	1st	Isoquinoline carboxamide	In clinical use (gold standard) poor signal to noise ratio.
[^{11}C]Ro5-4864	[^{11}C]7-chloro-5-(4-chlorophenyl)-1-methyl-1,3-dihydro-2*H*-benzo[e][1,4]diazepin-2-one	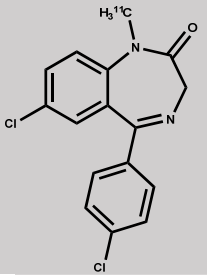	Not determined	Benzodiazepine	Clinical: poor in vivo binding.
[^{11}C]Diazepam	[^{11}C]7-chloro-1-methyl-5-phenyl-1,3-dihydro-2*H*-benzo[e][1,4]diazepin-2-one	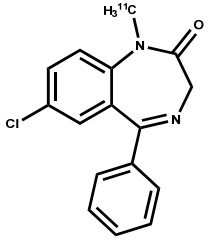	Not determined	Benzodiazepine	Preclinical: non-selective tracer, due to the affinity toward CBR.
[^{11}C]AC-5216	[^{11}C]*N*-benzyl-*N*-ethyl-2-(7-methyl-8-oxo-2-phenyl-7,8-dihydro-9*H*-purin-9-yl)acetamide	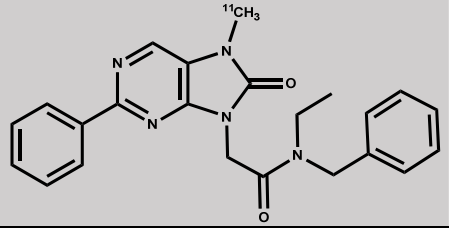	2nd	Dihydro-9*H*-purinacetamide	Clinical: promising ligand, although sensitive to rs6971 SNP.

[^{11}C]DAC	[^{11}C]*N*-benzyl-*N*-methyl-2-(7-methyl-8-oxo-2-phenyl-7,8-dihydro-9*H*-purin-9-yl)acetamide	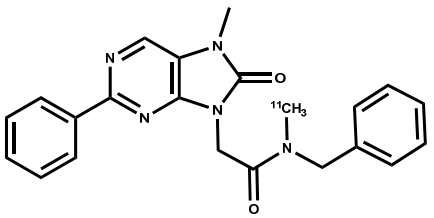	2nd	Dihydro-9*H*-purinacetamide	Preclinical: promising tracer, although sensitive to rs6971 SNP.
[^{11}C]DAA1106	[^{11}C]*N*-(5-fluoro-2-phenoxyphenyl)-*N*-(2-methoxybenzyl)acetamide	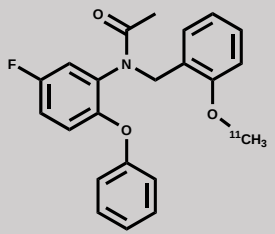	2nd	Phenoxy-acetamide	Clinical: replaced by other analogues. Sensitive to rs6971 SNP.
[^{18}F]FEDAA1106	*N*-(5-fluoro-2-phenoxyphenyl)-*N*-[^{18}F](2-(2-fluoroethoxy)-5-methoxybenzyl)acetamide	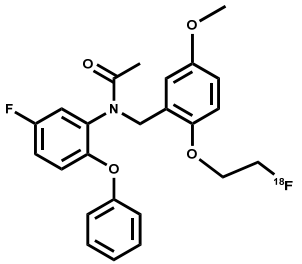	2nd	Phenoxy-acetamide	Clinical: promising tracer, although sensitive to rs6971 SNP.
[^{11}C]PBR28	[^{11}C]*N*-(2-methoxybenzyl)-*N*-(4-phenoxypyridin-3-yl)acetamide	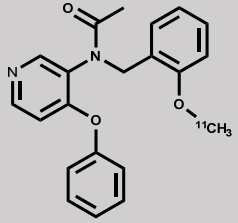	2nd	Phenoxy-acetamide	Clinical: promising tracer, although sensitive to rs6971 SNP.

[^{18}F]FEPPA	[^{18}F]*N*-(2-(2-fluoroethoxy)benzyl)-*N*-(4-phenoxypyridin-3-yl)acetamide	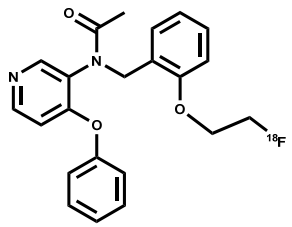	2nd	Phenoxy-acetamide	Clinical: promising tracer, although sensitive to rs6971 SNP.
[^{11}C]DAA1097	[2-*isopropyl*-^{11}C]*N*-(2-phenoxyphenyl)-*N*-(2-((propan-2-yl-2-oxy)benzyl)acetamide	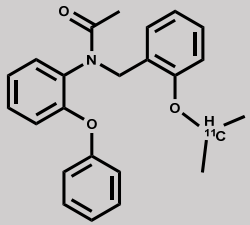	2nd	Phenoxy-acetamide	Preclinical: replaced by other analogues, sensitive to rs6971 SNP.
[^{11}C]PBR01	[*methyl*-^{11}C]2-((*N*-(2-phenoxyphenyl)acetamido)methyl) benzoate	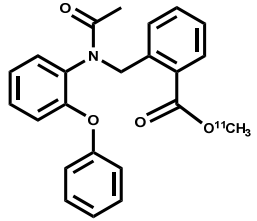	2nd	Phenoxy-acetamide	Preclinical: replaced by other analogues, sensitive to rs6971 SNP.
[^{18}F]PBR06	[^{18}F]*N*-(2,5-dimethoxybenzyl)-2-fluoro-*N*-(2-phenoxyphenyl)acetamide	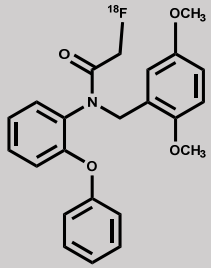	2nd	Phenoxyacetamide	Clinical: promising tracer, although sensitive to rs6971 SNP.

[^{18}F]fluoro-methyl-PBR28	[^{18}F]*N*-(2-(fluoromethoxy)benzyl)-*N*-(4-phenoxypyridin-3-yl)acetamide	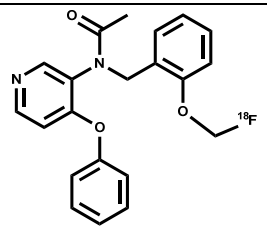	2nd	Phenoxyacetamide	Preclinical: promising tracer, although sensitive to rs6971 SNP.
[^{18}F]6-fluoroPBR28	[^{18}F]*N*-(6-fluoro-4-phenoxypyridin-3-yl)-*N*-(2-methoxybenzyl)acetamide	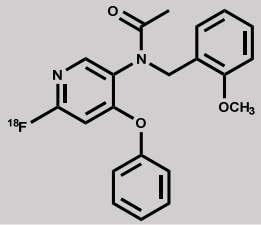	2nd	Phenoxyacetamide	Preclinical: promising tracer, although sensitive to rs6971 SNP.
[^{11}C]Vinpocetine	[*ethyl*-^{11}C](41S,13aS)-13a-ethyl-2,3,41,5,6,13a-hexahydro-1H-indolo[3,2,1-de]pyrido[3,2,1-ij][1,5]naphthyridine-12-carboxylate	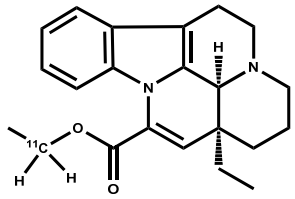	2nd	Vinca alkaloid	Clinical: promising tracer, although sensitive to rs6971 SNP.
[^{11}C]DPA-713	[*methoxy*-^{11}C]N,N-dibutyl-2-(2-(4-(methoxy-11C)phenyl)-5,7-dimethylpyrazolo[1,5-a]pyrimidin-3-yl)acetamide	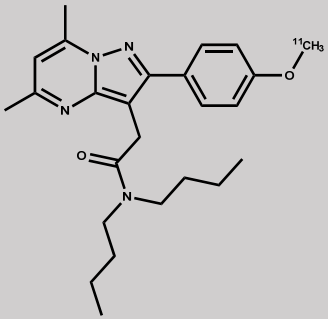	2nd	Pyrazolo-pyrimidine	Clinical: promising tracer, although sensitive to rs6971 SNP.

[^{18}F]DPA-714	[^{18}F]*N,N*-dibutyl-2-(2-(4-(2-fluoroethoxy)phenyl)-5,7-dimethylpyrazolo[1,5-a]pyrimidin-3-yl)acetamide	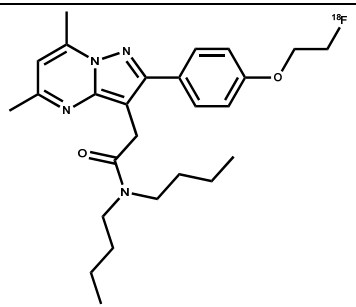	2nd	Pyrazolo-pyrimidine	Clinical: promising tracer, although sensitive to rs6971 SNP.
[^{18}F]VUIIS1008	[^{18}F]*N,N*-dibutyl-2-(5,7-diethyl-2-(4-(2-fluoroethoxy)phenyl)pyrazolo[1,5-a]pyrimidin-3-yl)acetamide	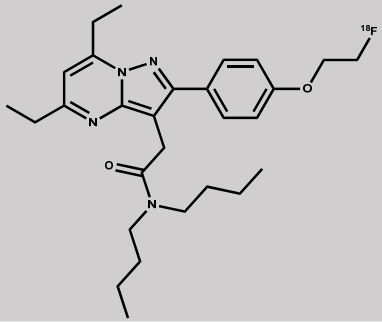	2nd	Pyrazolo-pyrimidine	Preclinical: promising tracer, although sensitive to rs6971 SNP.
[^{11}C]CLINME	[*methyl*-^{11}C]2-(6-chloro-2-(4-iodophenyl)imidazo[1,2-a]pyridin-3-yl)-*N*-ethyl-*N*-methylacetamide	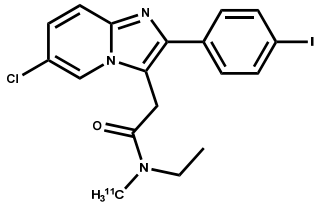	2nd	Imidazopyridine	Preclinical: promising tracer, although sensitive to rs6971 SNP.
[^{11}C]CB148	[^{11}C]2-(6,8-dichloro-2-(4-chlorophenyl)imidazo[1,2-a]pyridin-3-yl)-*N*-methyl-*N*-phenylacetamide	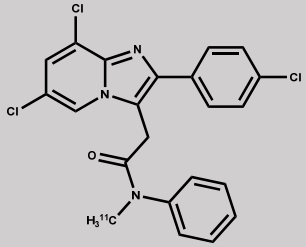	2nd	Imidazopyridine	Preclinical: promising tracer, although sensitive to rs6971 SNP.

[^{18}F]CB251	[^{18}F]2-(6,8-dichloro-2-(4-(2-fluoroethyl)phenyl)imidazo[1,2-a]pyridin-3-yl)-N,N-dipropylacetamide	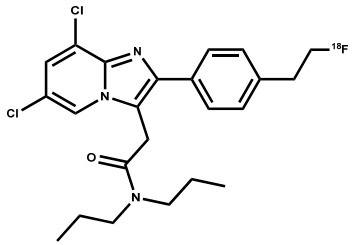	2nd	Imidazopyridine	Preclinical: promising tracer, although sensitive to rs6971 SNP.
[^{18}F]PBR111	[^{18}F]2-(6-chloro-2-(4-(3-fluoropropyl)phenyl)imidazo[1,2-a]pyridin-3-yl)-N,N-diethylacetamide	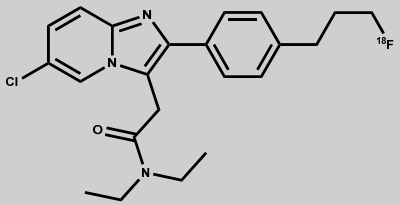	2nd	Imidazopyridine	Clinical: promising tracer, although sensitive to rs6971 SNP.
[^{18}F]PBR102	[^{18}F] 2-(6-chloro-2-(4-(2-fluoroethyl)phenyl)imidazo[1,2-a]pyridin-3-yl)-N,N-diethylacetamide	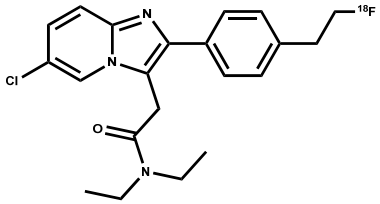	2nd	Imidazopyridine	Preclinical: promising tracer, although sensitive to rs6971 SNP.
[^{11}C]MBMP	[*methoxy*-^{11}C]2-(5-(4-methoxyphenyl)-2-oxobenzo[d]oxazol-3(2*H*)-yl)-N-methyl-*N*-phenylacetamide	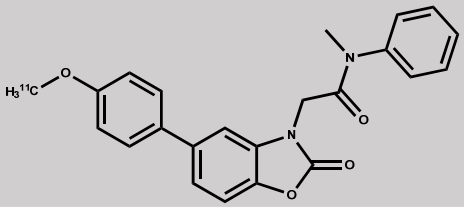	Not determined	Acetamido-benzoxazolone	Preclinical: poor stability.

[^{18}F]FEBMP	[^{18}F]2-(5-(4-(2-fluoroethoxy)phenyl)-2-oxobenzo[d]oxazol-3(2H)-yl)-*N*-methyl-*N*-phenylacetamide	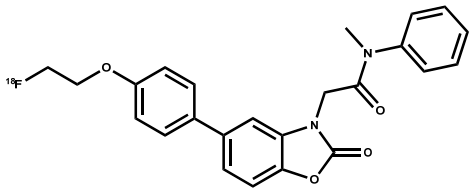	3rd	Acetamido-benzoxazolone	Preclinical: poor stability, slow brain kinetics.
[^{18}F]FEBMP	[^{18}F]2-(5-(6-fluoropyridin-3-yl)-2-oxobenzo[d]-oxazol-3(2H)-yl)-*N*-methyl-*N*-phenylacetamide	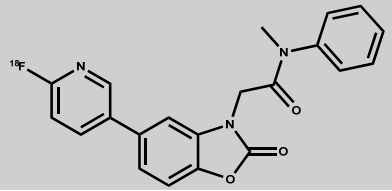	Not determined	Acetamido-benzoxazolone	Preclinical: promising tracer.
[^{18}F]GE-180	[^{18}F](4*S*)-*N,N*-diethyl-9-(2-fluoroethyl)-5-methoxy-2,3,4,4a,9,9a-hexahydro-1*H*-carbazole-4-carboxamide	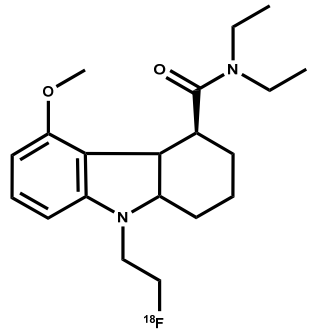	2nd: with really low sensitivity toward rs6971 SNP	Tetrahydro-carbazole	Clinical: promising tracer, although some sensitivity toward rs6971 SNP has been reported
(*R*)-[^{11}C]ER-176	(*R*)-[^{11}C]*N*-(sec-butyl)-4-(2-chlorophenyl)-*N*-methylquinazoline-2-carboxamide	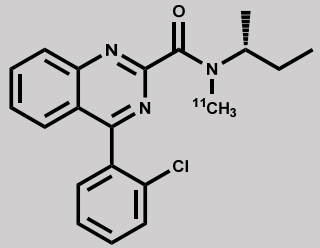	3rd	Quinazoline-carboxamide	Clinical: very promising compound. Unexpected *in vivo* sensitivity toward rs6971 SNP.

2.1.4.3.1. (*R*)-[^{11}C]PK11195 - FIRST GENERATION

Although initially labeled as a racemic mixture, (*R*)-[^{11}C]PK11195 was later identified as the active enantiomer responsible for TSPO binding.[182] Since then, it has been described as the gold standard TSPO PET tracer, exhibiting high affinity and selectivity. However, (*R*)-[^{11}C]PK11195 have been highly discredited as TSPO PET tracer due to its low brain availability and high non-specific binding, presumably attributed to the high lipophilicity, which ultimately leads to a poor signal to noise ratio. Moreover, although not discussed in the literature, the radiosynthesis of (*R*)-[^{11}C]PK11195 is known to be problematic.[215] Nevertheless, the initial observations made by Fujita *et al*.[124] regarding the apparent no-binding of a TSPO PET tracer, which was later explained on the basis of the rs6971 SNP, have not been perceived when using (*R*)-[^{11}C]PK11195. In this regard, (*R*)-[^{11}C]PK11195 offers very similar binding to all genotype groups which represents a clear advantage for clinical studies. Thus, it has been used as a TSPO PET radiopharmaceutical in an ample number of investigations.[216–219]

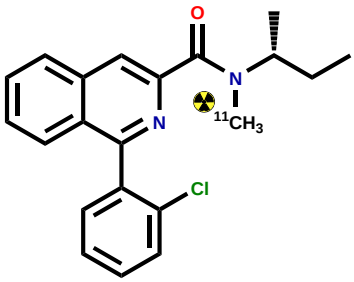

Figure 19. (R)-[^{11}C]PK11195

2.1.4.3.2. [^{11}C]PBR28 AND [^{18}]FEPPA - SECOND GENERATION

Both compounds are aryloxyanilide (phenoxyacetamide) analogues derived from DAA1106 and only differ in the radiolabeled residue: -methoxy vs. fluoroethoxy, as shown in figure 18. [^{11}C]PBR28 was first developed in the United States of America by Briard *et al*.[220] as an alternative for the disadvantages resulted from using (*R*)-[^{11}C]PK11195, while [^{18}]FEPPA was developed in Canada by Wilson *et al*.[221] Both tracers are highly affine and selective ligands, with [^{18}]FEPPA being a more potent one. Their radiosyntheses proceed straightforwardly, with the benefit of the more advantageous radionuclide in the case of [^{18}]FEPPA, due to the longer half-life. Metabolic stability as well as specific binding and *in vivo* pharmacokinetics are excellent in both situations, allowing the *in vivo* visualization and quantification of TSPO. Indeed, [^{11}C]PBR28 and [^{18}]FEPPA have been used in clinical settings in a tremendous way, including for comparison purposes between different PET radiopharmaceuticals. Unfortunately, a large dependence on the *in vivo* affinity

regarding the rs6971 SNP is notorious in PET studies. Certainly, as previously mentioned, effects of the rs6971 SNP were first observed by using [^{11}C]PBR28 and then confirmed for other compounds (imidazopyridine, indoleacetamides, pyrazolopyrimidines and others) including [^{18}]FEPPA. A common practice, following the use of second generation TSPO PET radiopharmaceuticals, is the exclusion of LAB from such studies, since low or no uptake of the radiotracers is observed. Indeed, the binding affinity of such ligands must be considered to properly quantify the radiotracer uptake and therefore interpret the data correctly.[222]

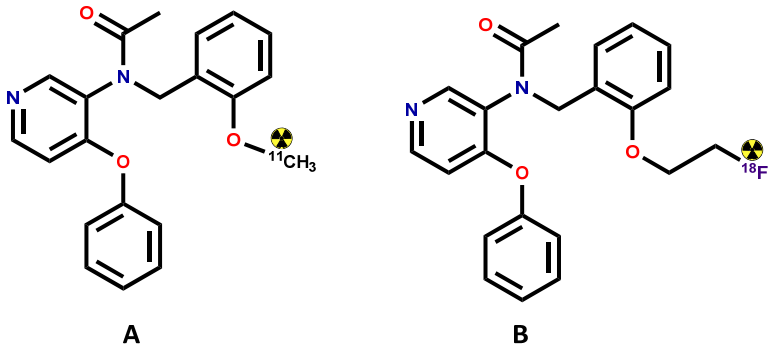

Figure 20. Aryloxyanilides PET tracers: (A) [^{11}C]PBR28 and (B) [^{18}F]FEPPA

2.1.4.3.3. (*R*)-[^{11}C]ER-176 - THIRD GENERATION

Recently, a close analogue of the (*R*)-[^{11}C]PK11195 was developed to overcome the problems associated with first and second generation TSPO PET radiopharmaceuticals. By using a clever strategy based on replacing the isoquinolinic aromatic ring of (*R*)-[^{11}C]PK11195 by a quinazolinic ring, the resulting quinazolinecarboxamide (*R*)-[^{11}C]ER-176 retains the high affinity and selectivity toward the TSPO, exhibited by (*R*)-[^{11}C]PK11195 and reduces the well discussed lipophilicity of (*R*)-[^{11}C]PK11195, through the incorporation of an additional nitrogen atom.[223] Moreover, this approach also preserves the low sensitivity of (*R*)-[^{11}C]PK11195 toward the rs6971 SNP in the newly developed radiotracer. Although posterior studies revealed an unexpected *in vivo* sensitivity of [^{11}C]ER-176 in humans, which differs from initial *in vitro* evaluations, (*R*)-[^{11}C]ER-176 seems to have enough sensitivity to image all three genotypes.[224,225]

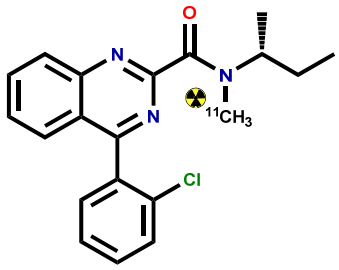

Figure 21. (R)-[^{11}C]ER-176

CHAPTER II
AIM

The involvement of TSPO in a plenitude of pathologies has favored the use of TSPO PET imaging as a leading diagnostic technique. Despite the attractive properties of TSPO as a biomarker and PET as very sensitive technique to follow changes in TSPO expression, TSPO PET imaging is still difficult due to the lack of adequate tracers. The challenges associated with the use of second generation TSPO PET radiopharmaceuticals and the disadvantages of (*R*)-[^{11}C]PK11195 urge the use of novel radiotracers with adequate pharmacokinetics and pharmacodynamics properties, in particular regarding the rs6971 SNP. Moreover, improving methods for the radiosyntheses of already existing TSPO PET radiopharmaceuticals, as well as gaining information for further characterization of the TSPO seems reasonable.

Therefore, the following objectives were envisioned for the elaboration of this doctoral thesis:

1. This doctoral thesis intended the synthesis of novel TSPO PET radiopharmaceuticals. Hence, the design of such ligands based on already known leading structures, as well as the planning of chemical routes to achieve references substances and radiolabeling precursors constituted the **first aim** for this work.
2. Since the molar activity of PET radiopharmaceuticals represents an important parameter in PET radiochemistry to avoid target saturation and undesired pharmacological effects, the **second aim** of this doctoral thesis lied in a comprehensive analysis of factors determining the outcome of this parameter in ^{11}C-tracers.
3. The **third aim** was the radiolabeling of the novel and already existing TSPO PET tracers. In this regard, the automated radiosynthesis of [^{18}F]FEPPA was time-optimized, whereas ideal reaction conditions were examined and subsequently automatized for the radiosyntheses of the newly developed radiotracers (*R*)-[^{11}C]Me@NEBIQUINIDE and (*R*)-[^{18}F]NEBIFQUINIDE.
4. Preclinical evaluation of the TSPO (radio)ligands represented the **fourth aim**. *In vitro* assessment included genotyping of different subjects, binding affinity investigations using competitive assays as well as autoradiographical methods, metabolic stability, lipophilicity and plasma protein binding. *In vivo* evaluation of novel TSPO PET radiopharmaceuticals comprised *in vivo* stability, biodistribution analysis and µPET imaging.

CHAPTER III
PUBLICATIONS

1. [^{18}F]FEPPA: IMPROVED AUTOMATED RADIOSYNTHESIS, BINDING AFFINITY PROFILE AND PRELIMINARY IN VITRO EVALUATION IN COLORECTAL CANCER

Berroterán-Infante N, Balber T, Fürlinger P, Bergmann M, Lanzenberger R, Hacker M, Mitterhauser M, Wadsak W.

ACS Med. Chem. Lett. 2018, 9, 177-181.

I developed the new radiosynthetical method and established it at the Medical University of Vienna. I performed all the radiosyntheses, the binding affinity and genotyping experiments, and contributed to the autoradiography and kinetic binding assays. Additionally, I carried out the data analysis and wrote the manuscript.

ACS Medicinal Chemistry Letters

Letter

Cite This: ACS Med. Chem. Lett. 2018, 9, 177−181

[^{18}F]FEPPA: Improved Automated Radiosynthesis, Binding Affinity, and Preliminary in Vitro Evaluation in Colorectal Cancer

Neydher Berroterán-Infante,[†,‡] Theresa Balber,[†,§] Petra Fürlinger,[†] Michael Bergmann,[∥] Rupert Lanzenberger,[⊥] Marcus Hacker,[†] Markus Mitterhauser,[†,§,#] and Wolfgang Wadsak*[,†,‡,▽]

[†]Division of Nuclear Medicine, Department of Biomedical Imaging and Image-guided Therapy, Medical University of Vienna, Vienna A-1090, Austria

[‡]Department of Inorganic Chemistry, Faculty of Chemistry, University of Vienna, Vienna A-1090, Austria

[§]Department of Pharmaceutical Technology, Faculty of Life Sciences, University of Vienna, Vienna A-1090, Austria

[∥]Surgical Research Laboratories, Department of Surgery, Medical University of Vienna, Vienna A-1090, Austria

[⊥]Department of Psychiatry and Psychotherapy, Medical University of Vienna, Vienna A-1090, Austria

[#]Ludwig Boltzmann Institute Applied Diagnostics, Vienna A-1090, Austria

[▽]Center for Biomarker Research in Medicine, CBmed GmbH, Graz A-8010, Austria

Supporting Information

ABSTRACT: The overexpression of the translocator protein (TSPO) has been amply reported for a variety of conditions, including neurodegenerative disorders, heart failure, and cancer. Thus, TSPO has been proposed as an excellent imaging biomarker, allowing, in this manner, to obtain an accurate diagnosis and to follow disease progression and therapy response. Accordingly, several radioligands have been developed to accomplish this purpose. In this work, we selected [^{18}F]FEPPA, as one of the clinical established tracers, and assessed its in vitro performance in colorectal cancer. Moreover, we setup an improved radiosynthesis method and assessed the in vitro binding affinity of the nonradioactive ligand toward the human TSPO. Our results show an excellent to moderate affinity, in the subnanomolar and nanomolar range, as well as the suitability of [^{18}F]FEPPA as an imaging agent for the TSPO in colorectal cancer.

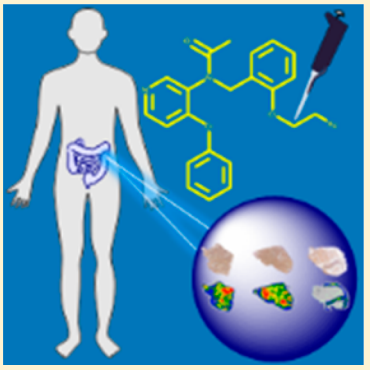

KEYWORDS: *TSPO, FEPPA, radiosynthesis, affinity, autoradiography, colorectal cancer*

The translocator protein (TSPO), previously known as the peripheral benzodiazepine receptor (PBR),[1] has emerged in the last years as an attractive target for diagnosis and treatment of several pathological conditions.[2−5] Its up-regulation has been especially reported in activated microglia of neuroinflammatory disorders such as multiple sclerosis, Parkinson's, Alzheimer's, and Huntington's diseases, as well in some type of cancers, including breast, colon, and glioblastomas.[6−8] Therefore, a variety of ligands have been developed for in vivo visualization, for instance, with positron emission tomography (PET), of the TSPO; including isoquinoline carboxamides, phenoxyphenyl acetamides, pyridazinoindoles, and others.[9−11] The isoquinoline carboxamide [^{11}C](*R*)-PK11195 ((*R*)-1-(2-chlorophenyl)-*N*-[^{11}C]methyl-*N*-(1-methylpropyl)-isoquinoline is one of the first and, until now, the most used ligand for TSPO imaging using PET.[12] However, a high nonspecific binding, due to its high lipophilicity, which ultimately leads to a low signal-to-noise ratio and a problematic radiosynthesis, have been a major drawback for the use of this tracer.[13] To overcome these issues, a second generation of TSPO PET ligands with improved affinity and lipophilicity has arisen over the years. Nevertheless, a single nucleotide polymorphism (rs6971) in the *TSPO* gene (Ala147Thr substitution) has hampered the development of such tracers because all these ligands exhibit different binding affinities toward human TSPO from subjects with different genotype. In this regard, three groups have been reported: high-affinity binders (HAB, homozygotes Ala147Ala), mixed-affinity binders (MAB, heterozygotes Ala147Thr), and low-affinity binders (LAB, homozygotes Thr147Thr).[14] Some of those PET tracers are still widely used, although it is common to exclude LAB from clinical studies since low or no uptake of the tracers is observed. The second disadvantage is the interpretation of the data since the difference in the binding affinity must be considered, causing difficulties on the appropriate quantification of the tracer uptake.[15] Among these tracers, the phenoxyphenyl acetamide [^{18}F]FEPPA (*N*-acetyl-*N*-(2-[^{18}F]-fluoroethoxyben-zyl)-2-phenoxy-5-pyridinamine) shows out-

Received: September 6, 2017
Accepted: February 21, 2018
Published: February 21, 2018

DOI: 10.1021/acsmedchemlett.7b00367
ACS Med. Chem. Lett. 2018, 9, 177−181

standing properties regarding affinity, stability, lipophilicity, and radiosynthesis.[16]

[^{18}F]FEPPA has been already used in several preclinical and clinical settings;[17,18] however, only the in vivo effect of the polymorphism has been reported.[19] To the best of our knowledge, no binding affinity profile, in terms of the inhibitory constant (K_i) toward the human TSPO, nor the evaluation in colorectal cancer have been performed. Hence, starting from the already reported automated radiosynthesis of [^{18}F]FEPPA, we first established an improved and reliable method for the tracer production and subsequently assessed the in vitro binding affinity profile regarding the polymorphism rs6971. Furthermore, since the overexpression of TSPO in colorectal cancer is amply described,[20−22] autoradiography experiments with [^{18}F]FEPPA, using human colorectal cancer and healthy colon tissues, as well as real-time kinetic experiments utilizing the colorectal cancer cell line HT-29 were conducted.

The TSPO-PET tracer [^{18}F]FEPPA was synthesized according to previously published procedures,[16,17] with some minor modifications as outlined in Scheme 1.

Scheme 1. Radiosynthesis of [^{18}F]FEPPA

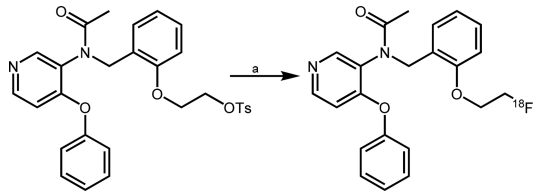

[a] [^{18}F]KF/K222$_{(dry)}$, ACN, 90 °C, 10 min. Purification: preparative HPLC, SPE.

Briefly, aliphatic nucleophilic substitution was automated in a nuclear interface synthesizer between dried [^{18}F]KF/K222 and the tosylate precursor (2-(2-((*N*-(4-phenoxypyridin-3-yl)-acetamido)methyl)phenoxy)ethyl-4-methylbenzenesulfonate). After the reaction time, the crude product was transferred to a semipreparative HPLC system, and the fraction containing the product ($t_R \approx 5$ min) was collected. The solvents were removed by SPE and the product reformulated in ethanol, sodium chloride, and phosphate-buffered saline. The (radio)chemical purity was assessed by means of analytical HPLC and TLC. All other quality control tests (visual inspection, pH, osmolality, radionuclide purity, K222, and residual solvents contents) were performed using regular procedures implemented in the PET Centre of the Vienna General Hospital. Complete details of the radiosynthesis and the quality control can be found in the Supporting Information.

The purity of [^{18}F]FEPPA always exceeded 99%, and 4.2 ± 0.8 GBq of the product was afforded, representing a nondecay corrected radiochemical yield of 38 ± 3% (based on [^{18}F]F$^-$ at EOB) with a molar radioactivity of 241 ± 13 GBq·μmol^{-1} (n = 15) in a total synthesis time of 30 min. The quality control was always in accordance to the guidelines of the European Pharmacopeia.[23]

With this new set of conditions, the main outcome was the time reduction of the purification step of the previously published method[17] from 23 to 5 min, which drastically reduces the total synthesis time and affords a small increase in the radiochemical yield.

The affinity toward human TSPO of nonradioactive FEPPA (cold standard, *N*-acetyl-*N*-(2-fluoroethoxybenzyl)-2-phenoxy-5-pyridinamine) was determined in a competitive binding assay, as reported elsewhere,[24] using [^{3}H]PK11195 and a TSPO-expressing platelet membrane, from individuals previously genotyped regarding the polymorphism rs6971 and subsequently identified as HAB, MAB, and LAB (approved by the Ethics Committee of the Medical University of Vienna).

Inhibition constants in the subnanomolar and nanomolar range were obtained for FEPPA (Figure 1). K_i (HAB) = (0.5 ± 0.1) nM, K_i (MAB) = (0.6 ± 0.1), (37 ± 5) nM, and K_i (LAB) = (37 ± 5) nM. As expected, the in vitro binding affinity of FEPPA shows the typical behavior of the second generation of TSPO ligands regarding the TSPO polymorphism rs6971. Moreover, the inhibition constant for LAB shows a moderate binding affinity, which is 70 times lower than for HAB.

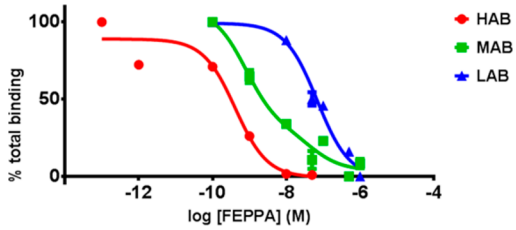

Figure 1. Competition binding assays of nonradioactive FEPPA in HAB, MAB, and LAB using [^{3}H]PK11195 and a TSPO-expressing platelet membrane.

Although the up-regulation of TSPO in colorectal cancer is well-known, little research has been performed regarding TSPO imaging in this disease. TSPO-PET research has been more focused on neuroinflammation disorders and glioblastomas, as a consequence of the significant role of TSPO in glial activation.[25] Therefore, we deemed to evaluate the appropriateness of [^{18}F]FEPPA as an imaging agent for colorectal cancer in vitro.

First, the expression of the TSPO in colon cancer and healthy mucosa (both obtained directly after tumorectomy with full informed consent from one patient bearing colon cancer and approved by the Ethics Committee of the Medical University of Vienna), as well as in HT-29 cells, was examined by Western blot. The presence of TSPO (above the 15 kDa mark, predicted molecular weight of 18 kDa) in HT-29 cells,[26] as well as in the tumor lysate, was confirmed (Figure 2). Interestingly, TSPO was not detected in healthy tissue lysate, although a moderate expression of TSPO in colon has been reported.[27]

Moreover, in order to ensure the suitability of [^{18}F]FEPPA for further evaluations and thus taking into account the polymorphism rs6971, we also conducted a PCR-based genotype assay on the cell line and the patient tissue, which distinguished the HT-29 cells and the patient bearing the tumor within the HAB group.

Accordingly, real-time binding experiments, to assess the tracer kinetics, were planned using HT-29 cells and LigandTracer Technology.[28] In a typical real-time binding experiment, the equilibrium was reached after 20 min, and in pursuance of displacing bonded [^{18}F]FEPPA and thereby demonstrating specific binding to the TSPO, solutions of unlabeled FEPPA, PBR28, or PK11195 were used.

As shown in Figure 3, specific binding was observed for [^{18}F]FEPPA since the signal decreased after the addition of displacement solutions, i.e., the radioactivity bound to the cells was reduced in all cases. Unlabeled FEPPA achieved a (50.2 ±

DOI: 10.1021/acsmedchemlett.7b00367
ACS Med. Chem. Lett. 2018, 9, 177−181

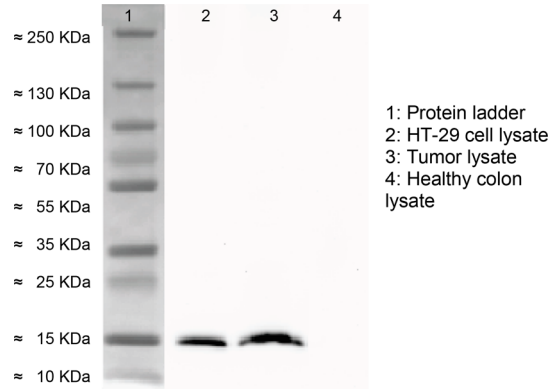

Figure 2. Protein bands of ~15 kDa (theoretical molecular weight of TSPO, 18 kDa) were detected via Western blot with a specific anti-TSPO antibody in HT-29 cell and colorectal cancer tissue lysates, however not in healthy colon tissue lysate.

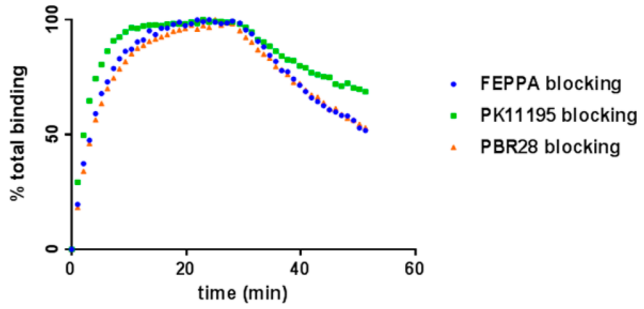

Figure 3. Normalized overlay real-time binding kinetics of [^{18}F]FEPPA in HT-29 cells using LigandTracer Technology. Association of [^{18}F]FEPPA was performed for 30 min, and subsequently, displacing agents (FEPPA, PK11195, or PBR28) were applied. Displacement was examined for additional 30 min.

11.2)% displacement, whereas PBR28 and PK11195 reached (48.2 ± 6.7)% and (32.2 ± 10.6)% displacement, respectively. In a similar set of experiments, only DMSO was used as vehicle control.

With these results in hand, we proceeded to perform autoradiography experiments with tumor and healthy colon tissues. Tissue slices were incubated with approximately 50 kBq per slice of freshly prepared [^{18}F]FEPPA for 1 h. Analogously, blocking experiments were accomplished by coincubating the slices with radiotracer and unlabeled FEPPA or PBR28 (10 μM). After exposing the slices to a phosphor screen, radiotracer uptake was analyzed, and the amount of compound (fmol·mm^{-2}) accumulated in each slice was determined.

Figure 4 shows a significantly higher (three to six times) uptake of the tracer in malignant tissue (baseline red) in comparison with healthy colon tissue (baseline blue), which is in accordance with the already mentioned upregulation of TSPO in colorectal cancer. Moreover, competitive blocking with unlabeled TSPO ligands was significantly observed in all cases.

Furthermore, an immunohistochemical investigation was realized in order to match the TSPO localization and the radiotracer uptake. For this purpose, an anti-TSPO antibody staining was performed using vicinal slices to those used for autoradiography. In Figure 5, a representative staining shows a stronger staining for tumor tissue in comparison to healthy colon. Accordingly, in the autoradiography counterpart, a higher uptake of the tracer in this tissue is observed as well,

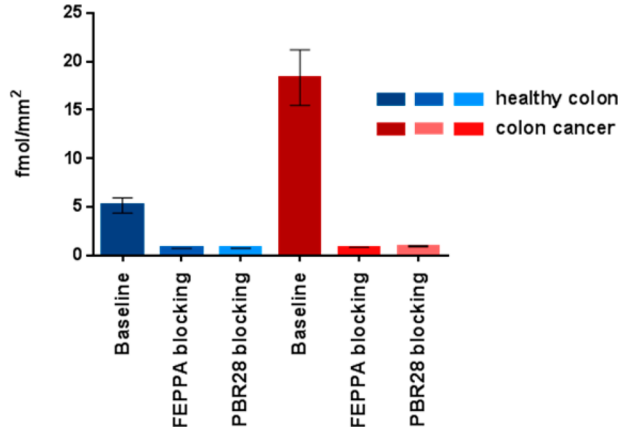

Figure 4. [^{18}F]FEPPA uptake (fmol·mm^{-2}) in healthy colon compared to colon cancer tissue slices. Specific uptake was confirmed by blocking experiments with cold FEPPA and PBR28.

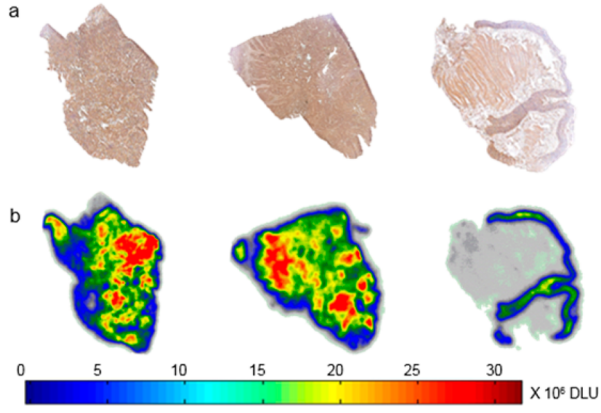

Figure 5. [^{18}F]FEPPA accumulation observed in autoradiography corresponded to TSPO expression in the vicinal slices as revealed by immunohistochemistry. (a) TSPO IHC. (b) [^{18}F]FEPPA autoradiography. Left/middle, colorectal tumor tissues. Right, healthy colon tissue. DLU, digital light units.

demonstrating once more the high sensitivity of [^{18}F]FEPPA for TSPO recognition in colon cancer.

PET imaging of TSPO in colonic diseases seems to be challenging mainly due to the basal expression of this protein in healthy tissues and in less grade due to the availability of several probes with different pharmacological properties, which difficult the comparison of the data. Several reports[29,30] suggest poor specificity of TSPO PET tracers for evaluation of such conditions; meanwhile, some investigations[31−33] support the use of TSPO in inflammatory bowel diseases and colorectal cancer. In view of the high level of specificity demonstrated by our in vitro results and also the relatively low uptake of [^{18}]FEPPA in vivo in healthy colon and stomach as demonstrated elsewhere,[17] we propose [^{18}F]FEPPA as a potentially appropriate probe to be further in vivo evaluated as a TSPO PET tracer to evaluate this malignancy.

In summary, we have developed a faster and still reliable method for the radiosynthesis of [^{18}F]FEPPA with higher radiochemical yields. Moreover, FEPPA showed similar behavior in vitro as other TSPO ligands regarding the polymorphism rs6971; although its affinity in human platelets is very potent in all identified genotypes. Additionally, we present here the first evaluation, to the best of our knowledge,

DOI: 10.1021/acsmedchemlett.7b00367
ACS Med. Chem. Lett. 2018, 9, 177−181

in colorectal cancer. Our results point toward the suitability of [^{18}F]FEPPA for imaging colorectal cancer with PET.

■ ASSOCIATED CONTENT

Supporting Information

The Supporting Information is available free of charge on the ACS Publications website at DOI: 10.1021/acsmedchemlett.7b00367.

Detailed information about radiosynthetic procedures, binding affinity assays, including genotyping and membrane preparation, cell culture, real-time kinetics, autoradiography, immunohistochemistry, Western blot, and additional results (PDF)

■ AUTHOR INFORMATION

Corresponding Author

*Tel: +43-1-40400-55330. E-mail: wolfgang.wadsak@meduniwien.ac.at.

ORCID

Wolfgang Wadsak: 0000-0003-4479-8053

Author Contributions

N.B.-I. performed all the radiosyntheses, the binding affinity experiments and genotyping assays, and writing of the paper and contributed to autoradiography and real-time binding assays. T.B. performed all immunohistochemistry, Western blot, autoradiography, and real-time binding experiments. P.F. contributed to autoradiography, immunohistochemistry, Western blot, and real-time binding experiments. M.B. performed the tumorectomy and contributed to the design of the study. M.H. and R.L. designed parts of the research and proofread the manuscript. M.M. conceived and supervised the in vitro experiments and proofread the manuscript. W.W. conceived and supervised the radiosyntheses and proofread the manuscript. All authors have given approval to the final version of the manuscript.

Notes

The authors declare no competing financial interest.

■ ACKNOWLEDGMENTS

This scientific project was performed with the support of the Medical Imaging Cluster of the Medical University of Vienna. The authors want to thank Friedrich Girschele for collecting the blood samples for membrane preparation and Stefan Schmitl for his collaboration in the binding affinity profile experiments.

■ ABBREVIATIONS

TSPO, translocator protein; PBR, peripheral benzodiazepine receptor; HAB, high-affinity binders 5; MAB, mixed-affinity binders; LAB, low-affinity binders; t_R, retention time; ACN, acetonitrile; HPLC, high performance liquid chromatography; SPE, solid phase extraction; TLC, thin layer chromatography; EOB, end of bombardment; PCR, polymerase chain reaction; IHC, immunohistochemistry; DLU, digital light units

■ REFERENCES

(1) Papadopoulos, V.; Baraldi, M.; Guilarte, T. R.; Knudsen, T. B.; Lacapère, J.-J.; Lindemann, P.; Norenberg, M. D.; Nutt, D.; Weizman, A.; Zhang, M.-R.; Gavish, M. Translocator Protein (18 kDa): New Nomenclature for the Peripheral-Type Benzodiazepine Receptor Based on Its Structure and Molecular Function. *Trends Pharmacol. Sci.* **2006**, *27*, 402−409.

(2) Kim, T.; Pae, A. N. Translocator Protein (TSPO) Ligands for the Diagnosis or Treatment of Neurodegenerative Diseases: A Patent Review (2010−2015; Part 1). *Expert Opin. Ther. Pat.* **2016**, *26*, 1325−1351.

(3) Kim, T.; Pae, A. N. Translocator Protein (TSPO) Ligands for the Diagnosis or Treatment of Neurodegenerative Diseases: A Patent Review (2010 − 2015; Part 2). *Expert Opin. Ther. Pat.* **2016**, *26*, 1353−1366.

(4) Rupprecht, R.; Papadopoulos, V.; Rammes, G.; Baghai, T. C.; Fan, J.; Akula, N.; Groyer, G.; Adams, D.; Schumacher, M. Translocator Protein (18 KDa) (TSPO) as a Therapeutic Target for Neurological and Psychiatric Disorders. *Nat. Rev. Drug Discovery* **2010**, *9*, 971−988.

(5) Mukherjee, S.; Das, S. K. Translocator Protein (TSPO) in Breast Cancer. *Curr. Mol. Med.* **2012**, *12*, 443−457.

(6) Dupont, A.-C.; Largeau, B.; Santiago Ribeiro, M. J.; Guilloteau, D.; Tronel, C.; Arlicot, N. Translocator Protein-18 KDa (TSPO) Positron Emission Tomography (PET) Imaging and Its Clinical Impact in Neurodegenerative Diseases. *Int. J. Mol. Sci.* **2017**, *18*, 785.

(7) Roncaroli, F.; Su, Z.; Herholz, K.; Gerhard, A.; Turkheimer, F. E. TSPO Expression in Brain Tumours: Is TSPO a Target for Brain Tumour Imaging? *Clin. Transl. Imaging* **2016**, *4*, 145−156.

(8) Mendonça-Torres, M. C.; Roberts, S. S. The Translocator Protein (TSPO) Ligand PK11195 Induces Apoptosis and Cell Cycle Arrest and Sensitizes to Chemotherapy Treatment in Pre- and Post-Relapse Neuroblastoma Cell Lines. *Cancer Biol. Ther.* **2013**, *14*, 319−326.

(9) Camsonne, R.; Crouzel, C.; Comar, D.; Mazière, M.; Prenant, C.; Sastre, J.; Moulin, M.; Syrota, A. Synthesis of N-(11C) Methyl, N-(Methyl-1 Propyl), (Chloro-2 Phenyl)-1 Isoquinoleine Carboxamide-3 (PK 11195): A New Ligand for Peripheral Benzodiazepine Receptors. *J. Labelled Compd. Radiopharm.* **1984**, *21*, 985−991.

(10) Briard, E.; Zoghbi, S. S.; Imaizumi, M.; Gourley, J. P.; Shetty, H. U.; Hong, J.; Cropley, V.; Fujita, M.; Innis, R. B.; Pike, V. W. Synthesis and Evaluation in Monkey of Two Sensitive 11C-Labeled Aryloxyanilide Ligands for Imaging Brain Peripheral Benzodiazepine Receptors In Vivo. *J. Med. Chem.* **2008**, *51*, 17−30.

(11) Cheung, Y.-Y.; Nickels, M. L.; Tang, D.; Buck, J. R.; Manning, H. C. Facile Synthesis of SSR180575 and Discovery of 7-Chloro-N,N,5-Trimethyl-4-Oxo-3(6-[18F]Fluoropyridin-2-Yl)-3,5-Dihydro-4H-Pyridazino[4,5-b]Indole-1-Acetamide, a Potent Pyridazinoindole Ligand for PET Imaging of TSPO in Cancer. *Bioorg. Med. Chem. Lett.* **2014**, *24*, 4466−4471.

(12) Guilarte, T. R. 13.31 - Molecular Imaging: The New Frontier in Neurotoxicology A2. In *Comprehensive Toxicology*, 2nd ed.; McQueen, C. A., Ed.; Elsevier: Oxford, 2010; pp 537−551.

(13) Boutin, H.; Prenant, C.; Maroy, R.; Galea, J.; Greenhalgh, A. D.; Smigova, A.; Cawthorne, C.; Julyan, P.; Wilkinson, S. M.; Banister, S. D.; Brown, G.; Herholz, K.; Kassiou, M.; Rothwell, N. J. [18F]DPA-714: Direct Comparison with [11C]PK11195 in a Model of Cerebral Ischemia in Rats. *PLoS One* **2013**, *8*, e56441.

(14) Owen, D. R.; Yeo, A. J.; Gunn, R. N.; Song, K.; Wadsworth, G.; Lewis, A.; Rhodes, C.; Pulford, D. J.; Bennacef, I.; Parker, C. A.; StJean, P. L.; Cardon, L. R.; Mooser, V. E.; Matthews, P. M.; Rabiner, E. A.; Rubio, J. P. An 18-KDa Translocator Protein (TSPO) Polymorphism Explains Differences in Binding Affinity of the PET Radioligand PBR28. *J. Cereb. Blood Flow Metab.* **2012**, *32*, 1−5.

(15) Owen, D. R.; Guo, Q.; Rabiner, E. A.; Gunn, R. N. The Impact of the Rs6971 Polymorphism in TSPO for Quantification and Study Design. *Clin. Transl. Imaging* **2015**, *3*, 417−422.

(16) Wilson, A. A.; Garcia, A.; Parkes, J.; McCormick, P.; Stephenson, K. A.; Houle, S.; Vasdev, N. Radiosynthesis and Initial Evaluation of [18F]-FEPPA for PET Imaging of Peripheral Benzodiazepine Receptors. *Nucl. Med. Biol.* **2008**, *35*, 305−314.

(17) Vasdev, N.; Green, D. E.; Vines, D. C.; McLarty, K.; McCormick, P. N.; Moran, M. D.; Houle, S.; Wilson, A. A.; Reilly, R. M. Positron-Emission Tomography Imaging of the TSPO with [18F]FEPPA in a Preclinical Breast Cancer Model. *Cancer Biother.Radiopharm.* **2013**, *28*, 254−259.

DOI: 10.1021/acsmedchemlett.7b00367
ACS Med. Chem. Lett. 2018, 9, 177−181

(18) Setiawan, E.; Wilson, A. A.; Mizrahi, R.; et al. Role of Translocator Protein Density, a Marker of Neuroinflammation, in the Brain during Major Depressive Episodes. *JAMA Psychiatry* **2015**, *72*, 268−275.
(19) Mizrahi, R.; Rusjan, P. M.; Kennedy, J.; Pollock, B.; Mulsant, B.; Suridjan, I.; De Luca, V.; Wilson, A. A.; Houle, S. Translocator Protein (18 KDa) Polymorphism (Rs6971) Explains in-Vivo Brain Binding Affinity of the PET Radioligand [18F]-FEPPA. *J. Cereb. Blood Flow Metab.* **2012**, *32*, 968−972.
(20) Katz, Y.; Eitan, A.; Amiri, Z.; Gavish, M. Dramatic Increase in Peripheral Benzodiazepine Binding Sites in Human Colonic Adenocarcinoma as Compared to Normal Colon. *Eur. J. Pharmacol.* **1988**, *148*, 483−484.
(21) Katz, Y.; Eitan, A.; Gavish, M. Increase in Peripheral Benzodiazepine Binding Sites in Colonic Adenocarcinoma. *Oncology* **2004**, *47*, 139−142.
(22) Han, Z.; Slack, R. S.; Li, W.; Papadopoulos, V. Expression of Peripheral Benzodiazepine Receptor (PBR) in Human Tumors: Relationship to Breast, Colorectal, and Prostate Tumor Progression. *J. Recept. Signal Transduction Res.* **2003**, *23*, 225−238.
(23) Council of Europe. *Europäisches Arzneibuch (European Pharmacopoeia)*, 8th ed; Verlag Österreich GmbH: Vienna, 2008; pp 995.
(24) Owen, D. R. J.; Gunn, R. N.; Rabiner, E. A.; Bennacef, I.; Fujita, M.; Kreisl, W. C.; Innis, R. B.; Pike, V. W.; Reynolds, R.; Matthews, P. M.; Parker, C. A. Mixed-Affinity Binding in Humans with 18-KDa Translocator Protein Ligands. *J. Nucl. Med.* **2011**, *52*, 24−32.
(25) Tronel, C.; Largeau, B.; Santiago Ribeiro, M. J.; Guilloteau, D.; Dupont, A.-C.; Arlicot, N. Molecular Targets for PET Imaging of Activated Microglia: The Current Situation and Future Expectations. *Int. J. Mol. Sci.* **2017**, *18*, 802.
(26) Ostuni, M.; Ducroc, R.; Péranzi, G.; Tonon, M.-C.; Papadopoulos, V.; Lacapère, J.-J. Translocator Protein (18 kDa) Ligand PK 11195 Induces Transient Mitochondrial Ca2+ Release Leading to Transepithelial Cl- Secretion in HT-29 Human Colon Cancer Cells. *Biology of the Cell* **2007**, *99*, 639−647.
(27) Tang, D.; Li, J.; Buck, J. R.; Tantawy, M. N.; Xia, Y.; Harp, J. M.; Nickels, M. L.; Meiler, J.; Manning, H. C. Evaluation of TSPO PET Ligands [18F]VUIIS1009A and [18F]VUIIS1009B: Tracers for Cancer Imaging. *Mol. Imaging Biol.* **2017**, *19*, 578−588.
(28) Zeilinger, M.; Pichler, F.; Nics, L.; Wadsak, W.; Spreitzer, H.; Hacker, M.; Mitterhauser, M. New Approaches for the Reliable in Vitro Assessment of Binding Affinity Based on High-Resolution Real-Time Data Acquisition of Radioligand-Receptor Binding Kinetics. *EJNMMI Res.* **2017**, *7*, 22.
(29) Takano, A.; Gulyás, B.; Varrone, A.; Karlsson, P.; Sjoholm, N.; Larsson, S.; Jonsson, C.; Odh, R.; Sparks, R.; Al Tawil, N.; Hoffmann, A.; Zimmermann, T.; Thiele, A.; Halldin, C. Biodistribution and Radiation Dosimetry of the 18 KDa Translocator Protein (TSPO) Radioligand [18F]FEDAA1106: A Human Whole-Body PET Study. *Eur. J. Nucl. Med. Mol. Imaging* **2011**, *38* (11), 2058−2065.
(30) Wu, C.; Yue, X.; Lang, L.; Kiesewetter, D. O.; Li, F.; Zhu, Z.; Niu, G.; Chen, X. Longitudinal PET Imaging of Muscular Inflammation Using 18F-DPA-714 and 18F-Alfatide II and Differentiation with Tumors. *Theranostics* **2014**, *4* (5), 546−555.
(31) Bernards, N.; Pottier, G.; Thézé, B.; Dollé, F.; Boisgard, R. In Vivo Evaluation of Inflammatory Bowel Disease with the Aid of MPET and the Translocator Protein 18 KDa Radioligand [18F]DPA-714. *Mol. Imaging Biol.* **2015**, *17* (1), 67−75.
(32) Kurtys, E.; Doorduin, J.; Eisel, U. L. M.; Dierckx, R. A. J. O.; de Vries, E. F. J. Evaluating [11C]PBR28 PET for Monitoring Gut and Brain Inflammation in a Rat Model of Chemically Induced Colitis. *Mol. Imaging Biol.* **2017**, *19* (1), 68−76.
(33) Powell, A. E.; Vlacich, G.; Zhao, Z.-Y.; McKinley, E. T.; Washington, M. K.; Manning, H. C.; Coffey, R. J. Inducible Loss of One Apc Allele in Lrig1-Expressing Progenitor Cells Results in Multiple Distal Colonic Tumors with Features of Familial Adenomatous Polyposis. *Am. J. Physiol. - Gastrointest. Liver Physiol.* **2014**, *307* (1), G16−G23.

DOI: 10.1021/acsmedchemlett.7b00367
ACS Med. Chem. Lett. 2018, 9, 177−181

2. MOLAR ACTIVITY - THE KEYSTONE IN ^{11}C-RADIOCHEMISTRY: AN EXPLORATIVE STUDY USING THE GAS PHASE METHOD

Pichler V, Zenz T, Philippe C, Vraka, C, Berroterán-Infante N, Pfaff S, Nics L, Ozenil M, Langer O, Willeit M, Traub-WeidingerT, Lanzenberger R, Mitterhauser M, Hacker M, Wadsak W.
Nuc. Med. Biol., 2018, 67, 21-26.

I performed several radiosyntheses and contributed to the analysis and interpretation of the data. I was also involved in the revision of the manuscript.

Nuclear Medicine and Biology 67 (2018) 21–26

Contents lists available at ScienceDirect

Nuclear Medicine and Biology

journal homepage: www.elsevier.com/locate/nucmedbio

Molar activity – The keystone in ^{11}C-radiochemistry: An explorative study using the gas phase method

Verena Pichler [a,*], Thomas Zenz [a], Cécile Philippe [a], Chrysoula Vraka [a], Neydher Berrotéran-Infante [a], Sarah Pfaff [a], Lukas Nics [a], Marius Ozenil [a], Oliver Langer [a,b,c], Matthäus Willeit [d], Tatjana Traub-Weidinger [a], Rupert Lanzenberger [d], Markus Mitterhauser [a,e], Marcus Hacker [a], Wolfgang Wadsak [a,f]

[a] Department of Biomedical Imaging and Image-guided Therapy, Division of Nuclear Medicine, Medical University of Vienna, Vienna, Austria
[b] Department of Clinical Pharmacology, Medical University of Vienna, Vienna, Austria
[c] Center for Health and Bioresources, AIT Austrian Institute of Technology GmbH, Seibersdorf, Austria
[d] Department of Psychiatry and Psychotherapy, Division of General Psychiatry, Medical University of Vienna, Vienna, Austria
[e] Ludwig-Boltzmann-Institute Applied Diagnostics, Vienna, Austria
[f] CBmed GmbH - Center for Biomarker Research in Medicine, Graz, Austria

ARTICLE INFO

Article history:
Received 10 July 2018
Received in revised form 28 September 2018
Accepted 29 September 2018
Available online xxxx

Keywords:
Molar activity
Specific activity
Carbon-11
Automated synthesis

ABSTRACT

Introduction: Radiochemists/radiopharmacists, involved in the preparation of radiopharmaceuticals are regularly confronted with the requirement of continuous high quality productions in their day-to-day business. One of these requirements is high specific or molar activity of the radiotracer in order to avoid *e.g.* receptor saturation and pharmacological or even toxic effects of the applied tracer for positron emission tomography. In the case of ^{11}C-labeled radiotracers, the reasons for low molar activity are manifold and often the search for potential ^{12}C-contaminations is time-consuming.
Methods: In this study, diverse ^{12}C-contaminations were analyzed and quantified, which occurred during >450 syntheses of six PET tracers using [^{11}C]CO_2 or [^{11}C]CH_3I generated *via* the gas phase method in a commercially available synthesizer. Additionally, non-radioactive syntheses were performed in order to identify the origins of carbon-12.
Results: The manifold contributions to low molar activity can be attributed to three main categories, namely technical parameters (*e.g.* quality of target gases, reagents or tubings), inter/intralaboratory parameters (*e.g.* maintenance interval, burden of the module, *etc.*) and interoperator parameters (*e.g.* handling of the module).
Conclusion: Our study provides a better understanding of different factors contributing to the overall carbon load of a synthesis module, which facilitates maintenance of high molar activity of carbon-11-labeled radiopharmaceuticals.

1. Introduction

^{11}C-labeled radiotracers for application in positron emission tomography (PET) play an important role in neuroimaging, especially for *in vivo* analysis of receptor expression and disease-induced alterations thereof in the brain. The concept of molar activity is especially relevant for potential receptor occupancy and saturation, as well as to avoid undesired pharmacological effects. In small-animal PET measurement, it is *e.g.* stated that the receptor saturation should be below 5%, and reasonably, an exceptionally high molar activity is necessary [1]. As a result, the radioactivity as well as the moles of the substance are determined for these PET-tracers and their ratio is called the molar activity. Just recently, Coenen et al. started a movement for standardization of radiopharmaceutical nomenclature und definitions. Accordingly, the term molar activity (A_m) is used for 'the measured radioactivity per mole of compound measured in Bq/mol or GBq/μmol'. Besides, the measured activity per gram of compound in Bq/g or GBq/g is designated as specific activity (A_S) [2].

It is obvious, that time is an important factor in radiochemistry, as the molar activity is continuously decreasing over time due to radioactive decay. Time has a higher impact on short-lived radionuclides (such as carbon-11) compared to longer-lived ones (like fluorine-18). Furthermore, ^{11}C-chemistry displays another characteristic making the molar activity even more crucial compared to productions of PET tracers with a different radiolabel. Most ^{11}C-tracer productions start with [^{11}C]CO_2 and, unfortunately, the non-radioactive contaminant CO_2 is ubiquitous in surrounding air, whereas it is rather unlikely that *e.g.* cyclotron produced fluorine-18 is, besides other sources, contaminated with high amounts of naturally occurring fluorine-19 *per se*.

* Corresponding author at: Waehringer Guertel 18-20, 1090 Vienna, Austria.
E-mail address: verena.pichler@meduniwien.ac.at (V. Pichler).

https://doi.org/10.1016/j.nucmedbio.2018.09.003
0969-8051/

Carbon-11, a cyclotron generated nuclide, is produced either by irradiation of N_2/O_2 or N_2/H_2 gas mixtures. In most cases, the generated [^{11}C]CO_2 (or [^{11}C]CH_4) is further processed to receive the most important synthon [^{11}C]CH_3I. Reasonably, the molar activity for syntheses starting from [^{11}C]CH_4 is generally higher than for those starting from [^{11}C]CO_2 [3]. The processing of [^{11}C]CO_2 to [^{11}C]CH_3I is performed either *via* the 'wet' method with $LiAlH_4$ and HI, or *via* a gas phase reaction using H_2 and I_2. Potential carbon-12 sources were extensively discussed for the 'wet' method [4,5] as well as for the single pass I_2 method [6]. However, less information is available for the synthesis of [^{11}C]CH_3I through the gas phase iodination reaction of commercially available modules such as GE TRACERlab FX C [7] or Synthra MeIplus. This fact is astonishing considering that most of ^{11}C-syntheses are performed during routine production or clinical trials, and the production has to be performed on a weekly or even daily base. Therefore, a constant aim is to keep the molar activity high and predictable. Every inexplicable decrease is the fear of a radiochemist specialized on ^{11}C-tracer preparation and also of technicians involved.

The aim of our investigations was the identification and evaluation of potential carbon-11 sources within the [^{11}C]CH_3I production unit of the GE TRACERlab FX C Pro. These investigations were based on six ^{11}C-labeled PET tracers, which were produced on a weekly to nearly daily base within our facility over the course of 1.5 years. Due to the clinical demand for high radiochemical yields, often 2–3 applications have to be possible with one radiochemical production. Hence, all syntheses were performed using the [^{11}C]CO_2 target. Additionally, we established a protocol to minimize potential risks for poor/decreased molar activities as well as to optimize the maintenance interval for the equipment in order to guarantee high and reproducible quality within our daily routine production of 2–3 ^{11}C-tracer preparations per day on the same synthesizer.

2. Experimental

2.1. Material and reagents

All chemicals and solvents were obtained from commercial sources with analytical grade and used without further purification. Iodine (sublimated grade for analysis; ACS, Pharm.Eur.) was purchased from Merck (Darmstadt, Germany; product number: 1.04761.0100). The nickel catalyst (Shimalilte Ni reduced, 80/100 mesh) was purchased from Shimadzu (Kyoto, Japan) and was mixed with a molecular sieve (4 Å, 80/100 mesh, purchased from Grace, Columbia, USA). The [^{11}C]CH_3I trap consisted of Porapak Q (50–80 mesh, Waters, Vienna, Austria). Silver triflate impregnated carbon was prepared by dissolving 1 g of silver trifluoromethanesulfonate (Sigma Aldrich, Vienna, Austria) in 20 mL acetonitrile (for DNA synthesis, ≤10 ppm H_2O, Merck, Darmstadt, Germany). To this solution, 3 g of Graphpac-GC (80/100 mesh, Alltech, Deerfield, Illinois, USA) was added and the suspension was stirred in the dark for about 30 min. The solvent was removed under reduced pressure and the obtained powder was further dried in the dark for 2 h (rotary evaporator). The three ascarite II traps (ascarite®, approx. 20–30 mesh, Sigma Aldrich, Vienna, Austria) were used to avoid contaminations with moisture within the methyl iodide production unit.

2.2. General method for the in-target [^{11}C]CO_2 production and delivery to the hot cell

[^{11}C]CO_2 was produced by means of a GE PETtrace 860 cyclotron (General Electric Healthcare, Uppsala, Sweden) and a GE [^{11}C]CO_2 high pressure target *via* the ^{14}N(p,α)^{11}C reaction by a high purity gas mixture of N_2 6.0 and 1% O_2 5.5 (Air Liquide, Vienna, Austria). Alphagaz™ 2 helium 6.0 (≥99.9999%, Air Liquide, Vienna Austria) and Alphagaz™ 2 hydrogen 6.0 (99.9999%, Air Liquide, Vienna Austria) was used as inert gas and reduction reagent, respectively. The target consisted of an aluminium alloy and target foils made of Havar (alloy of cobalt). Depending on the experimental schedules irradiation times and beam currents were varied. However, standard settings were an irradiation time of 30 min and beam current of 65 μA yielding approximately 120 GBq of [^{11}C]CO_2. Moreover, delivery time from target to the Hot Cells/TRACERlab FX C Pro synthesizer was 4 min, including an automatic, additional refill/delivery cycle to assure complete emptying of the target. Subsequently, the delivered [^{11}C]CO_2 was trapped on a molecular sieve at room temperature and either released by heating to 400 °C for Grignard reactions ([^{11}C]-(+)-PHNO, [*carbonyl*-^{11}C] WAY100635) or further processed according to Larsen et al. [8] by means of the in-built methylation process in the GE TRACERlab FX C Pro synthesizer (General Electric Healthcare, Uppsala, Sweden) (Fig. 1).

2.3. Maintenance interval for the GE TRACERlab FX C Pro

The maintenance interval recommended by the commercial supplier of the GE TRACERlab FX C Pro for the most common tasks was adapted to serve the needs of our facility. The adaptions are listed in Table 1.

2.4. Preparation of the GE TRACERlab FX C Pro for [^{11}C]CH_3I based productions

Module preparation started with flushing of the "[^{11}C]CH_3I preparation unit" with helium (20–50 mL/min) (*via* V24, V25, V29, VA, V15, V9, V17, V16) as well as flushing the lines to the reactor (*via* VB, V7 and V8) for around 1 min. Subsequently, the same pathways were checked for leakages with a helium flow of 100 mL/min. In order to guarantee tightness the flow had to decrease below 4 mL/min.

Heating to 200 °C under a continuous helium flow (50 mL/min) of the [^{11}C]CH_3I trap – and, if applied, the silver triflate column – was performed to remove traces of chemical contaminants from the previous synthesis. During that time, V1–V3 were washed two to three times with water followed by acetone *via* the reactor as well as the load and inject positions of the HPLC valve. The reactor as well as the lines from V1–V3 and the line to the injection valve were dried with a continuous helium stream *via* V18. V4, V5 and V6 were washed with either ethanol or water *via* the product vial or V11 and V12. The HPLC lines were washed with HPLC solvent *via* V14 into the waste bottle as well as into the bulb. The bulb line was washed with water and HPLC solvent *via* V11 and V12.

All lines associated with the reactor were afterwards checked for presence of solvent residues, which have to be fully removed.

15 min before the start of the synthesis, a pre-run sequence was started, consisting of a heating step of the [^{11}C]CO_2 trap ([^{11}C]CH_4 production unit) to 400 °C with a helium stream of 50 mL/min *via* V27 (2 min). The [^{11}C]CO_2 trap was pre-flushed with hydrogen gas (3 min) still at 400 °C and subsequently cooled down to at least 50 °C. Cooling of the CH_4 trap to −78 °C with liquid nitrogen was started before release of radioactivity from the target.

2.5. General procedure for the conversion of [^{11}C]CO_2 to [^{11}C]CH_3I

[^{11}C]CO_2 was trapped at room temperature on a molecular sieve including nickel as catalyst. Afterwards, the [^{11}C]CO_2 trap was flushed with helium (50 mL/min) and subsequently filled with hydrogen (120 mL/min). V27 was closed prior to V25 and the [^{11}C]CO_2 trap was heated to 400 °C. The formed [^{11}C]CH_4 was released with a helium stream *via* V10 (exhaust exit) and trapped on the [^{11}C]CH_4 trap, which was cooled to −75 °C. V10 was closed, V9 opened and [^{11}C]CH_4 was released into the circulation unit by heating the trap slowly to 80 °C. Inside the circulation unit, the [^{11}C]CH_4 was converted to [^{11}C]CH_3I, whereas an optimal result was achieved by around 10–11 circulations within approximately 3 min. Around 10% of the radioactivity were usually trapped on the [^{11}C]CH_3I trap within the first circulation and approximately 35–50% of the starting activity were trapped as [^{11}C]CH_3I after the circulation process had ended. Afterwards V16 (exhaust exit) was

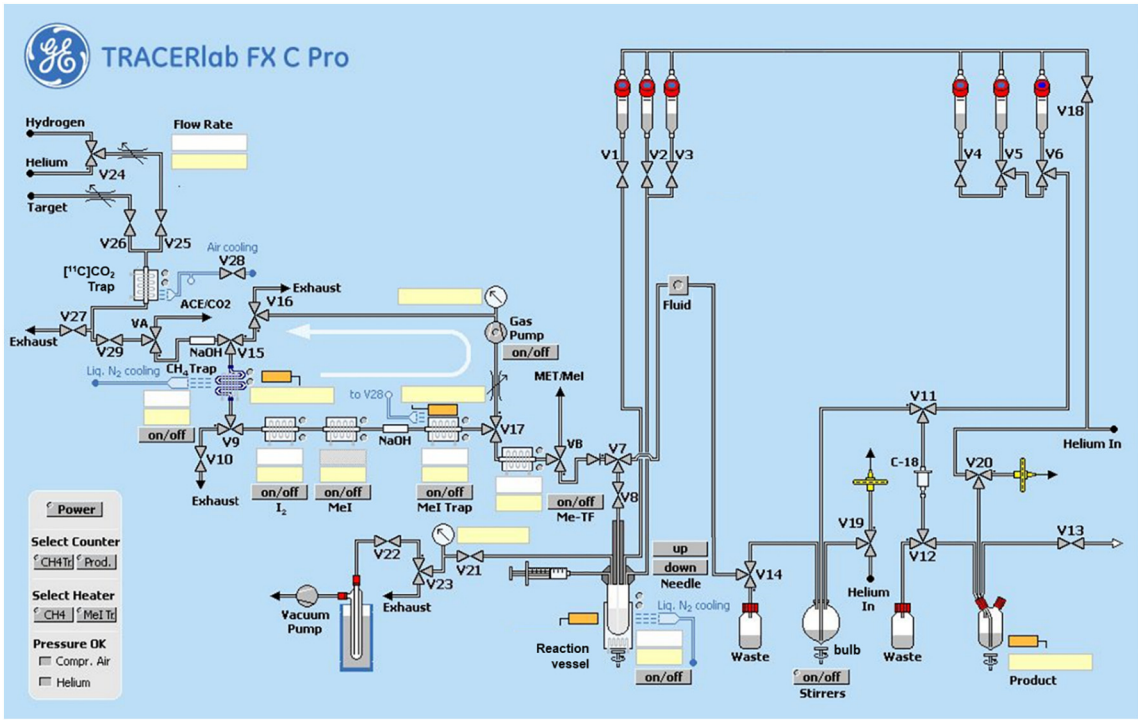

Fig. 1. Scheme of the [^{11}C]CH_3I production unit of the GE TRACERlab FX C Pro.

opened and the trap was heated to 90 °C to remove potential byproducts. Afterwards V16 was closed, the trap was further heated to 190 °C and the radioactivity was released into the reaction vessel *via* V17, VB (silver triflate column or bypass), V7 and V8. Around 75–90% of [^{11}C]CH_3I/[^{11}C]CH_3OTf was trapped inside of the reactor, highly depending on the employed trapping solvent.

2.6. General procedure for [^{11}C]CO_2 release for Grignard reactions

In general, Grignard reactions can be directly conducted using [^{11}C]CO_2 from the cyclotron. In our facility, firstly [^{11}C]CO_2 was trapped on the [^{11}C]CO_2 trap prior to the actual reaction start, in order to allow a controlled [^{11}C]CO_2 release into a plastic reaction loop, previously coated with the respective Grignard reagent. In advance, the cyclotron target was flushed twice with target gas.

Accordingly, the [^{11}C]CO_2 trap was heated for 5–10 min to 400 °C with a helium stream (20 mL/min) *via* V27 to remove potential CO_2 traces and subsequently cooled to room temperature. It is important to avoid accidental flushing of this trap with hydrogen gas to prevent the chemical reaction to [^{11}C]CH_4. Then, the cyclotron produced [^{11}C]CO_2 was trapped. The trap was successively heated to 300 °C with a gentle helium stream (5–10 mL/min) *via* the exhaust valve V27. When a temperature of 300 °C was reached, it was further increased to 400 °C, while V27 was closed, and V29 and VA were opened for release of the activity to the loop.

2.7. Tracer production

Four tracers were produced by methylation reactions, using [^{11}C]CH_3I or [^{11}C]CH_3OTf, respectively, and were therefore dependent on a good performance of the [^{11}C]CH_3I production unit: [^{11}C]DASB (n = 158), [^{11}C]harmine (n = 109), [^{11}C]PIB (n = 61) and [^{11}C]erlotinib (n = 49). The synthesis procedures were performed as described previously [9–12]. Two tracers were produced *via* Grignard reactions. A detailed description of the synthesis of [^{11}C]-(+)-PHNO (n = 49) as well as [*carbonyl*-^{11}C]WAY100635 (n = 31) was published elsewhere [13,14]. For analysis of the trapping efficiency of different solvents, additional data from productions for [^{11}C]methionine (n = 14) [15] and [^{11}C]tariquidar (n = 10) [16] were added.

2.8. Analytical procedure for the quantification of molar activity

For analysis of the molar activities, an Agilent 1260 system (Agilent Technologies GmbH, Santa Clara, CA, USA) equipped with a quaternary pump (G1311B), a multi wavelength UV-detector (G1365D), a manual injector (G1328C), a NaI (Tl) detector from Berthold Technologies (Bad Wildbad, Germany) and GINA Star controlling software (Elysia-Raytest; Straubenhardt, Germany) was used. The column was an X-Bridge BEH Shield RP-18, 4.6 × 50 mm, 2.5 μm, 130 Å (Waters, Austria). All details for the different mobile phases, limits of detection and quantification were presented recently [17].

Table 1
Recommended *versus* established maintenance interval for the most common tasks of module servicing in our facility.

Maintenance tasks	Recommended interval	Our interval
Leak test	Every 5th synthesis	Every synthesis
1st iodine trap	Every 5th synthesis	Once per week (approx. 7–10th synthesis)
2nd iodine trap	n.a.	Every 30th synthesis
Water traps	Every 20th synthesis	Every 15–20th synthesis
Iodine refill	Every 20th synthesis	Every 25th synthesis
Change of CH_3I trapping material	Every 20th synthesis	Dependent on synthesis performance (every 150–200th syntheses)
Change CO_2 trap/CH_4 oven material	Every 100th synthesis	Dependent on synthesis performance (every 200–400th syntheses)
Change CO_2 cooling trap material	n.a.	Dependent on synthesis performance (~1000th syntheses)

2.9. Partial runs for the analysis of potential contamination with ubiquitous CO_2

The identification of potential sources of non-radioactive carbon dioxide was performed by analysis of partial runs (*i.e.* simulated preparations interrupted after specific steps).

(1) For analysis of the precursor quality, the [^{11}C]DASB radiolabeling precursor (MASB) was solved in 0.4 mL DMSO and an HPLC run was performed in order to determine the amount of DASB contained in the precursor.
(2) For identification of potential carbon-12 contamination originating from the target (including target gas, tubings and distribution ways, but not from the irradiation process), the target was flushed twice with target gas without previous irradiation. The potential carbon-12 dioxide contamination was trapped in the CO_2 trap. The circulation process was performed as described before and the produced CH_3I was released into a solution of 1 mg MASB in 0.4 mL DMSO. Afterwards the reaction mixture was quenched with 1 mL of water and the amount of the formed DASB was analyzed.
(3) For identification of potential carbon-12 contamination resulting from the module or inert gas source: the [^{11}C]CO_2 trap was flushed with a stream of helium (50 mL/min) and the circulation process was performed as described before. The trapping and analysis of DASB was performed as described for (2).

2.10. Statistical analysis of molar activity for a set of PET tracers

The molar activities of the aforementioned six PET tracers were analyzed over a course of approximately 1.5 years with around 10–15 carbon-11 productions per week. Production records were statistically analyzed by Microsoft Excel 2010 and *t*-test was performed with Graph Pad Prism 6 (GraphPad Software, La Jolla, CA, USA). Moving average analysis was executed by trend line analysis also in Microsoft Excel 2010.

All calculation for molar activities and yields within the different processes were performed at the same time point (end of syntheses or end of the respective process) but non-decay corrected to depict the situation during a synthesis.

Box plot analysis (Fig. 3) shows the overall range of values (minimal to maximal value), the range between the 25th to 75th percentile as box and the median value is shown as intermediate line of the box. All data for Fig. 5 are expressed as mean ± SD, whereas in Figs. 2, 4, and 6 every point represents a single experiment/event to enable trend analysis.

3. Results and discussion

The molar activities of six PET-tracers, [^{11}C]DASB, [^{11}C]harmine, [^{11}C]PIB, [^{11}C]erlotinib, [^{11}C]-(+)-PHNO and [*carbonyl*-^{11}C]WAY100635, was monitored over the course of 1.5 years with a high turnover of around 10–15 carbon-11 productions per week produced on the same GE TRACERlab FX C Pro system (Fig. 2). Moving average analysis showed a continuous trend with a peak in molar activity around every 3 months (approx. 150 syntheses). Within our production scheme, the main reason for a fast drop in molar activity was found to be the filling level of the target gas bottle (major effect) or the inert gas bottle (helium bottle, minor effect).

On the other hand, the molar activity was highly dependent on the quality of the starting materials (different production lots of commercial suppliers, time of solvent usage, *etc.*). Therefore the average molar activity was also PET-tracer dependent. The highest A_m at end of synthesis (non-decay corrected) was achieved for [^{11}C]harmine (146 ± 108 GBq/μmol), [^{11}C]DASB (133 ± 110 GBq/μmol), as well as the Grignard reaction based tracers [^{11}C]-(+)-PHNO (132 ± 92 GBq/μmol) and [*carbonyl*-^{11}C]WAY100635 (137 ± 101 GBq/μmol), whereas [^{11}C]erlotinib (101 ± 57 GBq/μmol) and [^{11}C]PIB (103 ± 61 GBq/μmol) showed the lowest values.

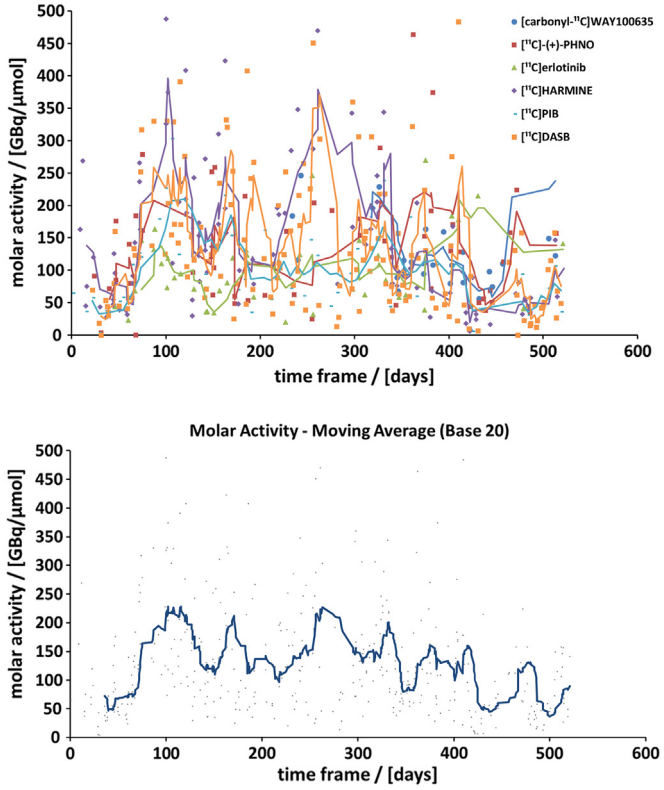

Fig. 2. Top: Overview on molar activities of an overall of 457 syntheses of the following PET-tracers: [*carbonyl*-^{11}C]WAY-100635 (n = 31), [^{11}C]-(+)-PHNO (n = 49), [^{11}C]erlotinib (n = 49), [^{11}C]harmine (n = 109), [^{11}C]PIB (n = 61) and [^{11}C]DASB (n = 158). The lines are the moving average analysis (base 4) for the respective radiotracer to visualize the trend over the time. Bottom: Moving average analysis over all molar activities with a period of 20 to show the fluctuation within approximately a month independent on the respective radiotracer.

Interestingly, we observed a slight trend to lower molar activities throughout the day when using the synthesizer repeatedly for ^{11}C-tracer preparations. In general, the first production resulted in higher molar activity than the successive ones. This trend is explicable either by residues from previous runs, which could not be removed by the cleaning procedure, or it is potentially a sum of effects caused by the type of tracer in combination with effects caused by the producer. However, a more extensive evaluation is necessary to fully explain this trend — performing three consecutive syntheses with the same tracer and the same producer. Unfortunately, we are not able to perform such experiments at the moment due to logistical restrictions in connection with the clinical routine schedule.

However rare, excessive or wrong use of the module by the producer can dramatically influence the performance. Intra- and interoperator variabilities were also clearly seen (Fig. 3).

When a reduction in molar activities was observed, it was essential to clearly distinguish between a drop (a) only for [^{11}C]CH_3I based tracers, (b) only for Grignard-reaction based tracers or (c) for both. In our facility, the main reasons for a decreasing molar activity only for [^{11}C]CH_3I based tracers were identified as (organic) contamination of the ascarite traps or molecular sieves, damaged tubing or clogging of valves. As the transformation of [^{11}C]CO_2 to [^{11}C]CH_3I was found to show a linear trend with around 37 ± 4% absolute yield of [^{11}C]CH_3I (Fig. 4) every drastic discrepancy indicated a beginning systematic disturbance of this process.

Once a poor performance (with unaltered turnover of [^{11}C]CO_2 to [^{11}C]CH_3I) was observed, it was mandatory to change all ascarite traps in order to gain sufficient molar activities again. Moreover, it was found that a few syntheses were necessary for regeneration of the system (*i.e.* additional methylation runs without tracer preparation).

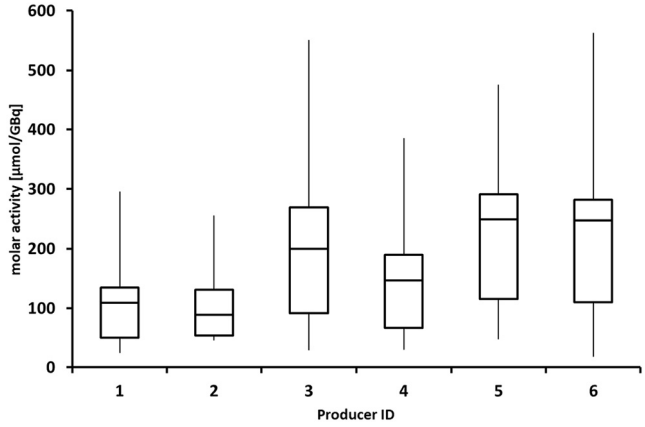

Fig. 3. Inter- and intraoperator variabilities in molar activities shown for [^{11}C]harmine. Box plot analysis includes the minimum to maximum value (upper and lower whisker), the range of the 25th to 75th percentile (box) as well as the median value (intermediate line of the box). In overall 86 syntheses were included in the analysis with the following assignment to the producers: producer 1 ($n = 10$); producer 2 ($n = 12$), producer 3 ($n = 29$), producer 4 ($n = 7$), producer 5 ($n = 16$), and producer 6 ($n = 12$). 23 syntheses were excluded as no assignment to a single producer was possible (productions in pairs due to teaching aspects) or when only ≤5 syntheses per producer were available.

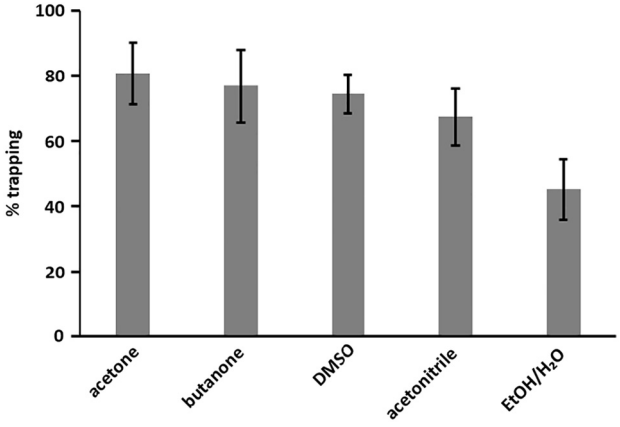

Fig. 5. Trapping efficiency of [^{11}C]CH_3I or [^{11}C]CH_3OTf, respectively, in five solvents, namely acetone ([^{11}C]tariquidar, $n = 10$), butanone ([^{11}C]PIB, $n = 48$), DMSO ([^{11}C]DASB and [^{11}C]harmine, $n = 31$), acetonitrile ([^{11}C]erlotinib, $n = 49$) and a mixture of ethanol/water ([^{11}C]methionine, $n = 14$) at room temperature. Values are expressed as mean ± SD.

When additionally to the drop in molar activity the radiochemical yield in [^{11}C]CH_3I decreased to less than approximately 30% it was mainly caused by partial clogging of the gas pump valve, which was recognizable by a reduction in the number of the cycles during the transformation of [^{11}C]CH_4 to [^{11}C]CH_3I *via* valves V9, V17, V16 and V15.

Although the reaction solvent did not influence the molar activity of the respective tracer, a distinct difference in the trapping efficiency and consequently on the yield was observable (Fig. 5). The most effective solvents for trapping [^{11}C]CH_3I or [^{11}C]CH_3OTf at room temperature were polar, aprotic solvents, like DMSO, acetone, and butanone, with a nearly quantitative recovery of the activity. The least effective ones were polar, protic solvents, such as a mixture of ethanol and water, which additionally were able to act as nucleophile themselves and, therefore, potentially produce side products, *e.g.* [^{11}C]methanol or [*methyl*-^{11}C]methylethylether.

As Grignard reactions, as used for *e.g.* the synthesis of [^{11}C]-(+)-PHNO, do not proceed *via* [^{11}C]CH_3I, a drop in molar activity solely for this kind of reactions was mainly caused by impurities of the used reagents. This problem was often caused by repeated usage of critical reagents (*e.g.* CO_2 enrichment in these containers). In most cases a significant increase of the molar activity was achieved by using a fresh batch of the applied chemical reagent.

However, when a drop in both, [^{11}C]CO_2 and [^{11}C]CH_3I based reactions, occurred, the main carbon source was either a contamination of the [^{11}C]CO_2 trap or within the cyclotron target. As mentioned before, this increased carbon load was mainly brought about by a low fill level of the target gas bottle.

For identification of the origin of organic contamination, we performed three successive syntheses, in which two partial runs and a full run were conducted on the same day. For molar activity measurement, the [^{11}C]DASB production scheme was used. The partial runs included the identification of the amount of DASB within the starting material, the contribution to the carbon load by the module and the cyclotron target, as well as measurement of the carbon load solely originating from the module.

The amount of DASB within the starting material was negligible for the following calculations. The results for the carbon load were opposed to the produced DASB. The correlation between the identified carbon load of the sum of the contributions of module and cyclotron and the obtained molar activity is depicted in Fig. 6. Here, it is obvious that small changes in the carbon-load influence the molar activity more drastically in the high molar activity range than in the low one. Thus, high fluctuations are more likely and common at high molar activities.

The experimental work-up using different partial runs was successfully applied to identify and eliminate carbon contaminations faster within our synthetic protocol and production routine. Hence, we recommend following this procedure in the set-up and during continuous monitoring of automated radiosyntheses of ^{11}C-tracers.

In summary, three clearly recognizable parameters for performance of carbon-11 syntheses in terms of molar activity were identified: technical, inter/intralaboratory and interoperator parameters (Fig. 7).

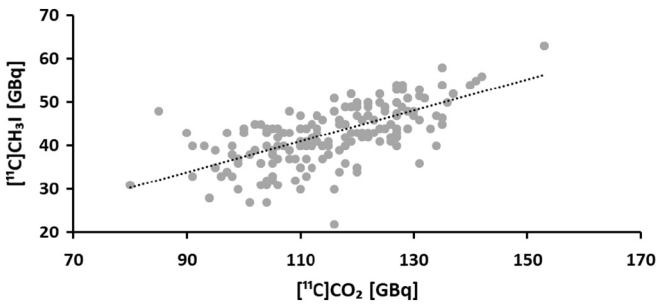

Fig. 4. Absolute yield of [^{11}C]CH_3I in relation to the starting activity of [^{11}C]CO_2 ($n = 262$). The linear regression analysis (dotted line) highlights the increasing trend ($y = 0.3558x + 1.9012$; $R2 = 0.449$).

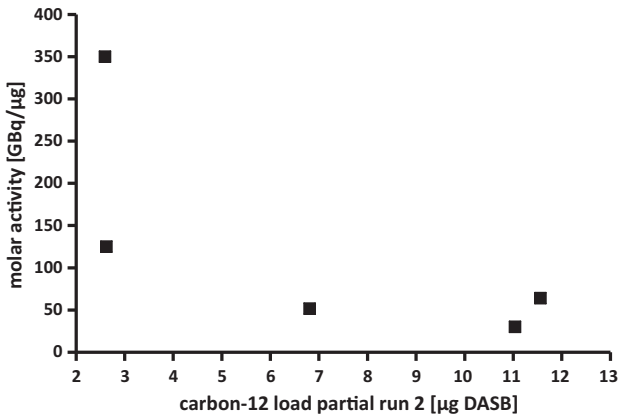

Fig. 6. Relationship between the ^{12}C-load (absolute amount of produced DASB) of the sum of contributions from synthesizer and cyclotron processes and molar activity of [^{11}C]DASB measured on the same day.

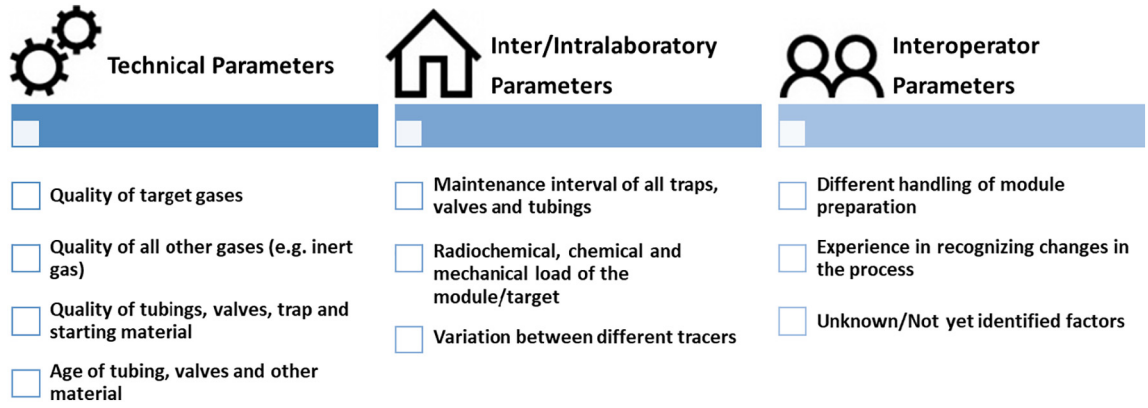

Fig. 7. Identified parameters influencing the molar activity of the six analyzed radiotracers.

The technical parameters included mostly external factors, such as the quality of the target and inert gas, the quality of the reagents and consumables, which were dependent on the commercial supplier and therefore often difficult to control.

Easier to adapt and modify were the inter-/intralaboratory parameters as, for instance, the maintenance intervals had to be changed to generate continuous high performance and to keep the carbon load within the module at a low level.

The trickiest part was the determination of interoperator parameters, such as varying module preparation procedures and monitoring of the synthetic process. Only extensive validation, (re-) training of the personnel and clear and concise standard operational procedures lead to satisfactory and consistent molar activities.

4. Conclusion

The aim of this extensive study was to identify carbon-12 contaminations within the synthetic procedure which influence the molar activities of six examined carbon-11 based PET tracers. The identified parameters were manifold and could be summarized into technical, inter/intralaboratory and interoperator parameters. For this purpose, both a retrospective analysis of >450 synthesis data and dedicated experiments (including partial synthetic runs as well as full radiochemical runs) were conducted in order to facilitate the identification process of the responsible parts within the synthesizer for reduced molar activities. Addressing the identified parameters before set-up and monitoring them during operation guarantees stable quality of ^{11}C-tracer preparations with constant molar activities.

Acknowledgement

We thank Andreas Krcal for his technical support and help with the maintenance of the GE TRACERlab FX C Pro module and Katharina Pallitsch for preparing silver triflate.

Disclosure statement

The authors declare that they have no conflict of interest.

This article does not contain any studies with human participants or animals performed by any of the authors.

References

[1] Lancelot S, Zimmer L. Small-animal positron emission tomography as a tool for neuropharmacology. Trends Pharmacol Sci 2010;31(9):411–7.
[2] Coenen HH, Gee AD, Adam M, Antoni G, Cutler CS, Fujibayashi Y, et al. Consensus nomenclature rules for radiopharmaceutical chemistry – setting the record straight. Nucl Med Biol 2017:55:v-xi.
[3] Andersson J, Truong P, Halldin C. In-target produced [^{11}C]methane: increased specific radioactivity. Appl Radiat Isot 2009;67(1):106–10.
[4] Iwata R, Ido T, Ujiie A, Takahashi T, Ishiwata K, Hatano K, et al. Comparative study of specific activity of [^{11}C]methyl iodide: a search for the source of carrier carbon. Int J Rad Appl Instrum A 1988;39(1):1–7.
[5] Gómez-Vallejo V, Llop J. Specific activity of [^{11}C]CH_3I synthesized by the "wet" method: main sources of non-radioactive carbon. Appl Radiat Isot 2009;67(1):111–4.
[6] Zhang M-R, Suzuki K. Sources of carbon which decrease the specific activity of [^{11}C]CH_3I synthesized by the single pass I2 method. Appl Radiat Isot 2005;62(3):447–50.
[7] Kniess T, Rode K, Wuest F. Practical experiences with the synthesis of [^{11}C]CH_3I through gas phase iodination reaction using a TRACERlabFXC synthesis module. Appl Radiat Isot 2008;66(4):482–8.
[8] Larsen P, Ulin J, Dahlstrøm K, Jensen M. Synthesis of [^{11}C]iodomethane by iodination of [^{11}C]methane. Appl Radiat Isot 1997;48(2):153–7.
[9] Haeusler D, Mien LK, Nics L, Ungersboeck J, Philippe C, Lanzenberger RR, et al. Simple and rapid preparation of [^{11}C]DASB with high quality and reliability for routine applications. Appl Radiat Isot 2009;67(9):1654–60.
[10] Philippe C, Haeusler D, Mitterhauser M, Ungersboeck J, Viernstein H, Dudczak R, et al. Optimization of the radiosynthesis of the Alzheimer tracer 2-(4-N-[^{11}C]methylaminophenyl)-6-hydroxybenzothiazole ([^{11}C]PIB). Appl Radiat Isot 2011;69(9):1212–7.
[11] Philippe C, Zeilinger M, Mitterhauser M, Dumanic M, Lanzenberger R, Hacker M, et al. Parameter evaluation and fully-automated radiosynthesis of [^{11}C]harmine for imaging of MAO-A for clinical trials. Appl Radiat Isot 2015;97:182–7.
[12] Philippe C, Mairinger S, Pichler V, Stanek J, Nics L, Mitterhauser M, et al. Comparison of fully-automated radiosyntheses of [^{11}C]erlotinib for preclinical and clinical use starting from in target produced [^{11}C]CO_2 or [^{11}C]CH_4. EJNMMI Radiopharm Chem 2018;3:8.
[13] Rami-Mark C, Ungersboeck J, Haeusler D, Nics L, Philippe C, Mitterhauser M, et al. Reliable set-up for in-loop 11C-carboxylations using Grignard reactions for the preparation of [carbonyl-^{11}C]WAY-100635 and [^{11}C]-(+)-PHNO. Appl Radiat Isot 2013;82:75–80.
[14] Wadsak W, Mien L-K, Ettlinger DE, Lanzenberger R, Haeusler D, Dudczak R, et al. Simple and fully automated preparation of [carbonyl-^{11}C]WAY-100635. Radiochim Acta 2007;95(7):417–22.
[15] Mitterhauser M, Wadsak W, Krcal A, Schmaljohann J, Eidherr H, Schmid A, et al. New aspects on the preparation of [^{11}C]Methionine — a simple and fast online approach without preparative HPLC. Appl Radiat Isot 2005;62:441–5.
[16] Bauer F, Kuntner C, Bankstahl JP, Wanek T, Bankstahl M, Stanek J, et al. Synthesis and in vivo evaluation of [^{11}C]tariquidar, a positron emission tomography radiotracer based on a third-generation P-glycoprotein inhibitor. Bioorg Med Chem 2010;18(15):5489–97.
[17] Nics L, Steiner B, Klebermass E-M, Philippe C, Mitterhauser M, Hacker M, et al. Speed matters to raise molar radioactivity: fast HPLC shortens the quality control of C-11 PET-tracers. Nucl Med Biol 2018;57:28–33.

3. SYNTHESIS AND IN VITRO EVALUATION OF NEW TRANSLOCATOR PROTEIN LIGANDS DESIGNED FOR POSITRON EMISSION TOMOGRAPHY

Kalina T[#], Berroterán-Infante N[#], Schmitl S, Vraka C, Hacker M, Mitterhauser M, Wadsak W, Pallitsch K.

Future Med. Chem., 2018, In Press.

[#]equally contributed

I designed and performed all radiochemical and *in vitro* experiments, including radiosynthesis optimization and automation, determination of binding affinities toward TSPO, metabolic stability assays and AGP binding experiments. Furthermore, I conceived and executed some of the chemical routes to obtain the reference substances and precursors. I also analyzed data and wrote parts of the manuscript.

Synthesis and *in vitro* evaluation of new translocator protein ligands designed for positron emission tomography

Thomas Kalina,[a,‡] Neydher Berroterán-Infante,[b,c,‡] Stefan Schmitl,[b] Chrysoula Vraka,[b] Marcus Hacker,[b] Markus Mitterhauser,[b,d,e] Katharina Pallitsch*[,a] and Wolfgang Wadsak.*[b,c,f]

[a]Department of Organic Chemistry, Faculty of Chemistry, University of Vienna, Vienna, Austria.

[b]Division of Nuclear Medicine, Department of Biomedical Imaging and Image-guided Therapy, Medical University of Vienna, Vienna, Austria.

[c]Department of Inorganic Chemistry, Faculty of Chemistry, University of Vienna, Vienna, Austria.

[d]Department of Pharmaceutical Technology, Faculty of Life Sciences, University of Vienna, Vienna Austria.

[e]Ludwig Boltzmann Institute Applied Diagnostics, Vienna, Austria.

[f]Center for Biomarker Research in Medicine, CBmed GmbH, Graz, Austria.

[‡] These authors contributed equally.

* Corresponding author

Abstract

Background: Dysregulated levels of the translocator protein 18 KDa (TSPO) have been reported in several disorders, particularly neurodegenerative diseases. This makes TSPO an interesting target for the development of diagnostic biomarkers. Even though several radioligands have already been developed for *in vivo* TSPO imaging, the ideal TSPO radiotracer has still not been found yet. **Results:** Here, we report the chemical synthesis of a set of new TSPO ligands designed for future application in positron emission tomography, together with the determination of their biological activity and applied ^{11}C-labeling strategy. **Conclusion:** The lead compound of our series, (*R*)-[^{11}C]Me@NEBIQUINIDE, showed very promising results and is therefore proposed to be further evaluated under *in vivo* settings.

Keywords:
TSPO, synthesis, radiosynthesis, preclinical evaluation, polymorphism rs6971, PET

1. Introduction

The translocator protein 18 kDa (TSPO), first described in 1977 as the peripheral benzodiazepine receptor, was found as an additional binding site for diazepam outside the brain [1,2]. Subsequent studies have determined its role in several pathological conditions [3–6], as well as its participation in some biological processes, including cell proliferation, apoptosis, immunomodulation and particularly steroidogenesis [7–10].

Expression levels of TSPO are usually high in several organs, including heart, kidneys, lungs, spleen, testis and adrenal glands; whereas they are low in the healthy human brain [3,11,12]. Interestingly, up-regulation of the TSPO has been shown in a variety of medical conditions, including heart failure, various cancer [9] types and especially in (neuro)inflammation [13] which highlights TSPO as a promising target for drug development, as well as an intriguing site for diagnosis and disease progression monitoring in the mentioned pathologies [14–16].

Accordingly, a plethora of substances have been synthesized for *in vivo* imaging of TSPO mainly relying on positron emission tomography (PET) (Figure 1). (*R*)-[^{11}C]PK11195 ((*R*)-[^{11}C]**1**) is the most prevalent TSPO PET tracer since the early 1990s [17], even though it suffers from a high non-specific binding, which causes a low signal-to-noise ratio [18–23]. To face this shortcoming, numerous radioligands (the so-called second generation of TSPO PET tracers) with improved properties have been developed over the last years [24–28]. One of them, [^{11}C]PBR28 ([^{11}C]**2**), showed no binding to TSPO in two out of twelve subjects [29]. This phenomenon is caused by a single-nucleotide polymorphism (rs6971) in the *TSPO* gene, which replaces alanine to threonine (Ala147Thr) in a non-conservative way. This polymorphism ultimately leads to a heterogeneous binding affinity of the radiotracer toward TSPO of subjects with different genotypes. Three affinity patters related to the genotypes can be distinguished as follows: high-affinity-binders (HAB,

homozygotes), mixed-affinity-binders (MAB, heterozygotes) and low-affinity-binders (LAB, homozygotes) [30,31]. Second generation radiotracers suffer from genotype sensitivity toward this polymorphism to various degrees. Due to these severe drawbacks of the already established tracers [32], there is an urgent need for a third generation of TSPO PET tracers to overcome these problems.

As a result, several compounds have been tested to obtain the much desired ideal TSPO PET tracer. Some attempts have been conducted [33–35] using analogues from [^{11}C](*R*)-**1** with reduced lipophilicity in order to diminish the high non-specific binding. Among those, [^{11}C]ER-176 ([^{11}C]**3**) showed outstanding in vitro and in vivo properties in monkeys [33]. Unfortunately, an unexpected sensitivity toward the rs6971 polymorphism was observed in first human studies [36]. Alternative tracers {[^{11}C]MBMP ([^{11}C]**4**) and [^{18}F]FEBMP ([^{18}F]**5**)} with no sensitivity toward the human TSPO polymorphism, showed poor metabolic stability as well as slow brain kinetics. Results concerning the rs6971 polymorphism of the recently developed radiofluorinated derivative [^{18}F]2-(5-(6-fluoropyridin-3-yl)-2-oxobenzo[*d*]-oxazol-3(2H)-yl)-*N*-methyl-*N*-phenylacetamide are still missing [37–39].

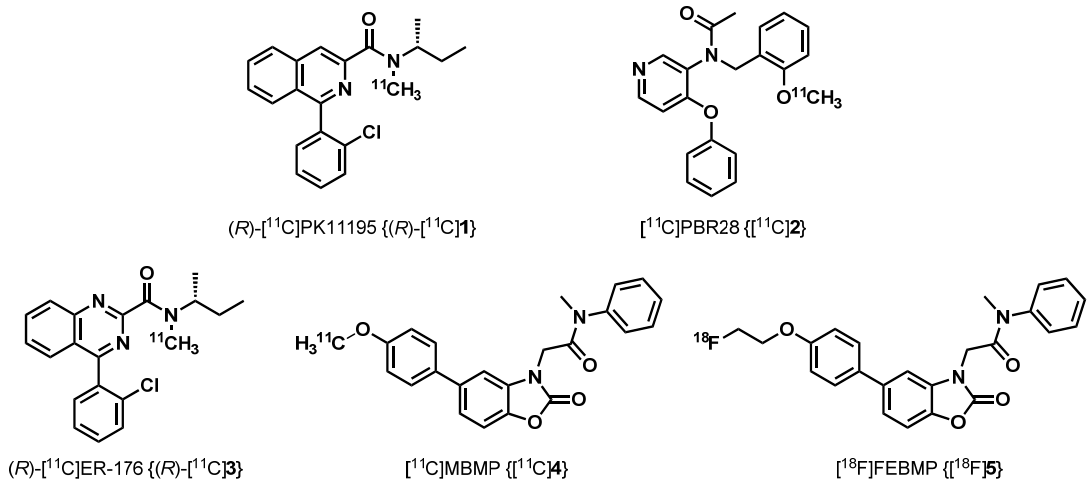

Figure 1. Selected TSPO PET tracers.

Clearly, there is still a huge demand for a novel, superior radiotracer for TSPO imaging. Herein, we report the synthesis and *in vitro* evaluation of four carboxamide analogues of **2** (VIE_TSPO_002, **6**, VIE_TSPO_004, **7**, VIE_TSPO_008, **8**, and VIE_TSPO_010, **9**) and one pyridine analog of **1**, [(*R*)-Me@NEBIQUINIDE, (*R*)-**10**] together with the radiolabeling strategy of the most promising compound.

2. Results and discussion

2.1. Design of lead structures

Unfortunately, there is no 3D structure of human TSPO available to date.[40] Therefore, we decided to develop a set of new TSPO ligands, based on established structural motifs that showed promising binding properties. As the amide functionality has been reported as a requirement for TSPO affinity, [41] we wanted to investigate the impact of alterations in the nature of the amide moiety on the binding affinity, regarding the rs6971 polymorphism, in several established second generation TSPO ligands [FEDAA1106 (**11**), PBR28 (**2**) and FEPPA (**12**)] (Figure 2). In addition, the *sec*-butyl amide of **1** was combined with a phenoxynicotinamide moiety (like in compound **2**) together in one molecule. In order to reduce the lipophilicity, compound **10** bears a chloropyridinyl- instead of a chlorophenyl moiety.

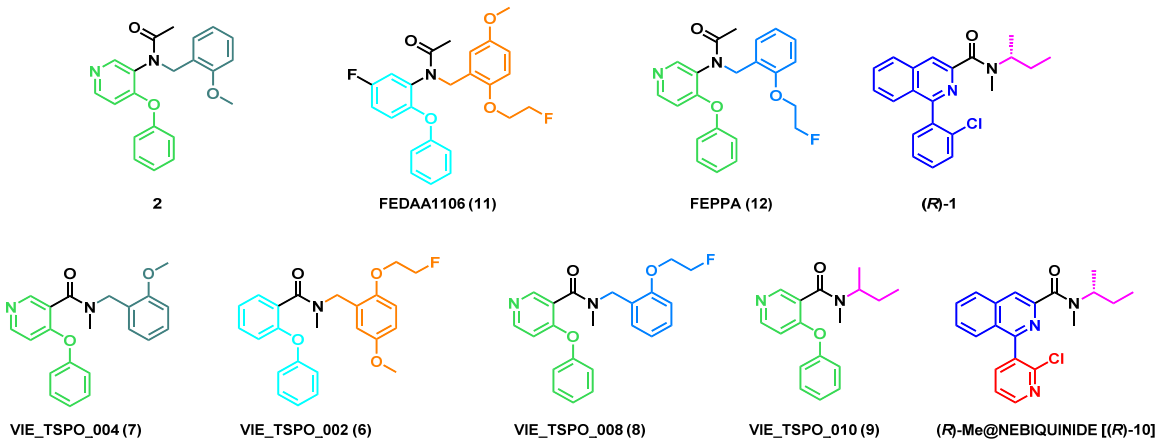

Figure 2. 1st row: established TSPO ligands; 2nd row: newly designed TSPO ligands; matching colors are used to highlight equal structural motifs.

2.2. Synthetic Chemistry

The evaluated compounds can be divided in three sets. One of the designed potential TSPO ligands is derived from benzoic acid (**6**), other target compounds bear a nicotinic acid core (**7**-**9**) and one compound bears an isoquinoline core (**10**). The discussion of the synthesis of the target compounds has thus been divided in three parts. Conveniently, a radiolabeling precursor was also synthesized for each substance.

Compounds derived from benzoic acid - synthesis of reference standards and radiolabeling precursors

We designed a synthetic strategy using the same key intermediate to obtain the tosylated precursor and the reference standard of the benzoic acid core structures in order to make the synthesis as convenient as possible. Commercially available 2-iodobenzoic acid was converted to 2-phenoxybenzoic acid (**13**) by a literature known procedure in moderate yield (42%) [42] (Figure 3).

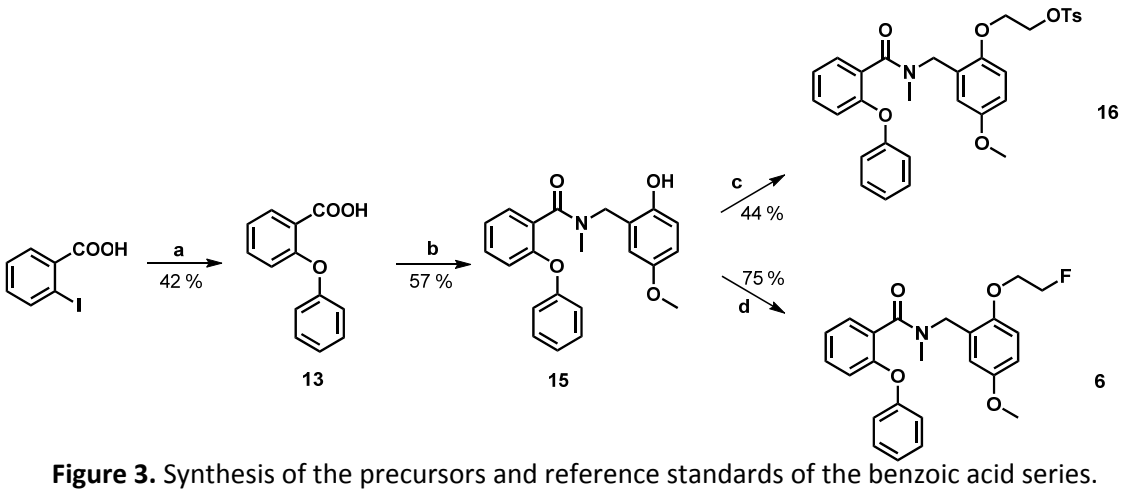

Figure 3. Synthesis of the precursors and reference standards of the benzoic acid series. Reagents and conditions: (a) PhOH, DBU, Cu(0), Cu(I)I, DMF, *reflux,* 2 h; (b) amine **14a**, HOBt, EDC·HCl, EtOH, 60°C, 24 h; (c) NaH, $TsOCH_2CH_2OTs$, DMF, r.t., 18 h; (d) NaH, $TsOCH_2CH_2F$, DMF, r.t., 18 h.

Amines **14a-c** which were used in the subsequent couplings of the nicotinic acid derived compounds, were easily accessible by a literature known procedure [43,44] (Figure 4).

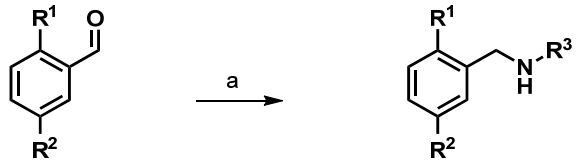

17a: R^1 = OH, R^2 = OMe
17b: R^1 = H, R^2 = OH
17c: R^1 = H, R^2 = OH

14a: R^1 = OH, R^2 = OMe, R^3 = Me (35 %)
14b: R^1 = H, R^2 = OH, R^3 = Me (45 %)
14c: R^1 = H, R^2 = OH, R^3 = H (27 %)

Figure 4. Synthesis of amines **14a-c**. Reagents and conditions *for **14a** and **b:*** 1. NH_2Me, EtOH, 60 °C, 24 h; 2. $NaBH_4$; *for **14c:*** 1. $H_2NOH{\cdot}HCl$, EtOH, r.t., 1 h; 2. HCl, zinc dust, EtOH, r.t., 15 min; 3. NH_3, NaOH, r.t., 15 min.

13 was coupled with amine **14a** in the presence of HOBt and EDC hydrochloride to give the desired key intermediate, **15**, in good yield. The amide was either converted to the fluorinated reference standard **6** or the tosylated precursor **16** for radio-fluorination, as depicted in figure 3.

Compounds derived from nicotinic acid - synthesis of reference standards and radiolabeling precursors

Three different nicotinic acid derived target structures were envisaged. The reference standards, as well as the necessary precursors for radiolabeling were synthesized. 2-Phenoxynicotinic acid (**18**) [45] was the common starting material for the synthesis of all target nicotinamide derivatives (Figure 5).

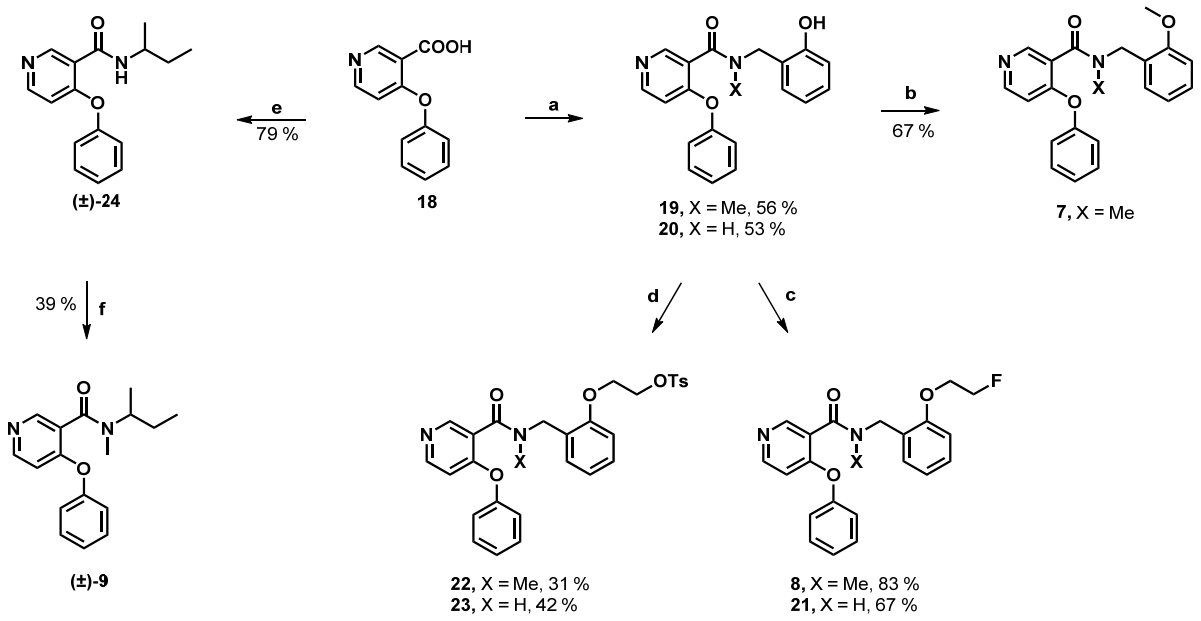

Figure 5. Synthesis of the precursors and reference standards of the nicotinic acid series.

Reagents and conditions: (a) HOBt, EDC·HCl, *then* **14b** *or* **14c,** CH_2Cl_2, r.t., 24 h; (b) *for X = Me:* 1. NaH, DMF, 0 °C; 45 min; 2. CH_3I, DMF; r.t., 2 h (c) *for X = H:* KO*t*Bu, $TsOCH_2CH_2F$, DMF, 50 °C, 18 h; *for X = Me:* NaH, $TsOCH_2CH_2F$, DMF, r.t., 18 h; (d) *for X* = H: KO*t*Bu, $TsOCH_2CH_2OTs$, CH_2Cl_2, 50 °C, 24 h; *for X* = Me: NaH, $TsOCH_2CH_2OTs$, CH_2Cl_2, r.t., 4.5 h; (e) 1. $(COCl)_2$,CH_2Cl_2 *reflux,* 2 h; 2. (±)-*sec*-butylamine, Et_3N. CH_2Cl_2, r.t., 18 h; (f) 1. NaH, DMF, 0 °C, 30 min; 2. CH_3I, DMF, r.t., 1 h.

Acid activation could either be accomplished using oxalyl chloride or a mixture of HOBt and EDC hydrochloride. The activated nicotinic acid derivatives were subsequently coupled with different amines. Both activation methods yielded the desired amide products in comparable yield.

Coupling with amines **14b** and **14c**, respectively, gave compounds **19** and **20** in moderate yields (56% and 53%, respectively). **19** is itself already one of the desired precursor compounds. Methylation of **19** under basic conditions yielded the corresponding reference standard **7**. **19** and **20** were used for the synthesis of all other reference standards and precursors, as shown in figure 5.

Coupling with (±)-*sec*-butylamine gave amide **24** in 79% yield, which was one of the desired precursors. Compound (±)-**9** could easily be obtained from the latter by reaction with methyl iodide after deprotonation with sodium hydride.

Compounds derived from isoquinoline - synthesis of reference standards and radiolabeling precursors

Compound **25** bears a pyridyl substituted isoquinoline core, which offers, in addition to the radiolabeling via *N*-methylation with carbon-11, a possibility for radiolabeling via nucleophilic aromatic substitution using [^{18}F]fluoride, as a result of the *N*-activation.

The radiolabeling precursor (*R*)-**25** and the unlabeled reference standard (*R*)-**10** were obtained starting from commercially available methyl 2-iodo-benzoate in 3 or 4 steps, respectively. Methyl 1-bromoisoquinoline-3-carboxylate (**26**) was synthesized according to the procedure described by Tucker *et al*. [46]. The bromide **26** was elongated *via* the Suzuki protocol. Surprisingly, this reaction failed in DMF as solvent, whereas the desired pyridyl substituted compound **27** was obtained in moderate yield after refluxing the reaction mixture for 16 h in 1,2-dimethoxyethane under basic conditions (Figure 6).

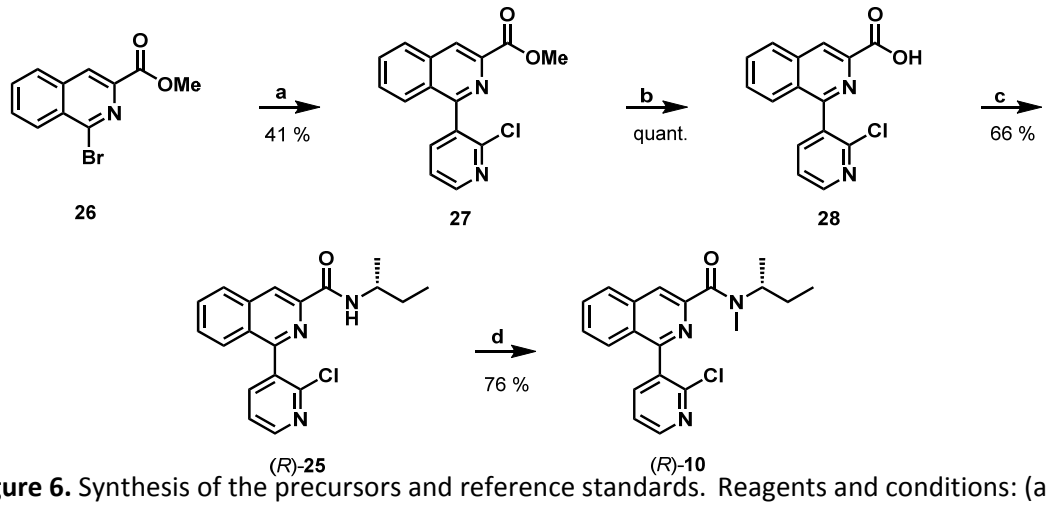

26 27 28 (*R*)-**25** (*R*)-**10**

Figure 6. Synthesis of the precursors and reference standards. Reagents and conditions: (a) 1. $Pd(dppf)Cl_2$, 2. (2-chloropyridine-3-yl) boronic acid, K_3PO_4, DME, 80 °C, 16 h, ; (b) NaOH, dioxane, H_2O, r.t., 4 h; (c) oxalyl chloride, CH_2Cl_2, *reflux,* 2 h; *then*: Et_3N, (*R*)-*sec*-butylamine, CH_2Cl_2, r.t., 16 h; (d) 1. NaH, DMF, 0 °C; 30 min, 2. CH_3I, DMF, r.t., 1.75 h.

Attempts to increase the yield of the Suzuki reaction by microwave irradiation failed under any of the tested conditions. Afterwards, saponification under basic conditions gave the corresponding free carboxylic acid **28** in excellent yield. Acid activation in the presence of oxalyl chloride, followed by nucleophilic substitution with (*R*)-*sec*-butylamine gave the desired substance (*R*)-**25**, which was subsequently methylated to obtain amide (*R*)-**10**. This transformation turned out to be more challenging than expected. Different bases, like NaHMDS or KO*t*Bu, and reaction temperatures have been tested. The best results were achieved using NaH for deprotonation at 0 °C. However, the yields still varied from one experiment to the other largely depending on the total reaction time. It proved best to keep the reaction time below 35 min, to avoid methylation of the isoquinoline and pyridine nitrogen atoms.

2.3. Binding affinity and lipophilicity

A broad spectrum of inhibition constants (K_i) was obtained for the newly developed ligands. All data fitted best to a single-site model, except for the MAB data of compound **7**, which fitted best to a two-site model. This behaviour has also been observed for other second generation TSPO ligands, as **2** [30]. Compounds **6**, **7**, **8** and **9** were rapidly discarded as potential PET ligands, due to their poor binding affinity (regarding the standards for PET tracers) toward TSPO, proving that the acetamide group is essential for the binding affinity of the second generation of TSPO ligands. Moreover, the affinity of those compounds is also largely affected by the rs6971 polymorphism, as demonstrated by the different K_i values of different genotype groups. Interestingly, the incorporation of a fluorine atom enhanced the binding affinities of the new substances as revealed by the K_i values of **6** and **8** compared to **7**, as reported for other drug candidates [47].

Table 1. Inhibition constants (K_i) of newly developed substances in high-affinity-binders (HAB), mixed-affinity-binders (MAB) and low-affinity-binders (LAB) and log*P* values (HPLC, pH 7.4). Given values represent arithmetic means of at least n=3 experiments ± standard deviation.

Compound	Ki_{HAB} (nM)	Ki_{MAB} (nM)	Ki_{LAB} (nM)	$Log P_{7.4pH}$
2[30,48]	3.4±0.2	4.0±1.2 313±38	188±7.0	3.01±0.11#
6	95±8	357±36	851±159	2.70±0.01
7	359±142	401±99 3850±459	4000±1000	2.69±0.01
8	135±11	497±79	925±83	3.63±0.02
9	>30000	>30000	>30000	1.72±0.03
1[30,49]	28±4	22±2	24±6	3.25±0.03
(*R*)-10	16±3	21±4	17±4	2.27±0.14

Shake-flask method

On the contrary, compound (*R*)-**10** showed excellent binding properties to TSPO, even better than **1**, showing a K_i value in the low nanomolar range as well as low sensitivity toward the polymorphism (K_{iHAB}/K_{iLAB} = 0.93).

Since the high lipophilicity of **1** has been reported as a major disadvantage for the use of this PET ligand, we also determined the log*P* values of the new candidates using an HPLC method and found a significantly lower lipophilicity of (*R*)-**10** in comparison to **1**.

2.4. Radiochemistry

In view of the weak affinity of compounds **6**, **7**, **8** and **9** toward TSPO, we focused our radiolabeling experiments on compound **10**. Hence, we first determined the optimal reaction conditions for the ^{11}C-labeling and afterwards used these conditions for the automated radiosynthesis. Typical

reaction conditions as reported for the production of [^{11}C]**1** were tested, which included the use of solid KOH as the base for the amide deprotonation and [^{11}C]methyl iodide as the ^{11}C-methylation reagent in DMSO [50]. Unexpectedly, only low radiochemical conversions (RCC) were achieved using these conditions even at high temperatures and longer reaction times (Figure 7A). [^{11}C]Methyl triflate was tested as alternative ^{11}C-source resulting in higher RCC. Several identical concentrations were tested for both ^{11}C-sources using the same precursor (**25**). A precursor concentration of 2 mg·mL^{-1} was found to be ideal, while higher concentrations did not offer better conversions (data not shown).

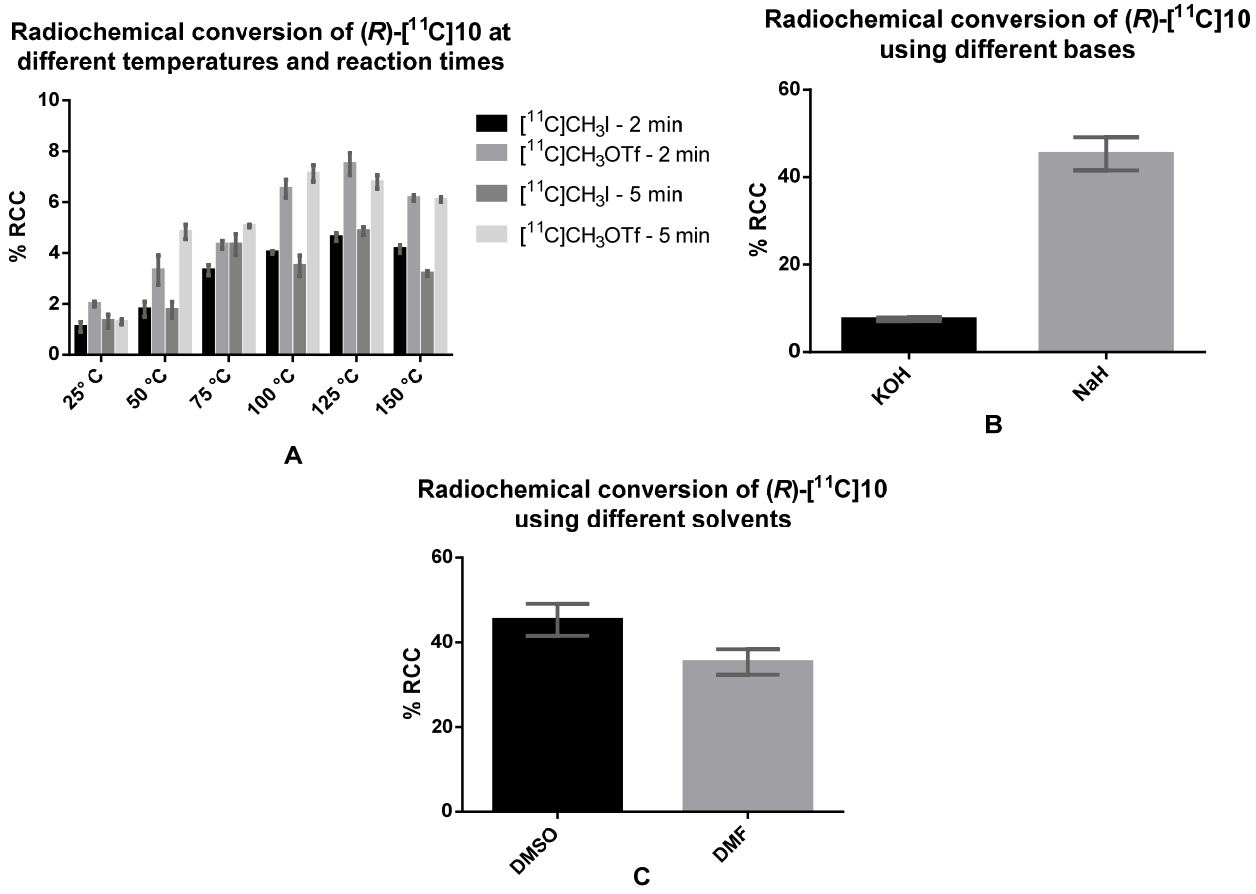

Figure 7. Radiochemical conversion of (*R*)-[^{11}C]**10** under different conditions. A: radiochemical conversion of (*R*)-[^{11}C]**10** at different temperatures and reaction times; B: radiochemical conversion of (*R*)-[^{11}C]**10** using different bases; C: radiochemical conversion of (*R*)-[^{11}C]**10** using different solvents. Columns represent arithmetic means of 3 independent experiments (n=3); error bars represent the standard deviation.

Best results were thus obtained using [^{11}C]CH_3OTf for 2 min at 125 °C. Subsequently, the effect of different bases was investigated (Figure 7B). NaH led to an improved RCC compared to the use of solid KOH. The first experiments showed that temperatures above 100 °C facilitate the ^{11}C-methylation, thus only DMF and DMSO were tested as solvents for radiolabeling. DMSO showed to be superior in these experiments (Figure 7C). In summary, the best results (RCC = 45±4) were obtained by reacting [^{11}C]CH_3OTf with **25** (2 mg·mL^{-1}) in DMSO activated with NaH for 2 min at 125 °C (Figure 8).

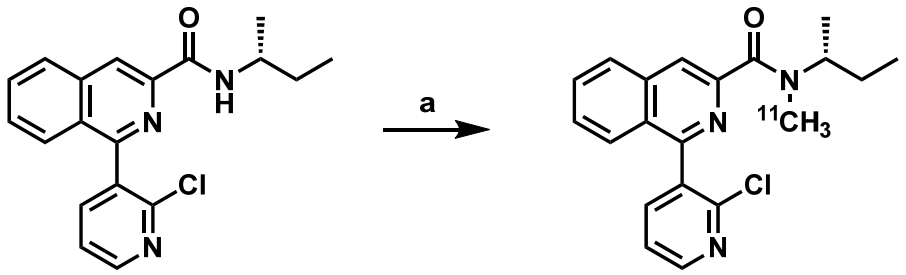

(*R*)-**25** (*R*)-[^{11}C]**10**

Figure 8. Optimized radiosynthesis of (*R*)-[**^{11}**C]**10**. (a) 1. NaH, 2. [^{11}C]CH_3OTf, 125 °C, DMSO.

For the automated production of (*R*)-[^{11}C]**10**, approximately 100 GBq of cyclotron produced [^{11}C]CO_2 were delivered to the synthesizer. (*R*)-[^{11}C]**10** was obtained in a final yield of 2.6±0.4 GBq (11.3±0.6% radiochemical yield, EOB; molar radioactivity = 101±16 GBq·µmol^{-1}, EOS, n = 5) after 44 min. The synthesis time included the production of [^{11}C]CH_3OTf, reaction of the latter with precursor **25**, purification, formulation, and quality control. All quality control parameters were in accordance with the acceptance criteria, based on the radiopharmaceutical preparations monograph of the European Pharmacopoeia [51] (see Table 2).

Table 2. Results of quality control of (*R*)-[^{11}C]**10.**

Test	Acceptance criteria [#]	Result
Vial contents	Clear, colorless, particle free	Pass
pH	4.5 – 8.5	7.5
Radiochemical purity	≥95%	≥98%
Radionuclide purity	Half-life: (20.3±2) min	(19.8±5) min
	γ-Spectrum: 511 keV	(507±6) keV
Ethanol content	≤100000 ppm	≤ 85000 ppm
DMSO content	≤5000 ppm	≤ 120 ppm
Sterility	Sterile	Pass
Endotoxins	≤10 EU/mL	≤ 1 EU/mL

[#] Acceptance criteria based on related monographs in the European Pharmacopoeia [51,52]

2.5. **AGP Binding**

Since α1-acid glycoprotein (AGP) has been described as the major plasma protein responsible for the binding of (*R*)-[^{11}C]**1** to plasma and this interaction influences the outcome of (*R*)-[^{11}C]**1** PET scans [23], we investigated the binding of (*R*)-[^{11}C]**10** to AGP using spin desalting columns. Our findings revealed a significant ($p<0.0001$) lower binding of (*R*)-[^{11}C]**10** compared to (*R*)-[^{11}C]**1** (68.8±0.7% vs. 89.8±0.7%), which in addition to the reduced lipophilicity, highlights our lead compound as a promising candidate for *in vivo* applications.

2.6. Metabolic stability

Incubation of (*R*)-[^{11}C]**10** with human liver microsomes under physiological conditions revealed no significant degradation of our lead compound (Figure 9). In fact, 98.2±0.2% (n=3) of intact tracer

was found after an incubation time of 60 min. Although microsomal incubation does not fully represent the complex *in vivo* situation, due to the lack of several enzymes [53], the observed *in vitro* stability of [^{11}C]**10** is significantly higher than for other established TSPO PET tracers [54].

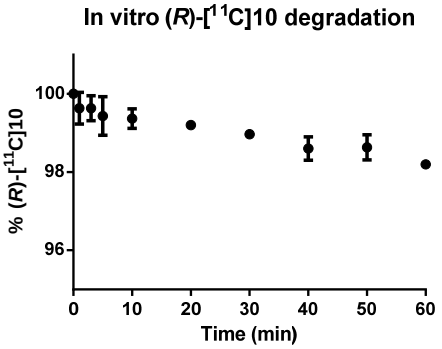

Figure 9. Stability of (*R*)-[^{11}C]**10** in microsomal incubation. Dots represent arithmetic means of 3 experiments (n=3); error bars represent the standard deviation.

3. Conclusions

An array of carboxamide derivatives targeting TSPO were synthesized in satisfactory yield. The conducted *in vitro* competition experiments emphasize the isoquinoline carboxamide moiety as a leading scaffold for TSPO ligands and prove the necessity of the acetamide moiety for TSPO binding with high affinity in second generation TSPO ligands. Accordingly, compound (*R*)-**10** demonstrated to be the most potent ligand among the prepared substances. Its radioactive counterpart, (*R*)-[^{11}C]**10**, was therefore prepared in more than sufficient radiochemical yield, high molar radioactivity and radiochemical purity. The introduction of the chloropyridinyl substituent enhanced, as expected, the physicochemical properties of (*R*)-**10** as demonstrated by the reduced lipophilicity and decreased binding to α1-AGP compared to compound **1**. Moreover, the chloropyridinyl moiety opens up the possibility for future incorporation of the more convenient radionuclide fluorine-18 (110 min half-life, compared to 20 min half-life for carbon-11) through a

Halex (halogen exchange) reaction using [^{18}F]fluoride, which is planned for the near future. The obtained results provide a basis for future *in vivo* evaluations of (*R*)-[^{11}C]**10** using µPET**.**

4. Future Perspective

The development of third generation TSPO PET tracers is already in its highest point. Some improved radiotracers have been already proposed. In the next years, complimentary information about the performance of those tracers in different TSPO-related diseases should be available, which will further highlight a general use of TSPO PET imaging for diagnosis and follow-up of such diseases.

5. Summary Points

- A new series of potent TSPO-PET ligands were synthesized and evaluated for their binding affinity to TSPO. The most promising candidate was further radiolabelled with [^{11}C]CH_3OTf.
- (*R*)-[^{11}C]**10** showed K_i values in the nanomolar range, as well as a lower lipophilicity, compared to the established PET tracer [^{11}C]**1**.
- The reaction conditions for the ^{11}C-labelling were optimized to obtain high radiochemical conversion in its fully automated synthesis.
- (*R*)-[^{11}C]**10** has a significant lower binding to α1-acid glycoprotein, than [^{11}C]**1**, thereof a higher specific binding is expected, regarding future *in vivo* applications.

6. Associated Content

The Supporting Information is available free of charge online and includes, experimental methods, determination of target compound purity by means of HPLC as well as ^{1}H, ^{13}C and ^{19}F NMR spectra of new compounds.

7. Author Information

Corresponding Author

*Dr. Katharina Pallitsch

Department of Organic Chemistry, Faculty of Chemistry

University of Vienna

Waehringer Strasse 38

A-1090 Vienna, Austria

E-Mail: katharina.pallitsch@univie.ac.at

ORCID

Neydher Berroterán-Infante: 0000-0002-9247-6457

Wolfgang Wadsak: 0000-0003-4479-8053

Katharina Pallitsch: 0000-0003-2648-1044

8. Acknowledgment

This scientific project was performed with the support of the Medical Imaging Cluster of the Medical University of Vienna. The authors want to thank Friedrich Girschele for collecting blood samples from membrane preparation. Further we thank S. Felsinger for recording NMR spectra.

9. Financial and competing interest disclosure

Wolfgang Wadsak is a part-time employee of CBmed GmbH. All other authors have nothing to disclose.

10. References

Publications of special note have been highlighted as: * of interest and **of considerable interest

1. Papadopoulos V, Baraldi M, Guilarte TR, *et al.* Translocator protein (18kDa): new nomenclature for the peripheral-type benzodiazepine receptor based on its structure and molecular function. *Trends Pharmacol. Sci.* 27(8), 402–409 (2006).

2. Braestrup C, Squires RF. Specific benzodiazepine receptors in rat brain characterized by high-affinity (3H)diazepam binding. *Proc. Natl. Acad. Sci. U. S. A.* 74(9), 3805–3809 (1977).

3. Liu G-J, Middleton RJ, Hatty CR, *et al.* The 18 kDa Translocator Protein, Microglia and Neuroinflammation. *Brain Pathol.* 24(6), 631–653 (2014).

4. Veenman L, Gavish M. The peripheral-type benzodiazepine receptor and the cardiovascular system. Implications for drug development. *Pharmacol. Ther.* 110(3), 503–524 (2006).

5. Kunduzova OR, Escourrou G, De La Farge F, *et al.* Involvement of peripheral benzodiazepine receptor in the oxidative stress, death-signaling pathways, and renal injury induced by ischemia-reperfusion. *J. Am. Soc. Nephrol. JASN*. 15(8), 2152–2160 (2004).

6. Jordà EG, Jiménez A, Verdaguer E, *et al.* Evidence in favour of a role for peripheral-type benzodiazepine receptor ligands in amplification of neuronal apoptosis. *Apoptosis Int. J. Program. Cell Death*. 10(1), 91–104 (2005).

7. Zhao AH, Tu LN, Mukai C, *et al.* Mitochondrial Translocator Protein (TSPO) Function Is Not Essential for Heme Biosynthesis. *J. Biol. Chem.* 291(4), 1591–1603 (2016).

8. Papadopoulos V, Fan J, Zirkin B. Translocator protein (18 kDa): an update on its function in steroidogenesis. *J. Neuroendocrinol.* 30(2), e12500 (2018).

9. Denora N, Natile G. An Updated View of Translocator Protein (TSPO). *Int. J. Mol. Sci*. 18(12), 2640-2644 (2017).

*** Interesting TSPO review.**

10. Bonsack F, Alleyne CH, Sukumari-Ramesh S. Augmented expression of TSPO after intracerebral hemorrhage: a role in inflammation? *J. Neuroinflammation*. 13, 151-164 (2016).

11. Tu LN, Zhao AH, Hussein M, Stocco DM, Selvaraj V. Translocator Protein (TSPO) Affects Mitochondrial Fatty Acid Oxidation in Steroidogenic Cells. *Endocrinology*. 157(3), 1110–1121 (2016).

12. Di Grigoli G, Monterisi C, Belloli S, *et al.* Radiosynthesis and Preliminary Biological Evaluation of [^{18}F]VC701, a Radioligand for Translocator Protein. *Mol. Imaging*. 14, 1535-3508 (2015).

13. Cagnin A, Kassiou M, Meikle SR, Banati RB. Positron emission tomography imaging of neuroinflammation. *Neurother. J. Am. Soc. Exp. Neurother.* 4(3), 443–452 (2007).

14. Rupprecht R, Papadopoulos V, Rammes G, *et al.* Translocator protein (18 kDa) (TSPO) as a therapeutic target for neurological and psychiatric disorders. *Nat Rev Drug Discov*. 9(12), 971–988 (2010).

15. O'Brien ER, Kersemans V, Tredwell M, *et al.* Glial activation in the early stages of brain metastasis: TSPO as a diagnostic biomarker. *J. Nucl. Med. Off. Publ. Soc. Nucl. Med.* 55(2), 275–280 (2014).

16. Dupont A-C, Largeau B, Santiago Ribeiro MJ, Guilloteau D, Tronel C, Arlicot N. Translocator Protein-18 kDa (TSPO) Positron Emission Tomography (PET) Imaging and Its Clinical Impact in Neurodegenerative Diseases. *Int. J. Mol. Sci.* 18(4), 785-821 (2017).

17. Shah F, Hume SP, Pike VW, Ashworth S, McDermott J. Synthesis of the enantiomers of [N-methyl-11C]PK 11195 and comparison of their behaviours as radioligands for PK binding sites in rats. *Nucl. Med. Biol.* 21(4), 573–581 (1994).

18. Bird JLE, Izquierdo-Garcia D, Davies JR, *et al.* Evaluation of translocator protein quantification as a tool for characterising macrophage burden in human carotid atherosclerosis. *Atherosclerosis*. 210(2), 388–391 (2010).

19. Kobayashi M, Jiang T, Telu S, *et al.* 11C-DPA-713 has much greater specific binding to translocator protein 18 kDa (TSPO) in human brain than 11C-(R)-PK11195. *J. Cereb. Blood Flow Metab. Off. J. Int. Soc. Cereb. Blood Flow Metab.* 38(3), 393–403 (2018).

20. Fujita M, Kobayashi M, Ikawa M, *et al.* Comparison of four 11C-labeled PET ligands to quantify translocator protein 18 kDa (TSPO) in human brain: (R)-PK11195, PBR28, DPA-713, and ER176-based on recent publications that measured specific-to-non-displaceable ratios. *EJNMMI Res.* 7(1), 84–88 (2017).

** **Interesting comparison among first, second, and third generation TSPO PET tracers.**

21. Kreisl WC, Fujita M, Fujimura Y, *et al.* Comparison of [11C]-(R)-PK 11195 and [11C]PBR28, two radioligands for translocator protein (18 kDa) in human and monkey: Implications for positron emission tomographic imaging of this inflammation biomarker. *NeuroImage*. 49(4), 2924–2932 (2010).

22. Vivash L, O'Brien TJ. Imaging Microglial Activation with TSPO PET: Lighting Up Neurologic Diseases? *J. Nucl. Med.* 57(2), 165–168 (2016).

23. Lockhart A, Davis B, Matthews JC, *et al.* The peripheral benzodiazepine receptor ligand PK11195 binds with high affinity to the acute phase reactant alpha1-acid glycoprotein: implications for the use of the ligand as a CNS inflammatory marker. *Nucl. Med. Biol.* 30(2), 199–206 (2003).

*** Description of the α1-AGP binding of [^{11}C]PK11195**

24. Guo Q, Owen DR, Rabiner EA, Turkheimer FE, Gunn RN. Identifying improved TSPO PET imaging probes through biomathematics: The impact of multiple TSPO binding sites in vivo. *Neuroimage*. 60(2), 902–910 (2012).

25. Wilson AA, Garcia A, Parkes J, *et al.* Radiosynthesis and initial evaluation of [18F]-FEPPA for PET imaging of peripheral benzodiazepine receptors. *Nucl. Med. Biol.* 35(3), 305–314 (2008).

26. James ML, Fulton RR, Henderson DJ, *et al.* Synthesis and in vivo evaluation of a novel peripheral benzodiazepine receptor PET radioligand. *Bioorg. Med. Chem.* 13(22), 6188–6194 (2005).

27. Boutin H, Prenant C, Maroy R, *et al.* [18F]DPA-714: Direct Comparison with [11C]PK11195 in a Model of Cerebral Ischemia in Rats. *PLOS ONE*. 8(2), e56441 (2013).

28. Imaizumi M, Kim H-J, Zoghbi SS, *et al.* PET imaging with [11C]PBR28 can localize and quantify upregulated peripheral benzodiazepine receptors associated with cerebral ischemia in rat. *Neurosci. Lett.* 411(3), 200–205 (2007).

29. Fujita M, Imaizumi M, Zoghbi SS, *et al.* Kinetic analysis in healthy humans of a novel positron emission tomography radioligand to image the peripheral benzodiazepine receptor, a potential biomarker for inflammation. *NeuroImage*. 40(1), 43–52 (2008).

30. Owen DRJ, Gunn RN, Rabiner EA, *et al.* Mixed-Affinity Binding in Humans with 18-kDa Translocator Protein Ligands. *J. Nucl. Med.* 52(1), 24–32 (2011).

31. Owen DR, Yeo AJ, Gunn RN, *et al.* An 18-kDa Translocator Protein (TSPO) Polymorphism Explains Differences in Binding Affinity of the PET Radioligand PBR28. *J. Cereb. Blood Flow Metab.* 32(1), 1–5 (2012).

32. Owen DR, Guo Q, Rabiner EA, Gunn RN. The impact of the rs6971 polymorphism in TSPO for quantification and study design. *Clin. Transl. Imaging*. 3(6), 417–422 (2015).

33. Zanotti-Fregonara P, Zhang Y, Jenko KJ, *et al.* Synthesis and evaluation of translocator 18 kDa protein (TSPO) positron emission tomography (PET) radioligands with low binding sensitivity to human single nucleotide polymorphism rs6971. *ACS Chem. Neurosci.* 5(10), 963–971 (2014).

34. Brouwer C, Jenko K, Zoghbi SS, Innis RB, Pike VW. Development of N-Methyl-(2-arylquinolin-4-yl)oxypropanamides as Leads to PET Radioligands for Translocator Protein (18 kDa). *J. Med. Chem.* 57(14), 6240–6251 (2014).

35. Castellano S, Taliani S, Milite C, *et al.* Synthesis and Biological Evaluation of 4-Phenylquinazoline-2-carboxamides Designed as a Novel Class of Potent Ligands of the Translocator Protein. *J. Med. Chem.* 55(9), 4506–4510 (2012).

36. Ikawa M, Lohith TG, Shrestha S, *et al.* 11C-ER176, a Radioligand for 18-kDa Translocator Protein, Has Adequate Sensitivity to Robustly Image All Three Affinity Genotypes in Human Brain. *J. Nucl. Med.* 58(2), 320–325 (2017).

** **Regarding the unexpected *in vivo* sensitivity of TSPO PET tracers toward the polymorphism rs6971 in humans.**

37. Tiwari AK, Ji B, Yui J, *et al.* [18F]FEBMP: Positron Emission Tomography Imaging of TSPO in a Model of Neuroinflammation in Rats, and in vitro Autoradiograms of the Human Brain. *Theranostics*. 5(9), 961–969 (2015).

38. Tiwari AK, Yui J, Fujinaga M, *et al.* Characterization of a novel acetamidobenzoxazolone-based PET ligand for translocator protein (18 kDa) imaging of neuroinflammation in the brain. *J. Neurochem.* 129(4), 712–720 (2014).

39. Fujinaga M, Luo R, Kumata K, *et al.* Development of a 18F-Labeled Radiotracer with Improved Brain Kinetics for Positron Emission Tomography Imaging of Translocator Protein (18 kDa) in Ischemic Brain and Glioma. *J. Med. Chem.* 60(9), 4047–4061 (2017).

40. Milenkovic VM, Bader S, Sudria-Lopez D, Siebert R, Brandl C, Nothdurfter C, *et al.* Effects of genetic variants in the TSPO gene on protein structure and stability. *PLoS ONE* 13(4), e0195627 (2018).

41. (a) Mokrov GV, Deeva OA, Gudasheva TA, Yarkov SA, Yarkova MA, Seredenin SB. Design, synthesis and anxiolytic-like activity of 1-arylpyrrolo[1,2-a]pyrazine-3-carboxamides. *Bioorg. Med. Chem.* 23(13), 3368–3378 (2015); (b) Lee Y-S, Siméon FG, Briard E, Pike VW. Solution structures of the prototypical 18 kDa translocator protein ligand, PK 11195, elucidated with 1H/13C NMR spectroscopy and quantum chemistry. *ACS Chem. Neurosci.* 3(4), 325–335 (2012).

** **Regarding the importance of amides groups for TSPO binding affinity.**

42. Giri R, Goodell JR, Xing C, *et al.* Synthesis and cancer cell cytotoxicity of substituted xanthenes. *Bioorg. Med. Chem.* 18(4), 1456–1463 (2010).

43. Andreu R, C. Ronda J. Synthesis of 3,4-Dihydro-2H-1,3-benzoxazines by Condensation of 2-Hydroxyaldehydes and Primary Amines: Application to the Synthesis of Hydroxy-Substituted and Deuterium-Labeled Compounds. *Synth. Commun.* 38, 2316–2329 (2008).

44. Ayedi MA, Le Bigot Y, Ammar H, Abid S, El Gharbi R, Delmas M. Synthesis of primary amines by one-pot reductive amination of aldehydes. *Synth. Commun.* 43(6), 2127–2133 (2013).

45. Zou Q, Duan H, Ning M, *et al.* 4-Benzofuranyloxynicotinamide derivatives are novel potent and orally available TGR5 agonists. *Eur. J. Med. Chem.* 82, 1–15 (2014).

****** **Regarding the synthesis of TSPO ligands.**

46. Tucker SC, Brown JM, Oakes J, Thornthwaite D. Resolution and coupling of 1-(2'-hydroxy-1'-naphthyl)isoquinolines. *Tetrahedron*. 57(13), 2545–2554 (2001).

***** **Regarding the synthesis of TSPO ligands.**

47. Shah P, Westwell AD. The role of fluorine in medicinal chemistry. *J. Enzyme Inhib. Med. Chem.* 22(5), 527–540 (2007).

48. Briard E, Zoghbi SS, Imaizumi M, *et al.* Synthesis and Evaluation in Monkey of Two Sensitive 11C-Labeled Aryloxyanilide Ligands for Imaging Brain Peripheral Benzodiazepine Receptors In Vivo. *J. Med. Chem.* 51(1), 17–30 (2008).

49. Vraka C, Nics L, Wagner K-H, Hacker M, Wadsak W, Mitterhauser M. LogP, a yesterday's value? *Nucl. Med. Biol.* 50(Supplement C), 1–10 (2017).

50. Cremer JE, Hume SP, Cullen BM, *et al.* The distribution of radioactivity in brains of rats given [N-methyl-11C]PK 11195 in vivo after induction of a cortical ischaemic lesion. *Int. J. Rad. Appl. Instrum. B*. 19(2), 159–166 (1992).

51. Council of Europe. Radiopharmaceutical preparations. In: Europäisches Arzneibuch (European Pharmacopoeia) (8th ed), Verlag Österreich GmbH, Vienna, Austria, pp 995 (2008).

52. Council of Europe. Raclopride ([^{11}C]methoxy) injection. In: *European pharmacopoeia* (7.0), European Pharmacopoeia Commission, Strasbourg, France, 988–90 (2010).

53. Jia L, Liu X. The Conduct of Drug Metabolism Studies Considered Good Practice (II): In Vitro Experiments. *Curr. Drug Metab.* 8(8), 822–829 (2007).

54. Eberl S, Katsifis A, Peyronneau MA, *et al.* Preclinical in vivo and in vitro comparison of the translocator protein PET ligands [^{18}F]PBR102 and [^{18}F]PBR111. *Eur. J. Nucl. Med. Mol. Imaging*. 44(2), 296–307 (2017).

4. (*R*)-[^{18}F]NEBIFQUINIDE: A TALE OF NEW THIRD GENERATION TRANSLOCATOR PROTEIN PET TRACER

Berroterán-Infante N[#]; Kalina T[#]; Fetty L; Janisch V; Velasco R; Hacker M; Haug AR; Pallitsch K; Wadsak W; Mitterhauser M.

[#]equally contributed

J Med Chem, Submitted.

I designed and performed all radiochemical, *in vitro* and *in vivo* experiments, including radiosynthesis optimization and automation, determination of binding affinities toward TSPO, metabolic stability assays, AGP and bone binding tests, as well as mice biodistribution experiments. Moreover, I analyzed the data and wrote the manuscript.

(*R*)-[^{18}F]NEBIFQUINIDE: A Tale of a New Third Generation Translocator Protein PET Tracer

Neydher Berroterán-Infante, [‡,a,b] *Thomas Kalina,* [‡,c] *Lukas Fetty,* [a] *Victoria Janisch,* [a] *Ramona Velasco,*[c] *Chrysoula Vraka,* [a] *Marcus Hacker,* [a] *Alexander R. Haug,* [a] *Katharina Pallitsch,* [*,c] *Wolfgang Wadsak,* [†,*,a,b,d] *and Markus Mitterhauser.* [†,a,e]

[a]Division of Nuclear Medicine, Department of Biomedical Imaging and Image-guided Therapy, Medical University of Vienna, Währinger Gürtel 18-20, 1090 Vienna, Austria.

[b]Institute of Inorganic Chemistry, Faculty of Chemistry, University of Vienna, Währinger Straße 42, 1090 Vienna, Austria.

[c]Institute of Organic Chemistry, Faculty of Chemistry, University of Vienna, Währinger Straße 38, 1090 Vienna, Austria.

[d]Center for Biomarker Research, CBmed, Stiftingtalstraße 5, 8010 Graz, Austria.

[e]Ludwig Boltzmann Institute Applied Diagnostics, Währinger Gürtel 18-20, 1090 Vienna, Austria.

Keywords: Fluorine-18 • Imaging agents • Preclinical evaluation • Radiopharmaceuticals • TSPO

Abstract: Positron emission tomography (PET) imaging of the 18 kDa translocator protein (TSPO), which is relevant to a multitude of diseases (especially neurodegenerative disorders), is considered a challenge for molecular imaging due to the poor availability of suitable radiotracers with adequate pharmacokinetic properties. Here, we describe the development of a radiofluorinated analogue of the established TSPO PET tracer (*R*)-[^{11}C]PK11195. We conducted a complete preclinical evaluation using *in vitro*, *in vivo* and *ex vivo* methods to assess the performance of this novel radiotracer, where we observed

high specific binding of the radiotracer to TSPO, as well as high metabolic stability. Therefore, we propose this radiolabeled compound for further evaluation in animal models as well as in clinical trials.

Introduction:

The 18 kDa translocator protein (TSPO) was first described in 1977 as the peripheral benzodiazepine receptor, as it showed the ability to bind diazepam in peripheral organs.[1,2] Its location at the outer mitochondrial membrane is of relevance due to the involvement of mitochondria in cell survival, as well as the role of mitochondrial dysfunctions in the development of several diseases. In this context, TSPO has been observed to be relevant in several physiological processes, including mitochondrial respiration, apoptosis, cell proliferation and particularly, the transport of cholesterol into the mitochondria for steroid synthesis.[3] TSPO dysregulation has been associated with a variety of diseases, such as several types of cancer, heart insufficiency, endocrine syndromes, and mostly neurodegenerative disorders.[4-7] Hence, assessment of alterations in TSPO expression levels has been suggested for diagnosis of these diseases using molecular imaging techniques such as positron emission tomography (PET).

Although numerous TSPO PET tracers have been developed up to now, they all have suffered from severe drawbacks, which have hampered their use.[8] The most frequently used TSPO PET tracer, generally referred to as the "gold standard" in this context, is (*R*)-[^{11}C]PK11195 {(*R*)-[^{11}C]**1**}. It exhibits a high lipophilicity, which results in a high non-specific *in vivo* binding, inevitably leading to a low signal-to-noise ratio,[9] whereas several other radioligands, such as [^{11}C]PBR28 {[^{11}C]**2**}, [^{18}F]FEPPA {[^{18}F]**3**, and [^{11}C]DPA-713 {[^{11}C]**4**} have shown outstanding properties in this context.[10-12] Unfortunately, this class of radioligands, known as the "second generation of TSPO PET tracers", binds to TSPO in a

heterogeneous fashion in different subjects, depending on the TSPO phenotype binding profile, *i.e.* high-affinity-binders (HAB), low-affinity-binders (LAB), and mixed-affinity-binders (MAB), which is directly related to a single-nucleotide polymorphism in the *TSPO* gene (rs6971).[13] Exclusion of LABs from clinical studies, as well as challenges in the quantification of the respective radiotracer uptake, are the main disadvantages for the application of these tracers.[14]

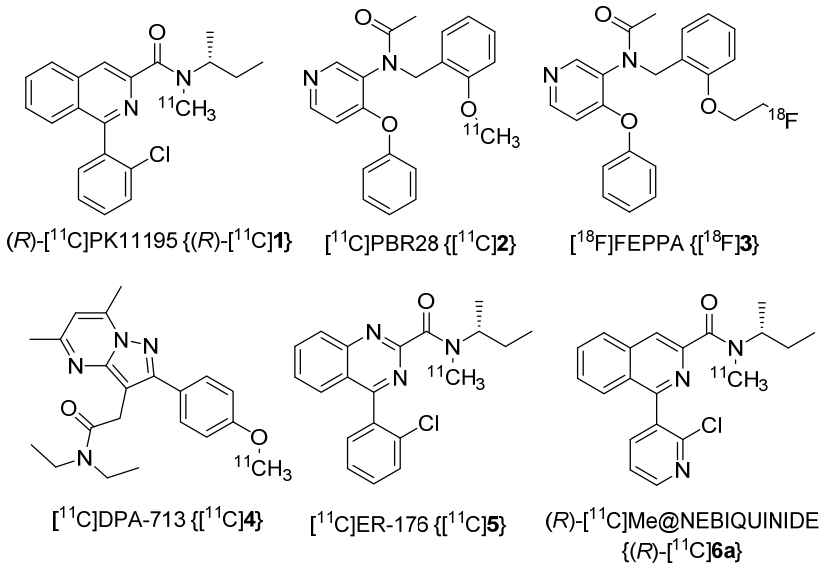

Figure 1. Chemical structures of known TSPO PET tracers.

Hence, the development of new TSPO PET tracers with adequate pharmacokinetic properties combined with a low sensitivity toward the polymorphism rs6971 has been the focus of many investigations. For instance, the quinazoline derivative [^{11}C]ER-176 {[^{11}C]**5**} has been tested in humans, with very promising outcome so far,[15-17] while a compound developed by our group, the pyridinyl isoquinoline derivative (*R*)-[^{11}C]Me@NEBIQUINIDE {(*R*)-[^{11}C]**6a**}, showed outstanding in vitro results in earlier examinations.[18] Nevertheless, the disadvantageous short half-life of carbon-11 ($t_{1/2}$ = 20.2 min), which was the radionuclide of choice in the latter compounds, encouraged us to develop a new pyridinyl isoquinoline analogue labeled with the longer-lived radionuclide

fluorine-18 ($t_{1/2}$ = 109.7 min). Herein, we report the synthesis, radiosynthesis and full preclinical evaluation of (*R*)-[^{18}F]NEBIFQUINIDE {*(R)*-[^{18}F]**6b**}.

Results and Discussion:

Chemistry: The radiolabeling precursor, (*R*)-**6a**, and the reference standard, (*R*)-**6b**, were synthesized as previously described (Scheme 1).[18] A Suzuki reaction between methyl 1-bromoisoquinoline-3-carboxylate (**7**)[19] and the corresponding halogenated pyridylboronic acid gave the coupled products (**8a** and **8b**) in moderate yields. These were hydrolyzed to the carboxylic acids **9a** and **9b**. Subsequent amidation proceeded smoothly after oxalyl chloride mediated activation and successive treatment with (*R*)-sec-butylamine to obtain amides **10a** and **10b**. Finally, methylation reactions, under basic conditions, gave the precursor (*R*)-**6a** and the reference standard (*R*)-**6b** in an overall yield of 20% and 17%, respectively.

Scheme 1. Synthesis of precursor and reference standard.

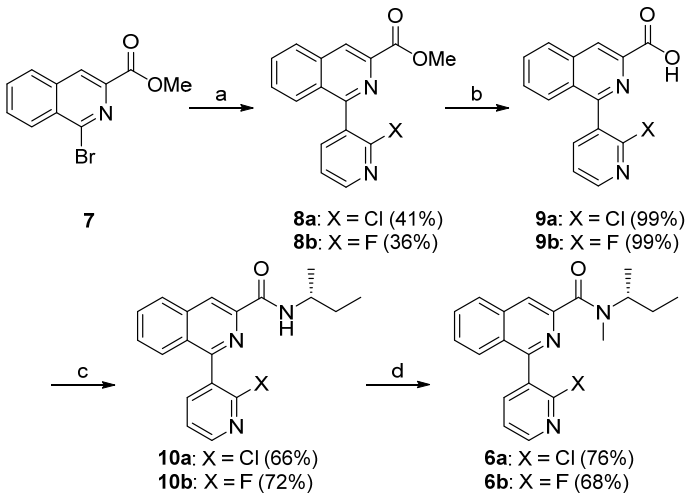

7

8a: X = Cl (41%)
8b: X = F (36%)

9a: X = Cl (99%)
9b: X = F (99%)

10a: X = Cl (66%)
10b: X = F (72%)

6a: X = Cl (76%)
6b: X = F (68%)

Reagents and conditions: (**a**) *for X* = Cl: $Pd(dppf)Cl_2$, (2-chloropyridine-3-yl) boronic acid, K_3PO_4, DME, 80 °C; *for X* = F: $Pd(dppf)Cl_2$, (2-fluoropyridine-3-yl) boronic acid, K_3PO_4, DME, 80 °C; (**b**) NaOH, 1,4-dioxane/H_2O; (**c**) oxalyl chloride, CH_2Cl_2, reflux; *then* Et_3N, (*R*)-sec-butylamine; (d) NaH, DMF, 0 °C; *then* CH_3I, 0 °C.

The impact of the halogen substituent (F *vs.* Cl) on the binding affinity toward TSPO was probed by means of competitive binding assays using thrombocyte membranes from subjects previously genotyped as HAB, MAB or LAB.[20] The observed inhibition constants (K_i) revealed a superior affinity of (*R*)-**6b** toward TSPO compared to (*R*)-**6a**, in the low nanomolar range. Moreover, a remarkably low sensitivity toward the TSPO polymorphism was conserved for the title compound K_i(HAB)/K_i(LAB) = 0.93). Thus, the introduction of fluorine clearly showed to improve the ligand-protein interactions, suggesting the suitability of [^{18}F]NEBIFQUINIDE for TSPO PET imaging.[21]

Biological Evaluation: Since the lipophilicity of TSPO radioligands has been described as a crucial factor on the pharmacokinetics of TSPO PET imaging,[22] determination of the log*P* value was performed. As expected, log*P* of (*R*)-**6b** was significantly reduced in comparison to **1** and remained in the same range as for (*R*)-**6a**.

Table 1. Inhibition constants (K_i) and log*P* values[a]

Compound	K_i(HAB) (nM)	K_i(MAB) (nM)	K_i(LAB) (nM)	Log*P*
1[20,23]	28±4	22±2	24±6	3.25±0.03
(*R*)-**6a**[18]	16±3	21±4	17±4	2.27±0.14
(*R*)-**6b**[b]	5.1±0.3	5.3±0.6	5.5±0.4	2.35±0.14

[a] Given values represent arithmetic means ± standard deviation of at least 3 independent experiments;

[b] This work

Scheme 2. A general approach for the radiolabeling of (*R*)-[^{18}F]**6b**.

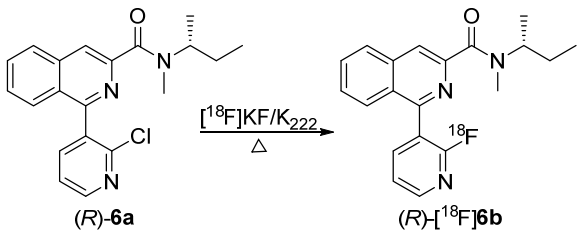

Next, we investigated ^{18}F-radiolabeling to obtain the desired new PET-tracer, (*R*)-[^{18}F]**6b**. Optimization was performed by small scale radiosyntheses (<100 MBq) using azeotropically dried [^{18}F]fluoride. The influence of the following parameters on the radiochemical conversion (RCC) was monitored via thin layer chromatography (TLC): reaction time, temperature, solvent, precursor concentration and the type of radiofluorinating agent. Unfortunately, very low RCCs (0.1% - 0.5%) were obtained even at high precursor concentrations, temperatures and after long reaction times using standard reaction setups.

^{18}F-Labeling proceeds via nucleophilic aromatic substitution, where the nitrogen of the pyridinyl substituent promotes the incorporation of [^{18}F]fluoride in the *ortho*-position to nitrogen, due to the stabilization of the reaction intermediate by both inductive and resonance effects (Scheme 2).[24] Despite the mentioned activation, successful radiofluorination of 2-halopyridines usually needs harsh conditions (20 min, ≥150 °C). Alternatively, microwave heating can be used for labeling of 2-halopyridines with fluorine-18 to achieve higher radiochemical yields in shorter reaction times.[25] Applying microwave heating, a RCC of 57±9% was obtained by reacting precursor (*R*)-**6a** (5 mg/mL) with a dried [^{18}F]KF/K2.2.2 complex for 10 min at 175 °C in DMSO (100 W, n=3). An alternative

approach using a recently published microfluidic radiofluorination method for 2-halopyridines[26] was not further investigated during the course of this study.

Table 2. Outcome of (*R*)-[^{18}F]**6b** radiosyntheses[a]

Parameter	Result	Acceptance criteria[b]
Starting activity [^{18}F]fluoride (GBq)	20±2	---
Isolated yield (*R*)-[^{18}F]**6b** (GBq)	7.6±0.9	---
Radiochemical yield, not corrected for decay (%)	38±3	---
Molar radioactivity (GBq/µmol)	107±12	---
Visual inspection	Clear, colorless	Clear, colorless
Radiochemical purity (%)	99.1±0.3	≥95
Radionuclide half-life (min)	108±3	109±10
Radionuclide decay energy (keV)	507±2	511±30
pH	7.49±0.01	4.5-8.5
Osmolality	324±10	200-400 mosm/kg

(mOsm/kg)		
DMSO content (ppm)	98±3	≤5000
Ethanol content (%)	9.8992±0.0002	≤10
K2.2.2 content (µg/mL)	≤50	≤50
Sterility	Sterile	Sterile
Endotoxin content (EU/mL)	≤1 EU/mL	≤10 EU/mL

[a] Given values represent arithmetic means ± standard deviation (n=3) [b] Based on the general monograph of radiopharmaceutical preparations in the European Pharmacopoeia[29].

Diarylsulfoxide or diaryliodonium salt based precursors,[27,28] or analogues containing more suitable groups, e.g. -NMe_3, -NO_2, which reasonably could lead to a less complex radiofluorination by means of conventional heating were not investigated due to the satisfactory results from the microwave assisted approach.

For subsequent experiments, semi-automated synthesis was performed using microwave heating followed by purification and formulation in a computer controlled synthesizer. The dried [^{18}F]KF/K2.2.2 complex was reacted with precursor (*R*)-**6a** under microwave heating followed by quenching with water. The reaction mixture was transferred to a semipreparative HPLC system for purification ($t_R \approx 5$ min). Collection in water followed by subsequent removal of solvents through solid-phase extraction (SPE) and further

formulation in ethanol, sodium chloride, and phosphate-buffered saline yielded the target compound in high radiochemical yields. A summary of the optimized radiochemical synthesis as well as of the quality control outcomes is shown in the Table 2.

The preclinical evaluation of this newly developed radiotracer included *in vitro* experiments to test the metabolic stability of (*R*)-[^{18}F]**6b**, bone binding assays to evaluate possible de-fluorination, and binding experiments to α1-acid glycoprotein (AGP) which has been described as the major protein responsible for plasma binding of (*R*)-[^{11}C]PK11195.[30] Accordingly, the stability of (*R*)-[^{18}F]**6b** was examined in human liver microsomal preparations over an incubation period of 60 min. Minimal degradation was observed after this time, with up to 98.5±0.6% (n=3) of tracer remaining intact, suggesting a higher stability of our new tracer compared to other established TSPO PET tracers.[31] Likewise, incubation of the tracer with hydroxyapatite was conducted over 90 min to determine binding of the tracer to inorganic bone matter, which was found to be negligible compared to [^{18}F]NaF (positive control) and similar to [^{18}F]FDG {2-deoxy-2-[^{18}F]fluoroglucose} (negative control),[32] as show in Figure 2.

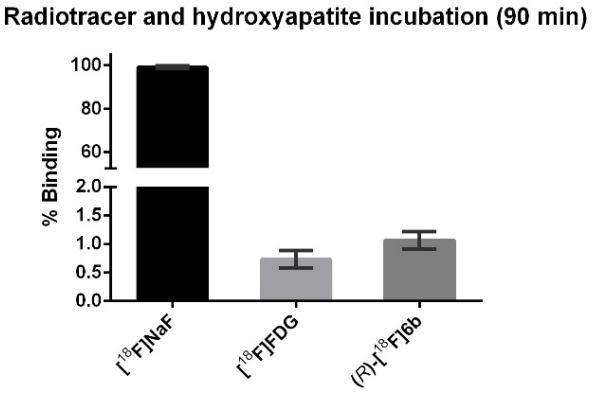

Figure 2. Incubation of radiotracers and hydroxyapatite for bone binding assays.

Incubations were conducted for 90 min and the bound radioactivity was counted. Incorporation of [^{18}F]NaF in bone matrix is well known, therefore acts as positive control. [^{18}F]FDG served as negative control (n=3).

As previously observed with (*R*)-[^{11}C]**6a**, we also noticed a significantly reduced AGP binding of our newly developed tracer (*R*)-[^{11}C]**6b** (67.9±0.9%) compared to the "gold standard" tracer (*R*)-[^{11}C]**1** (89.8±0.7%, $p<0.0001$), pointing to a higher concentration of free (*R*)-[^{11}C]**6b** in plasma. This consequently suggests a higher tracer concentration in the brain and minor binding to human serum albumin (HSA) compared to (*R*)-[^{11}C]PK11195.[30]

These satisfactory results encouraged us to perform *in vivo* imaging experiments. These investigations were combined with *ex vivo* biodistribution and stability studies of (*R*)-[^{18}F]**6b** in line with the 3R principle. The tracer was injected in C57BL/6 mice and a dynamic μPET scan was performed over 60 min followed by sacrificing the animals (baseline, n=3). To further characterize the specificity of (*R*)-[^{18}F]**6b**, displacement experiments were also conducted in C57BL/6 mice by administering PK11195 as a vehicle solution (5 mg/kg body weight, n=3) 30 min after radiotracer injection.

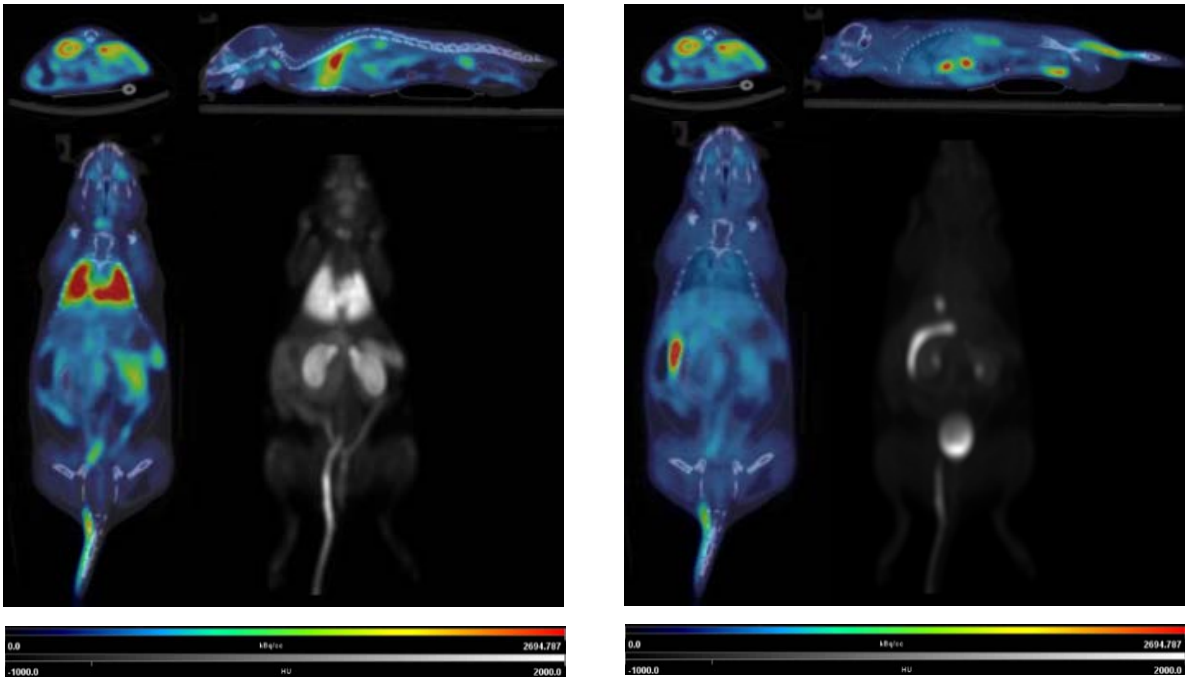

Figure 3. (*R*)-[^{18}F]**6b** µPET/CT image in a mouse.

A: pre-displacement; B: post-displacement. Anatomical planes in both cases: top-left: transaxial; top-right: sagittal; bottom-left: coronal; bottom-right: maximum intensity projection. Color scale is given in kBq/cc and it ranges from 0.00 to 2694.78. Gray scale is given in Hounsfield unit (HU) between -1000 and 2000.

Satisfyingly, µPET imaging revealed the highest uptake of (*R*)-[^{18}F]**6b** in TSPO-rich organs, e.g. heart and lungs, with uptake values (% ID/cc) of 12±4 and 11±4, respectively. As expected, low uptake (1.8±0.3% ID/cc) was observed in the brain, which is in line with the known poor expression of TSPO in healthy brain tissue. These findings were also confirmed in the *ex vivo* biodistribution measurements. Here, nearly complete clearance of the tracer from blood after 60 min was shown. Moreover, specific binding was demonstrated by injection of non-radioactive PK11195 (displacement), which achieved a significant reduction ($p=0.003$) of the uptake (up to 94±3% for the heart), compared to baseline scans.

A representative μPET/CT image is shown in Figure 3 (before and after displacement), while a detailed summary, including baseline scans and displacement experiments of %ID/g, is depicted in Figure 4. In particular, specific brain uptake suggests blood-brain-barrier penetration of (*R*)-[^{18}F]**6b**.

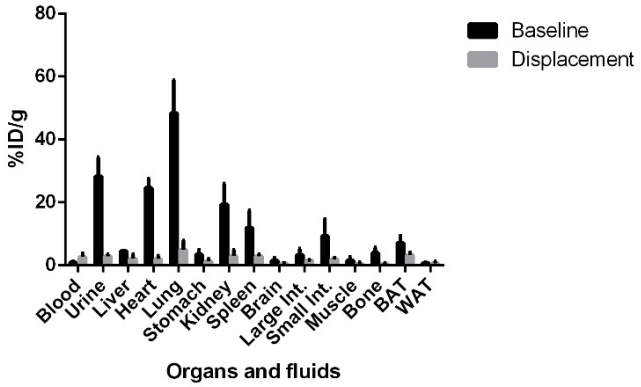

Figure 4. (*R*)-[^{18}F]**6b** biodistribution in C57BL/l mice 60 min *p.i.*. Weight-normalized percentage of injected radioactivity (baseline and displacement) are shown for several tissues (n=3).

Further analysis of organ radioactivity using radio-HPLC also revealed a high stability of the tracer. After 60 min more than 93±1% (n=3) of the radioactivity in the lungs and liver consisted of (*R*)-[^{18}F]**6b**, whereas up to 84±2% (n=3) of intact tracer was found in the brain. The residual activity indicated the emergence of a more hydrophilic metabolite (detailed chromatograms can be found in the supporting information).

Conclusion: In conclusion, we developed a new fluoropyridinyl quinoline derivative (*R*)-**6b**, which exhibits high and homogenous TSPO affinity in all phenotypes arising from the rs6971 polymorphism alongside a moderate lipophilicity. Its radiolabeled counterpart, (*R*)-[^{18}F]**6b**, was prepared with high radiochemical yields and purity. It displayed very promising *in vitro* and *in vivo* properties, which include high metabolic stability, low AGP

binding, blood-brain-barrier penetration, and high specific binding, in addition to the more convenient physical half-life of fluorine-18 compared to carbon-11. Thus, we propose further investigation of (*R*)-[^{18}F]**6b** in clinical trials, especially for complementary *in vivo* assessment of the sensitivity of (*R*)-[^{18}F]**6b** toward the polymorphism rs6971 in humans.

Experimental Section:

General Procedures:

All synthesized target compounds were checked for their purity (> 95%in all cases) via HPLC. (as indicated in "Instrumentation", for pictures see Supporting Information). All other chemicals and solvents were purchased from commercial sources and used without further purification (>95% purity). KP-Sil® (Biotage, Uppsala, Sweden) or Chromabond® (Macherey-Nagel, Düren, Germany) silica cartridges (80 g, 50 g, 25 g, 15 g or 10 g, depending on the total amount of substance to purify) were used for compound purification via flash chromatography. TLC was performed on 0.25 mm thick glass plates (or aluminum plates for radiochemical analysis) coated with silica gel 60 F_{254} (Merck Millipore, Darmstadt, Germany).

The radioligand [^{3}H]PK11195 (3,149 TBq.mmol^{-1}) as well as the Ultima Gold™ liquid scintillation cocktail for binding affinity experiments, were provided by Perkin Elmer (Walthman, USA), while Whatman® GF/B glass fiber papers were acquired from Brandel (Gaithersburg, USA) and a Pierce™ BCA Protein assay kit was obtained from ThermoFisher Scientific (Walthman, USA).

45 mg PS-HCO_3 cartridges from ABX (Radeberg, Germany), C18 plus SepPak® cartridges from Waters (Mildford, USA), 0.9% sodium chloride solution from B. Braun (Melsungen, Germany), phosphate-buffered saline solution produced by the Vienna General Hospital's

Pharmacy (Vienna, Austria), and low-protein binding Millex® GS 0.22 sterile filters manufactured by Millipore (Bedford, USA) were used for the radiosynthesis.

In vitro stability tests required human liver microsomes (20 mg/mL) and an NADPH-generating system from BD Biosciences (Woburn, USA). Micro Bio-spin chromatography columns packed with Bio-GEL P6 from Bio Rad (Hercules, USA) were used for AGP binding assays.

Instrumentation: Flash column chromatography was performed on a Biotage Isolera Prime (Biotage, Uppsala, Sweden) flash purification system. Melting points were determined on a Leica Galen III Reichert Thermovar instrument and are uncorrected. NMR spectra were recorded on a Bruker Avance AV III 600 (^{1}H: 600.27 MHz; ^{13}C: 150.93 MHz) or AV III HD 700 (^{19}F: 658.88 MHz) spectrometer. Chemical shifts were referenced to residual $CHCl_3$ (δ_H 7.24 ppm) or $(CD_2H)SO(CD_3)$ (δ_H 2.50 ppm) for proton NMR spectra, ^{13}C NMR spectra to $CDCl_3$ (δ_C 77.23 ppm) or $(CD_3)_2SO$ (δ_C 39.5). External CCl_3F (δ_F 0.00) served as reference for ^{19}F NMR spectra. Chemical shifts (δ) and coupling constants (*J*) are reported in ppm and in Hz, respectively. IR spectra were run on a Bruker VERTEX 70 IR spectrometer in ATR mode. Optical rotations were measured on a Perkin-Elmer 341 polarimeter in a 1 dm cell. $[\alpha]_D$ values are given in 10^{-1} deg cm^2 g^{-1}.

The total protein concentration in thrombocyte membranes used for affinity assays was determined in a Synergy HTX plate multimode reader (Biotek, Winooski, USA), whereas the protein-bound radioactivity required a Hidex 300SL beta counter (Hidex, Turku, Finland).

For the radiosynthesis, a GE PET trace cyclotron (PETtrace 860, GE Medical Systems, Uppsala, Sweden) was used to produce [^{18}F]fluoride, which was dried in a laptop-controlled (GINA Software, Elysia-Raytest, Straubenhardt, Germany) Nuclear Interface

synthesizer (GE Healthcare, Uppsala, Sweden). Subsequently, a PETwave microwave system (CEM, Matthews, USA) was utilized for radiolabeling, followed by purification of the product by semi-preparative reversed phase HPLC using a S1122 HPLC pump (Sykam, Fürstenfeldbruck, Germany) coupled to a UV- (Linear Instruments Model 200 Detector UV/VIS) and a radioactivity-detector, which are all integrated in the above mentioned synthesizer.

Radiochemical conversion (RCC), as well as [^{18}F]fluoride content in the final radiotracer formulation, were assessed by readout of radio-TLC using a Canberra-Packard Instant Imager (Perkin Elmer, Walthman, USA). Additional HPLC analysis was carried out for determination of the (radio)chemical purity and the molar radioactivity, on a HPLC system (Agilent Technologies, Vienna, Austria) owning a multi wavelength UV-detector and a sodium iodide - thallium detector. Quality control of the radiotracer further included determination of osmolality (Wescor Vapro® 5600 osmometer, Sanova Medical Systems, Vienna, Austria), pH (WTW inoLab 740 pH meter, WTW, Weilheim, Germany), and residual solvents content (430-GC gas chromatograph FID system, Bruker Billerica, USA).

A µPET/CT Inveon scanner (Siemens Medical Solution, Knoxville, USA) and a BioVet® physiological monitoring and heating system (m2m Imaging Corp, Cleveland, USA) were used for the *in vivo* imaging. A 2480 Wizard^2 gamma counter (Perkin Elmer, Walthman, USA) was utilized for measuring the radioactivity of organs and fluids of interest.

Animals: Five-weeks-old female C57BL/6 mice (Core Unit for Biomedical Research Division for Laboratory Animal Science and Genetics Medical University Vienna, Himberg, Austria) were kept under controlled housing conditions (22±1 °C; 40-70% humidity, 12 h day/night cycle). Animals were fed *ad libitum* with water and standard laboratory animal diet. All procedures involving animals were approved by the Ethics

Committee of the Medical University of Vienna, as well as by the Austrian Ministry of Science, Research and Economy (BMWFW-66.009/0029-WF/V36/2015) in accordance to the relevant guidelines and regulations.

Statistical Analysis: All quantitative data are specified as mean values ± standard deviation in text and figures. A student two-tailed t-test (α=0.95) was performed using GraphPad Prism® software for determination of significance. Therefore, *p* values <0.05 were considered to be significant. Error bars in figures represent the standard deviation; if not visual, they are within the icon margin.

Methods

Synthetic Chemistry: Methyl 1-(2-fluoropyridin-3-yl)isoquinoline-3-carboxylate (8b): Methyl 1-bromoisoquinoline-3-carboxylate**Error! Bookmark not defined.** (1.12 mmol, 0.300 g) and Pd(dppf)Cl_2 (0.1 equiv., 0.11 mmol, 0.082 g) were dissolved in DME (10 mL) under Ar-atmosphere. (2-fluoropyridine-3-yl) boronic acid (2 equiv., 2.24 mmol, 0.317 g), dissolved in DME (3 mL), and K_3PO_4 (2 equiv., 2.24 mmol, 0.479 g), dissolved in water (3 mL) were added and the reaction mixture was stirred at 80 °C for 16 h. After evaporation of the solvent, the residue was taken up in a 1:1 mixture of EtOAc and sat. aqueous $NaHCO_3$ solution (20 mL) and the precipitate was filtered off. The aqueous phase was extracted with EtOAc (2 × 15 mL), the combined organic phases were washed with brine (20 mL), dried ($MgSO_4$) and concentrated under reduced pressure. The residue was purified by medium pressure chromatography (heptanes/EtOAc, gradient: 8 → 80 % EtOAc) to yield methyl 1-(2-fluoropyridin-3-yl)isoquinoline-3-carboxylate (**8b**, 0.41 mmol, 0.116 g, 36 %, TLC: heptanes:EtOAc = 2:1, R_f = 0.13) as a colourless solid; mp = 220 °C (decomp.). ^{1}H NMR (600.27 MHz, $CDCl_3$): δ = 8.67 (s, 1H), 8.39 (d, *J* = 4.4 Hz, 1H), 8.08 (t, *J* = 8.5 Hz, 1H), 8.06 (d, *J* = 8.5, 1H), 7.81 (t, *J* = 7.5 Hz, 1H), 7.80 (d, *J* = 7.2 Hz, 1H), 7.73-7.68

(m, 1H), 7.44-7.38 (m, 1H), 4.04 (s, 3H, CH_3); ^{13}C NMR (150.93 MHz, CD_3OD): δ = 166.1 (s, 1C), 160.6 (d, *J* = 240.0 Hz, 1C, C-F), 154.5 (d, *J* = 4.2 Hz, 1C), 148.6 (d, *J* = 14.5 Hz, 1C), 143.0 (d, *J* = 4.1 Hz, 1C), 141.1 (s, 1C), 136.1 (s, 1C), 131.3 (s, 1C), 130.2 (s, 1C), 128.6 (s, 1C), 128.5 (s, 1C), 126.8 (d, *J* = 2.6 Hz, 1C), 124.7 (s, 1C), 122.0 (d, *J* = 4.4 Hz, 1C), 121.7 (d, *J* = 31.4 Hz, 1C), 53,1 (s, 1C, CH_3). ^{19}F NMR (658.88 MHz, $CDCl_3$): δ = –66.89 (s); IR (ATR): ν = 1721, 1435, 1247, 1231, 749 cm^{-1}; HRMS (ESI): m/z calculated for $C_{16}H_{11}N_2O_2F$ – Na^+ [M + Na^+]: 305.0697; found: 305.0699.

1-(2-Fluoropyridin-3-yl)isoquinoline-3-carboxylic acid (9b): Methyl ester **8b** (0.39 mmol, 0.110 g) was dissolved in a mixture of 1,4-dioxane and water(1:1, 5 mL) and NaOH pellets (3 equiv., 1.17 mmol, 0.047 g) were added. The reaction mixture was stirred at r.t. for 4 h. Afterwards the solvent was removed under reduced pressure, the residue was taken up in water (5 mL) and the pH of the resulting solution was adjusted to 2 (pH paper). The resulting precipitate was filtered off and dried, which gave 1-(2-fluoropyridin-3-yl)isoquinoline-3-carboxylic acid (**9b**, 0.38 mmol, 0.103 g, quant.) as a colorless solid; mp = 237-238 °C. ^1H NMR [600.27 MHz, $(CD_3)_2SO$]: δ = 13.26 (broad s, 1H, COOH), 8.76 (s, 1H), 8.50 (dd, *J* = 4.7 Hz, *J* = 1.3 Hz, 1H), 8.33 (d, *J* = 8.2 Hz, 1H), 8.26-8.21 (m, 1H), 7.96-7.92 (m, 1H), 7.85-7.81 (m, 1H), 7.79-7.76 (m, 1H), 7.65-7.62 (m, 1H); ^{13}C NMR [150.93 MHz, $(CD_3)_2SO$]: δ = 166.2 (s, 1C), 159.9 (d, *J* = 236.0 Hz, 1C, C-F), 153.7, (d, *J* = 4.2 Hz, 1C), 148.6 (d, *J* = 14.7 Hz, 1C), 143.3 (d, *J* = 3.9 Hz, 1C), 141.4 (s, 1C), 135.8 (s, 1C), 131.5 (s, 1C), 130.5 (s, 1C), 128.8 (s, 1C), 127.7 (s, 1C), 126.2 (s, 1C), 124.0 (s, 1C), 122.5 (d, *J* = 4.1 Hz, 1C), 120.9 (d, *J* = 31.4 Hz, 1C); ^{19}F NMR [658.88 MHz, $(CD_3)_2SO$]: δ = –69.43 (s); IR (ATR): ν = 1721, 1435, 1231, 1109, 780 cm^{-1}; HRMS (ESI): m/z calculated for $C_{15}H_9N_2O_2F$ – Na^+ [M + Na^+]: 291.0543; found: 291.0544.

(–)-*(R)*-*N*-(*sec*-Butyl)-1-(2-fluoropyridin-3-yl)isoquinoline-3-carboxyamide (10b): 1-(2-Fluoropyridin-3-yl)isoquinoline-3-carboxylic acid (**9b**, 0.36 mmol, 0.097 g) was

dissolved in CH_2Cl_2 (5 mL) and oxalyl chloride (5 equiv., 1.75 mmol, 0.229 g) was added. The reaction mixture was refluxed for 4 h and then the solvent was removed under reduced pressure and the residue was taken up in CH_2Cl_2 (5 mL). Et_3N (3 equiv., 1.08 mmol, 0.109 g), followed by (*R*)-*sec*-butylamine (1.5 equiv., 0.54 mmol, 0.029 g) was added under Ar-atmosphere. After stirring at r.t. for 16 h, water (10 mL) was added, the phases were separated and the organic phase was washed with water (2 × 10 mL), brine (10 mL), dried ($MgSO_4$) and concentrated under reduced pressure. The residue was purified by medium pressure chromatography (heptanes/EtOAc, gradient: 10 → 80 % EtOAc) to yield (–)-(*R*)-*N*-(*sec*-butyl)-1-(2-chloropyridin-3-yl)isoquinoline-3-carboxyamide (**10b**, 0.26 mmol, 0.084 g, 72 %, TLC: heptanes:EtOAc = 3:2, R_f = 0.33) as a yellowish solid. $[\alpha]_D^{22}$: –20.32 (CH_2Cl_2, *c* 0.925); mp = 107-109 °C; ^{1}H NMR (600.27 MHz, $CDCl_3$): δ = 8.70 (d, *J* = 0.6 Hz, 1H), 8.47-8.43 (m, 1H), 8.08 (d, *J* = 8.2 Hz, 1H), 8.05 (ddd, *J* = 9.7 Hz, *J* = 7.3 Hz, *J* = 2.0 Hz, 1H), 7.96 (d, *J* = 8.6 Hz, 1H), 7.82-7.76 (m, 2H), 7.66 (ddd, *J* = 8.2 Hz, *J* = 6.9 Hz, *J* = 1.1 Hz, 1H), 7.45 (ddd, *J* = 6.9 Hz, *J* = 4.9 Hz, *J* = 1.7 Hz, 1H), 4.21-4.14 (m, 1H, CH-N), 1.68-1.57 (m, 2H, CH_2), 1.27 (d, *J* = 6.7 Hz, 3H, C<u>H</u>$_3$-CH), 0.97 (t, *J* = 7.4 Hz, 3H, C<u>H</u>$_3$-CH_2); ^{13}C NMR (150.93 MHz, $CDCl_3$): δ = 163.7 (s, 1C), 160.7 (d, *J* = 240.7 Hz, 1C), 152.6 (d, *J* = 4.4 Hz, 1C), 148.4 (d, *J* = 14.4 Hz, 1C), 143.3 (s, 1C), 142.7 (d, *J* = 4.1 Hz, 1C), 136.9 (s, 1C), 131.1 (s, 1C), 129.2 (s, 1C), 128.7 (s, 1C), 128.1 (s, 1C), 126.5 (d, *J* = 2.1 Hz, 1C), 121.8 (d, *J* = 30.8 Hz, 1C), 121.7 (d, *J* = 4.4 Hz, 1C), 120.9 (s, 1C), 46.8 (s, 1C, CH-N), 29.8 (s, 1C, CH_2), 20.5 (s, 1C, CH_3-CH), 10.5 (s, 1C, CH_3-CH_2); ^{19}F NMR (658.88 MHz, $CDCl_3$): δ = –67.12 (s); IR (ATR): ν = 3217, 1667, 1518, 1437, 778 cm^{-1}; HRMS (ESI): m/z calculated for $C_{19}H_{18}N_3OF$ – Na^+ [M + Na^+]: 346.1319; found: 346.1326.

***(R)*-*N*-(*sec*-Butyl)-1-(2-fluoropyridin-3-yl)-*N*-methylisoquinoline-3-carboxamide (6b):** NaH (7.7 equiv., 0.33 mmol, 0.008 g) was added to a solution of amide **10b** (0.04

mmol, 0.014 g) in dry DMF (1.5 mL) at 0 °C and the reaction mixture was stirred for 30 min. Afterwards, methyl iodide (1.5 equiv., 0.07 mmol, 0.009 g) was added and stirring was continued for 1.75 h. The reaction was quenched by addition of HCl (1M, 1.5 mL) and water (5 mL). The aqueous phase was extracted with CH_2Cl_2 (3 × 5 mL), the combined org. phases were washed with brine (2 × 5 mL), dried ($MgSO_4$) and concentrated under reduced pressure. The residue was purified by medium pressure chromatography (heptanes/EtOAc, gradient: 10 → 80 % EtOAc) to yield (*R*)-*N*-(*sec*-butyl)-1-(2-fluoropyridin-3-yl)-*N*-methylisoquinoline-3-carboxamide (**6b**, 0.03 mmol, 0.010 g, 68 %, TLC: heptanes:EtOAc = 3:2, R_f = 0.22) as a yellowish solid. mp = 98-99 °C; ^{1}H NMR (600.27 MHz, $CDCl_3$, 2 conformers): δ = 8.41-8.39 (m, 2H, major conformer A + minor conformer B), 8.09-7.95 (m, 6H, 3 × A + 3 × B), 7.81-7.74 (m, 4H, 2 × A + 2 × B), 7.43-7.38 (m, 2H, A + B), 4.84-4.76 (m, 1H, CH-N, B), 3.92-3.83 (m, 1H, CH-N, A), 2.98 (s, 3H, CH_3-N, A), 2.89 (s, 3H, CH_3-N, B), 1.66-1.60 (m, 2H, CH_2, A + B), 1.59-1.51 (m, 1H, CH_2, B), 1.45-1.36 (m, 1H, CH_2, A), 1.24 (d, *J* = 6.8 Hz, 3H, C<u>H</u>$_3$-CH), 1.22 (d, *J* = 6.6 Hz, 3H, C<u>H</u>$_3$-CH, A), 0.99 (t, *J* = 7.4 Hz, 3H, C<u>H</u>$_3$-CH_2, B), 0.78 (t, *J* = 7.4 Hz, 3H, C<u>H</u>$_3$-CH_2, A). ^{13}C NMR (150.93 MHz, $CDCl_3$, 2 conformers): δ = 169.7 (s, 1C, A), 169.1 (s, 1C, B), 160.7 (d, *J* = 240.4 Hz, 1C, C-F B), 160.7 (d, *J* = 240.4 Hz, 1C, C-F A), 152.9 (d, *J* = 4.5 Hz, 1C, A), 152.7 (d, *J* = 4.6 Hz, 1C, B), 148.5 (s, 1C, B), 148.4 (s, 1C, A), 148.3 (d, *J* = 14.6 Hz, 1C, A), 148.3 (d, *J* = 14.5 Hz, 1C, B), 142.8 (d, *J* = 4.0 Hz, 1C, B), 142.7 (d, *J* = 4.1 Hz, 1C, A), 136.8 (s, 1C, A), 136.7 (s, 1C, B), 130.1 (s, 1C, A), 130.9 (s, 1C, B), 128.7 (s, 1C, B), 128.6 (s, 1C, A), 127.9 (s, 2C, A + B), 127.0 (s, 1C, A), 126.9 (s, 1C, B), 126.4 (s, 1C, A), 126.4 (s, 1C, B), 121.9 (s, 1C, B), 121.8 (s, 1C, A), 121.6 (d, *J* = 4.4 Hz, 1C, B), 121.6 (d, *J* = 4.3 Hz, 1C, A), 121.2 (s, 1C, B), 120.9 (s, 1C, A), 55.7 (s, 1C, A), 50.5 (s, 1C, B), 30.4 (s, 1C, B), 27.3 (s, 1C, A), 26.6 (s, 1C, B), 26.3 (s, 1C, A), 18.5 (s, 1C, A), 17.3 (s, 1C, B), 11.0 (s, 1C, B), 10.9 (s, 1C, A); ^{19}F NMR (658.88 MHz, $CDCl_3$, 2 conformers):

δ = –67.47 (s), –67.48 (s); IR (ATR): ν = 2960, 1657, 1421, 799, 672 cm^{-1}; HRMS (ESI): m/z calculated for $C_{20}H_{20}N_3OF$ – Na^+ [M + Na^+]: 360.1482; found: 360.1479; purity ≥99% as determined by HPLC (see experimental section).

Radiochemistry: [^{18}F]Fluoride was produced in a cyclotron by irradiation of [^{18}O]H_2O with a beam (55 μA) of protons [$^{18}O(p,n)^{18}F$], transferred to the synthesizer and fixed on a PS-HCO_3 cartridge. The radioactivity was eluted into the reactor's synthesizer by passing 0.8 mL of a K_2CO_3/K2.2.2 solution (4.5 $mg{\cdot}mL^{-1}$/22 $mg{\cdot}mL^{-1}$) in acetonitrile/water (80:20) or 0.8 mL of a $Me_4N{\cdot}HCO_3$ (15 $mg{\cdot}mL^{-1}$) in acetonitrile/water (80:20) through the cartridge. The resulting complex was heated to 100 °C under a flow of helium for azeotropic drying. Subsequently, two additional portions (0.7 mL each) of acetonitrile were added and the evaporation process was repeated to ensure complete removal of water.

The influence of several parameters, i.e. temperature, time, solvent, precursor concentration, and type of fluorinating agent, to enhance the RCC was investigated in the conventional heating experiments, by reacting small amounts of dried [^{18}F]fluoride (< 50 MBq) with precursor **6a** (in a total volume of 100 μL - 200 μL). After the desired reaction time, the reactions were quenched by adding water (100 μL) and the RCC was determined by analysis of a radio-TLC (hexanes:ethyl acetate = 50:50), comparing with the R_f of an authentic sample of (*R*)-**6b**.

Labeling conditions for microwave heating assays were chosen based on our experiences on the radiofluorination of 2-chloropyridine (data not shown): A solution of (*R*)-**6a** (0.5 mL, 5 $mg{\cdot}mL^{-1}$ in DMSO) was added to the dried [^{18}F]KF/K2.2.2 complex and the mixture was transferred to the microwave reactor. The temperature was set to 175 °C for 10 min by applying 100 W power. The reaction was stopped by addition of 0.5 mL of water and the reaction outcome was analyzed as described above.

Radiosynthesis of (*R*)-[^{18}F]**6b** was performed by reaction of precursor (*R*)-**6a** and dried [^{18}F]KF/K2.2.2 complex under microwave irradiation as above described. The reaction was stopped and the resulting mixture was transferred (fluid detector controlled) to a semi-preparative HPLC column (Waters µBondapak® C18, 300x7.8 mm, 10 µm particle size) under a flow (4 mL·min^{-1}) of a mixture of 0.01 M H_3PO_4/acetonitrile (60:40). The product (*R*)-[^{18}F]**6b** eluted from the column after 5 min and was immediately collected in distilled water (80 mL). This aqueous solution was successively passed through a pre-conditioned (10 mL ethanol, 20 mL water) C18 cartridge, which, after this process, was washed with additional water (10 mL). Ethanol (1 mL) followed by saline solution (0.9%, 3 mL,) were passed through the cartridge to elute the product and the product solution was mixed with phosphate-buffered saline solution (6 mL, pH 7.4). Finally, the pure and reformulated (*R*)-[^{18}F]**6b** solution was filtered under laminar air flow.

Quality control of the radiotracer included the determination of (radio)chemical purity and molar radioactivity *via* HPLC using an X-Bridge BEH Shield RP-18 column (4.6 × 50 mm, 2.5 µm, 130 Å) and a mixture of 60% acetonitrile and 40% phosphate buffer (pH = 9.3), as stationary and mobile phases, respectively. Additionally, a TLC based assay (acetonitrile:water = 70 : 30) was used to confirm the amount of [^{18}F]fluoride in the radiotracer formulation. Additional tests, i.e. pH, osmolality, radionuclide purity, K2.2.2 and residual solvents content, sterility and absence of endotoxins, were performed following standard procedures of the PET Centre of the Vienna General Hospital/Medical University of Vienna.

In vitro preclinical evaluation: Genotyping assays were performed similarly to our previous investigations for this study.[1]

Binding affinity: Assays were conducted as already described[1,2] incubating [^{3}H]PK11195 (5 nM), increasing concentration solutions of (*R*)-**6b**, and TSPO-expressing thrombocyte membranes[3] (from genotyped volunteers, 250 μg total protein.ml^{-1}, determined by colorimetric measurement at 562 nm, as described in the instructions' manual of the BCA kit) at 37 °C. A 20 μM PK11195 solution was used *in lieu* of (*R*)-**6b** in order to determine the non-specific binding, whereas total binding was assessed by incubating [^{3}H]PK11195 alone with membrane suspension. All dilutions were performed in tris-HCl buffer (50 mM tris base, 140 mM NaCl, 1.5 mM $MgCl_2$, 5 mM KCl, 1.5 mM $CaCl_2$, pH 7.4), to keep the concentration of DMSO [used for the initial dissolution of (*R*)-**6b**] lower than 1% of the final solution. IC_{50} values were obtained from competition plots (n=3) analyzed by GraphPad Prism® software and K_i values were calculated using the Cheng-Prusoff equation.[4]

Lipophilicity measurements: The log*P* was determined *via* a literature known UV-HPLC method (n=3).[5,6]

AGP binding: AGP binding assays (n=3) were carried out as previously reported[7] using our newly developed tracer (*R*)-[^{18}F]**6b** for the incubation with AGP. Stability testing in human liver microsomes and bone binding studies. Procedures described in detail by Rami-Mark *et al*. were followed.[8] In our case, incubations were performed with (*R*)-[^{18}F]**6b**.

***In vivo* imaging:** Mice were anesthetized using a mixture of isoflurane/oxygen (2.5:97.5; 1.5 mL·min^{-1}). During the scan time, vital signs of the animals were monitored. All animals received a cone beam CT, which was further processed for attenuation correction. Parameters of the small animal cone beam computed tomography scanner were set to full rotation with 360 projections, 4x4 binning, 80 KV voltage, 500 μA current and exposure time 200 ms (duration 7 min). The raw data were reconstructed with the implemented

Feldkamp algorithm with a ramp filter and x2 downsampling resulting in a 512 × 512 image resolution. After the CT, tracer application was performed dynamically via an intravenous injection of 8±2 MBq of (*R*)-[^{18}F]**6b** (128±9 GBq/μmol) during the PET measurement, which was performed for 60 min (baseline mice, n=3). For displacement experiments, PK11195 (5 mg/kg, n= 3) was administered 30 min after radiotracer injection and the dynamic scan was continued to a total scan time of 60 min. The dynamic list mode data were computed into three-dimensional sinograms with following frame durations: 1 × 3s, 3 × 2s, 1 × 6s, 1 × 15s, 1 × 35s, 1 × 145s, 2 × 270s, 1 × 445s, 1 × 600s, 2 × 20s, 2 × 30s, 1 × 500s, 1 × 200s, 1 × 5s. Images were reconstructed with the implemented OSEM3D/OP-MAP algorithm applying scatter and attenuation correction. The algorithm processed the reconstruction with 2 iterations for OSEM and 18 iterations for MAP algorithm. Image data had a matrix size of 256 × 256 and were corrected for random events, dead time and radioactive decay.

Post-processing: All postprocessing steps were performed with the PMOD software version 3.8 (PMOD Technologies Ltd., Zurich, Switzerland). PET images were pre-filtered isotopically with a 3D Gaussian of 0.5 mm. Image reduction by the factor 2 was applied to the CT images to result in the same matrix size. The reconstructed CT and PET images were aligned using rigid registration. Volumes of Interest (VOIs) were segmented on the fused images. Time-activity curves were extracted from defined VOIs and normalized to injected dose. Pre and postblocking images were calculated from the dynamic scans by defining the time average of the following frames: pre-blocking: 9-13 (210-1815 s) and post-blocking: 14-19 (1835-3600 s).

***Ex vivo* preclinical evaluation:** After the dynamic scans, the same animals were sacrificed and the organs and fluids of interest were removed. The radioactivity in the organs was

measured, weight-normalized, and expressed as the percentage of injected dose per gram of tissue (%ID/g).

***Ex vivo* stability:** Heart, lung, and brain from biodistribution studies were further processed to determine the amount of intact radiotracer present in such tissues. In detail, blood was centrifuged for 5 min (15,000 rpm; 4 °C) and the obtained plasma was mixed with an equal volume of an acetonitrile/methanol (10:1), vortexed and centrifuged again for 5 min (15,000 rpm; 4 °C). The resulting supernatant was analyzed by means of radio-HPLC. Likewise, lung and brain tissues were homogenized in acetonitrile/methanol (10:1) with a tissue disruptor and further centrifuged for 5 min (15,000 rpm; 4 °C). The resulting supernatants were similarly subjected to radio-HPLC analysis.

ASSOCIATED CONTENT

Supporting Information

Additional information available online free of charge (http://oubs.acs.org.) includes: ^{1}H, ^{13}C and ^{19}F NMR, compound determination (via HPLC), optimization of radiochemical reaction conditions, *ex vivo* evaluation of the target compound.

AUTHOR INFORMATION

Corresponding Author

Katharina Pallitsch: katharina.pallitsch@univie.ac.at. Phone: +43 (0) 1 4277 52105

Wolfgang Wadsak: wolfgang.wadsak@meduniwien.ac.at. Phone: +43 (0) 1 40400 55330

Author Contributions

[‡] These authors contributed equally as first authors.

[†] These authors contributed equally as last authors.

[*] These authors contributed equally as corresponding authors

Acknowledgements

This scientific project was performed with the support of the Medical Imaging Cluster of the Medical University of Vienna. The authors want to thank Friedrich Girschele and Mag. pharm. Stefan Schmitl for their collaboration in the binding affinity assays, as well as the Preclinical Imaging Laboratory Team from the Medical University of Vienna for its valuable support on the animal experiments.

Abbreviations used

K2.2.2, 4,7,13,16,21,24-Hexaoxa-1,10-diazabicyclo[8.8.8]hexacosane; EtOAc, Ethyl acetate; DMF, *N*,*N*-Dimethylformamide; DMSO, Dimethyl sulfoxide; DME, 1,2-Dimethoxyethane.

References

[1] Braestrup, C.; Squires, R. F. *Proc. Natl. Acad. Sci. U.S.A.* Specific Benzodiazepine Receptors in Rat Brain Characterized by High-Affinity (3H)Diazepam Binding. **1977**, *74*, 3805-3809.

[2] Papadopoulos, V.; Baraldi, M.; Guilarte, T. R.; Knudsen, T. B.; Lacapère, J.-J.; Lindemann, P.; Norenberg, M. D.; Nutt, D.; A. Weizman, A.; Zhang, M. R.; et al. *Trends Pharmacol. Sci.* Translocator Protein (18kda): New Nomenclature for the Peripheral-Type Benzodiazepine Receptor Based on its Structure and Molecular Function. **2006**, *27*, 402-409

[3] Denora, N.; Natile, G. *Int. J. Mol. Sci.* An Updated View of Translocator Protein (TSPO). **2017**, *18*, 2640-2644.

[4] Austin, C. J. D.; Kahlert, J.; Kassiou, M.; Rendina, L. M. *Int. J. Biochem. Cell Biol.* The Translocator Protein (TSPO): A Novel Target for Cancer Chemotherapy. **2013**, *45*, 1212-1216.

[5] Motloch, L. J.; Hu, J.; Akar, F. G. *Oxid. Med. Cell Longev.* The Mitochondrial Translocator Protein and Arrhythmogenesis in Ischemic Heart Disease. **2015**, Article ID 234104.

[6] Giannaccini, G.; Betti, L.; Palego, L.; Pirone, A.; Schmid, L.; Lanza, M.; Fabbrini, L.; Pelosini, C.; Maffei, M.; Santini, F.; et al. *BMC Neurosci.* Serotonin Transporter (SERT) and Translocator Protein (TSPO) Expression in the Obese Ob/Ob Mouse. **2011**, 12:18.

[7] Dupont, A.-C.; Largeau, B.; Santiago Ribeiro, M. J.; Guilloteau, D.; Tronel, C.; Arlicot, N. *Int. J. Mol. Sci.* Translocator Protein-18 Kda (TSPO) Positron Emission Tomography (PET) Imaging and its Clinical Impact in Neurodegenerative Diseases. **2017**, *18*, 785-821.

[8] Janssen, B.; Vugts, D.; Windhorst, A.; Mach, R.; Janssen, B.; Vugts, D. J.; Windhorst, A. D.; Mach, R. H. *Molecules* PET Imaging of Microglial Activation—Beyond Targeting TSPO. **2018**, *23*, 607-620.

[9] Boutin, H.; Prenant, C.; Maroy, R.; Galea, J.; Greenhalgh, A. D.; Smigova, A.; Cawthorne, C.; Julyan, P.; Wilkinson, S. M.; Banister, S. D.; et al. *PLOS One* [^{18}F]DPA-714: Direct Comparison with [^{11}C]PK11195 in a Model of Cerebral Ischemia in Rats. **2013**, *8*, e56441.

[10] Imaizumi, M.; Kim, H.-J.; Zoghbi, S. S.; Briard, E.; Hong, J.; Musachio, J. L.; Ruetzler, C.; Chuang, D.-M.; Pike, V. W.; Innis, R. B.; et al. *Neurosci. Lett.* PET Imaging with [^{11}C]PBR28 Can Localize and Quantify Upregulated Peripheral Benzodiazepine Receptors Associated with Cerebral Ischemia in Rat. **2007**, *411*, 200-205.

[11] Wilson, A. A.; Garcia, A.; Parkes, J.; McCormick, P.; Stephenson, K. A.; Houle, S.; Vasdev, N. *Nucl. Med. Biol.* Radiosynthesis and Initial Evaluation Of [^{18}F]-FEPPA for PET Imaging Of Peripheral Benzodiazepine Receptors. **2008**, *35*, 305-314.

[12] James, M. L.; Fulton, R. R.; Henderson, D. J.; Eberl, S.; Meikle, S. R.; Thomson, S.; Allan, R. D.; Dolle, F.; Fulham, M. J.; Kassiou, M. *Bioorg. Med. Chem.* Synthesis and in vivo Evaluation of a Novel Peripheral Benzodiazepine Receptor PET Radioligand. **2005**, *13*, 6188-6194.

[13] Owen, D. R.; Yeo, A. J.; Gunn, R. N.; Song, K.; Wadsworth, G.; Lewis, A.; Rhodes, C.; Pulford, D. J.; Bennacef, I.; Parker, C. A.; et al. *J. Cereb. Blood Flow Metab.* An 18-Kda Translocator Protein (TSPO) Polymorphism Explains Differences in Binding Affinity of the PET Radioligand PBR28. **2012**, *32*, 1-5.

[14] Owen, D. R.; Guo, Q.; Rabiner, E. A.; Gunn, R. N. *Clin. Transl. Imaging* The Impact of the rs6971 Polymorphism in TSPO for Quantification and Study Design. **2015**, *3*, 417-422.

[15] Zanotti-Fregonara, P.; Zhang, Y.; Jenko, K. J.; Gladding, R. L.; Zoghbi, S. S.; Fujita, M.; Sbardella, G.; Castellano, S.; Taliani, S.; Martini, C.; et al. *ACS Chem. Neurosci.* Synthesis and Evaluation of Translocator 18 Kda Protein (TSPO)

Positron Emission Tomography (PET) Radioligands with Low Binding Sensitivity to Human Single Nucleotide Polymorphism rs6971. **2014**, *5*, 963-971.

[16] Ikawa, M.; Lohith, T. G.; Shrestha, S.; Telu, S.; Zoghbi, S. S.; Castellano, S.; Taliani, S.; Settimo, F. D.; Fujita, M.; Pike, V. W.; et al. *J. Nucl. Med.* ^{11}C-ER176, A Radioligand for 18-Kda Translocator Protein, has Adequate Sensitivity to Robustly Image All Three Affinity Genotypes in Human Brain. **2017**, *58*, 320-325.

[17] Fujita, M.; Kobayashi, M.; Ikawa, M.; Gunn, R. N.; Rabiner, E. A.; Owen, D. R.; Zoghbi, S. S.; Haskali, M. B.; Telu, S.; Pike, V. W.; et al. *EJNMMI Res.* Comparison of Four ^{11}C-Labeled PET Ligands to Quantify Translocator Protein 18 Kda (TSPO) In Human Brain: (*R*)-PK11195, PBR28, DPA-713, and ER176-Based on Recent Publications that Measured Specific-to-Non-Displaceable Ratios. **2017**, *7(1)*, 84.

[18] Kalina, T.; Berroterán-Infante, N.; Schmitl, S.; Vraka, C.; Hacker, M.; Mitterhauser, M.; Pallitsch, K.; Wadsak, W. *Future Med. Chem.* Synthesis and in vitro Evaluation of New Translocator Protein Ligands Designed for Positron Emission Tomography. **2019** in press.

[19] Tucker, S. C.; Brown, J. M.; Oakes, J.; Thornthwaite, D. *Tetrahedron* Resolution And Coupling of 1-(2′-Hydroxy-1′-Naphthyl)Isoquinolines. **2001**, *57*, 2545-2554.

[20] Owen, D. R. J.; Gunn, R. N.; Rabiner, E. A.; Bennacef, I.; Fujita, M.; Kreisl, W. C.; Innis, R. B.; Pike, V. W.; Reynolds, R.; Matthews, P. M.; et al. *J. Nucl. Med.* Mixed-Affinity Binding in Humans with 18-Kda Translocator Protein Ligands. **2011**, *52*, 24-32.

[21] Shah, P.; Westwell, A. D. J. Enzyme Inhib. Med. Chem. The Role of Fluorine in Medicinal Chemistry. 2007, 22, 527-540.

[22] Owen, D. R. J., Matthews, P. M. in International Review of Neurobiology: Guest, P.C., Bahn S., Eds.; Academic Press: Cambridge, 2011, pp. 19–39.

[23] Vraka, C.; Nics, L.; Wagner, K.-H.; Hacker, M.; Wadsak, W.; Mitterhauser, M. Nucl. Med. Biol. Logp, A Yesterday's Value? 2017, 50, 1-10.

[24] Preshlock, S.; Tredwell, M.; Gouverneur, V. Chem. Rev. ^{18}F-Labeling of Arenes and Heteroarenes for Applications in Positron Emission Tomography. 2016, 116, 719-766.

[25] Dolci, L.; Dolle, F.; Jubeau, S.; Vaufrey, F.; Crouzel, C. J. Label. Compd. Radiopharm. 2[^{18}F]Fluoropyridines by No-Carrier-Added Nucleophilic Aromatic Substitution with [18F]FK-K222—A Comparative Study. 1999, 42, 975-985.

[26] Naumiec, G. R.; Cai, L.; Lu, S.; Pike, V. W. Eur. J. Org. Chem. Quinuclidine and DABCO Enhance the Radiofluorination of 5-Substituted 2-Halopyridines. 2017, 45, 6593-6603.

[27] Smits, R.; Fischer, S.; Hiller, A.; Deuther-Conrad, W.; Wenzel, B.; Patt, M.; Cumming, P.; Steinbach, J.; Sabri, O.; Brust, P.; et al., Bioorg. Med. Chem. Synthesis and Biological Evaluation of Both Enantiomers of [^{18}F]Flubatine, Promising Radiotracers with Fast Kinetics for the Imaging of α4β2-Nicotinic Acetylcholine Receptors. 2014, 22, 804-812.

[28] Yue, X.; Yan, X.; Wu, C.; Niu, G.; Ma, Y.; Jacobson, O.; Shen, B.; Kiesewetter, D. O.; Chen, X. Mol. Pharm. One-Pot Two-Step Radiosynthesis of a New ^{18}F-Labeled

Thiol Reactive Prosthetic Group and its Conjugate for Insulinoma Imaging. 2014, 11, 3875-3884.

[29] Council of Europe, Radiopharmaceutical preparations. In: Europäisches Arzneibuch (European pharmacopoeia), Verlag Österreich GmbH: Vienna, 2008, pp. 995.

[30] Lockhart, A. M; Davis, B.; Matthews, J. C.; Rahmoune, H.; Hong, G.; Gee, A.; Earnshaw, D.; Brown, J. *Nucl. Med. Biol.* The Peripheral Benzodiazepine Receptor Ligand PK11195 Binds with High Affinity to the Acute Phase Reactant A1-Acid Glycoprotein: Implications for the Use of the Ligand as a CNS Inflammatory Marker. **2003**, *30*, 199-206.

[31] Eberl, S.; Katsifis, A.; Peyronneau, M. A.; Wen, L.; Henderson, D.; Loc'h, C.; Greguric, I.; Verschuer, J.; Pham, T.; Lam, P.; et al. *Eur. J. Nucl. Med. Mol. Imaging* Preclinical in vivo and in vitro Comparison of the Translocator Protein PET Ligands [^{18}F]PBR102 and [^{18}F]PBR111. **2017**, *44*, 296-307.

[32] Rami-Mark, C.; Eberherr, N.; Berroterán-Infante, N.; Vanicek, T.; Nics, L.; Lanzenberger, R.; Hacker, M.; Wadsak, W.; Mitterhauser, M. *Nucl. Med. Biol.* [^{18}F]Fmener-D2: A Systematic in vitro Analysis of Radio-Metabolism. **2016**, *43*, 490-495.

5. BINDING AFFINITY OF SOME ENDOGENOUS AND SYNTHETIC TSPO LIGANDS REGARDING THE RS6971 POLYMORPHISM

Berroterán-Infante N, Tadik M, Hacker M, Wadsak W, Mitterhauser M.

Int J Mol Sci, In Press.

I designed and performed the binding affinity experiments. In addition, I analyzed the data and wrote the manuscript.

Communication

Binding Affinity of some Endogenous and Synthetic TSPO Ligands regarding the rs6971 Polymorphism

Neydher Berroterán-Infante [1,2], Monika Tadic [1], Marcus Hacker [1], Wolfgang Wadsak [1,2,3,*] and Markus Mitterhauser [1,4]

[1] Division of Nuclear Medicine, Department of Biomedical Imaging and Image-guided Therapy, Medical University of Vienna, Vienna, Austria.
[2] Department of Inorganic Chemistry, University of Vienna, Vienna, Austria.
[3] Center for Biomarker Research, CBmed, Graz, Austria.
[4] LBI Applied Diagnostics, Vienna, Austria.
* Correspondence: wolfgang.wadsak@meduniwien.ac.at; Tel.: +43-1-40400-55330.

Received: date; Accepted: date; Published: date

Abstract: The 18 kDa translocator protein (TSPO) is an intriguing target involved in several pathophysiological processes, whose exact functions remain elusive until now. A single nucleotide polymorphism in the *TSPO* gene influences the binding affinity of endogenous and synthetic TSPO ligands by facilitating a lower-affinity conformation, which modifies a potential ligand binding site, ultimately leading to a binding profile classification according to each genotype. For instance, some clinical effects of the distinctive binding affinity profile of cholesterol toward the TSPO of individuals with different genotypes have been extensively discussed. Therefore, we conducted an investigation based on a radioligand binding assay, to determine the inhibition constants of some reported endogenous TSPO ligands (diazepam binding inhibitor and protoporphyrin IX) as well as synthetic ligands (disulfiram and derivatives). We observed no dependency of the polymorphism on the binding affinity of the evaluated endogenous ligands, whereas a high dependency on the binding affinity of the tested synthetic ligands was evident.

Keywords: TSPO; rs6971 polymorphism; DBI; PPIX; disulfiram; binding affinity; radioligand.

1. Introduction

The 18 kDa translocator protein (TSPO) was first described as a peripheral binding site of some benzodiazepines [1,2]. It has been identified as a key component of the outer mitochondrial membrane (OMM), where it contributes to important mitochondrial tasks. Its involvement in a multitude of physiological functions, such as synthesis of steroids and heme, cell differentiation, and apoptosis, has been recently explained on the basis of the modulation of cell nuclear gene expression *via* the mitochondria-to-nucleus signaling pathway. Furthermore, the TSPO has been proposed to be dysregulated in a variety of diseases, including neurological and psychiatric disorders, several types of cancer and heart insufficiency [3–8]. Therefore, a plethora of endogenous and synthetic substances) have been suggested as (more or less specific) TSPO ligands to fully characterize the pathophysiological role of this protein. For instance, cholesterol has been pointed out as the main endogenous TSPO ligand due to the involvement of TSPO in steroidogenesis. Other endogenous ligands include the tetrapyrroles, heme and protoporphyrin IX (PPIX), as well as the polypeptide diazepam binding inhibitor (DBI). Likewise, several benzodiazepines, isoquinolinecarboxamides, aryolxyanilides, and other classes of compounds are known as TSPO-targeting ligands [9–11]. Independently of their high or low binding affinity, TSPO ligands have demonstrated their ability to modulate, in different grades, several TSPO functions and even have been proposed as therapeutic agents for TSPO-mediated diseases [12-15]. Interestingly, a single

nucleotide polymorphism (SNP) in the *TSPO* gene (rs6971 polymorphism), which replaces alanine by threonine (Ala147Thr) in a non-conservative way, is known to influence the binding affinity of some TSPO ligands (endogenous and synthetic) according to the exhibited genotype. In detail, the binding affinities of such ligands vary among individuals with different genotype. Three affinity patterns related to this SNP can be distinguished as follows: high-affinity-binders (HAB, homozygotes), mixed-affinity-binders (MAB, heterozygotes) and low-affinity-binders (LAB, homozygotes) [16,17]. The nature of this distinctive binding affinity has been explained based on allosteric modulations observed in LAB [18]. Although this heterogeneous binding affinity has mainly affected the development of appropriate radioligands for positron emission tomography (PET), this polymorphism has also been associated to several anxiety-related clinical conditions [19–22]. The link between the rs6971 polymorphism and such disorders has been recently explained on the basis of the lower affinity of cholesterol toward the TSPO in LAB [23]. Since the rs6971 polymorphism plays a pivotal role in the molecular characterization of the TSPO and consequently in the development of new TSPO ligands, we aimed to conduct a study to determine the influence of the rs6971 polymorphism on the binding affinity of two endogenous TSPO ligands: PPIX and DBI. In addition, disulfiram, a drug used for the treatment of alcoholism, and some of its derivatives were selected as synthetic TSPO ligands. This selection was based on a recent report by Yang *et al*, in which the disulfiram metabolite, dietyl-dithiocarbamate (DDC), was radiolabeled with the PET radionuclide copper-64 {[^{64}Cu]Cu-DDC} and proposed as a TSPO PET ligand without any information regarding its sensitivity towards the rs6971 polymorphism [24].

2. Results

The endogenous ligands, protoporphyrin IX (PPIX) and diazepam binding inhibitor (DBI), as well as the synthetic compounds disulfiram (DIS) and its derivatives: sodium diethyldithiocarbamate (DDC), cupric diethyldithiocarbamate (Cu-DDC), methyl diethyldithiocarbamate (Me-DDC), *S*-methyl-*N*,*N*-diethyldithiocarbamate Sulfoxide (Me-DDC Sulfoxide), *S*-methyl-*N*,*N*-diethylthiocarbamate (Me-DTC) and *N*,*N*-diethyl-1-(methylsulfinyl)methanamide (Me-DTC Sulfoxide) were selected to perform radioligand binding assays by inhibiting the binding of [^{3}H]PK11195 (a known TSPO ligand (K_d 29.25 nM), which binds to TSPO independent of the rs6971 polymorphism) in platelets membranes derived from subjects genotyped as HAB, MAB and LAB according to a well described assay [7]. Inhibition constants (K_i) are shown in table 1. All data fitted to single-site model.

Table 1. Inhibition constants (K_i) of the tested substances toward TSPO using [^{3}H]PK11195 as comparator (K_d 29.25 nM). Mean values ± SD are given (n=3)

Substance	HAB (μM)	MAB (μM)	LAB (μM)
PPIX	0.033±0.003	0.033±0.001	0.035±0.003
DBI	6.1±0.9	6.0±0.7	6±1
DIS	2.2±0.6	2.3±0.2	2.6±0.5
Cu-DDC	33±2	47±5	107±6
DDC	136±10	367±9	531±25
Me-DDC	166±20	347±30	574±42
Me-DDC Sulfoxide	314±5	1883±186	2666±253
Me-DTC	559±13	2732±80	3639±324
Me-DTC Sulfoxide	2822±206	4646±763	7118±972

3. Discussion

To the best of our knowledge, this is the first work reporting K_i values of the endogenous TSPO ligands PPIX and DBI, as binding affinity indicator, within a setup using human material. All other

studies involved the use of murine TSPO-expressing membranes. Nevertheless, our values are in agreement with those studies, in which nanomolar and micromolar ranges were reported for the binding affinities of PPIX and DBI, respectively. Moreover, our results show no dependency of the binding affinity of these two endogenous ligands regarding the rs6971 polymorphism. Hence, we propose that there will be no clinically relevant difference due to the biological binding of PPIX and DBI to TSPO of individuals of different genotype, as in the case of cholesterol [23].

Interestingly, affinities in the micromolar range were obtained for all disulfiram-related substances, including Cu-DDC. This is an interesting finding, due to the recent claim of [^{64}Cu]Cu-DDC as a potential TSPO PET tracer, for which a very high affinity (nanomolar range) is normally required [25]. In this regard, we suggest a re-evaluation of this compound as a TSPO PET tracer, especially considering the proposed *in vivo* radiosynthesis {by injecting disulfiram and [^{64}Cu]$CuCl_2$ separately} [20], since the binding affinity of disulfiram is higher than the binding affinity of Cu-DDC, as shown in table 1. Such evaluation should also consider the affinities of all potential disulfiram metabolites (DDC, Me-DDC, Me-DDC Sulfoxide, Me-DTC and Me-DTC Sulfoxide) toward TSPO as they will compete for the molecular target *in vivo*. Remarkably, we found for this series, that only disulfiram itself exhibited a K_i value independent of the genotype group, whereas all derivatives displayed a strong dependency on the rs6971 polymorphism.

Although only few substances were tested, this study highlights the importance of evaluating the effects of the rs6971 polymorphism on the binding affinity of TSPO ligands. To this list of compounds, additional substances may be added. For instance, none of the benzodiazepines proposed as TSPO ligands have been thoroughly investigated to the best of our knowledge, regarding their binding affinities considering the rs6971 polymorphism so far.

In the future, it will be interesting to evaluate how these findings might influence the understanding of TSPO functionality in healthy and pathological tissues during the course of disease. It became obvious that a thorough preclinical evaluation also considering the specific binding affinities using human tissue samples is of great importance, particularly combining these findings with the residence time of ligands at the TSPO binding sites.

4. Materials and Methods

All chemicals were obtained from commercial sources (Sigma Aldrich, TCI or Santa Cruz Biotechnology). All solvents and chemicals were used as purchased without further purification. The inhibition constants of all substances were determined through competitive radioligand binding assays, using TSPO-expressing membranes obtained from previously genotyped subjects regarding the rs6971 polymorphism [7] and prepared as described elsewhere [16,17]. Briefly, venous blood (80 mL) was collected in EDTA-containing tubes from healthy volunteers identified as HAB, MAB and LAB. Afterwards, whole blood was centrifuged at room temperature for 15 minutes (180*g). The resulting supernatant was centrifuged at room temperature for 15 minutes (1800*g) and a platelet pellet was obtained. Subsequently, the pellet was homogenized with buffer 1 (0.32 mM sucrose, 5 mM tris base, 1 mM $MgCl_2$, pH 7.4, 4 °C) and centrifuged at 4 °C for 15 minutes (48000*g) three times, with removal of the supernatant and re-homogenization of the pellet using buffer 2 (50 mM tris base, 1 mM $MgCl_2$, pH 7.4, 4 °C; *no sucrose*) after each centrifugation step. Finally, the resulting membrane was mixed with 3 mL of buffer 2 and aliquots were stored at −80 °C until use. The total protein concentration of the membrane was determined via colorimetric detection of cuprous cation (Cu^{1+}) by bicinchoninic acid (BCA) measuring the absorbance at 562 nm (Synergy HTX plate multimode reader, Biotek, Winooski, USA), following the instructions manual of the BCA kit (ThermoFisher Scientific, Waltham, USA).

Following the procedure described by Owen *et al*. [16], the radioligand binding assays were performed in test tubes, filled with 250 µL of the tested substance dissolved in assay buffer (50 mM tris base, 140 mM NaCl, 1.5 mM $MgCl_2$, 5 mM KCl, 1.5 mM $CaCl_2$, pH 7.4, 37 °C), 200 µL of the membrane suspension (250 $\mu g.mL^{-1}$) and 50 µL of a 10 nM [^{3}H]PK11195 (3,149 $TBq.mmol^{-1}$, Perkin Elmer, Waltham, USA) solution. Non-specific binding was determined using 20 µM PK11195

instead of the tested substance, whereas total binding was assessed by incubating only [^{3}H]PK11195 and membrane suspension. Incubations were carried out for 1 h at 37 °C. After this time, binding was terminated with ice cold wash buffer (50 mM tris base, 1.4 mM $MgCl_2$, pH 7.4, 4 °C), while filtrating the membrane bound through GF/B glass fiber filters (Brandel, Gaithersburg, USA) presoaked in assay buffer containing 0.05% polyethylene imine. In addition, 3 mL of wash buffer were passed through the filters and these were transferred into β-counting vials. Finally, 4 mL of β-scintillation cocktail (Perkin Elmer, Waltham, USA) were added and the radioactivity was counted (Hidex 300SL beta counter, Hidex, Turku, Finland). Data from the competition plots were analyzed and IC50 and K_i values were calculated using a dissociation constant of 29.25 nM for [^{3}H]PK11195 and GraphPad Prism® software.

Author Contributions: concept/design, N.B.I. and W.W.; methodology, N.B.I. and M.M.; validation, N.B.I., M.T., W.W. and M.M.; formal analysis, N.B.I.; investigation, N.B.I. and M.T.; resources, M.H., W.W. and M.M.; data curation, N.B.I., M.H., W.W., M.M.; writing—original draft preparation, N.B.I.; writing—reviewing and editing, N.B.I., M.T., M.H., W.W. and M.M..; supervision, W.W. and M.M; draft release – all authors.

Funding: This research received no external funding.

Acknowledgments: This scientific project was performed with the support of the Medical Imaging Cluster of the Medical University of Vienna.

Conflicts of Interest: Without relevance to this work, Wolfgang Wadsak discloses being a part-time employee of CBmed Ltd, Graz, Austria, and having received research grants from Eckert-Ziegler AG, Germany, Scintomics, Germany, Ipsen Pharma, Germany, and ITG GmbH, Germany. Neydher Berroterán-Infante is recipient of the Chemical Monthly Stipendium of the Austrian Academy of Sciences. The funding agency had no role in the design of the study; in the collection, analyses, or interpretation of data; in the writing of the manuscript, or in the decision to publish the results. All other authors declare no conflict of interest

Abbreviations

TSPO	18 kDa translocator protein
PPIX	Protoporphyrin IX
DBI	Diazepam binding inhibitor
HAB	High-affinity binders
MAB	Mixed-affinity binders
LAB	Low-affinity binders
DIS	Disulfiram
DDC	Sodium diethyldithiocarbamate
Cu-DDC	Cupric diethyldithiocarbamate
Me-DDC	Methyldiethyldithiocarbamate
Me-DDC Sulfoxide	*S*-methyl-*N*,*N*-diethyldithiocarbamate Sulfoxide
Me-DTC	*S*-methyl-*N*,*N*-diethylthiocarbamate Sulfoxide
Me-DTC Sulfoxide	*N*,*N*-diethyl-1-(methylsulfinyl)methanamide
PET	Positron emission tomography

References

1. Braestrup, C.; Squires, R.F. Specific benzodiazepine receptors in rat brain characterized by high-affinity (3H)diazepam binding. *Proc. Natl. Acad. Sci. U.S.A.* **1977**, *74*, 3805–3809.

2. Papadopoulos, V.; Baraldi, M.; Guilarte, T.R.; Knudsen, T.B.; Lacapère, J.-J.; Lindemann, P.; Norenberg, M.D.; Nutt, D.; Weizman, A.; Zhang, M.-R.; et al. Translocator protein (18kDa): new

nomenclature for the peripheral-type benzodiazepine receptor based on its structure and molecular function. *Trends in Pharmacological Sciences* **2006**, *27*, 402–409.

3. Yasin, N.; Veenman, L.; Singh, S.; Azrad, M.; Vainshtein, A.; Caballero, B.; Marek, I.; Gavish, M. Classical and Novel TSPO Ligands for the Mitochondrial TSPO Can Modulate Nuclear Gene Expression: Implications for Mitochondrial Retrograde Signaling. *Int J Mol Sci* **2017**, *18*, 786.

4. Bonsack, F.; Sukumari-Ramesh, S. TSPO: An Evolutionarily Conserved Protein with Elusive Functions. *Int J Mol Sci* **2018**, *19*.

5. Denora, N.; Natile, G. An Updated View of Translocator Protein (TSPO). *Int J Mol Sci* **2017**, *18*.

6. Papadopoulos, V.; Fan, J.; Zirkin, B. Translocator protein (18 kDa): an update on its function in steroidogenesis. *J. Neuroendocrinol.* **2018**, *30*.

7. Berroterán-Infante, N.; Balber, T.; Fürlinger, P.; Bergmann, M.; Lanzenberger, R.; Hacker, M.; Mitterhauser, M.; Wadsak, W. [18F]FEPPA: Improved Automated Radiosynthesis, Binding Affinity, and Preliminary in Vitro Evaluation in Colorectal Cancer. *ACS Med. Chem. Lett.* **2018**, *9*, 177–181.

8. Largeau, B.; Dupont, A.-C.; Guilloteau, D.; Santiago-Ribeiro, M.-J.; Arlicot, N. TSPO PET Imaging: From Microglial Activation to Peripheral Sterile Inflammatory Diseases? *Contrast Media Mol Imaging*, 2017, Article ID 6592139.

9. Veenman, L.; Vainshtein, A.; Yasin, N.; Azrad, M.; Gavish, M. Tetrapyrroles as Endogenous TSPO Ligands in Eukaryotes and Prokaryotes: Comparisons with Synthetic Ligands. *Int J Mol Sci* **2016**, *17*.

10. Kim, T.; Pae, A.N. Translocator protein (TSPO) ligands for the diagnosis or treatment of neurodegenerative diseases: a patent review (2010–2015; part 1). *Expert Opinion on Therapeutic Patents* **2016**, *26*, 1325–1351.

11. Kim, T.; Pae, A.N. Translocator protein (TSPO) ligands for the diagnosis or treatment of neurodegenerative diseases: a patent review (2010 – 2015; part 2). *Expert Opinion on Therapeutic Patents* **2016**, *26*, 1353–1366.

12. James, M.L.; Selleri, S.; Kassiu, M.; Development of ligands for the peripheral benzodiazepine receptor. *Curr. Med. Chem.* **2006**, *13*, 1991-2001.

13. Vainhstein, A.; Veenman, L.; Shterenberg, A.; Singh, S.; Masarwa, A.; Dutta, B.; Island, B.; Tsoglin, E.; Levin, E.; Leschiner, S.; et al. Quinazoline-based tricycilic compounds that regulate programme cell death, induce neuronal differentiation, and are curative in animal models for excitotoxicity and hereditary brain disease. *Cell Death Discovery* **2015**, *1*, 15027.

14. Costa, B.; Cavallini, C.; Da Pozzo, E.; Taliani, S.; Da Settimo, F.; Martini, C. The anxiolytic Etifoxine Binds to TSPO Ro5-4864 Binding Site with Long Residence Time Showing High Neurosteroidogenic Activity. *ACS Chem Neurosci* **2017**, *8*, 1448-1454.

15. Chen, Y.; Veenman, L.; Singh, S.; Ouyang, F.; Liang, J.; Huang, W.; Marek, I.; Zeng, J.; Gavish, M. 2-Cl-MGV-1 Ameloriates Apoptosis in the Thalamus and Hippocampus and Cognitive Deficits after Cortical Infarct Rats. *Stroke* **2017**, *48*, 3366–3374.

16. Owen, D.R.J.; Gunn, R.N.; Rabiner, E.A.; Bennacef, I.; Fujita, M.; Kreisl, W.C.; Innis, R.B.; Pike, V.W.; Reynolds, R.; Matthews, P.M.; et al. Mixed-Affinity Binding in Humans with 18-kDa Translocator Protein Ligands. *J Nucl Med* **2011**, *52*, 24–32.

17. Owen, D.R.; Yeo, A.J.; Gunn, R.N.; Song, K.; Wadsworth, G.; Lewis, A.; Rhodes, C.; Pulford, D.J.; Bennacef, I.; Parker, C.A.; et al. An 18-kDa Translocator Protein (TSPO) Polymorphism Explains Differences in Binding Affinity of the PET Radioligand PBR28. *J Cereb Blood Flow Metab* **2012**, *32*, 1–5.

18. Rojas, C.; Stathis, M.; Coughlin, J.M.; Pomper, M.; Slusher, B.S. The Low-Affinity Binding of Second Generation Radiotracers Targeting TSPO is Associated with a Unique Allosteric Binding Site. *J Neuroimmune Pharmacol* **2017**, 1–5.

19. Costa, B.; Pini, S.; Gabelloni, P.; Da Pozzo, E.; Abelli, M.; Lari, L.; Preve, M.; Lucacchini, A.; Cassano, G.B.; Martini, C. The spontaneous Ala147Thr amino acid substitution within the translocator protein influences pregnenolone production in lymphomonocytes of healthy individuals. *Endocrinology* **2009**, *150*, 5438–5445.

20. Costa, B.; Pini, S.; Martini, C.; Abelli, M.; Gabelloni, P.; Landi, S.; Muti, M.; Gesi, C.; Lari, L.; Cardini, A.; et al. Ala147thr substitution in translocator protein is associated with adult separation anxiety in patients with depression. *Psychiatric Genetics* **2009**, *19*, 110–111.

21. Nakamura, K.; Yamada, K.; Iwayama, Y.; Toyota, T.; Furukawa, A.; Takimoto, T.; Terayama, H.; Iwahashi, K.; Takei, N.; Minabe, Y.; et al. Evidence that variation in the peripheral benzodiazepine receptor (PBR) gene influences susceptibility to panic disorder. *Am. J. Med. Genet. B Neuropsychiatr. Genet.* **2006**, *141B*, 222–226.

22. Colasanti, A.; Owen, D.R.; Grozeva, D.; Rabiner, E.A.; Matthews, P.M.; Craddock, N.; Young, A.H. Bipolar Disorder is associated with the rs6971 polymorphism in the gene encoding 18 kDa Translocator Protein (TSPO). *Psychoneuroendocrinology* **2013**, *38*, 2826–2829.

23. Owen, D.R.; Fan, J.; Campioli, E.; Venugopal, S.; Midzak, A.; Daly, E.; Harlay, A.; Issop, L.; Libri, V.; Kalogiannopoulou, D.; et al. TSPO mutations in rats and a human polymorphism impair the rate of steroid synthesis. *Biochem. J.* **2017**, *474*, 3985–3999.

24. Yang, J.; Yang, J.; Wang, L.; Moore, A.; Liang, S.H.; Ran, C. Synthesis-free PET imaging of brown adipose tissue and TSPO via combination of disulfiram and 64CuCl2. *Scientific Reports* **2017**, *7*, 8298.

25. Wadsak, W.; Mitterhauser, M. Basics and principles of radiopharmaceuticals for PET/CT. *Eur. J. Radiol.* **2010**, *73*, 461-469.

CHAPTER IV
SUMMARY AND DISCUSSION

This doctoral thesis emphasizes the intimate associations between the TSPO and various clinical disorders. During the last years, PET imaging has served as the most prominent technique for *in vivo* assessment of such associations. Moreover, TSPO PET (radio)ligands have demonstrated to provide an important information of this complex target on a molecular level, which all together position them as invaluable tools for further characterization of the TSPO as well as the TSPO-related diseases. If looking at the big picture, these are precisely the class of figures we pursued in this work. Thus, two novel TSPO PET radiopharmaceuticals, (*R*)-[^{11}C]Me@NEBIQUINIDE and (*R*)-[^{18}F]NEBIFQUINIDE, were successfully synthesized and preclinically evaluated. Furthermore, additional insights regarding TSPO were gained: firstly, in colorectal cancer by using the clinical established TSPO PET radiotracer [^{18}F]FEPPA and secondly, in the rs6971 SNP by evaluating the binding affinities of synthetic and endogenous ligands toward the TSPO.

- Aryloxyanilides and their carboxamide derivatives

Despite its high sensitivity against the rs6971 SNP, the PET radiopharmaceutical [^{18}F]FEPPA has been extensively used for clinical investigations in search for TSPO expression changes in psychiatric and neurological disorders. Although interesting findings have been achieved in this regard, its radiosynthesis presented an inconvenient long time for purification of the radiolabeled product from the crude reaction mixture using HPLC, which eventually leads to lower radiochemical yields. An approach consisting in modifying the established conditions for this purification step was developed, which resulted in a significant time reduction affording a small increase in the radiochemical yield. Indeed, an additional method was recently published,[226] in which the purification time was substantially reduced and the removal of HPLC solvents was bypassed. Both methods are easily implemented and reflect the necessity of achieve PET radiopharmaceuticals in shorter reaction times.

The sensitivity of [^{18}F]FEPPA against the rs6971 SNP has been already documented *in vivo*. However, K_i values as indicators for such sensitivity were never reported. Accordingly, competitive binding assays using non-radioactive FEPPA were conducted within the framework of this doctoral thesis to determine the K_i values for each genotype. Interestingly, although the affinity of FEPPA is strongly genotype-dependent, it shows potent values in all groups (HAB, MAB, and LAB).

This work has highlighted the centrality of TSPO in several pathological disorders. Nevertheless, investigations regarding the involvement of TSPO in neurological conditions largely surpass any

other type of disease. The relative low expression of TSPO in healthy brain combined with the high expression observed during neuroinflammation processes offer the epitome for PET imaging. Thus, an *in vitro* study using [^{18}F]FEPPA was conducted in a colorectal cancer cell line as well as in tissues derived from a patient bearing this malignancy. A high and specific uptake was observed in the cell line and in the tumor tissue compared to negative cell line and healthy tissue, respectively. These preliminary results encourage the use of [^{18}F]FEPPA for further investigations, which may aid in the diagnosis and disease follow-up of colorectal cancer.

Based in the structure of the aryloxyanilides [^{18}F]FEPPA and [^{11}C]PBR28, several TSPO ligands were designed for the realization of this dissertation. The new series of compounds VIE_TSPO, named after the city of Vienna and depicted in figure 20, were synthesized along with their radiolabeling precursors with satisfactory yields. Unfortunately, all these ligands were rapidly discarded as potential TSPO PET radiopharmaceuticals due to the poor affinity toward TSPO in the high nanomolar to micromolar range. Moreover, the affinity of these ligands highly depended on the rs6971 SNP, i.e. the worst binding affinities were obtained for LAB. Although their unfavorable binding properties as PET radiopharmaceuticals, these substances (excepting VIE_TSPO_010, whose K_i value was only determined as higher than 30 µM) do exhibit affinity toward the TSPO and should be, therefore, considered as TSPO ligands. These results confirmed not only the requirement of an amide group for TSPO binding, but specifically an acetamide group in the case of aryloxyanilides.

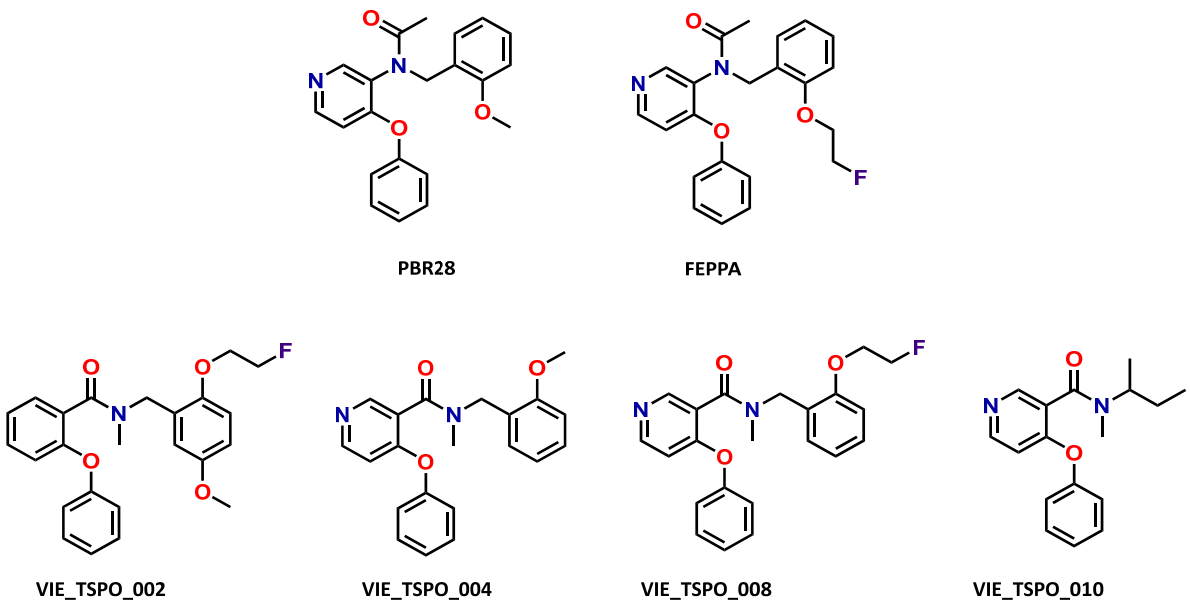

Figure 22. VIE_TSPO compounds developed within the framework of this doctoral thesis: derivatives from PBR28 and FEPPA

- Isoquinolinecarboxamide derivatives

Undeniably, (*R*)-[^{11}C]PK11195 exhibits numerous disadvantageous properties as TSPO PET radiopharmaceutical, which has prompted the search of suitable alternatives for the *in vivo* visualization of the TSPO. However, it serves as leading structure for TSPO ligand development, in particular due to its homogenous binding properties regarding the rs6971 SNP. In fact, the compound [^{11}C]ER-176, a quinazolinecarboxamide derivative of (*R*)-[^{11}C]PK11195 with an additional nitrogen atom in the core ring, has showed promising results, as previously discussed.

Using a similar strategy, two pyridinylisoquinilinecarboxamides analogues of (*R*)-[^{11}C]PK11195 were designed in the present research work, as shown in Figure 21. Strikingly, the two compounds, namely (*R*)-[^{11}C]Me@NEBIQUINIDE and (*R*)-[^{18}F]NEBIFQUINIDE proved to be excellent TSPO PET radiopharmaceuticals. In detail, analysis of their binding affinity demonstrated a high nanomolar affinity of both compounds toward the TSPO, which in addition did not exhibited significant differences regarding the rs971 SNP. Although the lipophilicity is a delicate parameter to judge the performance of a PET radiopharmaceutical, it has been pointed out as determinant property, alongside the plasma protein binding, for the poor pharmacokinetic profile of (*R*)-[^{11}C]PK11195. In this regard, (*R*)-[^{11}C]Me@NEBIQUINIDE and (*R*)-[^{18}F]NEBIFQUINIDE exhibited a reduced log*P* value as well as lower binding to α1-AGP (main plasma protein responsible for the binding of (*R*)-[^{11}C]PK11195) compared to (*R*)-[^{11}C]PK11195. Moreover, *in vitro* metabolic evaluations identified no significant degradation of the compounds. Apparently, the incorporation of the additional nitrogen atom in the aromatic substituent *in lieu* of the isoquinolinic ring offers similar results to the previous strategy. Moreover, it enables the radiolabeling, with the more practical radionuclide fluorine-18, at the halogen position *via* aromatic nucleophilic substitution of the chorine atom, due to the stabilization of the reaction intermediate by inductive and resonance effects exerted by the pyridinyl nitrogen. Due to this practical advantage, (*R*)-[^{18}F]NEBIFQUINIDE was tested in healthy mice. Likewise, excellent *in vivo* results were attained: high stability, biodistribution according to the relative expression of the TSPO, specificity and BBB penetration.

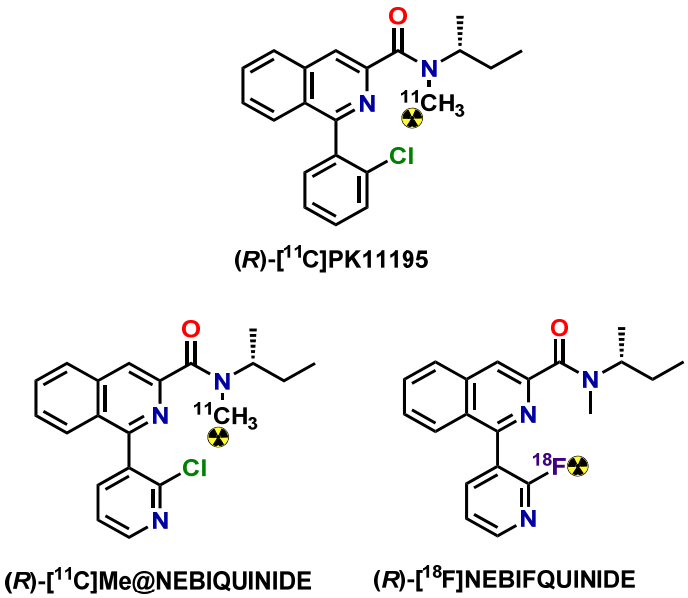

Figure 23. (R)-[^{11}C]Me@NEBIQUINIDE and (R)-[^{18}F]NEBIFQUINIDE derivatives of (R)-[^{11}C]PK11195. Both compounds developed within the framework of this doctoral thesis

- Other synthetic and endogenous TSPO ligands

Even though a countless amount of substances have been proposed as TSPO ligands, not all of them have been studied regarding the rs6971 SNP. Very recently, the low binding of TSPO ligands toward LAB has been rationalized on the basis of allosteric interactions, which are only present in this genotype group.[227] This interesting explanation presenting a further characterization of this intriguing target regarding its multiple binding sites. Moreover, it has been also demonstrated a genotype-dependent affinity of cholesterol toward TSPO,[118] which is associated with steroid-dependent stress and anxiety elements. These fascinating results were the impulse to follow an analysis of a battery of substances regarding their binding affinities toward the TSPO. Protoporphyrin IX as well as DBI served as endogenous ligands, whereas disulfiram and its related metabolites served as synthetic ligands. The choice of disulfiram was based on previous reports of a diethyldithiocarbamate (DDC, disulfiram derivative) ^{64}Cu-radiotracer.

Interestingly, micromolar affinities were obtained for disulfiram and all its metabolites, including Cu-DDC, which does not favor their use as TSPO PET radiopharmaceuticals. In view of these results, a further evaluation is proposed regarding the use of [^{64}Cu]Cu-DDC as potential TSPO PET radiopharmaceutical. A clear line of evidence, regarding the rs6971, polymorphism was not obtained, since some compounds showed genotype dependency, while others did not. Regarding the endogenous ligands, no significant differences were observed between all groups.

CHAPTER V
CONCLUSION AND OUTLOOK

Along the course of this dissertation, the synthesis and/or characterization of several substances as TSPO (PET) ligands have been described. Besides the excellent properties, in conjunction with potential future clinical application, of some substances here developed, the most significant conclusions resulting from this work are described below:

- Although several SAR studies have been conducted to determining ligand affinity toward TSPO, additional studies can provide valuable information for the generation of a new class of ligands, in particular if the diversity of TSPO binding sites is considered. The disclosure of the conformational TSPO structure, in particular the polymorphic variants, may support these investigations.

- Due to the variety of diseases in which TSPO is implicated, novel and established TSPO PET radiopharmaceuticals are powerful probes for further applications in the clinical management of not well studied disorders.

- Despite the last point, it is imperative to mention the description of TSPO as a very general and ubiquitous distributed target, which may not offer the specificity sometimes required to describe particular molecular events. Thus, other targets have been and may be identified to replace TSPO.

- The development of novel TSPO (PET)ligands must include an analysis of their binding affinities regarding the rs6971 SNP. This is of particular importance due to the omission in several publication of such examinations, which leads to a simplification of a very important issue.

In general, the results obtained in this doctoral thesis have been included in 5 peer-reviewed publications. From these articles, 4 publications have already been accepted, whereas 1 is in review process:
ACS Medicinal Chemistry Letters (impact factor 2017: 3.974): 1 peer-reviewed publication.
Nuclear Medicine and Biology (impact factor 2017: 2.203): 1 peer-reviewed publication.
Future Medicinal Chemistry (impact factor 2017: 3.969): 1 peer-reviewed publication.
Journal of Medicinal Chemistry (impact factor 2017: 6.259): 1 publication in review.
International Journal of Molecular Sciences (impact factor: 3.687): 1 peer-reviewed publication.

Moreover, an additional manuscript is in preparation, where the first application of (*R*)-[^{18}F]NEBIFQUINIDE in animal models of non-alcoholic fatty liver disease was examined. In this case, the investigation was also focused in peripheral diseases, whereby (*R*)-[^{18}F]NEBIQUINIDE showed promising results. Logically, additional studies are planned in animal models of neuroinflammation, which, as this doctoral thesis has highlighted, represents the main application of TSPO PET radiopharmaceuticals.

As mentioned in the introductory chapter, the path for PET radiopharmaceuticals into the clinic comprises several steps to assure an excellent performance in humans. Ideally, the results that arose in this dissertation will serve as foundation for the introduction of novel and promising TSPO PET radiopharmaceuticals.

CHAPTER VI
REFERENCES

1. Mankoff DA. A Definition of Molecular Imaging. Journal of Nuclear Medicine. 2007;48(6):18N-21N.

2. Silverman DHS, Melega WP. Molecular Imaging of Biological Processes with PET: Evaluating Biologic Bases of Cerebral Function. In: Phelps ME, editor. PET: Molecular Imaging and Its Biological Applications. New York, NY: Springer New York; 2004. p. 509–583.

3. Kherlopian AR, Song T, Duan Q, Neimark MA, Po MJ, Gohagan JK, Laine AF. A review of imaging techniques for systems biology. BMC Systems Biology. 2008;2(1):74.

4. Gambhir S. General Principles of Molecular Imaging. In: Weissleder R, Ross B, Rehemtulia A, Gambhir S, editors. Molecular Imaging: Principles and Practice. Shelton: Peoples's Medical Publishing House-USA; 2010.

5. Peterson TE, Manning HC. Molecular Imaging: 18F-FDG PET and a Whole Lot More. Journal of Nuclear Medicine Technology. 2009;37(3):151–161.

6. Popovtzer R, Agrawal A, Kotov NA, Popovtzer A, Balter J, Carey TE, Kopelman R. Targeted Gold Nanoparticles enable Molecular CT Imaging of Cancer. Nano letters. 2008;8(12):4593–4596.

7. Kircher MF, Hricak H, Larson SM. Molecular imaging for personalized cancer care. Molecular Oncology. 2012;6(2):182–195.

8. Jung K-H, Lee K-H. Molecular Imaging in the Era of Personalized Medicine. Journal of Pathology and Translational Medicine. 2015;49(1):5–12.

9. Chen Z-Y, Wang Y-X, Lin Y, Zhang J-S, Yang F, Zhou Q-L, Liao Y-Y. Advance of Molecular Imaging Technology and Targeted Imaging Agent in Imaging and Therapy. BioMed Research International. 2014.

10. Pysz MA, Gambhir SS, Willmann JK. Molecular Imaging: Current Status and Emerging Strategies. Clinical radiology. 2010;65(7):500–516.

11. Massoud TF, Gambhir SS. Molecular imaging in living subjects: seeing fundamental biological processes in a new light. Genes & Development. 2003;17(5):545–580.

12. James ML, Gambhir SS. A Molecular Imaging Primer: Modalities, Imaging Agents, and Applications. Physiological Reviews. 2012;92(2):897–965.

13. Cassidy PJ, Radda GK. Molecular imaging perspectives. Journal of the Royal Society Interface. 2005;2(3):133–144.

14. Belcari N, Del Guerra A. High-Resolution and Animal Imaging Instrumentation and Techniques. In: Grupen C, Buvat I, editors. Handbook of Particle Detection and Imaging. Berlin: Springer; 2012. p. 1124–1148.

15. Coleman RE. Radionuclide Imaging in Cancer Medicine. In: Kufe DW, Pollock RP, Weichselbaum RR, Bast RC, Gansler TS, Holland J, Frei E, editors. Holland-Frei Cancer Medicine. 6th edition. Hamilton: BC Decker; 2003.

16. Wu M, Shu J. Multimodal Molecular Imaging: Current Status and Future Directions. Contrast Media & Molecular Imaging. 2018. Article ID 1382183.

17. Hogg P, Lawson R. An overview of nuclear medicine imaging procedures. Nursing Standard (Royal College of Nursing). 2015;30(13):52–59.

18. Force S-TS of PT. Nuclear Medicine Technologist Scope of Practice and Performance Standards. Journal of Nuclear Medicine Technology. 2017;45(1):53–64.

19. Lee Y-S. Radiopharmaceuticals for Molecular Imaging. The Open Nuclear Medicine Journal. 2010; 2:178-185.

20. Imam SK. Molecular nuclear imaging: the radiopharmaceuticals (review). Cancer Biotherapy & Radiopharmaceuticals. 2005;20(2):163–172.

21. Frey KA. Methods in Positron Emission Tomography. In: Siegel GJ, Agranoff BW, Albers RW, Fisher SK, Uhler MD, editors. Basic Neurochemistry: Molecular, Cellular and Medical Aspects. 6th edition. Philadelphia: Lippincott-Raven; 1999.

22. Zanzonico P. Positron emission tomography: a review of basic principles, scanner design and performance, and current systems. Seminars in Nuclear Medicine. 2004;34(2):87–111.

23. Shukla AK, Kumar U. Positron emission tomography: An overview. Journal of Medical Physics / Association of Medical Physicists of India. 2006;31(1):13–21.

24. Vaquero JJ, Kinahan P. Positron Emission Tomography: Current Challenges and Opportunities for Technological Advances in Clinical and Preclinical Imaging Systems. Annual review of biomedical engineering. 2015;17:385–414.

25. Sanghvi D, Harisinghani MG. Modalities in modern radiology: A synopsis. Journal of Postgraduate Medicine. 2010;56(2):85.

26. Anand S, Singh H, Dash A. Clinical Applications of PET and PET-CT. Medical Journal, Armed Forces India. 2009;65(4):353–358.

27. Pichler BJ, Judenhofer MS, Pfannenberg C. Multimodal imaging approaches: PET/CT and PET/MRI. Handbook of Experimental Pharmacology. 2008;(185 Pt 1):109–132.

28. Zaidi H, Del Guerra A. An outlook on future design of hybrid PET/MRI systems. Medical Physics. 2011;38(10):5667–5689.

29. Jones T, Townsend DW. History and future technical innovation in positron emission tomography. Journal of Medical Imaging. 2017;4(1):011013.

30. Matthews PM, Rabiner EA, Passchier J, Gunn RN. Positron emission tomography molecular imaging for drug development. British Journal of Clinical Pharmacology. 2012;73(2):175–186.

31. Wang J, Maurer L. Positron Emission Tomography: applications in drug discovery and drug development. Current Topics in Medicinal Chemistry. 2005;5(11):1053–1075.

32. Kemp RA de, Epstein FH, Catana C, Tsui BMW, Ritman EL. Small-Animal Molecular Imaging Methods. Journal of Nuclear Medicine. 2010;51(Supplement 1):18S-32S.

33. Ametamey SM, Honer M, Schubiger PA. Molecular imaging with PET. Chemical Reviews. 2008;108(5):1501–1516.

34. Wuest F. Fluorine-18 labeling of small molecules: the use of 18F-labeled aryl fluorides derived from no-carrier-added [18F]fluoride as labeling precursors. Ernst Schering Research Foundation Workshop. 2007;(62):51–78.

35. Krasikova R. Synthesis modules and automation in F-18 labeling. Ernst Schering Research Foundation Workshop. 2007;(62):289–316.

36. Claggett SB, Quinn KM, Lazari M, Moore MD, van Dam RM. Simplified programming and control of automated radiosynthesizers through unit operations. EJNMMI Research. 2013;3:53.

37. Padgett HC, Schmidt DG, Luxen A, Bida GT, Satyamurthy N, Barrio JR. Computer-controlled radiochemical synthesis: a chemistry process control unit for the automated production of radiochemicals. International Journal of Radiation Applications and Instrumentation. Part A, Applied Radiation and Isotopes. 1989;40(5):433–445.

38. Alexoff DL, Russell JA, Shiue CY, Wolf AP, Fowler JS, MacGregor RR. Modular automation in PET tracer manufacturing: application of an autosynthesizer to the production of 2-deoxy-2-[18F]fluoro-D-glucose. International journal of radiation applications and instrumentation. Part A, Applied radiation and isotopes. 1986;37(10):1045–1061.

39. Vallabhajosula S, editor. Quality Control of PET Rediopharmaceuticals. In: Molecular Imaging: Radiopharmaceuticals for PET and SPECT. Berlin, Heidelberg: Springer Berlin Heidelberg; 2009. p. 197–204.

40. Schirrmacher R, Wängler C, Schirrmacher E. Fluorine-18 Radiochemistry: Theory and Practice. In: Pharmaceutical Radiochemistry (I). Vol. 1. Hans J. Wester. Fürstenfeldbrück: Scintomics Print Media and Publishing; 2010. (Munich Molecular Imaging Handbook Series).

41. Coenen HH, Gee AD, Adam M, Antoni G, Cutler CS, Fujibayashi Y, Jeong JM, Mach RH, Mindt TL, Pike VW, et al. Consensus nomenclature rules for radiopharmaceutical chemistry — Setting the record straight. Nuclear Medicine and Biology. 2017;55:v–xi.

42. Crane HR, Lauritsen CC. Radioactivity from Carbon and Boron Oxide Bombarded with Deutons and the Conversion of Positrons into Radiation. Physical Review. 1934;45(6):430–432.

43. Henriksen G. 11C-Labelled Tracers for use in PET: Concepts and Selected Labelling Strategies for Preparative Radiosynthesis. In: Pharmaceutical Radiochemistry (I). Vol. 1. Hans J. Wester. Fürstenfeldbrück: Scintomics Print Media and Publishing. (Munich Molecular Imaging Handbook Series).

44. Wolf AP, Redvanly CS. Carbon-11 and radiopharmaceuticals. The International Journal of Applied Radiation and Isotopes. 1977;28(1):29–48.

45. Comar D, Maziere M, Crouzel C. Radiopharmaceuticals and Labelled Compounds. IAEA. Vienna; 1973.

46. Larsen P, Ulin J, Dahlstrøm K, Jensen M. Synthesis of [11C]iodomethane by iodination of [11C]methane. Applied Radiation and Isotopes. 1997;48(2):153–157.

47. Jewett DM. A simple synthesis of [11C]methyl triflate. International Journal of Radiation Applications and Instrumentation. Part A, Applied Radiation and Isotopes. 1992;43(11):1383–1385.

48. Preshlock S, Tredwell M, Gouverneur V. (18)F-Labeling of Arenes and Heteroarenes for Applications in Positron Emission Tomography. Chemical Reviews. 2016;116(2):719–766.

49. Bejot R, Gouverneur V. 18F-Radionuclide Chemistry. In: Fluorine in Pharmaceutical and Medicinal Chemistry. Vol. Volume 6. IMPERIAL COLLEGE PRESS; 2011. p. 335–382. (Molecular Medicine and Medicinal Chemistry).

50. Ross TL, Ermert J, Hocke C, Coenen HH. Nucleophilic 18F-Fluorination of Heteroaromatic Iodonium Salts with No-Carrier-Added [18F]Fluoride. Journal of the American Chemical Society. 2007;129(25):8018–8025.

51. Richarz R, Krapf P, Zarrad F, Urusova EA, Neumaier B, Zlatopolskiy BD. Neither azeotropic drying, nor base nor other additives: a minimalist approach to 18F-labeling. Organic & Biomolecular Chemistry. 2014;12(40):8094–8099.

52. Zlatopolskiy BD, Zischler J, Krapf P, Zarrad F, Urusova EA, Kordys E, Endepols H, Neumaier B. Copper-Mediated Aromatic Radiofluorination Revisited: Efficient Production of PET Tracers on a Preparative Scale. Chemistry – A European Journal. 2015;21(15):5972–5979.

53. Van de Bittner GC, Ricq EL, Hooker JM. A Philosophy for CNS Radiotracer Design. Accounts of Chemical Research. 2014;47(10):3127–3134.

54. Wong DF, Gründer G, Brašić JR. Brain imaging research: Does the science serve clinical practice? International Review of Psychiatry. 2007;19(5):541–558.

55. Ametamey SM, Schubiger PA. PET radiopharmaceuticals for neuroreceptor imaging. Nuclear Science and Techniques. 2006;17(3):143–147.

56. McKinney JD, Richard A, Waller C, Newman MC, Gerberick F. The practice of structure activity relationships (SAR) in toxicology. Toxicological Sciences: An Official Journal of the Society of Toxicology. 2000;56(1):8–17.

57. Langer T, Krovat EM. Chemical feature-based pharmacophores and virtual library screening for discovery of new leads. Current Opinion in Drug Discovery & Development. 2003;6(3):370–376.

58. Hou T, Xu X. Recent development and application of virtual screening in drug discovery: an overview. Current Pharmaceutical Design. 2004;10(9):1011–1033.

59. Lange R, ter Heine R, Decristoforo C, Peñuelas I, Elsinga PH, van der Westerlaken MML, Hendrikse NH. Untangling the web of European regulations for the preparation of unlicensed radiopharmaceuticals: a concise overview and practical guidance for a risk-based approach. Nuclear Medicine Communications. 2015;36(5):414–422.

60. Aerts J, Ballinger JR, Behe M, Decristoforo C, Elsinga PH, Faivre-Chauvet A, Mindt TL, Kolenc Peitl P, Todde SC, Koziorowski J, et al. Guidance on current good radiopharmacy practice for the small-scale preparation of radiopharmaceuticals using automated modules: a European perspective. Journal of Labelled Compounds & Radiopharmaceuticals. 2014;57(10):615–620.

61. Verbruggen A, Coenen HH, Deverre J-R, Guilloteau D, Langstrom B, Salvadori PA, Halldin C. Guideline to regulations for radiopharmaceuticals in early phase clinical trials in the EU. European Journal of Nuclear Medicine and Molecular Imaging. 2008;35(11):2144–2151.

62. De Vos FJ, De Decker M, Dierckx RA. The good laboratory practice and good clinical practice requirements for the production of radiopharmaceuticals in clinical research. Nuclear Medicine Communications. 2005;26(7):575–579.

63. Harapanhalli RS. Food and Drug Administration requirements for testing and approval of new radiopharmaceuticals. Seminars in Nuclear Medicine. 2010;40(5):364–384.

64. Barth V, Need A. Identifying novel radiotracers for PET imaging of the brain: application of LC-MS/MS to tracer identification. ACS chemical neuroscience. 2014;5(12):1148–1153.

65. Pike VW. PET radiotracers: crossing the blood-brain barrier and surviving metabolism. Trends in Pharmacological Sciences. 2009;30(8):431–440.

66. Hulme EC, Trevethick MA. Ligand binding assays at equilibrium: validation and interpretation. British Journal of Pharmacology. 2010;161(6):1219–1237.

67. Yung-Chi C, Prusoff WH. Relationship between the inhibition constant (KI) and the concentration of inhibitor which causes 50 per cent inhibition (I50) of an enzymatic reaction. Biochemical Pharmacology. 1973;22(23):3099–3108.

68. Young WS, Kuhar MJ. A new method for receptor autoradiography: [3H]opioid receptors in rat brain. Brain Research. 1979;179(2):255–270.

69. Varrone A, Steiger C, Schou M, Takano A, Finnema SJ, Guilloteau D, Gulyás B, Halldin C. In vitro autoradiography and in vivo evaluation in cynomolgus monkey of [18F]FE-PE2I, a new dopamine transporter PET radioligand. Synapse. 2009;63(10):871–880.

70. Dickson CJ, Gee AD, Bennacef I, Gould IR, Rosso L. Further evaluation of quantum chemical methods for the prediction of non-specific binding of positron emission tomography tracers. Physical chemistry chemical physics: PCCP. 2011;13(48):21552–21557.

71. Rosso L, Gee AD, Gould IR. Ab initio computational study of positron emission tomography ligands interacting with lipid molecule for the prediction of nonspecific binding. Journal of Computational Chemistry. 2008;29(14):2397–2405.

72. Sharma R, Aboagye E. Development of radiotracers for oncology – the interface with pharmacology. British Journal of Pharmacology. 2011;163(8):1565–1585.

73. Kratochwil NA, Huber W, Müller F, Kansy M, Gerber PR. Predicting plasma protein binding of drugs: a new approach. Biochemical Pharmacology. 2002;64(9):1355–1374.

74. Singh SS, Mehta J. Measurement of drug–protein binding by immobilized human serum albumin-HPLC and comparison with ultrafiltration. Journal of Chromatography B. 2006;834(1):108–116.

75. Valko K, Nunhuck S, Bevan C, Abraham MH, Reynolds DP. Fast Gradient HPLC Method to Determine Compounds Binding to Human Serum Albumin. Relationships with Octanol/Water and Immobilized Artificial Membrane Lipophilicity. Journal of Pharmaceutical Sciences. 2003;92(11):2236–2248.

76. Alavijeh MS, Chishty M, Qaiser MZ, Palmer AM. Drug Metabolism and Pharmacokinetics, the Blood-Brain Barrier, and Central Nervous System Drug Discovery. NeuroRX. 2005;2(4):554–571. (Drug Discovery for Disorders of the Central Nervous System).

77. Lewis DF, Dickins M, Eddershaw PJ, Tarbit MH, Goldfarb PS. Cytochrome P450 substrate specificities, substrate structural templates and enzyme active site geometries. Drug Metabolism and Drug Interactions. 1999;15(1):1–49.

78. Jia L, Liu X. The Conduct of Drug Metabolism Studies Considered Good Practice (II): In Vitro Experiments. Current drug metabolism. 2007;8(8):822–829.

79. Halldin C, Bjurling P, Stålnacke CG, Jossan SS, Oreland L, Långström B. 11C-labelling of dimethylphenethylamine in two different positions and biodistribution studies. International Journal of Radiation Applications and Instrumentation. Part A, Applied Radiation and Isotopes. 1989;40(7):557–560.

80. Kilbourn MR, Carey JE, Koeppe RA, Haka MS, Hutchins GD, Sherman PS, Kuhl DE. Biodistribution, dosimetry, metabolism and monkey PET studies of [18F]GBR 13119. Imaging the dopamine uptake system in vivo. International Journal of Radiation Applications and Instrumentation. Part B, Nuclear Medicine and Biology. 1989;16(6):569–576.

81. Shiue CY, Bai LQ, Teng RR, Arnett CD, Wolf AP. No-carrier-added N-(3-[18F]fluoropropyl)spiroperidol: biodistribution in mice and tomographic studies in a baboon. Journal of Nuclear Medicine: Official Publication, Society of Nuclear Medicine. 1987;28(7):1164–1170.

82. Riemann B, Schäfers KP, Schober O, Schäfers M. Small animal PET in preclinical studies: opportunities and challenges. The quarterly journal of nuclear medicine and molecular imaging. 2008;52(3):215–221.

83. Schnöckel U, Hermann S, Stegger L, Law M, Kuhlmann M, Schober O, Schäfers K, Schäfers M. Small-animal PET: A promising, non-invasive tool in pre-clinical research. European Journal of Pharmaceutics and Biopharmaceutics. 2010;74(1):50–54.

84. Yao R, Lecomte R, Crawford ES. Small-animal PET: what is it, and why do we need it? Journal of Nuclear Medicine Technology. 2012;40(3):157–165.

85. STERNBACH LH, REEDER E. Quinazolines and 1,4-Benzodiazepines. II.1 The Rearrangement of 6-Chloro-2-chloromethyl-4-phenylquinazoline 3-Oxide into 2-Amino Derivatives of 7-Chloro-5-phenyl-3H-1,4-benzodiazepine 4-Oxide. The Journal of Organic Chemistry.

86. RANDALL LO, SCHALLEK W, HEISE GA, KEITH EF, BAGDON RE. The psychosedative properties of methaminodiazepoxide. The Journal of pharmacology and experimental therapeutics. 1960;129:163–171.

87. Randall LO. Pharmacology of methaminodiazepoxide. Diseases of the Nervous System. 1960;21(3)Suppl:7–10.

88. Harris TH. METHAMINODIAZEPOXIDE. Journal of the American Medical Association. 1960;172(11):1162–1163.

89. STERNBACH LH, REEDER E. Quinazolines and 1,4-Benzodiazepines. IV.1,2 Transformations of 7-Chloro-2-methylamino-5-phenyl-3H-1,4-benzodiazepine 4-Oxide3. The Journal of Organic Chemistry. 1961;26(12):4936–4941.

90. López-Muñoz F, Álamo C, García-García P. The discovery of chlordiazepoxide and the clinical introduction of benzodiazepines: Half a century of anxiolytic drugs. Journal of Anxiety Disorders. 2011;25(4):554–562.

91. López-Muñoz F, Alamo C. Historical evolution of the neurotransmission concept. Journal of Neural Transmission. 2009;116(5):515–533.

92. Bowery NG, Smart TG. GABA and glycine as neurotransmitters: a brief history. British Journal of Pharmacology. 2006;147(S1):S109–S119.

93. Schmidt RF, Vogel ME, Zimmermann M. Die Wirkung von Diazepam auf die präsynaptische Hemmung und andere Rückenmarksreflexe. Naunyn-Schmiedebergs Archiv für Pharmakologie und experimentelle Pathologie. 1967;258(1):69–82.

94. Costa E, Greengard P, American College of Neuropsychopharmacology. Mechanism of action of benzodiazepines. New York: Raven Press; 1975.

95. Polc P, Möhler H, Haefely W. The effect of diazepam on spinal cord activities: Possible sites and mechanisms of action. Naunyn-Schmiedeberg's Archives of Pharmacology. 1974;284(4):319–337.

96. Griffin CE, Kaye AM, Bueno FR, Kaye AD. Benzodiazepine Pharmacology and Central Nervous System–Mediated Effects. The Ochsner Journal. 2013;13(2):214–223.

97. Braestrup C, Squires RF. Specific benzodiazepine receptors in rat brain characterized by high-affinity (3H)diazepam binding. Proceedings of the National Academy of Sciences of the United States of America. 1977;74(9):3805–3809.

98. Woods MJ, Williams DC. Multiple forms and locations for the peripheral-type benzodiazepine receptor. Biochemical Pharmacology. 1996;52(12):1805–1814.

99. Gavish M, Bachman I, Shoukrun R, Katz Y, Veenman L, Weisinger G, Weizman A. Enigma of the peripheral benzodiazepine receptor. Pharmacological Reviews. 1999;51(4):629–650.

100. Leschiner S, Weizman R, Shoukrun R, Veenman L, Gavish M. Tissue-specific regulation of the peripheral benzodiazepine receptor by antidepressants and lithium. Neuropsychobiology. 2000;42(3):127–134.

101. Papadopoulos V, Baraldi M, Guilarte TR, Knudsen TB, Lacapère J-J, Lindemann P, Norenberg MD, Nutt D, Weizman A, Zhang M-R, et al. Translocator protein (18kDa): new nomenclature for the peripheral-type benzodiazepine receptor based on its structure and molecular function. Trends in Pharmacological Sciences. 2006;27(8):402–409.

102. Leneveu-Jenvrin C, Connil N, Bouffartigues E, Papadopoulos V, Feuilloley MGJ, Chevalier S. Structure-to-function relationships of bacterial translocator protein (TSPO): a focus on Pseudomonas. Frontiers in Microbiology. 2014 5:631.

103. Milenkovic VM, Bader S, Sudria-Lopez D, Siebert R, Brandl C, Nothdurfter C, Weber BHF, Rupprecht R, Wetzel CH. Effects of genetic variants in the TSPO gene on protein structure and stability. PLOS ONE. 2018;13(4):e0195627.

104. Bonsack F, Sukumari-Ramesh S. TSPO: An Evolutionarily Conserved Protein with Elusive Functions. International Journal of Molecular Sciences. 2018;19(6).

105. Anholt RR, Pedersen PL, De Souza EB, Snyder SH. The peripheral-type benzodiazepine receptor. Localization to the mitochondrial outer membrane. The Journal of Biological Chemistry. 1986;261(2):576–583.

106. Midzak A, Rone M, Aghazadeh Y, Culty M, Papadopoulos V. Mitochondrial protein import and the genesis of steroidogenic mitochondria. Molecular and Cellular Endocrinology. 2011;336(1–2):70–79.

107. Papadopoulos V, Aghazadeh Y, Fan J, Campioli E, Zirkin B, Midzak A. TRANSLOCATOR PROTEIN-MEDIATED PHARMACOLOGY OF CHOLESTEROL TRANSPORT AND STEROIDOGENESIS. Molecular and cellular endocrinology. 2015;408:90–98.

108. Rone MB, Midzak AS, Issop L, Rammouz G, Jagannathan S, Fan J, Ye X, Blonder J, Veenstra T, Papadopoulos V. Identification of a Dynamic Mitochondrial Protein Complex Driving Cholesterol Import, Trafficking, and Metabolism to Steroid Hormones. Molecular Endocrinology. 2012;26(11):1868–1882.

109. Chang YJ, McCabe RT, Rennert H, Budarf ML, Sayegh R, Emanuel BS, Skolnick P, Strauss JF. The human “peripheral-type” benzodiazepine receptor: regional mapping of the gene and characterization of the receptor expressed from cDNA. DNA and cell biology. 1992;11(6):471–480.

110. Riond J, Vita N, Le Fur G, Ferrara P. Characterization of a peripheral-type benzodiazepine-binding site in the mitochondria of Chinese hamster ovary cells. FEBS Letters. 1989;245(1–2):238–244.

111. Bućan M, Gatalica B, Nolan P, Chung A, Leroux A, Grossman MH, Nadeau JH, Emanuel BS, Budarf M. Comparative mapping of 9 human chromosome 22q loci in the laboratory mouse. Human Molecular Genetics. 1993;2(8):1245–1252.

112. Costa B, Salvetti A, Rossi L, Spinetti F, Lena A, Chelli B, Rechichi M, Pozzo ED, Gremigni V, Martini C. Peripheral Benzodiazepine Receptor: Characterization in Human T-Lymphoma Jurkat Cells. Molecular Pharmacology. 2006;69(1):37–44.

113. Hardwick M, Fertikh D, Culty M, Li H, Vidic B, Papadopoulos V. Peripheral-Type Benzodiazepine Receptor (PBR) in Human Breast Cancer: Correlation of Breast Cancer Cell Aggressive Phenotype with PBR Expression, Nuclear Localization, and PBR-mediated Cell Proliferation and Nuclear Transport of Cholesterol. Cancer Research. 1999;59(4):831–842.

114. Costa B, Pini S, Gabelloni P, Da Pozzo E, Abelli M, Lari L, Preve M, Lucacchini A, Cassano GB, Martini C. The spontaneous Ala147Thr amino acid substitution within the translocator protein influences pregnenolone production in lymphomonocytes of healthy individuals. Endocrinology. 2009;150(12):5438–5445.

115. Nakamura K, Yamada K, Iwayama Y, Toyota T, Furukawa A, Takimoto T, Terayama H, Iwahashi K, Takei N, Minabe Y, et al. Evidence that variation in the peripheral benzodiazepine receptor (PBR) gene influences susceptibility to panic disorder. American Journal of Medical Genetics. Part B, Neuropsychiatric Genetics: The Official Publication of the International Society of Psychiatric Genetics. 2006;141B(3):222–226.

116. Costa B, Pini S, Martini C, Abelli M, Gabelloni P, Landi S, Muti M, Gesi C, Lari L, Cardini A, et al. Ala147thr substitution in translocator protein is associated with adult separation anxiety in patients with depression. Psychiatric Genetics. 2009;19(2):110–111.

117. Colasanti A, Owen DR, Grozeva D, Rabiner EA, Matthews PM, Craddock N, Young AH. Bipolar Disorder is associated with the rs6971 polymorphism in the gene encoding 18 kDa Translocator Protein (TSPO). Psychoneuroendocrinology. 2013;38(11):2826–2829.

118. Owen DR, Fan J, Campioli E, Venugopal S, Midzak A, Daly E, Harlay A, Issop L, Libri V, Kalogiannopoulou D, et al. TSPO mutations in rats and a human polymorphism impair the rate of steroid synthesis. The Biochemical Journal. 2017;474(23):3985–3999.

119. Li F, Liu J, Zheng Y, Garavito RM, Ferguson-Miller S. Crystal structures of translocator protein (TSPO) and mutant mimic of a human polymorphism. Science. 2015;347(6221):555–558.

120. Owen DRJ, Gunn RN, Rabiner EA, Bennacef I, Fujita M, Kreisl WC, Innis RB, Pike VW, Reynolds R, Matthews PM, et al. Mixed-Affinity Binding in Humans with 18-kDa Translocator Protein Ligands. Journal of Nuclear Medicine. 2011;52(1):24–32.

121. Owen DR, Yeo AJ, Gunn RN, Song K, Wadsworth G, Lewis A, Rhodes C, Pulford DJ, Bennacef I, Parker CA, et al. An 18-kDa Translocator Protein (TSPO) Polymorphism Explains Differences in Binding Affinity of the PET Radioligand PBR28. Journal of Cerebral Blood Flow & Metabolism. 2012;32(1):1–5.

122. Kreisl WC, Fujita M, Fujimura Y, Kimura N, Jenko KJ, Kannan P, Hong J, Morse CL, Zoghbi SS, Gladding RL, et al. Comparison of [(11)C]-(R)-PK 11195 and [(11)C]PBR28, two radioligands for translocator protein (18 kDa) in human and monkey: Implications for positron emission tomographic imaging of this inflammation biomarker. NeuroImage. 2010;49(4):2924–2932.

123. Ramensky V, Bork P, Sunyaev S. Human non-synonymous SNPs: server and survey. Nucleic Acids Research. 2002;30(17):3894–3900.

124. Fujita M, Imaizumi M, Zoghbi SS, Fujimura Y, Farris AG, Suhara T, Hong J, Pike VW, Innis RB. Kinetic analysis in healthy humans of a novel positron emission tomography radioligand to image the peripheral benzodiazepine receptor, a potential biomarker for inflammation. NeuroImage. 2008;40(1):43–52.

125. Selvaraj V, Stocco DM. The changing landscape in translocator protein (TSPO) function. Trends in Endocrinology & Metabolism. 2015;26(7):341–348.

126. Šileikytė J, Blachly-Dyson E, Sewell R, Carpi A, Menabò R, Lisa FD, Ricchelli F, Bernardi P, Forte M. Regulation of the Mitochondrial Permeability Transition Pore by the Outer Membrane Does Not Involve the Peripheral Benzodiazepine Receptor (Translocator Protein of 18 kDa (TSPO)). Journal of Biological Chemistry. 2014;289(20):13769–13781.

127. Li F, Liu J, Liu N, Kuhn LA, Garavito RM, Ferguson-Miller S. Translocator Protein 18 kDa (TSPO): An Old Protein with New Functions? Biochemistry. 2016;55(20):2821–2831.

128. Denora N, Natile G. An Updated View of Translocator Protein (TSPO). International Journal of Molecular Sciences. 2017;18(12):2640.

129. Papadopoulos V. Structure and function of the peripheral-type benzodiazepine receptor in steroidogenic cells. Proceedings of the Society for Experimental Biology and Medicine. Society for Experimental Biology and Medicine (New York, N.Y.). 1998;217(2):130–142.

130. Azarashvili T, Krestinina O, Yurkov I, Evtodienko Y, Reiser G. High-affinity peripheral benzodiazepine receptor ligand, PK11195, regulates protein phosphorylation in rat brain mitochondria under control of Ca(2+). Journal of Neurochemistry. 2005;94(4):1054–1062.

131. Hirsch JD, Beyer CF, Malkowitz L, Beer B, Blume AJ. Mitochondrial benzodiazepine receptors mediate inhibition of mitochondrial respiratory control. Molecular Pharmacology. 1989;35(1):157–163.

132. Hirsch T, Decaudin D, Susin SA, Marchetti P, Larochette N, Resche-Rigon M, Kroemer G. PK11195, a ligand of the mitochondrial benzodiazepine receptor, facilitates the induction of apoptosis and reverses Bcl-2-mediated cytoprotection. Experimental Cell Research. 1998;241(2):426–434.

133. Lee DH, Kang SK, Lee RH, Ryu JM, Park HY, Choi HS, Bae YC, Suh KT, Kim YK, Jung JS. Effects of peripheral benzodiazepine receptor ligands on proliferation and differentiation of human mesenchymal stem cells. Journal of Cellular Physiology. 2004;198(1):91–99.

134. Morin D, Musman J, Pons S, Berdeaux A, Ghaleb B. Mitochondrial translocator protein (TSPO): From physiology to cardioprotection. Biochemical Pharmacology. 2016;105:1–13.

135. De Souza EB, Anholt RR, Murphy KM, Snyder SH, Kuhar MJ. Peripheral-type benzodiazepine receptors in endocrine organs: autoradiographic localization in rat pituitary, adrenal, and testis. Endocrinology. 1985;116(2):567–573.

136. Papadopoulos V, Fan J, Zirkin B. Translocator protein (18 kDa): an update on its function in steroidogenesis. Journal of Neuroendocrinology. 2018;30(2).

137. Rone MB, Fan J, Papadopoulos V. Cholesterol transport in steroid biosynthesis: Role of protein-protein interactions and implications in disease states. Biochimica et biophysica acta. 2009;1791(7):646.

138. Fan J, Papadopoulos V. Evolutionary Origin of the Mitochondrial Cholesterol Transport Machinery Reveals a Universal Mechanism of Steroid Hormone Biosynthesis in Animals. PLOS ONE. 2013;8(10):e76701.

139. Romeo E, Cavallaro S, Korneyev A, Kozikowski AP, Ma D, Polo A, Costa E, Guidotti A. Stimulation of brain steroidogenesis by 2-aryl-indole-3-acetamide derivatives acting at the mitochondrial diazepam-binding inhibitor receptor complex. The Journal of Pharmacology and Experimental Therapeutics. 1993;267(1):462–471.

140. Krueger KE, Papadopoulos V. Peripheral-type benzodiazepine receptors mediate translocation of cholesterol from outer to inner mitochondrial membranes in adrenocortical cells. The Journal of Biological Chemistry. 1990;265(25):15015–15022.

141. Papadopoulos V, Nowzari FB, Krueger KE. Hormone-stimulated steroidogenesis is coupled to mitochondrial benzodiazepine receptors. Tropic hormone action on steroid biosynthesis is inhibited by flunitrazepam. The Journal of Biological Chemistry. 1991;266(6):3682–3687.

142. Midzak A, Akula N, Lecanu L, Papadopoulos V. Novel androstenetriol interacts with the mitochondrial translocator protein and controls steroidogenesis. The Journal of Biological Chemistry. 2011;286(11):9875–9887.

143. Denora N, Laquintana V, Pisu MG, Dore R, Murru L, Latrofa A, Trapani G, Sanna E. 2-Phenyl-imidazo[1,2-a]pyridine Compounds Containing Hydrophilic Groups as Potent and Selective Ligands for Peripheral Benzodiazepine Receptors: Synthesis, Binding Affinity and Electrophysiological Studies. Journal of Medicinal Chemistry. 2008;51(21):6876–6888.

144. Midzak AS, Akula N, Rone MB, Papadopoulos V. Computational modeling and biological validation of novel non-steroidal ligands for the cholesterol recognition/interaction amino acid consensus (CRAC) motif of the mitochondrial translocator protein (TSPO). Pharmacological Research. 2015;99:393–403.

145. Papadopoulos V, Amri H, Li H, Boujrad N, Vidic B, Garnier M. Targeted disruption of the peripheral-type benzodiazepine receptor gene inhibits steroidogenesis in the R2C Leydig tumor cell line. The Journal of Biological Chemistry. 1997;272(51):32129–32135.

146. Hauet T, Yao Z-X, Bose HS, Wall CT, Han Z, Li W, Hales DB, Miller WL, Culty M, Papadopoulos V. Peripheral-type benzodiazepine receptor-mediated action of steroidogenic acute regulatory protein on cholesterol entry into leydig cell mitochondria. Molecular Endocrinology (Baltimore, Md.). 2005;19(2):540–554.

147. Kelly-Hershkovitz E, Weizman R, Spanier I, Leschiner S, Lahav M, Weisinger G, Gavish M. Effects of peripheral-type benzodiazepine receptor antisense knockout on MA-10 Leydig cell proliferation and steroidogenesis. The Journal of Biological Chemistry. 1998;273(10):5478–5483.

148. Tu LN, Zhao AH, Hussein M, Stocco DM, Selvaraj V. Translocator Protein (TSPO) Affects Mitochondrial Fatty Acid Oxidation in Steroidogenic Cells. Endocrinology. 2016;157(3):1110–1121.

149. Morohaku K, Pelton SH, Daugherty DJ, Butler WR, Deng W, Selvaraj V. Translocator protein/peripheral benzodiazepine receptor is not required for steroid hormone biosynthesis. Endocrinology. 2014;155(1):89–97.

150. Fan J, Campioli E, Midzak A, Culty M, Papadopoulos V. Conditional steroidogenic cell-targeted deletion of TSPO unveils a crucial role in viability and hormone-dependent steroid formation. Proceedings of the National Academy of Sciences. 2015;112(23):7261–7266.

151. Selvaraj V, Tu LN, Stocco DM. Crucial Role Reported for TSPO in Viability and Steroidogenesis is a Misconception. Commentary: Conditional Steroidogenic Cell-Targeted Deletion of TSPO Unveils a Crucial Role in Viability and Hormone-Dependent Steroid Formation. Frontiers in Endocrinology. 2016;7:91.

152. Gatliff J, Campanella M. The 18 kDa translocator protein (TSPO): a new perspective in mitochondrial biology. Current Molecular Medicine. 2012;12(4):356–368.

153. Veenman L, Papadopoulos V, Gavish M. Channel-like functions of the 18-kDa translocator protein (TSPO): regulation of apoptosis and steroidogenesis as part of the host-defense response. Current Pharmaceutical Design. 2007;13(23):2385–2405.

154. Zeno S, Veenman L, Katz Y, Bode J, Gavish M, Zaaroor M. The 18 kDa mitochondrial translocator protein (TSPO) prevents accumulation of protoporphyrin IX. Involvement of reactive oxygen species (ROS). Current Molecular Medicine. 2012;12(4):494–501.

155. Gavish M, Veenman L. Chapter Six - Regulation of Mitochondrial, Cellular, and Organismal Functions by TSPO. In: Pasternak GW, Coyle JT, editors. Advances in Pharmacology. Vol. 82. Academic Press; 2018. p. 103–136.

156. Yasin N, Veenman L, Singh S, Azrad M, Bode J, Vainshtein A, Caballero B, Marek I, Gavish M. Classical and Novel TSPO Ligands for the Mitochondrial TSPO Can Modulate Nuclear Gene Expression: Implications for Mitochondrial Retrograde Signaling. International Journal of Molecular Sciences. 2017. 18(4):786.

157. James ML, Selleri S, Kassiou M. Development of ligands for the peripheral benzodiazepine receptor. Current Medicinal Chemistry. 2006;13(17):1991–2001.

158. Fantini J, Di Scala C, Evans LS, Williamson PTF, Barrantes FJ. A mirror code for protein-cholesterol interactions in the two leaflets of biological membranes. Scientific Reports. 2016;6:21907.

159. Jamin N, Neumann J-M, Ostuni MA, Vu TKN, Yao Z-X, Murail S, Robert J-C, Giatzakis C, Papadopoulos V, Lacapère J-J. Characterization of the cholesterol recognition amino acid consensus sequence of the peripheral-type benzodiazepine receptor. Molecular Endocrinology (Baltimore, Md.). 2005;19(3):588–594.

160. Baier CJ, Fantini J, Barrantes FJ. Disclosure of cholesterol recognition motifs in transmembrane domains of the human nicotinic acetylcholine receptor. Scientific Reports. 2011;1:69.

161. Verma A, Nye JS, Snyder SH. Porphyrins are endogenous ligands for the mitochondrial (peripheral-type) benzodiazepine receptor. Proceedings of the National Academy of Sciences. 1987;84(8):2256–2260.

162. Pastorino JG, Simbula G, Gilfor E, Hoek JB, Farber JL. Protoporphyrin IX, an endogenous ligand of the peripheral benzodiazepine receptor, potentiates induction of the mitochondrial permeability transition and the killing of cultured hepatocytes by rotenone. Journal of Biological Chemistry. 1994;269(49):31041–31046.

163. Veenman L, Vainshtein A, Yasin N, Azrad M, Gavish M. Tetrapyrroles as Endogenous TSPO Ligands in Eukaryotes and Prokaryotes: Comparisons with Synthetic Ligands. International Journal of Molecular Sciences. 2016.17(6):880.

164. Zhao AH, Tu LN, Mukai C, Sirivelu MP, Pillai VV, Morohaku K, Cohen R, Selvaraj V. Mitochondrial Translocator Protein (TSPO) Function Is Not Essential for Heme Biosynthesis. Journal of Biological Chemistry. 2016;291(4):1591–1603.

165. Guidotti A, Forchetti CM, Corda MG, Konkel D, Bennett CD, Costa E. Isolation, characterization, and purification to homogeneity of an endogenous polypeptide with agonistic action on benzodiazepine receptors. Proceedings of the National Academy of Sciences of the United States of America. 1983;80(11):3531–3535.

166. Costa E, Guidotti A. Diazepam binding inhibitor (DBI): a peptide with multiple biological actions. Life Sciences. 1991;49(5):325–344.

167. Bovolin P, Schlichting J, Miyata M, Ferrarese C, Guidotti A, Alho H. Distribution and characterization of diazepam binding inhibitor (DBI) in peripheral tissues of rat. Regulatory Peptides. 1990;29(2–3):267–281.

168. Guarneri P, Papadopoulos V, Pan B, Costa E. Regulation of pregnenolone synthesis in C6-2B glioma cells by 4'-chlorodiazepam. Proceedings of the National Academy of Sciences of the United States of America. 1992;89(11):5118–5122.

169. Garnier M, Boujrad N, Ogwuegbu SO, Hudson JR, Papadopoulos V. The polypeptide diazepam-binding inhibitor and a higher affinity mitochondrial peripheral-type benzodiazepine receptor sustain constitutive steroidogenesis in the R2C Leydig tumor cell line. Journal of Biological Chemistry. 1994;269(35):22105–22112.

170. Lee Y-S, Siméon FG, Briard E, Pike VW. Solution structures of the prototypical 18 kDa translocator protein ligand, PK 11195, elucidated with 1H/13C NMR spectroscopy and quantum chemistry. ACS chemical neuroscience. 2012;3(4):325–335.

171. Anzini M, Cappelli A, Vomero S, Giorgi G, Langer T, Bruni G, Romeo MR, Basile AS. Molecular Basis of Peripheral vs Central Benzodiazepine Receptor Selectivity in a New Class of Peripheral Benzodiazepine Receptor Ligands Related to Alpidem. Journal of Medicinal Chemistry. 1996;39(21):4275–4284.

172. Mokrov GV, Deeva OA, Gudasheva TA, Yarkov SA, Yarkova MA, Seredenin SB. Design, synthesis and anxiolytic-like activity of 1-arylpyrrolo[1,2-a]pyrazine-3-carboxamides. Bioorganic & Medicinal Chemistry. 2015;23(13):3368–3378.

173. Schoemaker H, Bliss M, Yamamura HI. Specific high-affinity saturable binding of [3H] Ro5-4864 To benzodiazepine binding sites in the rat cerebral cortex. European Journal of Pharmacology. 1981;71(1):173–175.

174. Marangos PJ, Patel J, Boulenger JP, Clark-Rosenberg R. Characterization of peripheral-type benzodiazepine binding sites in brain using [3H]Ro 5-4864. Molecular Pharmacology. 1982;22(1):26–32.

175. Farges R, Joseph-Liauzun E, Shire D, Caput D, Le Fur G, Ferrara P. Site-directed mutagenesis of the peripheral benzodiazepine receptor: identification of amino acids implicated in the binding site of Ro5-4864. Molecular Pharmacology. 1994;46(6):1160–1167.

176. Tokuda K, O'Dell KA, Izumi Y, Zorumski CF. Midazolam inhibits hippocampal long-term potentiation and learning through dual central and peripheral benzodiazepine receptor activation and neurosteroidogenesis. The Journal of Neuroscience. 2010;30(50):16788–16795.

177. Kalk NJ, Owen DR, Tyacke RJ, Reynolds R, Rabiner EA, Lingford-hughes AR, Parker CA. Are prescribed benzodiazepines likely to affect the availability of the 18 kDa translocator protein (TSPO) in PET studies? Synapse. 2013;67(12):909–912.

178. Fiorini I, Nacci V, Ciani SM, Garofalo A, Campiani G, Savini L, Novellino E, Greco G, Bernasconi P, Mennini T. Novel Ligands Specific for Mitochondrial Benzodiazepine Receptors: 6-arylpyrrolo[2,1-d][1,5]benzothiazepine Derivatives. Synthesis, Structure-Activity Relationships, and Molecular Modeling Studies. Journal of Medicinal Chemistry. 1994;37(10):1427–1438.

179. Campiani G, Nacci V, Fiorini I, De Filippis M, Garofalo A, Ciani S, Greco G, Novellino E, Manzoni C, Mennini T. New pyrrolobenzothiazepine derivatives as molecular probes of the 'peripheral-type' benzodiazepine receptor (PBR) binding site. European Journal of Medicinal Chemistry. 1997;32(3):241–251.

180. Campiani G, Ramunno A, Fiorini I, Nacci V, Morelli E, Novellino E, Goegan M, Mennini T, Sullivan S, Zisterer DM, et al. Synthesis of New Molecular Probes for Investigation of Steroid Biosynthesis Induced by Selective Interaction with Peripheral Type Benzodiazepine Receptors (PBR). Journal of Medicinal Chemistry. 2002;45(19):4276–4281.

181. Le Fur G, Vaucher N, Perrier ML, Flamier A, Benavides J, Renault C, Dubroeucq MC, Guérémy C, Uzan A. Differentiation between two ligands for peripheral benzodiazepine binding sites, [3H]R05-4864 and [3H]PK 11195, by thermodynamic studies. Life Sciences. 1983;33(5):449–457.

182. Shah F, Hume SP, Pike VW, Ashworth S, McDermott J. Synthesis of the enantiomers of [N-methyl-11C]PK 11195 and comparison of their behaviours as radioligands for PK binding sites in rats. Nuclear Medicine and Biology. 1994;21(4):573–581.

183. Rao VLR, Butterworth RF. Characterization of binding sites for the ω3 receptor ligands [3H]PK11195 and [3H]RO5-4864 in human brain. European Journal of Pharmacology. 1997;340(1):89–99.

184. Lockhart A, Davis B, Matthews JC, Rahmoune H, Hong G, Gee A, Earnshaw D, Brown J. The peripheral benzodiazepine receptor ligand PK11195 binds with high affinity to the acute phase reactant alpha1-acid glycoprotein: implications for the use of the ligand as a CNS inflammatory marker. Nuclear Medicine and Biology. 2003;30(2):199–206.

185. Kim T, Pae AN. Translocator protein (TSPO) ligands for the diagnosis or treatment of neurodegenerative diseases: a patent review (2010–2015; part 1). Expert Opinion on Therapeutic Patents. 2016;26(11):1325–1351.

186. Pascali C, Luthra SK, Pike VW, Price GW, Ahier RG, Hume SP, Myers R, Manjil L, Cremer JE. The radiosynthesis of [18F]PK 14105 as an alternative radioligand for peripheral type benzodiazepine binding sites. International Journal of Radiation Applications and Instrumentation. Part A, Applied Radiation and Isotopes. 1990;41(5):477–482.

187. Cappelli A, Pericot Mohr G la, Gallelli A, Giuliani G, Anzini M, Vomero S, Fresta M, Porcu P, Maciocco E, Concas A, et al. Structure-activity relationships in carboxamide derivatives based on the targeted delivery of radionuclides and boron atoms by means of peripheral benzodiazepine receptor ligands. Journal of Medicinal Chemistry. 2003;46(17):3568–3571.

188. Cappelli A, Matarrese M, Moresco RM, Valenti S, Anzini M, Vomero S, Turolla EA, Belloli S, Simonelli P, Filannino MA, et al. Synthesis, labeling, and biological evaluation of halogenated 2-quinolinecarboxamides as potential radioligands for the visualization of peripheral benzodiazepine receptors. Bioorganic & Medicinal Chemistry. 2006;14(12):4055–4066.

189. Yu W, Wang E, Voll RJ, Miller AH, Goodman MM. Synthesis, fluorine-18 radiolabeling, and in vitro characterization of 1-iodophenyl-N-methyl-N-fluoroalkyl-3-isoquinoline carboxamide derivatives as potential PET radioligands for imaging peripheral benzodiazepine receptor. Bioorganic & Medicinal Chemistry. 2008;16(11):6145–6155.

190. Castellano S, Taliani S, Viviano M, Milite C, Da Pozzo E, Costa B, Barresi E, Bruno A, Cosconati S, Marinelli L, et al. Structure-activity relationship refinement and further assessment of 4-phenylquinazoline-2-carboxamide translocator protein ligands as antiproliferative agents in human glioblastoma tumors. Journal of Medicinal Chemistry. 2014;57(6):2413–2428.

191. Castellano S, Taliani S, Milite C, Pugliesi I, Da Pozzo E, Rizzetto E, Bendinelli S, Costa B, Cosconati S, Greco G, et al. Synthesis and Biological Evaluation of 4-Phenylquinazoline-2-

carboxamides Designed as a Novel Class of Potent Ligands of the Translocator Protein. Journal of Medicinal Chemistry. 2012;55(9):4506–4510.

192. Shah F, Pike V, Turton DR. Synthesis of homochiral 11C labelled radioligands for peripheral benzodiazepine binding sites. Journal of Radiolabeled Compounds. 1993;32.

193. Stevenson L, Tavares AAS, Brunet A, McGonagle FI, Dewar D, Pimlott SL, Sutherland A. New iodinated quinoline-2-carboxamides for SPECT imaging of the translocator protein. Bioorganic & Medicinal Chemistry Letters. 2010;20(3):954–957.

194. Okuyama S, Chaki S, Yoshikawa R, Ogawa S, Suzuki Y, Okubo T, Nakazato A, Nagamine M, Tomisawa K. Neuropharmacological profile of peripheral benzodiazepine receptor agonists, DAA1097 and DAA1106. Life Sciences. 1999;64(16):1455–1464.

195. Mizrahi R, Rusjan PM, Kennedy J, Pollock B, Mulsant B, Suridjan I, De Luca V, Wilson AA, Houle S. Translocator protein (18 kDa) polymorphism (rs6971) explains in-vivo brain binding affinity of the PET radioligand [18F]-FEPPA. Journal of Cerebral Blood Flow & Metabolism. 2012;32(6):968–972.

196. Guo Q, Colasanti A, Owen DR, Onega M, Kamalakaran A, Bennacef I, Matthews PM, Rabiner EA, Turkheimer FE, Gunn RN. Quantification of the specific translocator protein signal of 18F-PBR111 in healthy humans: a genetic polymorphism effect on in vivo binding. Journal of Nuclear Medicine. 2013;54(11):1915–1923.

197. Culty M, Silver P, Nakazato A, Gazouli M, Li H, Muramatsu M, Okuyama S, Papadopoulos V. Peripheral benzodiazepine receptor binding properties and effects on steroid synthesis of two new phenoxyphenyl-acetamide derivatives, DAA1097 and DAA1106. Drug Development Research. 2001;52(3):475–484.

198. Langer SZ, Arbilla S, Benavides J, Scatton B. Zolpidem and alpidem: two imidazopyridines with selectivity for omega 1- and omega 3-receptor subtypes. Advances in biochemical psychopharmacology. 1990;46:61–72.

199. Bourguignon JJ. Endogenous and Synthetic Ligand of Mitochondrial Benzodiazepine Receptors: Structure-Affinity Relationships. In: Peripheral Benzodiazepine Receptors. Giesen-Crouse, E. London: Academic Press; 1993. p. 59–85.

200. Trapani G, Franco M, Ricciardi L, Latrofa A, Genchi G, Sanna E, Tuveri F, Cagetti E, Biggio G, Liso G. Synthesis and Binding Affinity of 2-Phenylimidazo[1,2-a]pyridine Derivatives for both Central and Peripheral Benzodiazepine Receptors. A New Series of High-Affinity and Selective Ligands for the Peripheral Type. Journal of Medicinal Chemistry. 1997;40(19):3109–3118.

201. Georges G, Vercauteren D, Evrard G, Durant F, George P, Wick A. Characterization of the physico-chemical properties of the imidazopyridine derivative Alpidem. Comparison with Zolpidem. European Journal of Medicinal Chemistry. 1993;28(4):323–335.

202. George P, Rossey G, Depoortere H, Allen J, Wick A. Le Zolpidem: un Nouvel Hypnotique de Structure Imidazo[1,2-a]Pyridine. (Topics in Med. Chem.). Act. Chim. Terap. 1991;18:215–239.

203. Almirante L, Mugnaini A, Rugarli P, Gamba A, Zefelippo E, De Toma N, Murmann W. Derivatives of imidazole. III. Synthesis and pharmacological activities of nitriles, amides, and carboxylic acid derivatives of imidazo[1,2-a]pyridine. Journal of Medicinal Chemistry. 1969;12(1):122–126.

204. Abignente E, Caprariis PD, Fattorusso E, Mayol L. Research on heterocyclic compounds. XXIII. Phenyl derivatives of fused imidazole systems. Journal of Heterocyclic Chemistry. 1989;26(6):1875–1880.

205. Durand A, Thénot JP, Bianchetti G, Morselli PL. Comparative pharmacokinetic profile of two imidazopyridine drugs: zolpidem and alpidem. Drug Metabolism Reviews. 1992;24(2):239–266.

206. Trapani G, Franco M, Latrofa A, Carotti A, Serra M, Sanna E, Biggio G, Liso G. Novel 2-Phenylimidazo[1,2-a]pyridine Derivatives as Potent and Selective Ligands for Peripheral Benzodiazepine Receptors: Synthesis, Binding Affinity, and in Vivo Studies. Journal of Medicinal Chemistry. 1999;42(19):3934–3941.

207. Selleri S, Bruni F, Costagli C, Costanzo A, Guerrini G, Ciciani G, Costa B, Martini C. 2-Arylpyrazolo[1,5-a]pyrimidin-3-yl acetamides. New potent and selective peripheral benzodiazepine receptor ligands. Bioorganic & Medicinal Chemistry. 2001;9(10):2661–2671.

208. Kozikowski AP, Ma D, Brewer J, Sun S, Costa E, Romeo E, Guidotti A. Chemistry, binding affinities, and behavioral properties of a new class of “antineophobic” mitochondrial DBI receptor complex (mDRC) ligands. Journal of Medicinal Chemistry. 1993;36(20):2908–2920.

209. Sokias R, L. Werry E, W. Chua S, A. Reekie T, Munoz L, N. Wong EC, M. Ittner L, Kassiou M. Determination and reduction of translocator protein (TSPO) ligand rs6971 discrimination. MedChemComm. 2017;8(1):202–210.

210. Miettinen H, Kononen J, Haapasalo H, Helén P, Sallinen P, Harjuntausta T, Helin H, Alho H. Expression of peripheral-type benzodiazepine receptor and diazepam binding inhibitor in human astrocytomas: relationship to cell proliferation. Cancer Research. 1995;55(12):2691–2695.

211. Miyazawa N, Hamel E, Diksic M. Assessment of the peripheral benzodiazepine receptors in human gliomas by two methods. Journal of Neuro-Oncology. 1998;38(1):19–26.

212. Vlodavsky E, Soustiel JF. Immunohistochemical expression of peripheral benzodiazepine receptors in human astrocytomas and its correlation with grade of malignancy, proliferation, apoptosis and survival. Journal of Neuro-Oncology. 2007;81(1):1–7.

213. Dupont A-C, Largeau B, Santiago Ribeiro MJ, Guilloteau D, Tronel C, Arlicot N. Translocator Protein-18 kDa (TSPO) Positron Emission Tomography (PET) Imaging and Its Clinical Impact in Neurodegenerative Diseases. International Journal of Molecular Sciences. 2017;18(4):785.

214. Alam MM, Lee J, Lee S-Y. Recent Progress in the Development of TSPO PET Ligands for Neuroinflammation Imaging in Neurological Diseases. Nuclear Medicine and Molecular Imaging. 2017;51(4):283–296.

215. Boutin H, Prenant C, Maroy R, Galea J, Greenhalgh AD, Smigova A, Cawthorne C, Julyan P, Wilkinson SM, Banister SD, et al. [18F]DPA-714: Direct Comparison with [11C]PK11195 in a Model of Cerebral Ischemia in Rats. PLOS ONE. 2013;8(2):e56441.

216. Plavén-Sigray P, Matheson GJ, Cselényi Z, Jucaite A, Farde L, Cervenka S. Test-retest reliability and convergent validity of (R)-[11C]PK11195 outcome measures without arterial input function. EJNMMI research. 2018;8(1):102.

217. Ammirati E, Moroni F, Magnoni M, Busnardo E, Di Terlizzi S, Villa C, Sizzano F, Scotti I, Palini A, Presotto L, et al. Carotid artery plaque uptake of 11C-PK11195 inversely correlates with

circulating monocytes and classical CD14++CD16- monocytes expressing HLA-DR. International Journal of Cardiology. Heart & Vasculature. 2018;21:32–35.

218. Kang Y, Schlyer D, Kaunzner UW, Kuceyeski A, Kothari PJ, Gauthier SA. Comparison of two different methods of image analysis for the assessment of microglial activation in patients with multiple sclerosis using (R)-[N-methyl-carbon-11]PK11195. PloS One. 2018;13(8):e0201289.

219. Morris RS, Simon Jones P, Alawneh JA, Hong YT, Fryer TD, Aigbirhio FI, Warburton EA, Baron J-C. Relationships between selective neuronal loss and microglial activation after ischaemic stroke in man. Brain: A Journal of Neurology. 2018;141(7):2098–2111.

220. Briard E, Zoghbi SS, Imaizumi M, Gourley JP, Shetty HU, Hong J, Cropley V, Fujita M, Innis RB, Pike VW. Synthesis and Evaluation in Monkey of Two Sensitive 11C-Labeled Aryloxyanilide Ligands for Imaging Brain Peripheral Benzodiazepine Receptors In Vivo. Journal of Medicinal Chemistry. 2008;51(1):17–30.

221. Wilson AA, Garcia A, Parkes J, McCormick P, Stephenson KA, Houle S, Vasdev N. Radiosynthesis and initial evaluation of [18F]-FEPPA for PET imaging of peripheral benzodiazepine receptors. Nuclear Medicine and Biology. 2008;35(3):305–314.

222. Owen DR, Guo Q, Rabiner EA, Gunn RN. The impact of the rs6971 polymorphism in TSPO for quantification and study design. Clinical and Translational Imaging. 2015;3(6):417–422.

223. Zanotti-Fregonara P, Zhang Y, Jenko KJ, Gladding RL, Zoghbi SS, Fujita M, Sbardella G, Castellano S, Taliani S, Martini C, et al. Synthesis and evaluation of translocator 18 kDa protein (TSPO) positron emission tomography (PET) radioligands with low binding sensitivity to human single nucleotide polymorphism rs6971. ACS chemical neuroscience. 2014;5(10):963–971.

224. Ikawa M, Lohith TG, Shrestha S, Telu S, Zoghbi SS, Castellano S, Taliani S, Settimo FD, Fujita M, Pike VW, et al. 11C-ER176, a Radioligand for 18-kDa Translocator Protein, Has Adequate Sensitivity to Robustly Image All Three Affinity Genotypes in Human Brain. Journal of Nuclear Medicine. 2017;58(2):320–325.

225. Fujita M, Kobayashi M, Ikawa M, Gunn RN, Rabiner EA, Owen DR, Zoghbi SS, Haskali MB, Telu S, Pike VW, et al. Comparison of four 11C-labeled PET ligands to quantify translocator protein 18 kDa (TSPO) in human brain: (R)-PK11195, PBR28, DPA-713, and ER176-based on recent publications that measured specific-to-non-displaceable ratios. EJNMMI research. 2017;7(1):84.

226. Vignal N, Cisternino S, Rizzo-Padoin N, San C, Hontonnou F, Gelé T, Declèves X, Sarda-Mantel L, Hosten B. [18F]FEPPA a TSPO Radioligand: Optimized Radiosynthesis and Evaluation as a PET Radiotracer for Brain Inflammation in a Peripheral LPS-Injected Mouse Model. Molecules. 2018;23(6).

227. Rojas C, Stathis M, Coughlin JM, Pomper M, Slusher BS. The Low-Affinity Binding of Second Generation Radiotracers Targeting TSPO is Associated with a Unique Allosteric Binding Site. Journal of Neuroimmune Pharmacology. 2017 Sep 5:1–5.

CHAPTER VII
APPENDIX – SUPPORTING INFORMATION PUBLICATIONS

1. [^{18}F]FEPPA: IMPROVED AUTOMATED RADIOSYNTHESIS, BINDING AFFINITY PROFILE AND PRELIMINARY IN VITRO EVALUATION IN COLORECTAL CANCER

Neydher Berroterán-Infante,[†,‡] Theresa Balber,[†,∓] Petra Fürlinger,[†] Michael Bergmann,[⊥] Rupert Lanzenbeger,[⊥⊥] Marcus Hacker,[†] Markus Mitterhauser,[†, ∓,⧺] Wolfgang Wadsak[†,‡,§]

[†] Division of Nuclear Medicine, Department of Biomedical Imaging and Image-guided Therapy, Medical University of Vienna, Vienna, Austria.

[‡] Department of Inorganic Chemistry, Faculty of Chemistry, University of Vienna, Vienna, Austria.

[∓] Department of Pharmaceutical Technology, Faculty of Life Sciences, University of Vienna, Vienna, Austria.

[⊥] Surgical Research Laboratories, Department of Surgery, Medical University of Vienna, Vienna, Austria.

[⊥⊥] Department of Psychiatry and Psychotherapy, Medical University of Vienna, Vienna, Austria

[⧺] Ludwig Boltzmann Institute Applied Diagnostics, Vienna, Austria.

[§] Center for Biomarker Research in Medicine, CBmed GmbH, Graz, Austria.

Supporting Information

1. Material and Methods

Caution: ^{18}F is a β+ emitter (511 keV) with a half-life of 109.77 min. ^{3}H is a β- emitter (18.6 keV) with a half-life of 12.32 years. All reactions and experiments involving ^{18}F and/or ^{3}H were performed in a laboratory approved for the handling of radionuclides, and appropriate safety procedures were followed at all times to prevent radioactive contamination

1.1. Materials

FEPPA tosylate precursor (2-(2-((*N*-(4-phenoxypyridin-3-yl)acetamido)methyl)phenoxy)ethyl 4-methylbenzenesulfonate), FEPPA reference standard (*N*-Acetyl-*N*-(2-fluoroethoxybenzyl)-2-phenoxy-5-pyridinamine), (*R*)-PK11195 ((*R*)-1-(2-chlorophenyl)-*N*-methyl-*N*-(1-methylpropyl)-isoquinoline-3-carboxami-de), PBR28 (*N*-Acetyl-*N*-(2-methoxybenzyl)-2-phenoxy-5-pyridinamine) and PS-HCO_3 cartridges (45 mg) were obtained from ABX Advanced Biochemical Compounds (Radeberg, Germany). Acetonitrile (for DNA synthesis and HPLC grade), Kryptofix $K_{2.2.2}$ (4,7,13,16,21,24-hexaoxa-1,10-diazabicyclo[8.8.8]hexacosane for synthesis >99%), potassium carbonate (≥99%), potassium chloride (≥99.5), anhydrous calcium chloride (≥98%), anhydrous magnesium chloride (≥98), ethanol (absolute), hydrochloric acid 1 M, haematoxylin, n-butyl acetate, 10X RIPA lysis buffer concentrate and silica gel 60 F254S plates were purchased from Merck (Darmstadt, Germany). Tris base (ACS reagent, ≥99.8%), ammonium formate (≥99.995%), sodium chloride (≥99%), anhydrous dimethyl sulfoxide (≥99.9%), Triton X-100 (0.2%), 2-methylbutane (≥99%), bovine serum albumin, protease inhibitor and aqueous polyethylene imine (50% w/v) were obtained from Sigma Aldrich (Vienna, Austria). C18 plus SepPak® cartridges were purchased from Waters (Milford, USA). For formulation of the radiotracer, 0.9% sodium chloride solution from B. Braun (Melsungen, Germany) and a sterile phosphate-buffered saline solution from the Vienna General Hospital's Pharmacy (Vienna, Austria) were used. Mini-PROTEAN® TGX™ precast gels were acquired from BIO-RAD (Hercules, USA) and Amersham Protran™ Premium 0.2 µm NC nitrocellulose blotting membranes from GE Healthcare Life Sciences (Little Chalfont, United Kingdom). For immunochemistry assays, 10X phosphate-buffered saline concentrate was obtained from Morphisto (Frankfurt am Main, Germany) and diluted to obtain 1X PBS solution. Bloxall™ blocking solution and Vectastain® ABC Kit (PK-4001) were purchased from Vector Laboratories (Burlingame, USA). Avidin/Biotin blocking kit and PureLink® Genomic DNA extraction kit, Taqman® Genotyping Assay C_2512465_20, Taqman® PCR Master Mix, nuclease-free water, SuperSignal™ West Pico chemiluminescent susbtrate kit, Menzel Superfrost® Plus positively charged microscope slides as well as purified rabbit IgG (1 $mg.mL^{-1}$) and Pierce™ BCA Protein Assay kit were acquired from ThermoFisher Scientific (Waltham, USA). Rabbit monoclonal anti-TSPO antibody (ab109497) and DAB-Substrate kit were purchased from Abcam (Cambridge, United Kingdom). Histofluid® mounting medium was obtained from Paul Marienfeld (Lauda-Königshofen, Germany). Low-protein binding Millex® GS 0.22 µm sterile filters were obtained from Millipore (Bedford, USA). $H_2{}^{18}O$ (> 98%) was purchased from Rotem Europe (Leipzig, Germany). All cell culture media and supplements were purchased from ThermoFisher Scientific (Waltham, USA). [^{3}H]PK11195 (3,149 $TBq.mmol^{-1}$), Ultima Gold™ liquid scintillation cocktail and multisensitive

phosphor screens all three from Perkin Elmer (Waltham, USA) and Whatman® GF/B glass fiber paper from Brandel (Gaithersburg, USA) were used. All chemicals and solvents were used without further purification.

1.2. Instrumentation

[^{18}F]Fluoride was produced in a GE PET trace cyclotron (PETtrace 860, GE Medical Systems, Uppsala, Sweden) and the [^{18}F]FEPPA radiosynthesis was performed using a Nuclear Interface synthesizer (GE Healthcare, Uppsala, Sweden); remotely controlled by a laptop with the dedicated software GINA (Elysia-Raytest, Straubenhardt, Germany). Purification of [^{18}F]FEPPA was performed by semi-preparative reversed phase HPLC using the synthesizer-integrated system equipped with a radioactivity-, and UV-detector (Linear Instruments Model 200 Detector UV/VIS) and a S1122 HPLC pump (Sykam, Fürstenfeldbruck, Germany).

For quality control and molar radioactivity determination of [^{18}F]FEPPA, an Agilent 1260 system (Agilent Technologies GmbH, Austria) equipped with a quaternary pump (G1311B), a multi wavelength UV-detector (G1365D), and a NaI (Tl) detector from Berthold Technologies (Bad Wildbad, Germany), controlled with the GINA Star software (Elysia-Raytest, Straubenhardt, Germany) was used. The osmolality of the tracer was measured with a Wescor osmometer Vapro® 5600 (Sanova Medical Systems, Vienna, Austria) and the pH was controlled using a WTW inoLab 740 pH meter (WTW, Weilheim, Germany). Gas chromatography analysis for solvents residual content was performed with a Bruker Gas Chromatography System 430-GC. Analyses of radio-TLC plates were performed using a Canberra-Packard Instant Imager (Perkin Elmer, Waltham, USA).

Gel electrophoresis, semi-dry transfer and chemiluminescence imaging were performed using a MINI-PROTEAN® Tetra Cell - PowerPac™ Basic Power Supply system, a Trans-Blot® SD Semi-dry Transfer Cell and a VersaDoc™ Imaging system, all three from Bio-Rad (Hercules, California), respectively. Tissues were sliced using a microcryotome Microm HM 560 (Thermo Fisher Scientific, Waltham, USA) and imaged in a TissueFAXS scanner (Tissue Gnostics, Vienna, Austria). The autoradiography screens were processed using a cyclone plus phosphor imager (Perkin Elmer, Waltham, USA). DNA concentration was determined using a Nanodrop™ 1000 spectrophotometer (ThermoFisher Scientific, Waltham, USA) and PCR, for genotyping assay, was performed using a real-time PCR system OnePlus (Applied Biosystems, ThermoFisher Scientific, Waltham, USA). Total protein concentration of the membranes and lysates was measured in a Synergy HTX plate multimode reader (Biotek, Winooski, USA). For binding affinity experiments, a Hidex 300SL beta counter (Hidex, Turku, Finland) was used. For real-time binding kinetics, cells were counted with a Scepter™ 2.0 cell counter (Merck, Darmstadt, Germany) and the experiments were performed using LigandTracer® Yellow (Ridgeview Instruments AB, Uppsala, Sweden).

1.3. Methods

1.3.1. Radiochemistry

The synthesis of [^{18}F]FEPPA was conducted according to previously published procedures[1,2] with some modifications. For the radiosynthesis, cyclotron-produced [^{18}F]fluoride (^{18}O(p,n)^{18}F^{-}) was transferred to the synthesizer module and fixed on a PS-HCO_3 cartridge. In order to start the labeling reaction, the activity was eluted with 0.8 mL of a potassium carbonate (4.5 mg.mL^{-1}) and Kriptofix (22 mg.mL^{-1}) solution in acetonitrile/water 80/20 from the cartridge and transferred to the reactor with vacuum. The complex was azeotropically dried at 100 °C by addition of 0.6 mL of acetonitrile. After complete drying, 0.5 mL of a 6.25 mg.mL^{-1} solution of the FEPPA tosylate precursor in acetonitrile was added to the activated and dried [^{18}F]fluoride/$K_{2.2.2}$ complex and the reaction vessel was heated at 90 °C. After 10 min, the reaction was quenched with 2 mL of water and the crude product was transferred to a semi-preparative HPLC column (Phenomenex Onyx™ Monolithic Semi-PREP C18 Column 100x10 mm) and eluted with a solution of 60% 10 mM ammonium formate adjusted at pH 7.2 and 40% acetonitrile (flow at 4 mL.min^{-1}). The fraction containing the product was collected and dissolved in 60 mL of water. Subsequently, the solvents were removed by solid-phase extraction using a pre-conditioned (10 mL ethanol and 20 mL water) C18plus SepPak cartridge. The cartridge was washed with water and the product ([^{18}F]FEPPA) was eluted with ethanol (1.5 mL) and formulated with sodium chloride (10 mL) and phosphate-buffered saline (6 mL). Finally, the (radio)chemical purity was assessed via HPLC using a column (Phenomenex Onyx™ Monolithic C18 Column 100x4.6 mm) as stationary phase and a solution of 70% 10 mM ammonium formate and 30% acetonitrile (flow at 3 mL.min^{-1}) as the mobile phase.

1.3.2. Western Blot

1.3.2.1. Preparation of the tissue lysate

The tissue was homogenized in enough volume of RIPA lysis buffer using an Ultra-Turrax®. The resulting suspension was transferred into a reaction tube and protease inhibitor was added. The tube was gently shaken at 4 °C for 30 min and afterwards centrifuged at 4 °C for 20 min (12000 rpm). The pellet was discarded and the supernatant aliquoted and stored at -80 °C. The total protein concentration of the lysate was measured reading the absorbance at 562 nm, following the instructions of the BCA kit.

1.3.2.2. Gel electrophoresis and western blot

Lysate samples were diluted with Laemmli buffer and heated to 95 °C for 5 min. 20 µg protein per well were loaded onto the gel and gel electrophoresis was performed at 200 V for 28 min using conventional page buffer (25 mM tris base, 193 mM glycine and 3.5 mM SDS). Semi-dry transfer to nitrocellulose blotting membrane was performed at 80 mA per gel for 1 h. Membranes were blocked for 1 h at room temperature using 5% dry milk powder in TBS-T (tris buffered saline containing 0.1% Tween-20). Incubation with primary antibody

(rabbit monoclonal anti-PBR, 1:10,000) was performed for 2 h at room temperature. After washing the membrane three times with TBS-T, incubation with secondary antibody (goat anti rabbit IgG, HRP-conjugate, 1:2500) was conducted under the same conditions. Detection was performed using the dedicated chemiluminescent kit.

1.3.3. Genotyping

Venous blood (≈2 mL) was obtained from healthy volunteers in EDTA-containing tubes. Genomic DNA (gDNA) was extracted from blood, the HT-29 cells and the colon cancer tissue using the PureLink Genomic DNA Kit, according to the instructions manual. Subsequently, the gDNA concentration (A_{260}) and purity (A_{260}/A_{280}) was determined by means of NanoDrop® spectrophotometry. 20 ng of the gDNA were placed in a 96-well fast plate and dried. Subsequently, 10 µL of a 50/5/45 v/v mixture, containing the Taqman® Master Mix (2X), the Taqman® Assay (20X) and nuclease-free water, were added. After centrifugation, to spin down the contents and to eliminate the air bubbles from the plate, the PCR was performed using the thermal cycling conditions specified in the table 1. A final post-PCR fluorescence-read revealed the corresponding genotype: homozygous for one of the alleles (HAB or LAB) or heterozygous (MAB).

Table 1. Thermal conditions for PCR

Step	Temperature (°C)	Duration (s)	Cycles
AmpliTaqGold®, UP, Enzyme activation	95	600	HOLD
Denaturation	95	15	40
Annealing / Extension	60	60	40

1.3.4. Binding affinity profile

The affinity of FEPPA was determined in a TSPO-expressing membrane binding protocol, according to Owen et al.[3] The membranes were prepared following already described procedures.[4] In detail, venous blood (≈80 mL) was obtained in EDTA-containing tubes from previously genotyped healthy volunteers, i.e. the volunteers were identified as HAB, MAB and LAB. The whole blood was centrifuged at room temperature for 15 min (180 *g*). The resulting platelet-rich plasma was re-centrifuged at room temperature for 15 min (1800 *g*), to obtain a platelet pellet. Subsequently, the pellet was homogenized with buffer 1 (0.32 mM sucrose, 5 mM tris base, 1 mM $MgCl_2$, pH 7.4, 4 °C). Homogenates were centrifuged at 4 °C for 15 min (48000 *g*), followed by removal of the supernatant. The pellet was re-homogenized in 10 times w/v buffer 2 (50 mM tris base, 1 mM $MgCl_2$, pH 7.4, 4 °C) and re-centrifuged two times under the same conditions, with

an intermediate resuspension step with buffer 2. The resulting membrane was mixed with approximately 4 mL of buffer 2 and aliquots were stored at -80 °C until use. The total protein concentration of the membrane was measured reading the absorbance at 562 nm, following the instructions manual of the BCA kit.

The competitive binding experiments were performed in test tubes, filled with 250 µL of non-radioactive reference compound (FEPPA) dissolved in assay buffer (50 mM tris base, 140 mM NaCl, 1.5 mM $MgCl_2$, 5 mM KCl, 1.5 mM $CaCl_2$, pH 7.4, 37 °C, 2% DMSO), 200 µL of the membrane suspension (250 $\mu g.mL^{-1}$) and 50 µL of a 10 nM [^{3}H]PK11195 solution. For determining non-specific binding, 20 µM PK11195 was used; and for total binding, only [^{3}H]PK11195 and membrane suspension were incubated. All dilutions were performed in assay buffer, whereby the final concentration of DMSO never exceeded 1%. After incubation time, binding was quenched with ice cold wash buffer (50 mM tris base, 1.4 mM $MgCl_2$, pH 7.4, 4 °C) and membrane bound radioactivity was recovered by rapid filtration through GF/B glass fiber filters presoaked in assay buffer containing 0.05% polyethylene imine. Filters were washed 3 times with 1 mL wash buffer and transferred into β-counting vials. 4 mL of β-scintillation cocktail were added and finally the tubes were counted. Data from the competition plots (from three independent experiments, performed in triplicate) were analyzed and successively IC50 and Ki values were calculated using a dissociation constant of 29.25 nM for [^{3}H]PK11195 and GraphPad Prism® software.

1.3.5. Real-time kinetics

1.3.5.1. Cell Culture

Human colorectal adenocarcinoma cell line, HT-29 were purchased from ATCC (Manassas, USA) and were grown and maintained at 37 °C and 5% CO_2 in a cell incubator. HT-29 cells were cultivated using RPMI medium supplemented with 10% fetal bovine serum (FBS), 2 mM L-glutamine and 10 $\mu g.mL^{-1}$ gentamicin sulfate. $1x10^6$ cells were seeded in a 100/20 mm cell culture dish two days prior to the experiment. The cell culture dishes were slightly tilted and the cells were incubated for 24 h in this position to allow adherence at only one side of the petri dish (Figure 1a). On the next day, the medium was discarded and the dishes were evenly incubated in 10 mL medium to obtain a confluent cell layer (Figure 1b).

1.3.5.2. Real-time kinetics measurements

Real-time kinetics measurements were performed using a LigandTracer® Yellow device (Figure 1c). First, a background measurement was performed for 5 min. Growth medium was replaced by 2 mL of supplement-free medium and the dishes were placed in the LigandTracer® device. Taking into account the molar radioactivity of the [^{18}F]FEPPA batches, a small volume of the freshly prepared radiotracer was added to the cells, to reach a final concentration of 15 – 30 nM. After the equilibrium was reached, the measurement was paused and 1 µL of a solution of non-labeled TSPO ligand (FEPPA, PK11195 or PBR28) in DMSO was added and the measurement was re-started (final concentration of TSPO ligand 1.5 µM, DMSO content never exceeded 0.5%).[5]

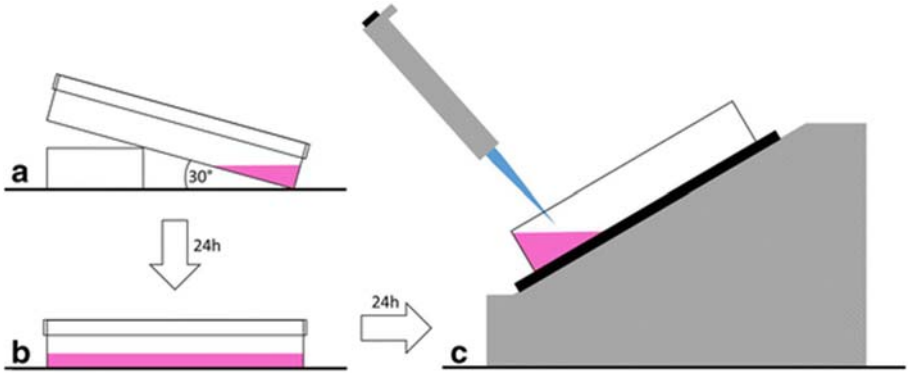

Figure 1. Cultivation of cells for real-time kinetics measurements (Adapted from Zeitlinger et al)[5]

1.3.6. Immunohistochemistry and autoradiography

1.3.6.1. Tissue preparation

Healthy mucosa and tumor tissues were obtained directly after tumorectomy from the Department of Surgery at the Medical University Vienna and quickly frozen in 2-methylbutane at -40 °C and subsequently stored at -80 °C until further processing. Tissue blocks were thawed within 12 h to -20 °C and cut using a microcryotome into 10 µm thick slices. Slices were mounted onto positively charged glass slides and stored at -80 °C until use.

1.3.6.2. Immunohistochemistry

Cryoslices were fixed in 96% ethanol for 10 min at room temperature. Permeabilization was performed with 0.2%1 Triton X-100 in PBS for 5 min. Tissue slices were surrounded with a Barrier-Pen and endogenous peroxidases were blocked by incubating the slices with 2 drops of Bloxall™ blocking solution for 10 min in a humid, dark chamber. Endogenous avidin and biotin were blocked using the dedicated kit, following the instructions of the user manual. Additionally, slices were incubated for 20 min with goat serum (1:10, PBS) to reduce non-specific binding. Primary antibody incubation was performed for 1 h in a humid, dark chamber (1:100; 0.1% BSA in PBS). Purified rabbit IgG was used as an isotype control. Slices were washed with PBS containing 0.1% Tween-20 and incubated for 30 min under same conditions with a biotinylated anti-rabbit IgG antibody provided by the Vectastain® kit (1:200, 5% goat serum in PBS). Subsequently, slices were washed three times for 5 min at room temperature using 0.1% Tween-20 in PBS. The preparation of the avidin/biotin-complex solution, provided by the Vectastain® ABC kit, was prepared and used according to the manufacturer´s instructions. After filtered a washing step, a freshly prepared 1:50 dilution of DAB reagent was incubated for 1 minute and the following washing step was achieved with tap water. Haematoxylin (1:7, deionized water) was filtrated onto the slices and incubated for 3 min. Development of the staining was accomplished in tap water. Slices were dehydrated using increasing concentrations of ethanol and n-butyl acetate. Finally, the slides were embedded in Histofluid® mounting medium and ulteriorly scanned.

1.3.6.3. Autoradiography

Tissue sections were allowed to thaw to room temperature until disappearing of condense water residues and pre-incubated with assay buffer (50 mM tris-HCl in deionized water, pH 7.4) at room temperature for 30 min in a Coplin jar. After careful removal of buffer, tissue slices were promptly incubated for 60 min with 100 µL of the freshly prepared radioligand [^{18}F]FEPPA in assay buffer (≈50 kBq per slice). For blocking experiments, non-labeled FEPPA and PBR28 were co-incubated at different concentrations. After the incubation time, the radioactive solution was cautiously discarded and the slides were washed twice for 5 min in a jar with ice-cold assay buffer, then with water and ultimately dried under an air stream and exposed to a phosphor screen until the next day. Tracer uptake was expressed as fmol of FEPPA.mm^{-2} of tissue.

1.4. Statistical analysis

Quantitative data are reported as arithmetic mean ± standard deviation. For the determination of significance, a Tukey's multiple comparison test (α=0.99) was performed using GraphPad Prism® software.

2. Results

2.1. Preparative HPLC purification

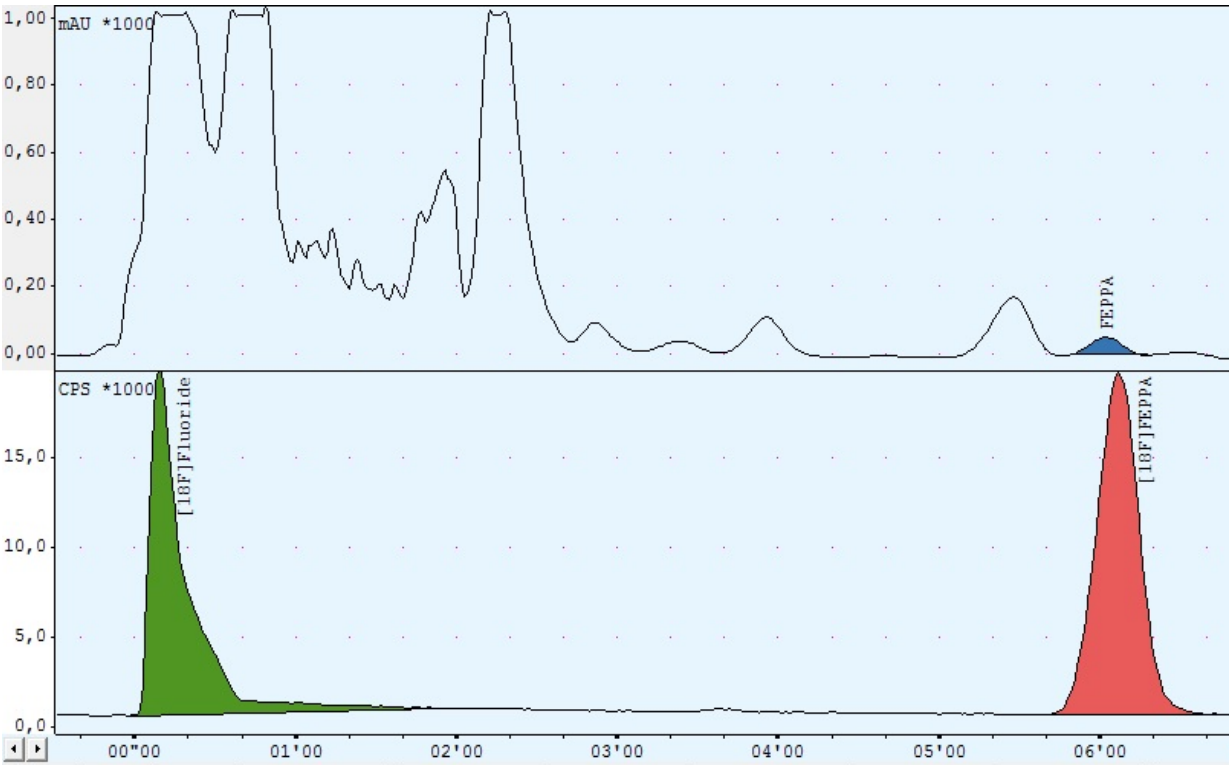

Figure 2. Representative preparative chromatogram for [^{18}F]FEPPA purification

2.2. Quality control

Table 2. Quality control assessment of [^{18}F]FEPPA

Test	Acceptance criteria	Result
Vial contents	Clear, colorless, particle free	Pass
pH	4.5 – 8.5	7.5
Radiochemical purity	≥95%	≥99%
Chemical (non-radioactive) impurities detected by HPLC (UV channel)	<1%	<0.1%
Radionuclidic purity	Half-life: (109±10) min	(112±5) min
	γ-Spectrum: 511 keV	(505±4) keV
Ethanol content	≤100000 ppm	≤ 85000 ppm
Acetonitrile content	≤400 ppm	≤ 214 ppm
Kryptofix content	≤50 µg.mL^{-1}	≤ 20 µg.mL^{-1}

A typical analytical chromatogram is shown in Figure 3. In order to determine the amount of cold FEPPA present in the radiotracer formulation, FEPPA standards were injected in the analytical HPLC using the same conditions for the quality control of [^{18}F]FEPPA. Accordingly, a calibration curve was prepared to calculate the corresponding amount.

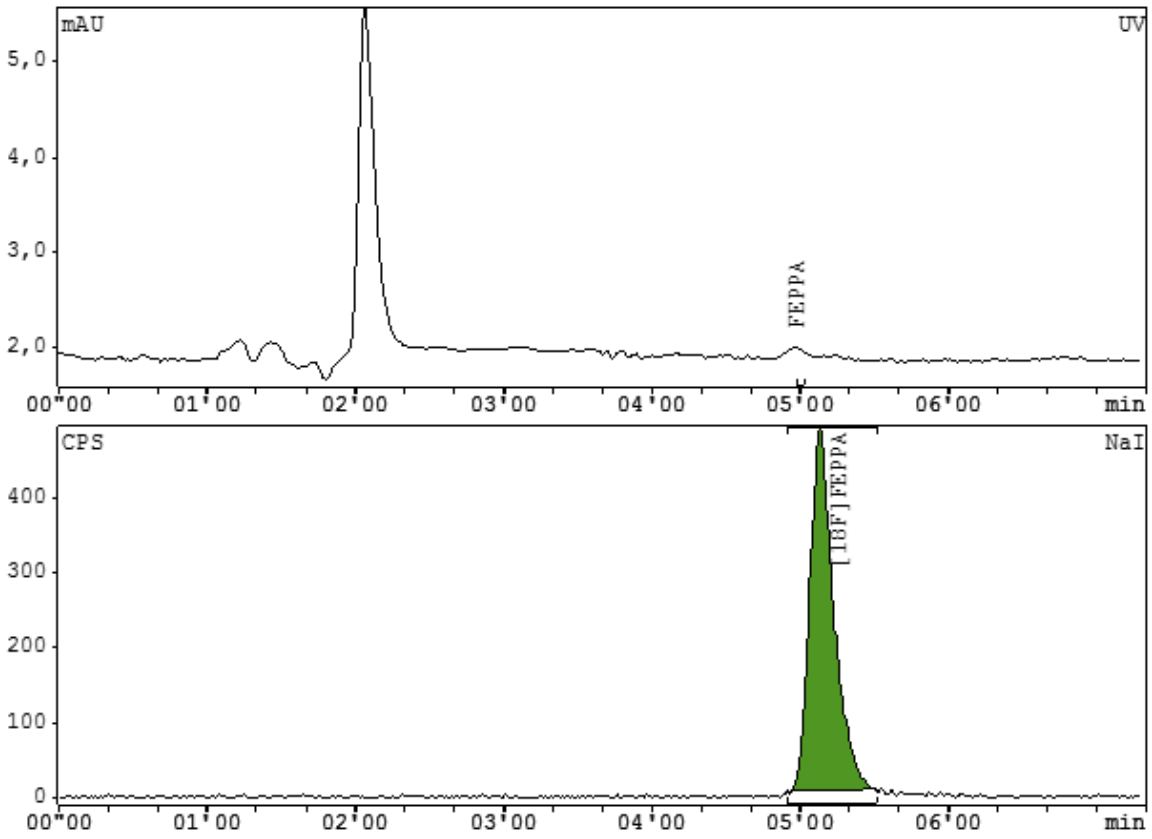

Figure 3. Representative analytical HPLC chromatogram

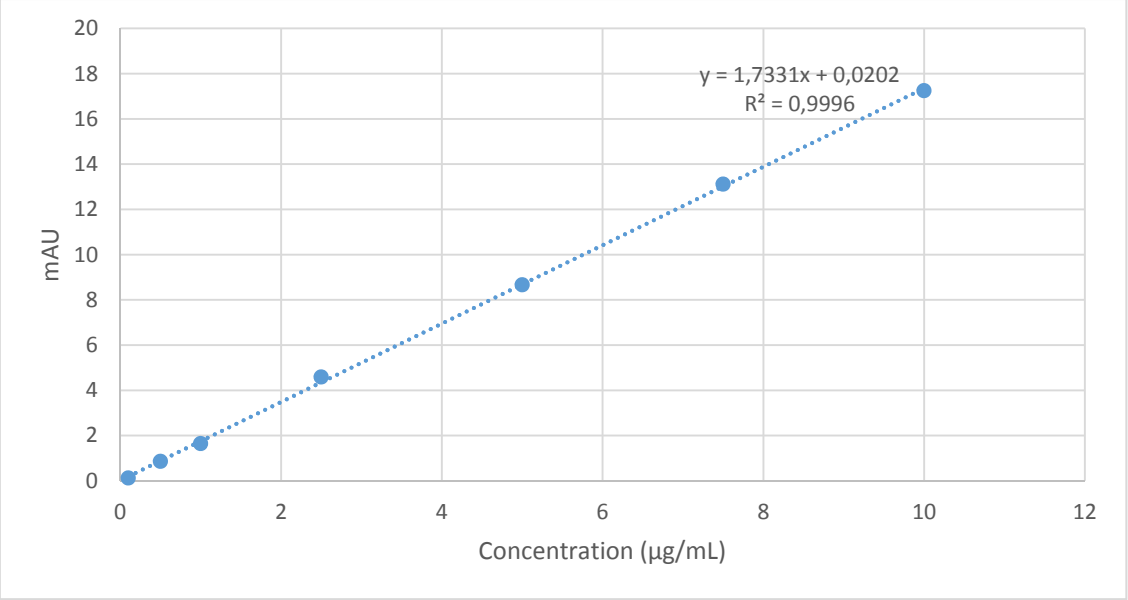

Figure 4. Calibration curve of FEPPA

2.3. Genotyping

A typical allelic discrimination plot is shown in Figure 5. Three different clusters can be observed, representing the three different genotypes: homozygous (red; Allele 1/Allele 1; Thr147Thr; LAB); homozygous (blue; Allele 2/Allele 2; Ala147Ala) and heterozygous (green; Allele 1/Allele 2; Ala147Thr; MAB).

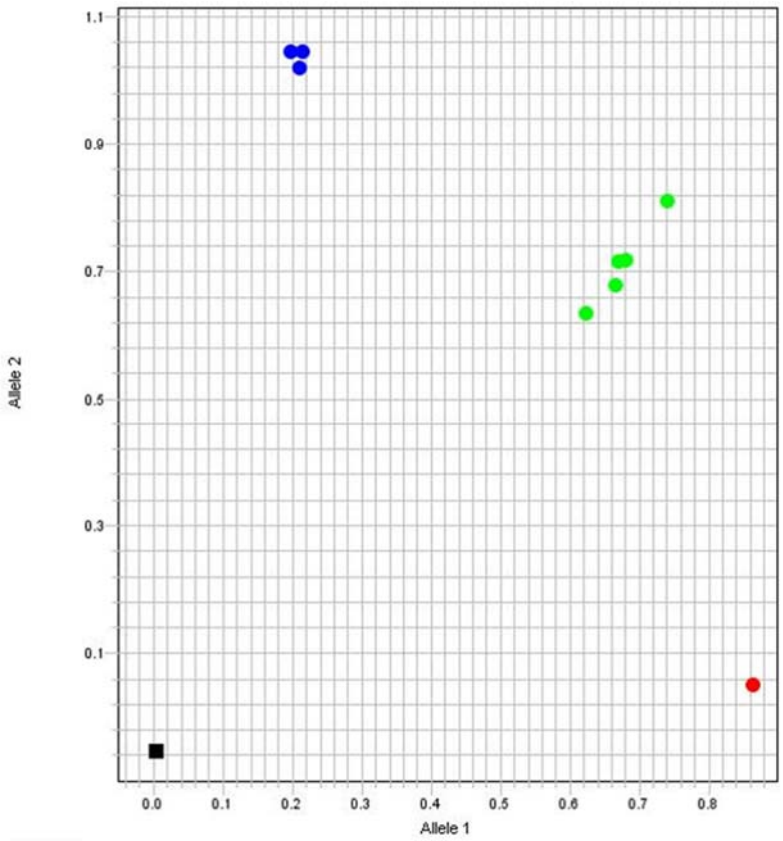

Figure 5. Allelic discrimination plot

2.4. Real-time kinetics

In Figure 6, a vehicle control indicates no effect in the signal after the addition of DMSO.

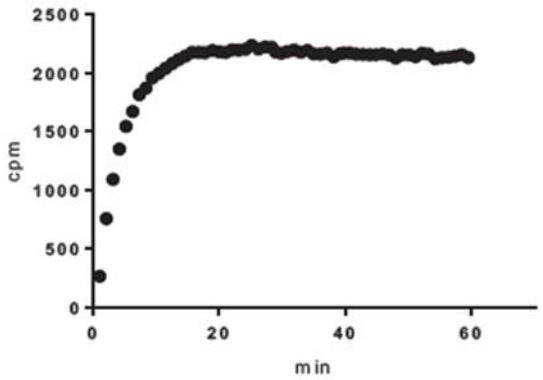

Figure 6. Vehicle controls in real-time kinetics measurements

3. References

(1) Wilson, A. A.; Garcia, A.; Parkes, J.; McCormick, P.; Stephenson, K. A.; Houle, S.; Vasdev, N. Radiosynthesis and Initial Evaluation of [18F]-FEPPA for PET Imaging of Peripheral Benzodiazepine Receptors. *Nucl. Med. Biol.* **2008**, *35* (3), 305–314.

(2) Vasdev, N.; Green, D. E.; Vines, D. C.; McLarty, K.; McCormick, P. N.; Moran, M. D.; Houle, S.; Wilson, A. A.; Reilly, R. M. Positron-Emission Tomography Imaging of the TSPO with [18F]FEPPA in a Preclinical Breast Cancer Model. *Cancer Biother. Radiopharm.* **2013**, *28* (3), 254–259.

(3) Owen, D. R. J.; Gunn, R. N.; Rabiner, E. A.; Bennacef, I.; Fujita, M.; Kreisl, W. C.; Innis, R. B.; Pike, V. W.; Reynolds, R.; Matthews, P. M.; Parker, C. A. Mixed-Affinity Binding in Humans with 18-KDa Translocator Protein Ligands. *J. Nucl. Med.* **2011**, *52* (1), 24–32.

(4) Owen, D. R.; Yeo, A. J.; Gunn, R. N.; Song, K.; Wadsworth, G.; Lewis, A.; Rhodes, C.; Pulford, D. J.; Bennacef, I.; Parker, C. A.; StJean, P. L.; Cardon, L. R.; Mooser, V. E.; Matthews, P. M.; Rabiner, E. A.; Rubio, J. P. An 18-KDa Translocator Protein (TSPO) Polymorphism Explains Differences in Binding Affinity of the PET Radioligand PBR28. *J. Cereb. Blood Flow Metab.* **2012**, *32* (1), 1–5.

(5) Zeilinger, M.; Pichler, F.; Nics, L.; Wadsak, W.; Spreitzer, H.; Hacker, M.; Mitterhauser, M. New Approaches for the Reliable in Vitro Assessment of Binding Affinity Based on High-Resolution Real-Time Data Acquisition of Radioligand-Receptor Binding Kinetics. *EJNMMI Res.* **2017**, *7*, 22.

(6) Mizrahi, R.; Rusjan, P. M.; Kennedy, J.; Pollock, B.; Mulsant, B.; Suridjan, I.; De Luca, V.; Wilson, A. A.; Houle, S. Translocator Protein (18 KDa) Polymorphism (Rs6971) Explains in-Vivo Brain Binding Affinity of the PET Radioligand [18F]-FEPPA. *J. Cereb. Blood Flow Metab.* **2012**, *32* (6), 968–972.

SUPPORTING INFORMATION

2. SYNTHESIS AND *IN VITRO* EVALUATION OF NEW TRANSLOCATOR PROTEIN LIGANDS DESIGNED FOR POSITRON EMISSION TOMOGRAPHY

Thomas Kalina,[a,‡] Neydher Berroterán-Infante,[b,c,‡] Stefan Schmitl,[b] Chrysoula Vraka,[b] Marcus Hacker,[b] Markus Mitterhauser,[b,d,e] Wolfgang Wadsak,*[,b,c,f] and Katharina Pallitsch*[,a]

[a]Department of Organic Chemistry, Faculty of Chemistry, University of Vienna, Vienna, Austria.

[b]Division of Nuclear Medicine, Department of Biomedical Imaging and Image-guided Therapy, Medical University of Vienna, Vienna, Austria.

[c]Department of Inorganic Chemistry, Faculty of Chemistry, University of Vienna, Vienna, Austria.

[d]Department of Pharmaceutical Technology, Faculty of Life Sciences, University of Vienna, Vienna Austria.

[e]Ludwig Boltzmann Institute Applied Diagnostics, Vienna, Austria.

[f]Center for Biomarker Research in Medicine, CBmed GmbH, Graz, Austria.

[‡] These authors contributed equally.

* Corresponding authors.

11. Experimental section

11.1. Materials

All chemicals were used as purchased from Sigma Aldrich, Acros, Alfa Aesar or Apollo Scientific (> 95% purity). Solvents were reagent grade and when necessary were dried by standard methods. All solvents and chemicals were used as purchased without further purification. Purity of synthesized compounds was determined via HPLC. TLC was carried out on 0.25 mm thick Millipore Sigma plates coated with silica gel 60 F254. Spots were visualized by UV light and/or dipping the plate into a solution of $(NH_4)_6Mo_7O_{24} \times 4\ H_2O$ (25.0 g) and $Ce(SO_4)_2 \times 4\ H_2O$ (1.0 g) in aqueous 10% H_2SO_4 (500 mL), followed by heating with a heat gun, if not stated differently. Flash (column) chromatography was performed with Macherey-Nagel silica gel 60 (230-400 mesh).

[^{3}H]PK11195 (3,149 TBq.mmol^{-1}) and Ultima Gold™ liquid scintillation cocktail were acquired from Perkin Elmer (Waltham, USA) and Whatman® GF/B glass fiber paper was purchased from Brandel (Gaithersburg, USA). Pierce™ BCA Protein Assay kit was acquired from ThermoFisher Scientific (Waltham, USA)

For formulation of the radiotracer, C18 plus SepPak® cartridges from Waters (Milford, USA), 0.9% saline solution from B. Braun (Melsungen, Germany), a sterile phosphate-buffered saline solution from the Vienna General Hospital's Pharmacy (Vienna, Austria) and low-protein binding Millex® GS 0.22 µm sterile filters from Millipore (Bedford, USA) were used.

11.2. Instrumentation

^{1}H, ^{13}C and ^{19}F NMR spectra were recorded in $CDCl_3$ or CD_3OD on a Bruker Avance AV III 400 (^{1}H: 400.27 MHz, ^{13}C: 100.65 MHz), AV III 600 (^{13}C: 150.93 MHz) or AV III HD 700 (^{1}H: 700.40 MHz, ^{13}C: 176.12 MHz, ^{19}F: 658.88 MHz) spectrometer. Proton NMR chemical shifts were referenced to residual $CHCl_3$ (δ_H 7.24 ppm) or CD_2HOD (δ_H 3.31 ppm). ^{13}C NMR spectra were referenced to $CDCl_3$ (δ_C 77.23 ppm) and CD_3OD (δ_C 49.00). ^{19}F NMR spectra were referenced to external CCl_3F (0.00 ppm). Chemical shifts (δ) are given in ppm and coupling constants (J) in Hz. IR spectra were run on a Bruker VERTEX 70 IR spectrometer in ATR mode. Melting points were determined on a Leica Galen III Reichert Thermovar instrument and are uncorrected.

A GE PETtrace 860 cyclotron and a TRACERlab™ FX C Pro synthesizer, both from GE Healthcare (Uppsala, Sweden), were used for the production of [^{11}C]CO_2 and the automation of the radiosynthesis of (*R*)-[^{11}C]**10**, respectively. The synthesizer has an integrated semi-preparative HPLC system, which allows the purification of the crude product, provided with a radioactivity- and UV-detector (Linear Instruments Model 200 Detector UV/VIS) in series and a LaPrep HPLC pump (VWR International, Radnor, USA).

An HPLC system (Agilent Technologies, Vienna, Austria) with a multi wavelength UV-detector and a sodium iodide - thallium detector controlled with the GINA Star software (Elysia-Raytest, Straubenhardt, Germany) was utilized for verifying the radiochemical conversions as well as for the quality control of the tracer, i.e. for determining the (radio)chemical purity and the molar radioactivity. In order to determine the osmolality of (*R*)-[^{11}C]**10**, a Wescor Vapro® 5600 osmometer was used (Sanova Medical Systems, Vienna, Austria), whereas the pH was measured using a WTW inoLab 740 pH meter (WTW, Weilheim, Germany). Gas chromatography was performed according to the general monograph on residual solvents of the European Pharmacopoeia [1], for analyzing the amount of organic volatile impurities in the tracer formulation, using a 430-GC system from Bruker (Billerica, USA), equipped with a flame ionization detector (FID).

Binding affinity experiments required the measurement of the total protein concentration (in the membranes) in a Synergy HTX plate multimode reader (Biotek, Winooski, USA) as well as liquid scintillation counting using a Hidex 300SL beta counter (Hidex, Turku, Finland).

11.3. Synthetic Chemistry

2-Phenoxybenzoic acid (13) [2]**:** 2-Iodobenzoic acid (12.4 mmol, 3.075 g) was dissolved in DMF (100 mL), phenol (2 equiv., 24.8 mmol, 2.334 g), DBU (1 ,8-diazabicyclo[5.4.0]undec-7-ene,3 equiv., 37.2 mmol, 5.663 g), copper powder (0.1 g) copper(I)iodide (0.1 g) and pyridine (0.2 mL) were added. The reaction mixture was refluxed for 2 h. The product **13** (5.59 mmol, 1.198 g, 42%) was collected as a colourless solid after precipitation with HCl (1 M, 25 mL). It was washed with water (2 × 10 mL) and dried *in vacuo.* The obtained spectroscopic data were identical to those reported in literature [2].

4-Methoxy-2-((methylamino)methyl)phenol (14a): NH_2Me (5 mmol, 0.155 g) was dissolved in EtOH (10 mL) under Ar-atmosphere. 2-Hydroxy-5-methoxybenzaldehyde (1 equiv., 5 mmol, 0.760 g) was slowly added and the reaction mixture was heated to 60 °C for 24 h. $NaBH_4$ (0.5 equiv., 2.5 mmol, 0.094 g) was added after cooling to r.t., and stirring was continued for 1 h. The reaction was quenched with water (10 mL) and extracted with EtOAc (3 × 10 mL). The combined organic phases were washed with water (10 mL), dried ($MgSO_4$) and concentrated under reduced pressure. The residue was purified by flash chromatography (CH_2Cl_2:EtOH = 6:1, R_f = 0.52) to yield 4-methoxy-2-((methylamino)methyl)phenol (**14a**, 1.73 mmol, 0.290 g, 35%) as colourless crystals; mp = 79-81 °C. ^{1}H NMR (700.40 MHz, CD_3OD): δ = 6.75-6.65 (m, 3H), 3.78 (s, 2H, CH_2), 3.72 (s, 3H, CH_3-O), 2.39 (s, 3H, CH_3-N); ^{13}C NMR (176.13 MHz, CD_3OD): δ = 154.08 (s, 1C), 151.93 (s, 1C), 125.57 (s, 1C), 116.91 (s, 1C), 116.28 (s, 1C), 114.70 (s, 1C), 56.16 (s, 1C, CH_3-N), 53.16 (s, 1C, CH_2-N), 34.98 (s, 1C, CH_3-O); IR (ATR): ν = 3292, 1453, 1269, 1082, 801 cm^{-1}; HRMS (ESI): m/z calculated for $C_9H_{13}NO_2 – H^+$ [M – H$^+$]: 168.1019. Found: 168.1015.

***N*-(2-hydroxy-5-methoxybenzyl)-*N*-methyl-2-phenoxybenzamide (15):** 2-Phenoxybenzoic acid (**13**, 1.73 mmol, 0.371 g) and 4-methoxy-2-((methylamino)methyl)phenol (**14a**, 1 equiv., 1.73 mmol, 0.290 g) were dissolved in CH_2Cl_2 (10 mL) under Ar-atmosphere. HOBt (1 equiv., 2.07 mmol, 0.280 g) was slowly added followed by EDC×HCl (1 equiv., 2.07 mmol, 0.397 g). Then, the reaction mixture was stirred at r.t. for 16 h. EtOAc (5 mL) was added and the organic phase was washed with water (10 mL), $NaHCO_3$ (sat. aqueous sol., 10 mL), brine (10 mL). Finally it was dried ($MgSO_4$) and concentrated under reduced pressure. The residue was purified by flash chromatography (heptanes:EtOAc = 2:1, R_f = 0.51) to yield *N*-(2-hydroxy-5-methoxybenzyl)-*N*-methyl-2-phenoxybenzamide (**15**, 0.98 mmol, 0.357 g, 57%) as a highly viscous oil. ^{1}H NMR (700.40 MHz, CD_3OD): δ = 7.42-7.31 (m, 8H, 4x major conformer A + 4x minor conformer B), 7.21 (td, *J* = 7.5 Hz, *J* = 0.7 Hz, 2H, B), 7.18-7.11 (m, 2H, A), 7.04-7.01 (m, 2H, A), 7.01-6.98 (m, 2H, B), 6.91 (d, *J* = 8.2 Hz, 1H, A), 6.85 (d, *J* = 8.3 Hz, 1H, B), 6.81 (d, *J* = 3 Hz, 1H, A), 6.74-6.65 (m, 4H, 2x A + 2x B), 6.63-6.61 (m, 1H, B), 4.80-4.30 (m, 4H, CH_2-N, 2x A + 2x B), 3.63 (s, 3H, CH_3-O, B), 3.55 (s, 3H CH_3-O, A), 2.96 (s, 3H CH_3-N, B), 2.95 (s, 3H, CH_3-N, A); ^{13}C NMR (176.13 MHz, CD_3OD): δ = 171.67 (s, 1C, C=O, B), 171.67 (s, 1C, C=O, A), 157.69 (s, 1C, A), 157.64 (s, 1C, B), 154.90 (s, 1C, B), 154.69 (s, 1C, A), 154.53 (s, 1C, A), 154.40 (s, 1C, B), 150.54 (s, 1C, A), 150.41 (s, 1C, B), 132.08 (s, 1C, A), 131.92 (s, 1C, B), 131.01 (s, 2C, A), 130.98 (s, 2C, B), 129.83 (s, 1C, B), 129.34 (s, 1C, A), 129.09 (s, 1C, A), 129.01 (s, 1C, B), 125.18 (s, 1C, B), 125.17 (s, 1C, A), 124.78 (s, 1C, A), 124.35 (s, 1C, B), 124.33 (s, 1C, B), 124.28 (s, 1C, A), 120.55 (s, 2C, B), 120.33 (s, 2C, A), 119.26 (s, 1C, A), 118.82 (s, 1C, B), 117.21 (s, 1C, B), 116.76 (s, 1C, B), 115.46 (s, 1C, A), 115.34 (s, 1C, A), 115.32 (s, 1C, B), 114.85 (s,

1C, B), 56.10 (s, 1C, CH_3-O, A), 56.08 (s, 1C, CH_3-O, B), 51.18 (s, 1C, CH_2-N, B), 46.81 (s, 1C, CH_2-N, A), 37.05 (s, 1C, CH_3-N, A), 33.16 (s, 1C, CH_3-N, B); IR (ATR): ν = 3306, 1601, 1490, 1237, 631 cm^{-1}; HRMS (ESI): m/z calculated for $C_{22}H_{21}NO_4$ – Na^+ [M – Na^+]: 386.1368. Found: 386.1355.

***N*-(2-(2-tosylethoxy)-5-methoxybenzyl)-*N*-methyl-2-phenoxybenzamide (16):** NaH (1.2 equiv., 0.33 mmol, 0.008 g) and ethylene ditosylate (2 equiv., 0.55 mmol, 0.203 g) were added to a solution of *N*-(2-hydroxy-5-methoxybenzyl)-*N*-methyl-2-phenoxybenzamide (**15**, 0.27 mmol, 0.100 g) in dry DMF (4 mL), under Ar-atmosphere,. After stirring for 18 h at r.t., acetic acid (conc., 5 drops) was added and the solvent was removed under reduced pressure. The residue was taken up in EtOAc (5 mL) and washed with water (2 × 5 mL). The combined organic phases were dried ($MgSO_4$) and concentrated under reduced pressure. The residue was purified by flash chromatography (heptanes:EtOAc = 3:1, R_f = 0.46) to yield the desired tosylated precursor **16** (0.12 mmol, 0.068 g, 44%) as highly viscous oil. ^{1}H NMR (700.40 MHz, CD_3OD): δ = 7.79 (d, *J* = 8.3 Hz, 2H, major conformer A), 7.71 (d, *J* = 8.3 Hz, 2H, minor conformer B), 7.44-7.30 (m, 12H, 6x A + 6x B), 7.23 (t, *J* = 7.5 Hz, 1H, A), 7.18-7.13 (3H, 1x A + 2x B), 7.04 (d, *J* = 8.5 Hz, 2H, A), 7.00 (d, *J* = 8.5 Hz, 2H, B), 6.90 (d, *J* = 8.1 Hz, 1H, A), 6.854 (d, *J* = 7.7 Hz, 1H, B), 6.851 (d, *J* = 7.7 Hz, 1H, A), 6.79 (d, *J* = 12.6 Hz, 1H, B), 6.78 (d, *J* = 12.7 Hz, 1H, A), 6.74 (dd, *J* = 8.9 Hz, *J* = 2.9 Hz, B), 6.72 (dd, *J* = 8.9 Hz, *J* = 3.0 Hz, 1H, A), 6.65 (d, *J* = 2.9 Hz, 1H, B), 4.73 (m, 2H, CH_2-N, A), 4.46 (broad s, 2H, CH_2-N, B), 4.35 (broad s, 2H, CH_2-O, A), 4.29 (t, *J* = 4.3 Hz, 2H, CH_2-OTs, B), 4.12 (t, *J* = 4.3 Hz, CH_2-OTs, A), 4.08 (broad s, 2H, CH_2-O, B), 3.66 (s, 3H, CH_3-O, B), 3.54 (s, 3H, CH_3-O, A), 2.92 (s, 3H, CH_3-N, B), 2.87 (s, 3H, CH_3-N, A), 2.40 (s, 6H, CH_3-Ph, 3x A + 3x B); ^{13}C NMR (176.13 MHz, CD_3OD): δ = 171.68 (s, 1C, C=O, B), 171.35 (s, 1C, C=O, A), 157.61 (s, 1C, A), 157.52 (s, 1C, B), 155.81 (s, 1C, A), 155.68 (s, 1C, B), 154.97 (s, 1C, B), 154.70 (s, 1C, A), 151.49 (s, 1C, A), 151.12 (s, 1C, B), 146.59 (s, 1C, A), 146.53 (s, 1C, B), 134.42 (s, 1C, B), 134.40 (s, 1C, A), 132.07 (s, 1C, B), 131.99 (s, 1C, A), 131.12 (s, 2C, A), 131.07 (s, 2C, B), 131.06 (s, 2C, B), 131.05 (s, 2C, A), 129.66 (s, 1C, B), 129.27 (s, 1C, A), 129.25 (s, 1C, A), 129.05 (s, 2C, A), 128.94 (s, 2C, B), 128.79 (s, 1C, B), 127.16 (s, 1C, A), 125.30 (s, 1C, B), 125.27 (s, 1C, A), 124.77 (s, 1C, A), 124.45 (s, 1C, B), 120.68 (s, 2C, B), 120.52 (s, 2C, A), 118.99 (s, 1C, A), 118.89 (s, 1C, B), 115.58 (s, 1C, B), 115.45 (s, 1C, A), 114.26 (s, 1C, A), 114.23 (s, 1C, B), 114.23 (s, 1C, A), 114.10 (s, 1C, B), 70.22 (s, 1C, CH_2-OTs, A), 70.03 (s, 1C, CH_2-OTs, B), 67.77 (s, 1C, CH_2-O, A), 67.60 (s, 1C, CH_2-O, B), 55.99 (s, 1C, CH_3-O, B), 55.95 (s, 1C, CH_3-O, A), 50.69 (s, 1C, CH_2-N, A), 46.10 (s, 1C, CH_2-N, B), 37.20 (s, 1C, CH_3-N, A), 33.48 (s, 1C, CH_3-N, B), 21.60 (s, 1C, CH_3-Ph, A), 21.57 (s, 1C, CH_3-Ph, B); IR (ATR): ν = 1632, 1487, 1212, 918, 751 cm^{-1}; HRMS (ESI): m/z calculated for $C_{31}H_{31}NO_7S$ – Na^+ [M – Na^+]: 584.1713. Found: 584.1701.

***N*-(2-(2-fluoroethoxy)-5-methoxybenzyl)-*N*-methyl-2-phenoxybenzamide (6):** *N*-(2-hydroxy-5-methoxybenzyl)-*N*-methyl-2-phenoxybenzamide (**15**, 0.27 mmol, 0.100 g) was dissolved in DMF (4 mL), under Ar-atmosphere, NaH (1.2 equiv., 0.33 mmol, 0.008 g) and 2-fluoroethyl 4-methylbenzenesulonate (1.2equiv., 0.33 mmol, 0.072 g) were added. After stirring for 18 h at r.t. acetic acid (conc., 5 drops) was added and the solvent was removed under reduced pressure. The residue was taken up in EtOAc (5 mL) and washed with water (2 × 5 mL). The combined organic phases were dried ($MgSO_4$) and concentrated under reduced pressure. The residue was purified by flash chromatography (heptanes:EtOAc = 3:1, R_f = 0.48) to yield *N*-(2-(2-fluoroethoxy)-5-methoxybenzyl)-*N*-methyl-2-phenoxybenzamide (**6**, 0.21 mmol, 0.084 g, 75%) as a highly viscous oil. ^{1}H NMR (700.40 MHz, CD_3OD): δ = 7.44 (m, 8H, 4x major conformer A + 4x minor conformer B), 7.21 (td, *J* =7.6 Hz, *J* = 0.8 Hz, 1H, A), 7.17-7.13 (m, 3H, 1x A + 2x B), 7.05-7.02 (m, 2H, A), 6.99-6.96 (m, 2H, B), 6.93-6.99 (m, 4H, 2x A + 2x B), 6.84 (d, *J* = 8.3 Hz, 1H, B), 6.78 (td, *J* = 9.4 Hz, *J* = 3.1 Hz, 2H, A), 6.68 (d, *J* = 3.1 Hz, 1H, B), 4.77 (m, 8H, CH_2-F, CH_2-N, 4x A + 4x B), 4.23 (m, 4H, CH_2-O, 2x A+ 2x B), 3.67 (s, 3H, CH_3-O, B), 3.56 (s, 3H CH_3-O, A), 3.00 (s, 3H, CH_3-N, B), 2.93 (s, 3H, CH_3-N, A); ^{13}C NMR (176.13 MHz, CD_3OD): δ = 171.78 (s, 1C, C=O, B), 171.35 (s, 1C, C=O, A), 157.65 (s, 1C, A), 157.54 (s, 1C, B), 155.76 (s, 1C, A), 155.63 (s, 1C, B), 154.95 (s, 1C, B), 154.67 (s, 1C, A), 152.01 (s, 1C, A), 151.65 (s, 1C, B). 131.99 (s, 1C, B), 131.95 (s, 1C, A), 131.03 (s, 2C, A), 131.00 (s, 2C, B), 129.63 (s, 1C, B), 129.33 (s, 1C, A), 129.26 (s, 1C, A), 128.84 (s, 1C, B), 127.27 (s, 1C, A), 127.08 (s, 1C, B), 125.25 (s, 1C, B), 125.21 (s, 1C, A), 124.74 (s, 1C, A), 124.39 (s, 1C, B), 120.59 (s, 2C, B), 120.44 (s, 2C, A), 119.03 (s, 1C, A), 118.83 (s, 1C, B), 115.69 (s, 1C, A), 115. 62 (s, 1C, B), 114.51 (s, 1C, A), 114.45 (s, 1C, A), 114.40 (s, 1C, B), 114.18 (s, 1C, B), 83.29 (d, *J* = 168.7 Hz, 1C, CH_2-F, A), 83.18 (d, *J* = 168.9 Hz, 1C, CH_2-F, B), 69.82 (d, *J* = 19.8 Hz, 1C CH_2-O, A), 69.62 (d, *J* = 19.7 Hz, 1C, CH_2-O, B), 55.99 (s, 1C, CH_3-O, B), 55.98 (s, 1C, CH_3-O, A), 50.94 (s, 1C, CH_2-N, A), 46.35 (s, 1C, CH_2-N, B), 37.15 (s, 1C, CH_3-N, A), 35.54 (s, 1C, CH_3-N, B); ^{19}F NMR (658.88 MHz, CD_3OD): δ = –225.03 (s, 1F CH_2-F, B), –225.08 (s, 1F, CH_2-F, A); IR (ATR): ν =1632, 1486, 1211, 1038, 752 cm^{-1}.
HRMS (ESI): m/z calculated for $C_{24}H_{24}FNO_4$ – Na^+ [M – Na^+]: 432.1581. Found: 432.1574.

Ethyl 4-chloronicotinate [3]**:** 4-Chloronicotinic acid (30 mmol, 4.726 g) was dissolved in dry CH_2Cl_2 (60 mL). Thionyl chloride (3 equiv., 90 mmol, 6.52 mL) and DMF (3 drops) were added and the reaction mixture was refluxed for 16 h. The solvent was evaporated under reduced pressure, the residue was dissolved in dry EtOH (48 ml) and Et_3N (2 equiv., 60 mmol, 8.32 mL) was added. After stirring 18 h at r.t., the solvent was evaporated und the residue taken up in a 1:1 mixture of H_2O and CH_2Cl_2 (30 mL). The phases were separated and the aqueous phase was extracted with CH_2Cl_2 (2 × 7 mL). The combined organic phases were washed with brine, dried ($MgSO_4$) and concentrated

under reduced pressure. The residue was purified by flash chromatography (heptanes:EtOAc = 1:1) to yield ethyl 4-chloronicotinate (3.970 g, 21.4 mmol, 71%) as a colourless oil. The obtained spectroscopic data were identical to those reported in literature [3].

Ethyl 4-phenoxynicotinate [4]**:** A solution of ethyl 4-chloronicotinate (5 mmol, 0.928 g) and K_2CO_3 (3 equiv., 15 mmol, 2.073 g) in dry DMF (20 mL) was stirred for 5 min before phenol (1.1 equiv., 5.5 mmol, 0.517 g) was slowly added. The resulting reaction mixture was heated at 90 °C for 3 h. Then, water (20 mL) was added and the mixture was extracted with EtOAc (3 × 20 mL), the combined organic phases were washed with brine (20 mL), dried ($MgSO_4$) and concentrated under reduce pressure. The residue was purified by flash chromatography (heptanes:EtOAc = 4:1, R_f = 0.23) to yield nicotinate (3.68 mmol, 0.896 g, 74%). The obtained spectroscopic data were identical to those reported in the literature [4].

4-Phenoxynicotinic acid (18): Ethyl 4-phenoxynicotinate (3.86 mmol, 0.896 g) was dissolved in 1,4-dioxane:H_2O (1:1, 30 mL) and NaOH (2 equiv., 7.36 mmol, 0.294 g) was added to the resulting solution. Stirring was continued for 3 h, the solvent was evaporated and the residue was taken up in H_2O (20 mL). The pH was adjusted to 3 (using 2 M HCl) and the product was extracted with EtOAc (18 × 20 mL). The combined organic phases were dried ($MgSO_4$) and concentrated under reduce pressure. The residue was purified by flash chromatography (EtOAc = 100%, R_f = 0.14) to yield ethyl 4-phenoxynicotinic acid (**18**, 0.17 mmol, 0.373 g, 47%) as colourless crystals. The recorded data were identical to those reported in literature [5].

***N*-(2-hydroxybenzyl)-*N*-methyl-4-phenoxynicotinamide (19):** 4-Phenoxynicotinic acid (**18**, 1.34 mmol, 0.290 g) and 2-((methylamino)methyl)phenol [6] (1 equiv., 1.34 mmol, 0.184 g) were combined in CH_2Cl_2 (5 mL) under Ar-atmosphere. After slow addition of HOBt (hydroxybenzotriazole, 1 equiv., 1.34 mmol, 0.182 g) and EDC×HCl [*N*-(3-Dimethylaminopropyl)-*N*'-ethylcarbodiimide hydrochloride, 1 equiv., 1.34 mmol, 0.257 g] the reaction mixture was stirred at r.t. for 24 h. EtOAc (5 mL) was added and the organic phase was extracted with water (10 mL), $NaHCO_3$ (saturated aqueous solution, 10 mL), brine (10 mL), dried ($MgSO_4$), and concentrated under reduced pressure. Recrystallization from EtOAc gave *N*-(2-hydroxybenzyl)-*N*-methyl-4-phenoxynicotinamide (**19**, 0.75 mmol, 0.249 g, 56%) as colourless crystals; mp = 182-184 °C. ^{1}H NMR (400.27 MHz, CD_3OD): δ = 8.49 (s, 1H, minor conformer B), 8.46 (s, 1H, major conformer A), 8.43 (d, *J* = 5.9 Hz, 1H, B), 8.37 (d, *J* = 5.9 Hz, 1H, A), 7.52-7.45 (m, 4H, A+B), 7.35-7.07 (m, 10H, A+B), 6.83-6.70 (m, 6H, A+B), 4.78 (signal overlapping with OD, 2H, A+B, 2 x OH), 3.03 (s, 3H, A,

CH_3), 3.00 (s, 3H, B, CH_3); ^{13}C NMR (100.65 MHz, CD_3OD): δ = 168.76 (s, 1C, C=O), 168.67 (s, 1C, C=O), 162.80 (s, 1C), 162.61 (s, 1C), 156.92 (s, 1C), 156.90 (s, 1C), 154.95 (s, 1C), 154.92 (s, 1C), 152.95 (s, 1C), 152.49 (s, 1C), 150.55 (s, 1C), 150.09 (s, 1C), 131.58 (s, 1C), 131.52 (s, 1C), 130.70 (s, 1C), 130.27 (s, 1C), 130.15 (s, 1C), 129.99 (s, 1C), 127.19 (s, 1C), 124.87 (s, 1C), 124.85 (s, 1C), 123.37 (s, 1C), 121.95 (s, 1C), 121.68 (s, 1C), 120.70 (s, 1C), 120.57 (s, 1C), 116.62 (s, 1C), 116.22 (s, 1C), 112.09 (s, 1C), 111.77 (s, 1C), 51.63 (s, 1C, CH_2), 47.12 (s, 1C, CH_2), 36.86 (s, 1C, CH_3), 33.34 (s, 1C, CH_3); IR (ATR): ν = 3059, 1627, 1463, 1191, 748 cm^{-1}; HRMS (ESI): m/z calculated for $C_{20}H_{18}N_2O_3 – H^+$ [M – H^+]: 335.1390. Found: 335.1391.

***N*-(2-hydroxybenzyl)-4-phenoxynicotinamide (20):** After slow addition of HOBt (1 equiv., 2.07 mmol, 0.280 g) and EDC×HCl (1 equiv., 2.07 mmol, 0.397 g) were slowly added to a solution of **18** (2.07 mmol, 0.447 g) and 2-(aminomethyl)phenol [7] (1 equiv., 2.07 mmol, 0.256 g) in dry CH_2Cl_2 (5 mL) under Ar-atmosphere. The reaction mixture was stirred at r.t. for 16 h before the addition of EtOAc (5 mL).The organic phase was washed with water (10 mL), $NaHCO_3$ (sat. aqueous solution, 10 mL), brine (10 mL), dried ($MgSO_4$) and concentrated under reduced pressure. The residue was purified by flash chromatography (CH_2Cl_2:EtOH = 19:1, R_f = 0.64) to yield *N*-(2-hydroxybenzyl)-4-phenoxynicotinamide (**20**, 1.11 mmol, 0.355 g, 53%) as colourless crystals. mp = 174-175 °C. ^1H NMR (700.40 MHz, CD_3OD): δ = 8.91 (s, 1H), 8.41 (d, *J* = 5.9 Hz, 1H), 7.54-7.49 (m, 2H), 7.38-7.34 (m, 1H), 7.24-7.21 (dd, *J* = 7.5 Hz, *J* = 1.26 Hz, 1H), 7.23-7.21 (m, 2H), 7.08 (td, *J* = 8.0 Hz, *J* = 1.6 Hz, 1H), 6.78-6.72 (m, 3H), 4.60 (s, 2H, CH_2-N); ^{13}C NMR (176.13 MHz, CD_3OD): δ = 165.75 (s, 1C, C=O), 164.52 (s, 1C), 156.78 (s, 1C), 154.44 (s, 1C), 153.84 (s, 1C), 152.85 (s, 1C), 131.68 (s, 2C), 130.39 (s, 1C), 129.80 (s, 1C), 127.57 (s, 1C), 125.57 (s, 1C), 125.38 (s, 1C), 122.26 (s, 1C), 121.53 (s, 1C), 116.12 (s, 1C), 111.97 (s, 1C), 40.81 (s, 1C, CH_2-N); IR (ATR): ν = 3365, 2500, 2076, 1650, 971 cm^{-1}; HRMS (ESI): m/z calculated for $C_{19}H_{16}N_2O_3 – H^+$ [M – H^+]: 321.1233. Found: 321.1229.

***N*-(2-methoxybenzyl)-*N*-methyl-4-phenoxynicotinamide (7): 19** (0.15 mmol, 0.053 g) was dissolved in DMF (2 mL), under Ar-atmosphere, and cooled to 0 °C. NaH (1.5 equiv., 0.23 mmol, 0.005 g), dissolved in DMF (1 mL), was added and the reaction was allowed to stir for 45 min. Afterwards, CH_3I (2 equiv., 0.31 mmol, 0.044 g) was slowly added and stirring was continued for 2 h. The reaction mixture was quenched with HCl (2 M, 2 mL) and the aqueous phase was extracted with CH_2Cl_2 (3 × 4 mL). The combined organic phases were washed with brine (5 mL), dried ($MgSO_4$) and concentrated under reduced pressure. The residue was purified by flash chromatography (EtOAc = 100%, R_f = 0.27) to yield *N*-(2-methoxybenzyl)-*N*-methyl-4-

phenoxynicotinamide (**7**, 0.11 mmol, 0.0367 g, 67%) as white crystals; mp = 106-110 °C. ^{1}H NMR (400.27 MHz, CD_3OD): δ = 8.52 (s, 1H, minor conformer B), 8.47 (s, 1H, major conformer A), 8.45 (d, *J* = 6.0 Hz, 1H, B), 8.41 (d, *J* = 5.9 Hz, 1H, A), 7.56-7.46 (m, 4H, 2x A + 2x B), 7.39-7.17 (m, 8H, 4x A + 4x B), 7.15-7.01 (m, 2H, A + B), 7.01-6.96 (m, 2H, A + B), 6.93 (td, *J* = 7.4 Hz, *J* = 0.9 Hz, 1H, A), 6.86 (td, *J* = 7.4 Hz, *J* = 0.9 Hz, 1H, B), 6.82 (d, *J* = 5.9 Hz, 1H, B), 6.74 (*d, J* = 5.9 Hz, 1H, A), 4.79-4.33 (m, 4H, CH_2-N, A + B), 3.84 (s, 3H, CH_3-O, B), 3.79 (s, 3H, CH_3-O, A), 3.06 (s, 3H, CH_3-N, A), 2.99 (s, 3H, CH_3-N, B); ^{13}C NMR (150.93 MHz, CD_3OD): δ = 168.65 (s, 1C, B), 168.34 (s, 1C, A), 162.86 (s, 1C, A), 162.65 (s, 1C, B), 159.07 (s, 1C, B), 158.96 (s, 1C, A), 154.75 (s, 1C, A), 154.67 (s, 1C, B), 152.87 (s, 1C, B), 152.65 (s, 1C, A), 150.35 (s, 1C, A), 149.94 (s, 1C, B), 131.72 (s, 2C, B), 131.63 (s, 2C, A), 130.57 (s, 1C, A), 130.32 (s, 1C, A), 129.98 (s, 1C, B), 129.71 (s, 1C, B), 127.38 (s, 1C, B), 127.37 (s, 1C, A), 124.97 (s, 1C, A), 124.91 (s, 1C, B), 124.86 (s, 1C, A), 124.60 (s, 1C, B), 122.03 (s, 2C, A), 121.86 (s, 2C, B), 121.60 (s, 1C, A), 121.58 (s, 1C, B), 111.85 (s, 1C, B), 111.70 (s, 1C, A), 111.69 (s, 1C, B), 111.51 ((s, 1C, A), 55.84 (s, 1C, CH_3-O, B), 55.73 (s, 1C, CH_3-O, A), 51.55 (s, 1C, CH_2-N, A), 46.82 (s, 1C, CH_2-N, B), 36.97 (s, 1C, CH_3-N, B), 33.42 (s, 1C, CH_3-N, A); IR (ATR): ν = 1622, 1474, 1254, 1198, 752 cm^{-1}; HRMS (ESI): m/z calculated for $C_{21}H_{20}N_2O_3 - H^+$ [M – H^+]: 349.1547. Found: 349.1539.

***N*-(2-(2-fluoroethoxy)benzyl)-*N*-methyl-4-phenoxynicotinamide (8): 19** (0.30 mmol, 0.100 g) was dissolved in DMF (4 mL), under Ar-atmosphere. Then, NaH (1.2 equiv., 0.36 mmol, 0.008 g) and 2-fluoroethyl 4-methylbenzenesulfunate (1.2 equiv., 0.36 mmol, 0.078 g) were added one after the other. Acetic acid (conc., 5 drops) was added to the reaction mixture after 18 h at r.t. and the solvent was removed under reduced pressure. The residue was taken up in EtOAc (5 mL) and extracted with water (2 × 5 mL). The combined organic phases were dried ($MgSO_4$) and concentrated under reduced pressure. The residue was purified by flash chromatography (EtOAc = 100%, R_f = 0.31) to yield the desired fluoroethyl derivative **8** (0.25 mmol, 0.094 g, 83%) as a highly viscous oil. ^{1}H NMR (700.40 MHz, CD_3OD): δ = 8.50 (s, 1H, major conformer A), 8.44 (s, 1H, minor conformer B), 8.43 (d, *J* = 5.9 Hz, A), 8.37 (d, *J* = 5.9 Hz, B), 7.52-7.48 (m, 2H, A), 7.48-7.45 (m, 2H, B), 7.37-7.30 (m, 3H, A), 7.29-7.23 (m, 2H, B), 7.18 (d, *J* = 8.2 Hz, 2H, A), 7.15 (d, *J* = 7.1 Hz, 1H, B), 7.09 (d, *J* = 8.2 Hz, 2H, B), 6.98 (t, *J* = 8.3 Hz, 2H, A + B), 6.94 (t, *J* = 7.5 Hz, 1H, B), 6.89 (t, *J* = 7.4 Hz, 1H, A), 6.80 (d, *J* = 5.8 Hz, 1H, A), 6.70 (d, *J* = 6.0 Hz, 1H, B), 4.84-4.47 (broad m, 4H, 2x A + 2x B), 4.79 (s, 1H, A), 4.74-4.69 (m, 1H, A), 4.67-4.63 (m, 1H, A), 4.27 (s, 1H, B), 4.25-4.21 (m, 1H, B), 4.21-4.18 (m, 1H, B), 3.10 (s, 3H, CH_3, B), 2.98 (s, 3H, CH_3,B); ^{13}C NMR (176.13 MHz, CD_3OD): δ = 168.82 (s, 1C, C=O, B), 168.29 (s, 1C, C=O, A), 162.90 (s, 1C, B), 162.26 (s, 1C, A), 158.10 (s, 1C, A), 157.69 (s, 1C, B), 154.77 (s, 1C, A), 154.65 (s, 1C, B), 152.84 (s, 1C, A), 152.70 (s, 1C, B), 150.12 (s, 1C, B),

149.99 (s, 1C, A), 131.68 (s, 2C, A), 131.61 (s, 2C, B), 130.44 (s, 1C, A), 130.34 (s, 1C, B), 130.09 (s, 1C, A), 129.80 (s, 1C, B), 127.37 (s, 1C, B), 127.33 (s, 1C, A), 125.61 (s, 1C, B), 125.60 (s, 1C, A), 124.93 (s, 1C, A), 124.54 (s, 1C, B), 122.24 (s, 1C, B), 122.17 (s, 1C, A), 122.05 (s, 2C, B), 121.81 (s, 2C, A), 113.00 (s, 1C, B), 112.85 (s, 1C, A), 111.88 (s, 1C, A), 111.68 (s, 1C, B), 83.21 (d, *J* = 168.8, 1C, CH_2-F, B), 83.04 (d, *J* = 169.0 Hz, 1C, CH_2-F, A), 68.95 (d, *J* = 19.9 Hz, 1C, CH_2-O, A), 68.90 (d, *J* = 19.6 Hz, 1C, CH_2-O, B), 51.27 (s, 1C, CH_2-N, B), 46.82 (s, 1C, CH_2-N, A), 36.95 (s, 1C, CH_3-N, A), 33.91 (s, 1C, CH_3-N, B); ^{19}F NMR (658.88 MHz, CD_3OD): δ = –224.91 (s, 1F, CH_2-F, A), –225.01 (s, 1F, CH_2-F, B); IR (ATR): ν = 1631, 1480, 1266, 1199, 631 cm^{-1}; HRMS (ESI): m/z calculated for $C_{22}H_{21}FN_2O_3$ – H^+ [M – H^+]: 381.1609. Found: 381.1596.

***N*-(2-(2-fluoroethoxy)benzyl)-4-phenoxynicotinamide (21): 20** (0.312 mmol, 0.100 g) was dissolved in DMF (4 mL), under Ar-atmosphere, KO*t*Bu (1.1 equiv., 0.343 mmol, 0.038 g) and 2-fluoroethyl 4-methylbenzenesulfunate (1.2 equiv., 0.374 mmol, 0.080 g) were added subsequently and the reaction mixture was stirred at 50 °C for 18 hThe solvent was removed under reduce pressure and the residue taken up in EtOAc (10 mL), washed with water (2 × 10 mL), dried ($MgSO_4$) and concentrated under reduced pressure. The residue was purified by flash chromatography (heptanes:EtOAc = 1:3, R_f = 0.45) to yield the desired fluoroethoxyderivative **21** (0.21 mmol, 0.076 g, 67%) as highly viscous oil. ^{1}H NMR (700.40 MHz, CD_3OD): δ = 8.87 (s, 1H), 8.41 (d, *J* = 5.9 Hz, 1H), 7.53-7.49 (m, 2H), 7.37-7.33 (m, 2H), 7.25 (td, *J* = 8.1 Hz, *J* = 1.6 Hz, 1H), 7.22-7.19 (m, 2H), 6.96 (d, *J* = 8.2 Hz, 1H), 6.91 (td, *J* = 7.5 Hz, *J* = 0.5 Hz, 1H), 6.74 (d, *J* = 5.9 Hz, 1H), 4.68 -4.65 (m, 1H, CH_2-F), 4.64 (s, 2H, CH_2-NH), 4.61-4.58 (m, 1H, CH_2-F), 4.22-4.20 (m, 1H, CH_2-O), 4.18-4.15 (m, 1H, CH_2-O); ^{13}C NMR (176.13 MHz, CD_3OD): δ = 165.75 (s, 1C, C=O), 164.38 (s, 1C), 157.90 (s, 1C), 154.53 (s, 1C), 153.73 (s, 1C), 152.65 (s, 1C), 131.69 (s, 2C), 130.25 (s, 1C), 129.96 (s, 1C), 127.65 (s, 1C), 127.57 (s, 1C), 122.22 (s, 2C), 122.12 (s, 1C), 122.07 (s, 1C), 112.85 (s, 1C), 112.06 (s, 1C), 83.09 (d, *J* = 168.91 Hz, 1C, CH_2-F), 68.92 (d, *J* = 19.9 Hz, 1C, CH_2-O), 40.48 (s, 1C, CH_2-NH); ^{19}F NMR (658.88 MHz, CD_3OD): δ = –225.13 (d, *J* = 1.3 Hz, 1F, CH_2-F); IR (ATR): ν = 3422, 1648, 1476, 1251, 631 cm^{-1}; HRMS (ESI): m/z calculated for $C_{21}H_{19}FN_2O_3$ – H^+ [M – H^+]: 367.1452. Found: 367.1444.

***N*-(2-(2-tosylethoxy)benzyl)-*N*-methyl-4-phenoxynicotinamide (22): 19** (0.44 mmol, 0.150 g) was dissolved in CH_2Cl_2 (5 mL), under Ar-atmosphere and NaH (1.2 equiv., 0.54 mmol, 0.012 g) followed by ethylene ditosylate (1.2 equiv., 0.54 mmol, 0.193 g) were added. After stirring for 4.5 h at r.t., the reaction was quenched by addition of NH_4Cl (sat. aqueous solution, 4 mL). The aqueous phase was extracted with EtOAc (2 × 10 mL). The combined organic phases were washed with HCl (1 M,

5 mL) and brine (5 mL), dried ($MgSO_4$) and concentrated under reduce pressure. The residue was purified by flash chromatography (EtOAc = 100%, R_f = 0.48) to yield the desired tosylate **22** (0.137 mmol, 0.073 g, 31%) as colourless crystals; mp = 244-245 °C (decomp.). ^{1}H NMR (700.40 MHz, CD_3OD): δ = 8.52 (s, 1H, major conformer A), 8.45 (d, *J* = 5.9 Hz, 1H, A), 8.41 (s, 1H, minor conformer B), 8.36 (d, *J* = 5.9 Hz, 1H, B), 7.80 (d, *J* = 8.3 Hz, 2H, B), 7.71 (d, *J* = 8.3 Hz, 2H, A), 7.51 (t, *J* = 7.7 Hz, 2H, A), 7.47 (t, *J* = 7.7 Hz, 2H, B), 7.39 (d, *J* = 7.9 Hz, 2H, A), 7.35 (d, *J* = 7.9 Hz, 2H, B), 7.35-7.29 (m, 2H, A+B), 7.24-7.18 (m, 3H, 2A+B), 7.19 (d, *J* = 7.7 Hz, 2H, A), 7.12 (d, *J* = 7.7 Hz, 2H, B), 6.93 (t, *J* = 7.5 Hz, 1H, B), 6.88 (t, *J* = 7.7 Hz, 2H, A+B), 6.87 (t, *J* = 7.5 Hz, 1H, A), 6.80 (d, *J* = 5.9 Hz, 1H, A), 6.71 (d, *J* = 5.9 Hz, 1H, B), 4.72 (broad s, 2H CH_2-N, B), 4.52 (broad s, 2H, CH_2-N, A), 4.39 (broad t, *J* = 4.1 Hz, 2H, O-CH_2, A), 4.31 (broad t, *J* = 3.8 Hz, 2H, O-CH_2, B), 4.19 (t, *J* = 4.2 Hz, 2H, -CH_2-OTs, A), 4.17 (broad s, 2H, -CH_2-OTs, B), 3.05 (s, 3H, N-CH_3, B), 2.94 (s, 3H, N-CH_3, A), 2.41 (s, 3H, Ts-CH_3, B), 2.40 (s, 3H, Ts-CH_3, A); ^{13}C NMR (176.13 MHz, CD_3OD): δ = 168.81 (s, 1C, C=O, B), 168.37 (s, 1C, C=O, A), 162.88 (s, 1C, A), 162.59 (s, 1C, B), 157.56 (s, 1C, A), 157.08 (s, 1C, B), 154.73 (s, 1C, A), 154.63 (s, 1C, B), 152.92 (s, 1C, A), 152.78 (s, 1C, B), 150.02 (s, 1C, A), 149.98 (s, 1C, B), 146.62 (s, 1C, A), 146,58 (s, 1C, B), 134.44 (s, 1C, B), 134.39 (s, 1C, A), 131.73 (s, 2C, A) 131.63 (s, 2C, B), 131.13 (s, 2C, A), 131.08 (s, 2C, B), 130.17 (s, 1C, B), 129.93 (s, 1C, A), 129.50 (s, 1C, A), 129.40 (s, 1C, B), 70.09 (s, 1C, A), 69.65 (s, 1C, B), 67.04 (s, 1C, A), 66.94 (s, 1C, B), 50.94 (s, 1C, A), 46.40 (s, 1C, B), 37.12 (s, 1C, A), 33.98 (s, 1C, B), 21.60 (s, 1C, A), 21.56 (s, 1C, B); IR (ATR): ν = 1631, 1477, 1173, 752 cm^{-1}; HRMS (ESI): m/z calculated for $C_{29}H_{28}N_2O_6S - H^+$ [M – H^+]: 533.1740. Found: 533.1730.

***N*-(2-(2-tosylethoxy)benzyl)-4-phenoxynicotinamide (23):** KO*t*Bu (1.1 equiv., 0.39 mmol, 0.044 g) and ethylene ditosylate (2 equiv., 0.72 mmol, 0.265 g) were added to a solution of **20** (0.35 mmol, 0.115 g) in dry CH_2Cl_2 (5 mL), under Ar-atmosphere. The solvent was removed under reduce pressure after stirring for 24 h at 50 °C. The residue was taken up in EtOAc (10 mL), extracted with water (2 × 10 mL), dried ($MgSO_4$) and concentrated under reduced pressure. The residue was purified by flash chromatography (EtOAc = 100%, R_f = 0.33) to yield the desired tosylated product **23** (0.15 mmol, 0.078 g, 42%) as colourless crystals; mp = 144-145 °C (decomp). ^{1}H NMR (700.40 MHz, CD_3OD): δ = 8.90 (s, 1H), 8.42 (d, *J* = 5.9 Hz, 1H), 7.72 (d, *J* = 8.3 Hz, 2H), 7.51 (t, *J* = 7.7 Hz, 2H), 7.37 (d, *J* = 7.8 Hz, 2H), 7.36 (t, *J* = 7.5 Hz, 1H), 7.32 (dd, *J* = 7.4 Hz, *J* = 1.2 Hz, 1H), 7.21 (td, *J* = 8.1 Hz, *J* = 1.5 Hz, 1H), 7.19 (d, *J* = 7.6 Hz, 2H), 6.90 (t, *J* = 7.5 Hz, 1H), 6.85 (d, *J* = 8.2 Hz, 1H), 6.75 (d, *J* = 5.9 Hz, 1H), 4.48 (s, 2H, CH_2-N), 4.26-4.22 (m, 2H, O-CH_2), 4.12-4.10 (m, 2H, CH_2-OTs), 2.39 (s, 3H, Ts-CH_3); ^{13}C NMR (176.13 MHz, CD_3OD): δ = 165.58 (s, 1C, C=O), 164.36 (s, 1C), 157.45 (s, 1C), 154.46 (s, 1C), 153.82 (s, 1C), 152.77 (s, 1C), 146.59 (s, 1C), 134.38 (s, 1C), 131.75 (s, 2C),

131.13 (s, 2C), 130.22 (s, 1C), 129.92 (s, 1C), 128.94 (s, 2C), 127.63 (s, 1C), 127.55 (s, 1C), 122.26 (s, 2C), 122.22 (s, 1C), 121.86 (s, 1C), 112.55 (s, 1C), 112.10 (s, 1C), 69.95 (s, 1C, CH_2-OTs), 66.94 (s, 1C, CH_2O), 40.44 (s, 1C, CH_2-NH), 21.58 (s, 1C, CH_3); IR (ATR): ν = 1669, 1471, 1032, 1171, 751 cm^{-1}; HRMS (ESI): m/z calculated for $C_{28}H_{26}N_2O_6S$ – H^+ [M – H^+]: 519.1584. Found: 519.1573.

(±)-*N*-(*sec*-butyl)-4-phenoxynicotinamide [(±)-24]: 4-phenoxynicotinic acid (**18**, 1.12 mmol, 0.241 g) and oxalyl chloride (4 equiv., 4.5 mmol, 0.571 g) were dissolved in CH_2Cl_2 (15 mL). DMF (5 drops) was added and the reaction mixture was refluxed for 2 h. After removal of the solvent under reduced pressure, the residue was dissolved in CH_2Cl_2 (15 mL) and (±)-*sec*-butylamine (1 equiv., 1.12 mmol, 0.082 g) followed by triethylamine (3 equiv., 3.36 mmol, 0.340 g) was added. The reaction mixture was stirred for 18 h at r.t. The organic phase was extracted with water (3 × 15 mL), washed with brine (15 mL), dried ($MgSO_4$) and concentrated under reduce pressure. The residue was purified by flash chromatography (heptanes:EtOAc = 1:2) to yield **24** (0.88 mmol, 0.240 g, 79%) as a yellowish oil. ^{1}H NMR (400.27 MHz, $CDCl_3$): δ = 9.30 (s, 1H), 8.44 (d, *J* = 5.8 Hz, 1H), 7.51-7.44 (m, 2H), 7.36-7.29 (m, 1H), 7.25 (broad s, 1H), 7.16-7.08 (m, 2H), 6.58 (d, *J* = 5.8 Hz, 1H), 4.16 (sept, *J* = 6.6 Hz, 1H, CH), 1.54 (quin d, *J* = 7.4 Hz, *J* = 0.9 Hz, 2H, CH_2), 1.20 (d, 3H, *J* = 6.6 Hz, 3H, CH_3-CH), 0.92 (t, *J* = 7.4 Hz, 3H, C<u>H</u>$_3$-CH_2); ^{13}C NMR (100.65 MHz, $CDCl_3$): δ = 162.85 (s, 1C, C=O), 162.70 (s, 1C, C=O), 154.44 (s, 1C), 153.32 (s, 1C), 153.10 (Cs, 1C), 130.87 (s, 2C), 126.70 (s, 1C), 121.14 (s, 2C), 118.96 (s, 1C), 110.61 (s, 1C), 47.28 (s, 1C, CH), 29.77 (s, 1C, CH_2), 20.59 (s, 1C, <u>C</u>H_3-CH), 10.41 (s, 1C, <u>C</u>H_3-CH_2); IR (ATR): ν = 3420, 3281, 3059, 1647, 1587, 1478, 1263, 1199 cm^{-1}; HRMS (ESI): m/z calculated for $C_{16}H_{18}N_2O_2$ – Na^+ [M – Na^+]: 293.1266. Found: 293.1259.

(±)-*N*-*sec*-butyl-*N*-methyl-4-phenoxynicotinamide [(±)-9]: (±)-24 (0.17 mmol, 0.047 g) was dissolved in DMF (2 mL) under Ar-atmosphere at 0 °C, before the addition of a solution of NaH (1.5 equiv., 0.25 mmol, 0.006 g) in DMF (1 mL). After 0.5 h CH_3I (2 equiv., 0.34 mmol, 0.048 g) was added and stirring was continued for 1 h. Then, the reaction mixture was quenched with cooled HCl (1 M, 10 mL) and the aqueous phase was extracted with CH_2Cl_2 (3 × 10 mL). The combined organic phases were washed with brine (10 mL), dried ($MgSO_4$) and concentrated under reduced pressure. The residue was purified by flash chromatography (EtOAc = 100%) to yield the desired methylated product **9** (0.07 mmol, 0.019 g, 39%) as a yellowish oil. ^{1}H NMR (600.25 MHz, $CDCl_3$): δ = 8.54-8.32 (m, 6H, 3 conformers, 2x A, 2x B, 2x C), 7.44-7.37 (m, 6H, 2x A, 2x B, 2x C), 7.28-7.21 (m, 3H, A + B + C), 7.09-7.04 (m, 6H, 2x A, 2x B, 2x C), 6.64-6.52 (m, 3H, A + B + C), 4.84-4.72 (m, 1H, C), 3.65-3.51 (m, 2H, A + B), 2.95 (s, 3H, C, CH_3-N), 2.94 (s, 3H, B, CH_3-N), 2.78 (s, 3H, A, CH_3-N), 1.97-1.34 (m, 9H, 3x A, 3x B, 3x C, CH-N, CH_2), 1.27-1.10 (m, 9H, 3x A, 3x B, 3x C, C<u>H</u>$_3$-CH), 0.95-

0.76 (m, 9H, 3x A, 3x B, 3x C, C<u>H</u>$_3$-CH$_2$); ^{13}C NMR (150.93 MHz, $CDCl_3$): δ = 166.41 (s, 1C, A), 166.40 (s, 1C, B), 166.32 (s, 1C, C), 160.95 (s, 1C, C), 160.59 (s, 2C, A + B), 153.42 (s, 1C, B), 153.40 (s, 1C, C), 153.31 (s, 1C, A), 151.54 (s, 1C, A), 151.41 (s, 1C, C), 151.28 (s, 1C, B), 150.00 (s, 1C, A), 149.71 (s, 1C, C), 148.33 (s, 1C, B), 130.34 (s, 2C, B), 130.29 (s, 2C, A), 130.25 (s, 2C, C), 125.88 (s, 1C, B), 125.78 (s, 1C, C), 125.75 (s, 1C, A), 124.18 (s, 2C, B + C), 123.82 (s, 1C, A), 120.96 (s, 2C, C), 120.94 (s, 2C, B), 120.71 (s, 2C, A), 110.25 (s, 1C, B), 109.74 (s, 2C, A + C), 56.19 (s, 1C, C, CH_3-N), 55.83 (s, 1C, B, CH_3-N), 50.05 (s, 1C, A, CH_3-N), 29.37 (s, 1C, C, CH-N), 27.30 (s, 1C, A, CH_2), 27.04 (s, 1C, C, CH_2), 26.44 (s, 1C, B, CH_2), 25.92 (s, 1C, B, CH-N), 25.79 (s, 1C, A, CH-N), 19.27 (s, 1C, A, CH_3-CH), 18.69 (s, 1C, B, CH_3-CH), 17.67 (s, 1C, C, CH_3-CH), 11.15 (s, 1C, B, <u>C</u>H_3-CH_2), 10.91 (s, 1C, A, <u>C</u>H_3-CH_2), 10.77 (s, 1C, C, <u>C</u>H_3-CH_2); IR (ATR): ν = 1623, 1475, 1255, 1199, 752 cm^{-1}; HRMS (ESI): m/z calculated for $C_{17}H_{20}N_2O_2$– H^+ [M – Na^+]: 307.1417. Found: 307.1419.

Methyl 1-(2-chloropyridin-3-yl)isoquinoline-3-carboxylate (27): Methyl 1-bromoisoquinoline-3-carboxylate (**26**, 1.42 mmol, 0.380 g) [8] and Pd(dppf)Cl_2 (0.1 equiv., 0.14 mmol, 0.104 g) were dissolved in 1,2-dimethoxyethane (DME, 10 mL) under Ar-atmosphere. (2-chloropyridine-3-yl) boronic acid (2 equiv., 2.86 mmol, 0.449 g), dissolved in DME (3 mL), and K_3PO_4 (2 equiv., 2.86 mmol, 0.606 g), dissolved in water (3 mL) were added and the reaction mixture was stirred at 80 °C for 16 h. The solvent was evaporated and the residue was taken up in a 1:1 mixture of EtOAc and sat. aqueous $NaHCO_3$ solution (20 mL) and the resulting precipitate was filtered off. The aqueous phase was extracted with EtOAc (2 × 15 mL), the combined organic phases were washed with brine, dried ($MgSO_4$) and concentrated under reduced pressure. The residue was purified by medium pressure chromatography (heptanes/EtOAc, gradient: 8 → 66% EtOAc) to give methyl 1-(2-chloropyridin-3-yl)isoquinoline-3-carboxylate (**27**, 0.58 mmol, 0.175 g, 41%, TLC: heptanes:EtOAc = 1:2, R_f = 0.16) as a colourless solid; mp = 202 °C (decomp.). ^{1}H NMR (600.27 MHz, $CDCl_3$): δ = 8.90 (s, 1H), 8.56 (d, *J* = 3.4 Hz, 1H), 8.06 (d, , *J* = 8.2 Hz, 1H), 7.86 (d, *J* = 6.8 Hz, 1H), 7.81 (t, *J* = 7.4 Hz, 1H), 7.70-7.62 (m, 2H), 7.46-7.42 (m, 1H), 4.04 (s, 3H, CH_3); ^{13}C NMR (150.93 MHz, $CDCl_3$): δ = 166.11 (s, 1C), 157.12 (s, 1C), 150.24 (s, 1C), 150.08 (s, 1C) 140.98 (s, 1C), 140.40 (s, 1C), 136.05 (s, 1C), 134.37 (s, 1C), 131.29 (s, 1C), 130.08 (s, 1C), 128.62 (s, 1C), 128.41 (s, 1C), 126.93 (s, 1C), 124.76 (s, 1C), 122.61 (s, 1C), 53.11 (s, 1C, CH_3); IR (ATR): ν = 2924, 1735, 1720, 1243, 761 cm^{-1}; HRMS (ESI): m/z calculated for $C_{16}H_{11}N_2O_2Cl$ – Na^+ [M + Na^+]: 321.0401; found: 321.0399.

1-(2-chloropyridin-3-yl)isoquinoline-3-carboxylic acid (28): Methyl ester **27** (0.41 mmol, 0.122 g) was dissolved in mixture of 1,4-dioxane and water (1:1, 5 mL) and solid NaOH (3 equiv., 1.22 mmol,

0.049 g) was added. The reaction mixture was stirred at r.t. for 4 h. The solvent was removed under reduced pressure, the residue was taken up in water (5 mL) and the pH of the resulting solution was adjusted to 2 (pH paper). The resulting precipitate was dried to give 1-(2-chloropyridin-3-yl)isoquinoline-3-carboxylic acid (**28**, 0.40 mmol, 0.114 g, quant.) as a colorless solid; mp = 193 °C (decomp.). ^{1}H NMR (600.27 MHz, CD_3OD): δ = 8.90 (s, 1H), 8.65 (dd, *J* = 4.9 Hz, *J* = 1.9 Hz, 1H), 8.32 (d, *J* = 8.2 Hz, 1H), 8.07 (dd, *J* = 7.5 Hz, *J* = 1.8 Hz, 1H), 8.04-8.00 (m, 1H), 7.90-7.86 (m, 1H), 7.77 (d, *J* = 8.4 Hz, 1H), 7.67 (dd, *J* = 7.5 Hz, *J* = 4.9 Hz, 1H); ^{13}C NMR (150.93 MHz, CD_3OD): δ = 166.68 (s, 1C), 157.87 (s, 1C), 151.92 (s, 1C), 150.77 (s, 1C), 142.20 (s, 1C), 140.22 (s, 1C), 138.41 (s, 1C), 134.31 (s, 1C), 133.65 (s, 1C), 132.42 (s, 1C), 130.20 (s, 1C), 129.68 (s, 1C), 128.46 (s, 1C), 126.63 (s, 1C), 124.34 (s, 1C); IR (ATR): ν = 1719, 892, 759, 631, 600 cm^{-1}; HRMS (ESI): m/z calculated for $C_{15}H_8N_2O_2Cl$ – Na^+ [M – H^+]: 283.0279 Found: 283.0282.

(–)-*(R)*-*N*-(*sec*-butyl)-1-(2-chloropyridin-3-yl)isoquinoline-3-carboxyamide [(–)-(*R*)-25]: Oxalyl chloride (1.75 mmol, 0.229 g) was added to a solution of carboxylic acid **28** (0.2 equiv., 0.35 mmol, 0.100 g) in dry CH_2Cl_2 (5 mL) and the reaction mixture was refluxed for 2 h. The solvent was removed under reduced pressure and the residue was taken up in CH_2Cl_2 (5 mL). Et_3N (3 equiv., 1.05 mmol, 0.106 g), followed by (*R*)-*sec*-butylamine (1.5 equiv., 0.52 mmol, 0.028 g) was added under Ar-atmosphere. After stirring at r.t. for 16 h, water was added and the organic phase was extracted with water (3 × 10 mL). The combined organic phases were washed with brine (10 mL), dried ($MgSO_4$) and concentrated under reduced pressure. The residue was purified by medium pressure chromatography (heptanes /EtOAc, gradient: 25 → 38% EtOAc) to yield the desired product **25** as yellowish solid (0.23 mmol, 0.079 g, 66%, TLC: heptanes:EtOAc = 3:2, R_f = 0.46). $[\alpha]_D^{22}$: –10.60 (CH_2Cl_2, *c* = 0.953); mp = 160-162 °C; ^{1}H NMR (600.27 MHz, $CDCl_3$): δ = 8.68 (s, 1H), 8.60 (dd, *J* = 4.9, *J* = 1.8 Hz, 1H), 8.06 (d, *J* = 8.2 Hz, 1H), 7.98-7.89 (m, 1H) 7.83 (dd, *J* = 7.4, *J* = 1.7 Hz, 1H), 7.79-7.73 (m, 1H), 7.67-7.59 (m, 2H), 7.47 (t, *J* = 6.3 Hz, 1H), 4.20-4.10 (m, 1H, CH-N), 1.70-1.53 (m, 2H, CH_2), 1.25 (d, *J* = 6.5 Hz, 3H, C$\underline{H}_3$-CH), 0.94 (t, *J* = 7.4 Hz, 3H, CH_3-CH_2). ^{13}C NMR (150.93 MHz, $CDCl_3$, 2 conformers): δ = 163.95 (s, 1C), 155.41 (s, 1C), 155.36 (s, 1C), 150.56 (s, 1C), 150.50 (s, 1C), 150.20 (s, 1C), 150.18 (s, 1C), 143.31 (s, 1C), 143. 27 (s, 1C), 140.45 (s, 1C), 137.03 (s, 1C), 136.99 (s, 1C), 134.61 (s, 1C), 134.52 (s, 1C), 131.27 (s, 1C), 129.38 (s, 1C), 128.99 (s, 1C), 128.98 (s, 1C), 128.11 (s, 1C), 126.88 (s, 1C), 126.84 (s, 1C), 122.63 (s, 1C), 122.57 (s, 1C), 121.00 (s, 1C), 120.97 (s, 1C), 47.00 (s, 2 × 1C, CH-N of both conformers), 30.01 (s, 1C, CH_2), 29.97 (s, 1C, CH_2), 20.77 (s, 1C, $\underline{C}H_3$-CH), 20.72 (s, 1C, $\underline{C}H_3$-CH), 10.81 (s, 1C, $\underline{C}H_3$-CH_2), 10.75 (s, 1C, $\underline{C}H_3$-CH_2); IR (ATR): ν = 2964, 1661, 1513, 1403, 1378 cm^{-1}; HRMS (ESI): m/z calculated for $C_{19}H_{18}N_3OCl$ – Na^+ [M + Na^+]: 362.1030; found: 362.1033.

***(R)-N*-(*sec*-butyl)-1-(2-chloropyridin-3-yl)-*N*-methylisoquinoline-3-carboxamide [(*R*)-10]:** NaH (7.7 equiv., 1.39 mmol, 0.033 g) was added to a solution of amide **25** (0.18 mmol, 0.060 g) in dry DMF (1.5 mL). The reaction mixture was stirred for 30 min at 0 °C. Then, methyl iodide (1.5 equiv., 0.27 mmol, 0.038 g) was added and stirring was continued for 1.75 h. The reaction was quenched with HCl (1M, 1.5 mL) and water (5 mL). The aqueous phase was extracted with CH_2Cl_2 (3 × 10 mL). The combined organic phases were washed with brine (2 × 5 mL), dried ($MgSO_4$) and concentrated under reduced pressure. The residue was purified by medium pressure chromatography (heptanes/EtOAc, gradient: 10 → 80% EtOAc) to yield *(R)-N*-(*sec*-butyl)-1-(2-chloropyridin-3-yl)-*N*-methylisoquinoline-3-carboxaminde (**10**, 0.14 mmol, 0.048 g, 76%, TLC: heptanes:EtOAc = 3:2, R_f = 0.28) as a yellowish solid. mp = 136-138 °C; ^{1}H NMR (600.27 MHz, $CDCl_3$, 4 conformers: ratio = 2.4 [A] : 1.9 [B]: 1.1 [C]: 1.0 [D]): δ = 8.58-8.51 (m, 4H, A-D), 8.10-7.98 (m, 4H, A-D), 7.97-7.92 (m, 4H, A-D), 7.81-7.70 (m, 8H, 2 × A-D), 7.62-7.54 (m, 8H, 2 × A-D), 7.44-7.38 (m, 4H, A-D), 4.84-471 (m, 2H, C+D), 3.92-3.80 (m, 2H, A+B), 2.96 (s, 3H, CH_3, B), 2.98 (s, 3H, CH_3, A), 2.88 (s, 3H, CH_3, D), 2.87 (s, 3H, CH_3, C), 1.68-1.48 (m, 4H, CH_2, A+B), 1.44-1.32 (m, 4H, CH_2, C+D), 1.24-1.13 (m, 12H, CH-C$\underline{H}_3$, A-D), 0.99-0.93 (m, 6H, C$\underline{H}_3$-CH_2, C+D), 0.80-0.72 (m, 6H, C$\underline{H}_3$-CH_2, A+B). ^{13}C NMR (150.93 MHz, $CDCl_3$, 4 conformers: ratio = 2.4 [A]: 1.9 [B]: 1.1 [C]: 1.0 [D]): δ = 169.76 (s, 1C, A), 169.67 (s, 1C, B), 169.09 (s, 1C, C), 169.05 (s, 1C, D), 155.83 (s, 1C, B), 155.59 (s, 1C, A), 155.46 (s, 1C, D), 155.34 (s, 1C, C), 150.23 (s, 1C, B), 150.17 (s, 1C, A), 150.10 (s, 2C, C+D), 149.92 (s, 1C, B), 149.89 (s, 2C, A+D), 149.85 (s, 1C, C), 148.50 (s, 1C, D), 148.49 (s, 1C, C), 148.38 (s, 1C, A), 148.28 (s, 1C, B), 140.20 (s, 1C, D), 140.17 (s, 1C, C), 140.07 (s, 1C, B), 139.94 (s, 1C, A), 136.85 (s, 1C, A), 136.72 (s, 2C, C+D), 136.66 (s, 1C, B), 134.53 (s, 1C, B), 134.50 (s, 1C, D), 134.41 (s, 1C, C), 134.30 (s, 1C, A), 130.98 (s, 1C, A), 130.96 (s, 1C, B), 130.90 (s, 1C, C), 130.86 (s, 1C, D), 128.64-128.56 (m, 4C, A-D), 127.89 (s, 1C, D), 127.89 (s, 1C, A), 127.84 (s, 1C, C), 127.81 (s, 1C, B), 126.59 (s, 1C, A), 126.86 (s, 2C, C+D), 126.82 (s, 1C, B), 126.59 (s, 1C, B), 126.50 (s, 2C, C+D), 126.40 (s, 1C, A), 122.42 (s, 2C, C+D), 122.37 (s, 1C, B), 122.28 (s, 1C, A), 121.26 (s, 1C, D), 121.04 (s, 1C, C), 120.95 (s, 1C, A), 120.53 (s, 1C, B), 55.86 (s, 1C, CH-N, A) 55.56 (s, 1C, CH-N, B), 50.63 (s, 1C, CH-N, D), 50.45 (s, 1C, CH-N, C), 30.50 (s, 1C, CH_3-N, D), 30.41 (s, 1C, CH_3-N, C), 27.35 (s, 1C, CH_2, A), 27.31 (s, 1C, CH_2, B), 26.63 (s, 1C, CH_2, D), 26.58 (s, 1C, CH_2, C), 26.29 (s, 2C, CH_3-N, A+B), 18.61 (s, 1C, $\underline{C}H_3$-CH, A), 18.46 (s, 1C, $\underline{C}H_3$-CH, B), 17.32 (s, 1C, $\underline{C}H_3$-CH C), 17.25 (s, 1C, $\underline{C}H_3$-CH, D), 11.06 (s, 1C, CH_3-CH_2, C), 11.03 (s, 2C, CH_3-CH_2, A+D), 10.86 (s, 1C, CH_3-CH_2, B); IR (ATR): ν = 2967, 1625, 1403, 802, 680 cm^{-1}; HRMS (ESI): m/z calculated for $C_{20}H_{20}N_3OCl$ – Na^+ [M + Na^+]: 376.1187; found: 376.1186.

11.4. Radiochemistry

11.4.1. General Experimental

[^{11}C]CO_2 was produced in a cyclotron by irradiation of highest grade N_2 (+1% O_2) with a beam of protons, following the nuclear reaction $^{14}N(p,\alpha)^{11}C$. After desired amounts of activity (beam current 65 µA) were reached, the produced [^{11}C]CO_2 was transferred to the synthesizer and trapped on molecular sieves (4 Å). Subsequently, it was reduced (under nickel catalysed conditions at 400 °C) to [^{11}C]CH_4 by passing a flow of H_2 through the molecular sieves. [^{11}C]CH_4 was converted to [^{11}C]CH_3I using sublimated iodine at 738 °C, as previously reported [9]. This process was finished after release of the produced [^{11}C]CH_3I from a Porapak® N column by heating the column to 200 °C. Likewise, [^{11}C]CH_3OTf was synthesized by passing the released [^{11}C]CH_3I through a column containing silver triflate on activated charcoil at 200 °C [10].

11.4.2. Evaluation of reaction conditions

Different reaction conditions for the synthesis of (*R*)-[^{11}C]**10** were evaluated by performing manual small scale reactions (activity < 2 GBq, total volume 100 µL - 150 µL), using aliquots (50 µL - 100 µL) of [^{11}C]CH_3I or [^{11}C]CH_3OTf solutions in a pre-selected organic solvent. The influence of the following parameters was examined:

- Precursor concentration
- Reaction temperature
- Reaction time
- Solvent
- Methylating agent

After the corresponding time, the reactions were stopped by adding 100 µL of distilled water and the radiochemical conversion (RCC) was determined by means of HPLC (details on flow rates and retention times are given below) using an X-Bridge BEH Shield RP-18 column (4.6 × 50 mm, 2.5 µm, 130 Å) as stationary phase and a mixture of 60% acetonitrile and 40% phosphate buffer (pH = 9.3) as mobile phase, following our concept for accelerating the quality control of ^{11}C-tracers, as described by Nics *et al.* [11]. Identity of the radiolabeled product (*R*)-[^{11}C]**10** was performed by co-injection in the HPLC system of an authentic sample of (*R*)-**10**.

11.4.3. Synthesis automation

The conditions for the ^{11}C-methylation reaction with the higher RCC were transferred to the software of the synthesizer and the complete radiosynthesis of (*R*)-[^{11}C]**10** was automated. The produced [^{11}C]CH_3OTf was trapped at room temperature in a glass reactor containing 1 mg of precursor NEBIQUINIDE ((*R*)-N-(sec-butyl)-1-(2-chloropyridin-3-yl)-*N*-methylisoquinoline-3-carboxamide, **25**) dissolved in 0.5 mL DMSO as well as 4 mg of NaH as mineral oil suspension (60% NaH). Subsequently, the reactor was sealed and heated to 120 °C for 2 min. After this time, the reactor was cooled to 25 °C with liquid nitrogen and the reaction was stopped by adding 1 mL of water. The reaction mixture was transferred (controlled by a fluid detector) to a semi-preparative HPLC column (Waters µBondapak® C18, 300 × 7.8 mm, 10 µm particle size) under a flow (5 $mL \cdot min^{-1}$) of a mixture 50/50 0.01 M H_3PO_4/acetonitrile. The fraction containing the pure ($t_R \approx 6$ min) (*R*)-[^{11}C]**10** was collected in a round-bottom flask containing 60 mL of distilled water. The resulting solution was pushed through a C18 cartridge in order to remove the HPLC solvents. The cartridge was consequently washed with 10 mL of distilled water and the product was eluted with 1.5 mL of ethanol, formulated with physiological saline solution (10 mL) and phosphate-buffered saline solution (6 mL). Finally, the product was sterile filtered under laminar air flow.

Radio(chemical) purity and molar radioactivity were determined via HPLC using the same conditions as for the RCC analysis. The quality control of the freshly prepared tracer, including sterility and absence of endotoxins tests, was performed using standard procedures of the PET Centre of the Vienna General Hospital/Medical University of Vienna and following the recommendations described in the European Pharmacopoeia [1].

11.5. *In vitro* preclinical evaluation

11.5.1. Genotyping

The used genotyping assays were the same, as reported for our previous studies [12].

11.5.2. Binding affinity studies

Compounds **6**, **7**, **8, 9** and **10** were dissolved in DMSO and their affinities towards TSPO was assessed by dint of the inhibition constants values (K_i) derived from competitive binding experiments, as described elsewhere [13], using TSPO-expressing membranes obtained from genotyped healthy volunteers (approved by the Ethics Committee of the Medical University of Vienna) and prepared following published methods [14]. Assay tubes were filled each with 250 µL of solutions of increasing concentration of one of the non-radioactive reference compounds (**6**, **7**, **8**, **9** or **10**), 50 µL of a 10 nM [^{3}H]PK11195 solution and 200 µL of membrane suspension (250 µg total protein·mL^{-1}, determined via colorimetric detection of cuprous cation (Cu^{1+}) by bicinchoninic acid (BCA) measuring the absorbance at 562 nm, following the instructions manual of the BCA kit). For determination of non-specific binding, 20 µM PK11195 was used instead of the non-radioactive reference compound; and for total binding, only [^{3}H]PK11195 and membrane suspension were incubated. All dilutions were performed in assay buffer [13], thus resulting in a final concentration of DMSO < 1%. Data from the competition plots (from three independent experiments, performed in triplicates) were analyzed and successively IC_{50} and K_i values were calculated using Cheng-Prusoff's equation [15] and a dissociation constant (K_d) of 29.25 nM for [^{3}H]PK11195 [13] and GraphPad Prism® software (single-site fit K_i and two-sites fit K_i, respectively).

11.5.3. LogP analysis

The Log*P* value of all reference compounds was determined using an UV-HPLC method as reported elsewhere [16,17]. Briefly, a solution of the substances was co-injected (n=3) with triphenylene and toluene (as internal standards) into a polymeric apHERA column under a gradient flow (1.5 mL·min^{-1}), starting from 10% methanol and 90% 25 mM phosphate buffer (pH 7.4) to 100% methanol within 9.4 min. Detection was performed at 254 nm and 285 nm.

11.5.4. AGP Binding

AGP binding assays were performed as described elsewhere [18]. For these assays, in house produced (*R*)-[^{11}C]**1** was used instead of [^{3}H]**1**. Binding to AGP was calculated as the percentage of total activity eluted from the spin desalting column. Incubation in PBS (without AGP) was used as reference.

11.5.5. Stability testing

Pooled human microsomes were pre-incubated for 5 min at 37 °C (pH 7.4) with a NADPH-generating system. A 10 µL aliquot of freshly prepared tracer (*R*)-[^{11}C]**10** was added and the resulting mixture was further incubated at 37 °C. In order to stop the enzymatic reaction, a mixture of methanol/acetonitrile (10% methanol in acetonitrile) was added at determined time points. The resulting suspensions were vortexed and centrifuged at room temperature for 5 min (23000 g). The amount of intact tracer was determined using radio-HPLC, by injection of the supernatant.

11.6. Statistical analysis

In text and figures, all quantitative data are specified as mean values ± standard deviation. A student two-tailed t-test (α=0.95) was performed using GraphPad Prism® software for determination of significance. Error bars in figures represent the standard deviation; if not visual, they are within the icon margin.

12. Results – NMR Spectra

12.1. NMR Spectra

^{1}H, ^{13}C and ^{19}F NMR spectra of all synthetized compounds are available as additional material. All assignments, solvents and measuring frequencies are given above (experimental section). The first spectrum shown in each series is the full ^{1}H NMR spectrum. Expansions are depicted where they were regarded as necessary. Then the ^{13}C NMR spectrum, followed by the ^{19}F NMR, are depicted in the same manner. The x-axes are in ppm, while the peak labels are in Hz for all given spectra. Structures are always given on top of the full ^{1}H NMR spectrum. Integrals are denoted below the x-axes where they are regarded as necessary and the integration range is marked. The numbering of compounds is in accordance with the numbering of substances in the main text. All ^{13}C NMR spectra were recorded j-modulated. HPLC chromatograms were recorded to determine the purities of the target compounds, using the same system as described in the main text.

^{1}H NMR of 4-Methoxy-2-((methylamino)methyl)phenol:

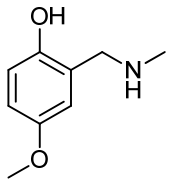

14a

^{13}C NMR of 4-Methoxy-2-((methylamino)methyl)phenol:

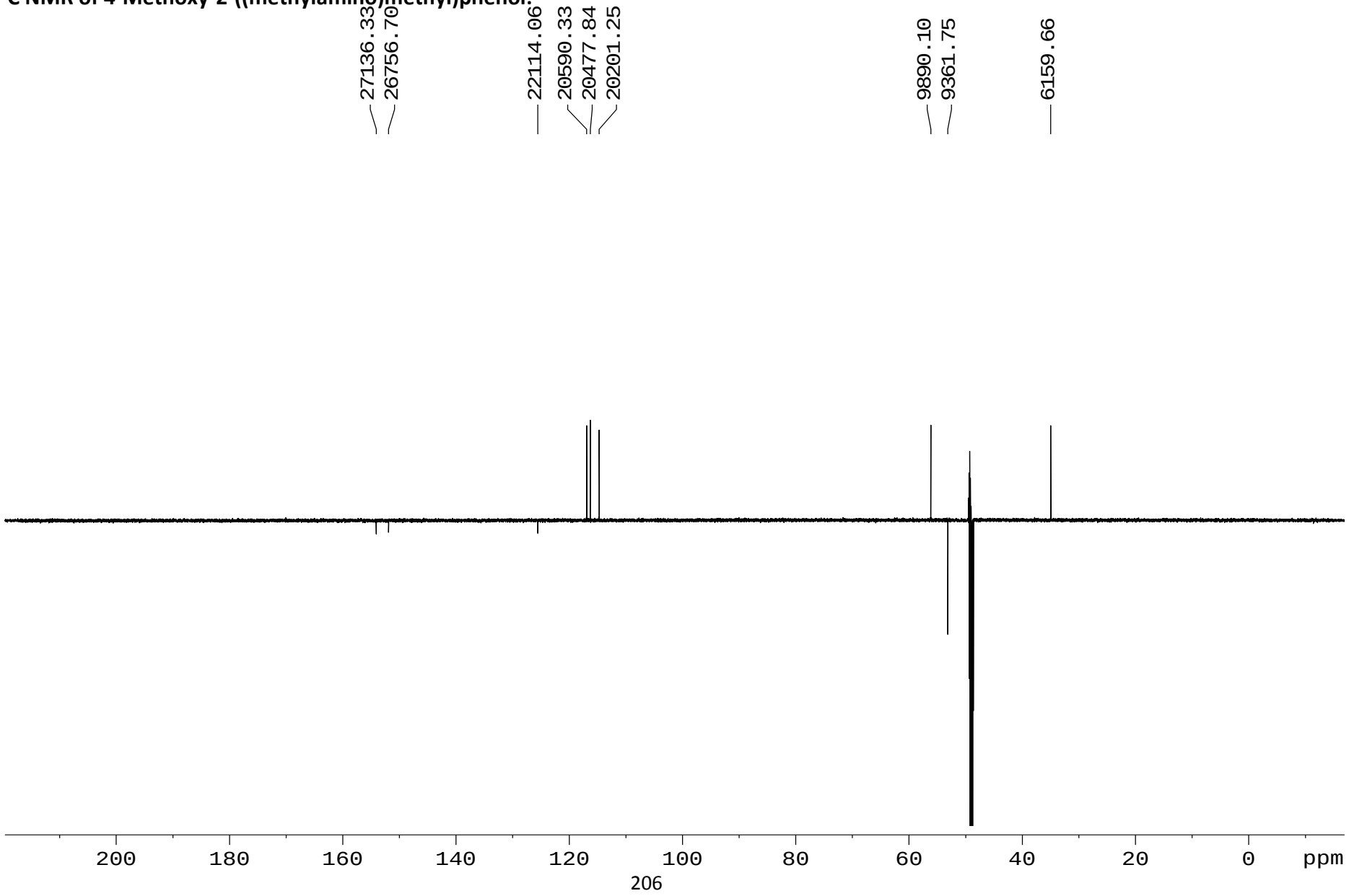

^{1}H NMR of *N*-(2-Hydroxy-5-methoxybenzyl)-*N*-methyl-2-phenoxybenzamide:

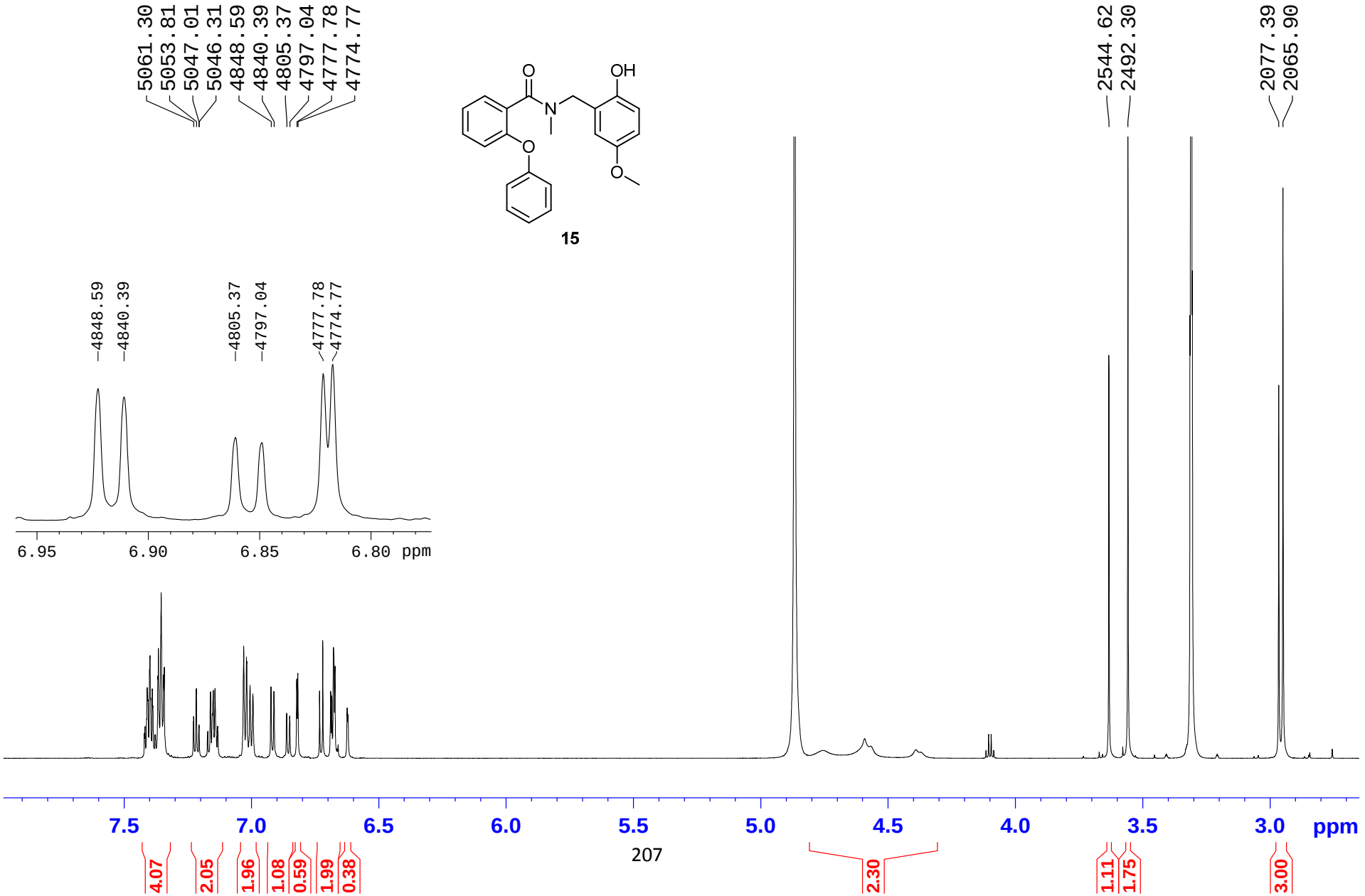

^{13}C NMR of *N*-(2-Hydroxy-5-methoxybenzyl)-*N*-methyl-2-phenoxybenzamide:

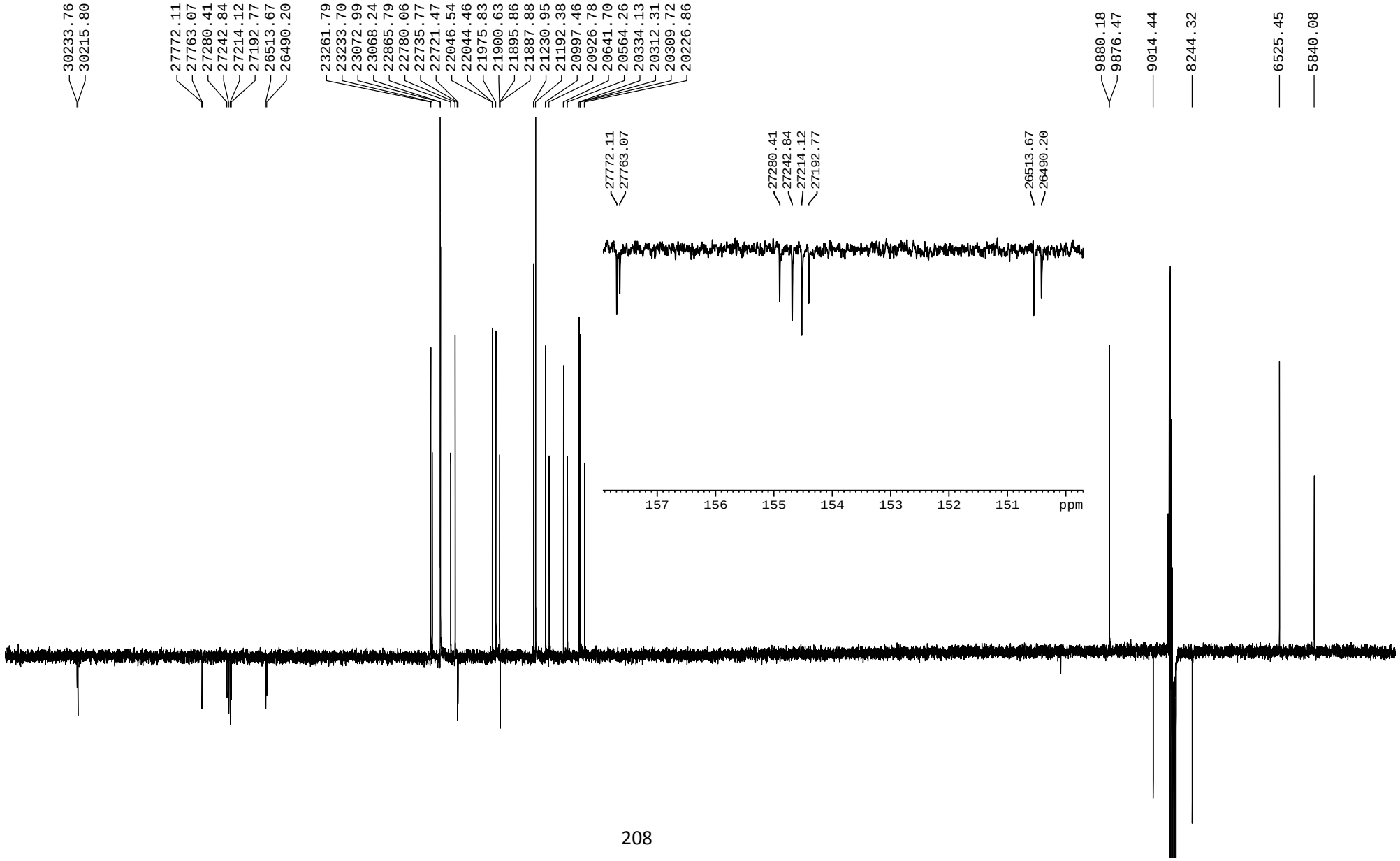

^{1}H NMR of *N*-(2-(2-Tosylethoxy)-5-methoxybenzyl)-*N*-methyl-2-phenoxybenzamide:

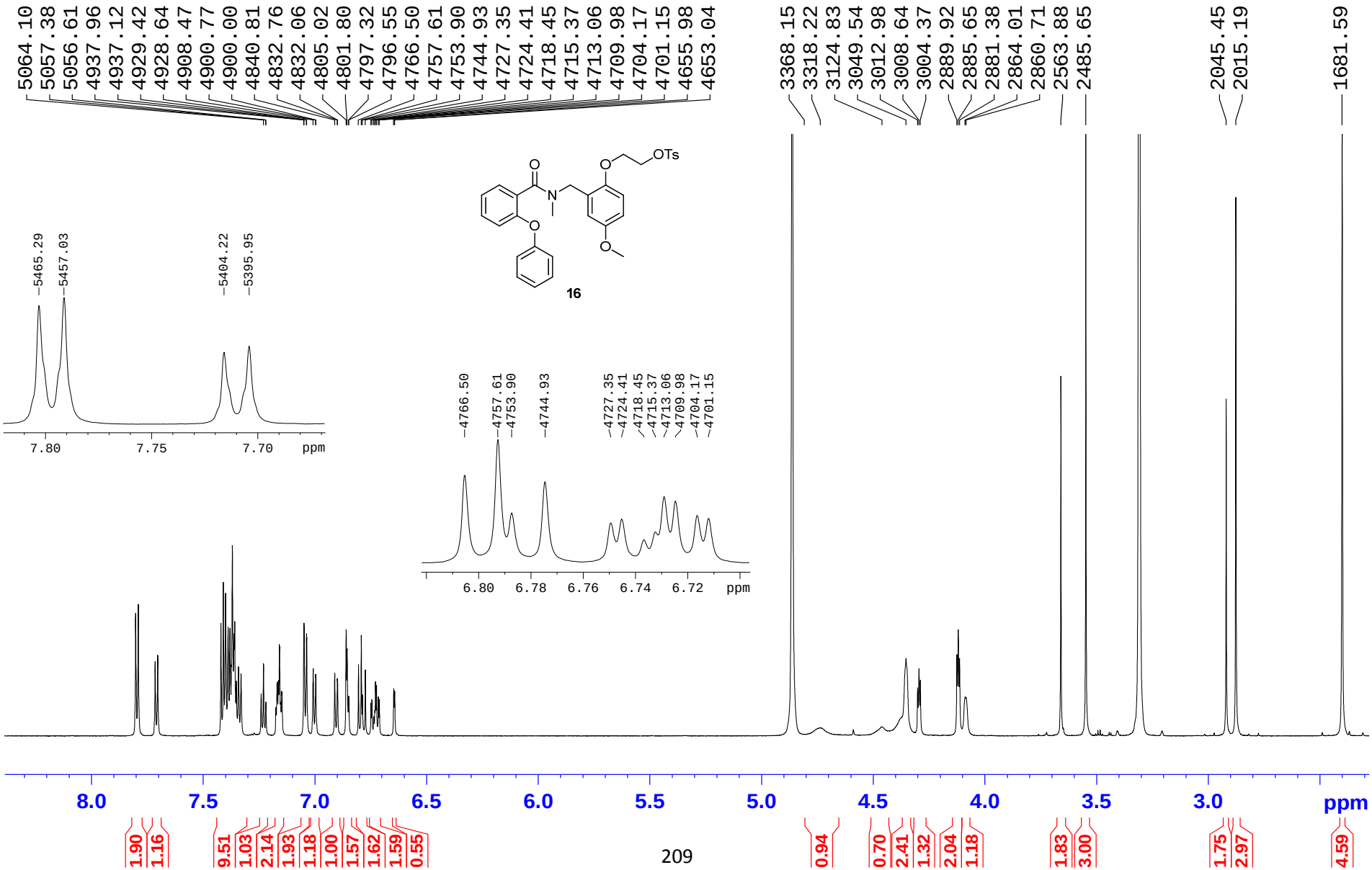

^{13}C NMR of *N*-(2-(2-Tosylethoxy)-5-methoxybenzyl)-*N*-methyl-2-phenoxybenzamide:

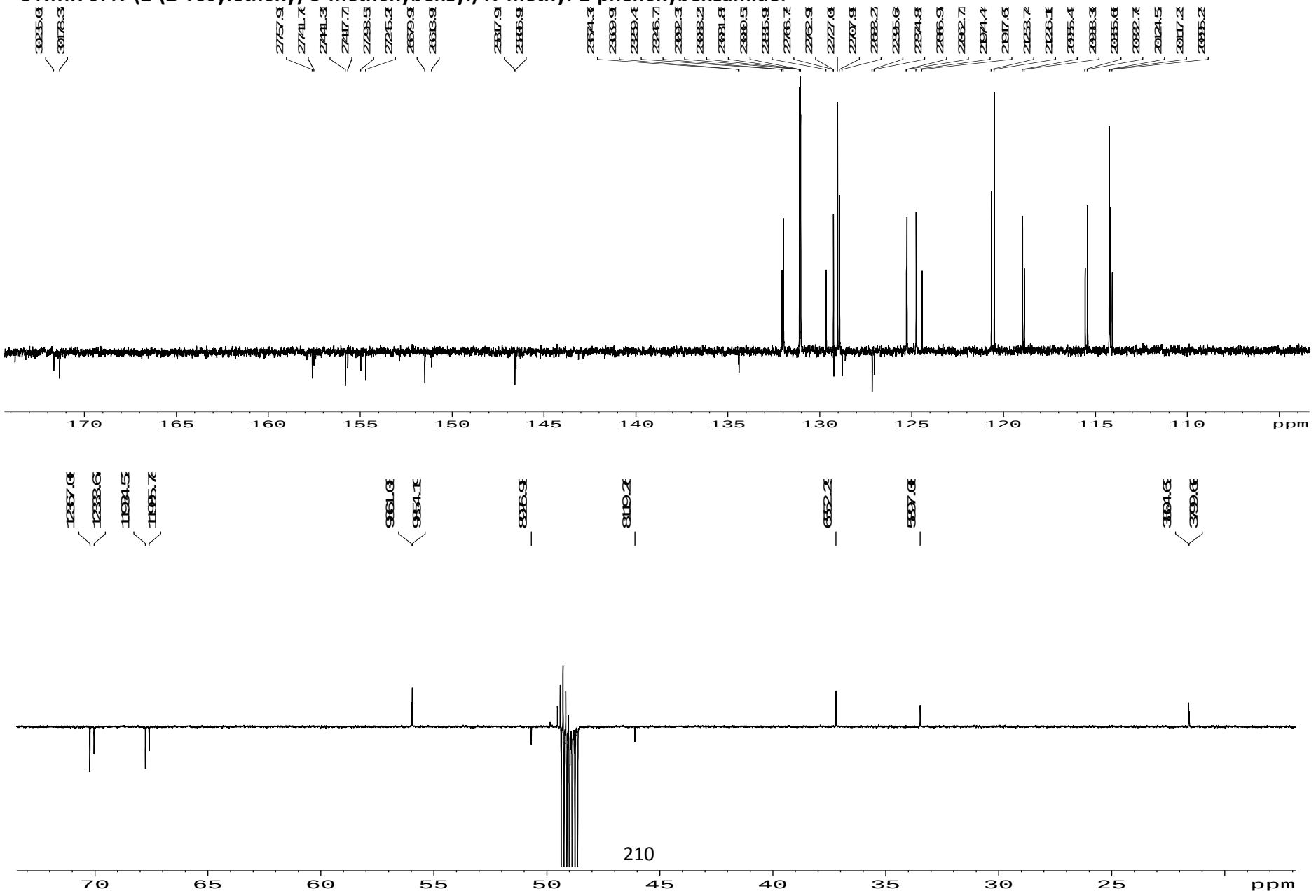

^{1}H NMR of *N*-(2-(2-Fluoroethoxy)-5-methoxybenzyl)-*N*-methyl-2-phenoxybenzamide:

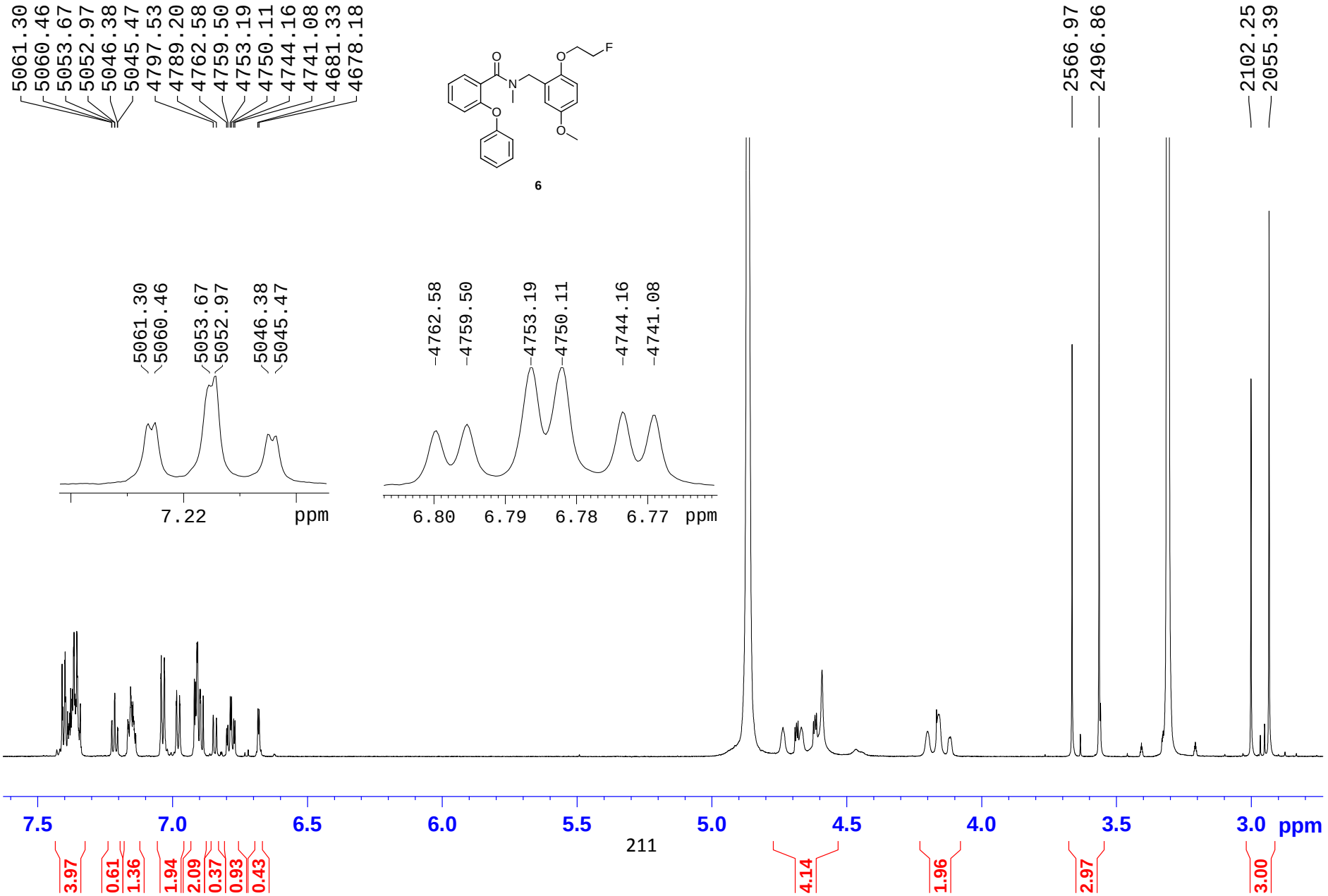

^{13}C NMR of *N*-(2-(2-Fluoroethoxy)-5-methoxybenzyl)-*N*-methyl-2-phenoxybenzamide:

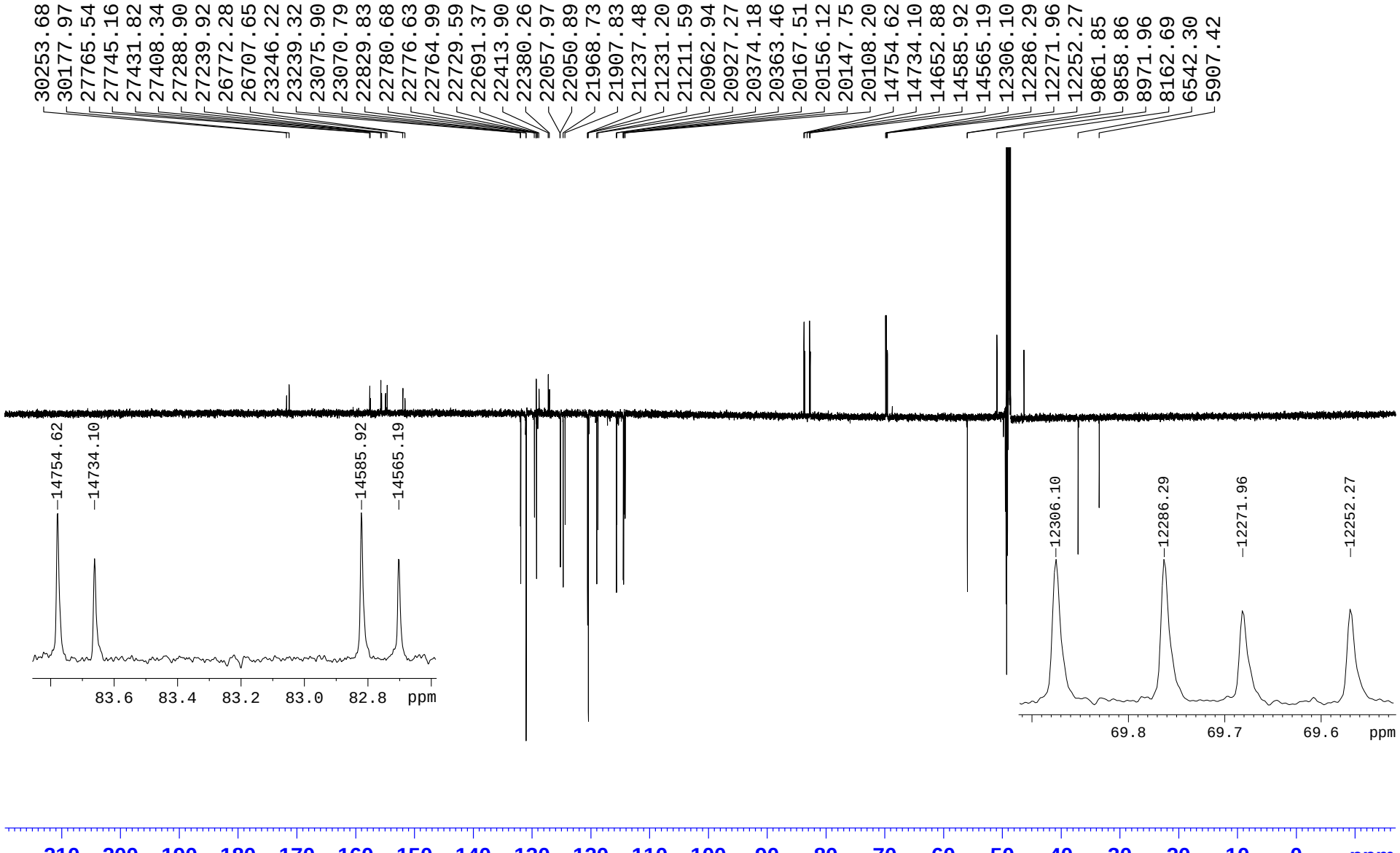

^{19}F NMR of *N*-(2-(2-Fluoroethoxy)-5-methoxybenzyl)-*N*-methyl-2-phenoxybenzamide:

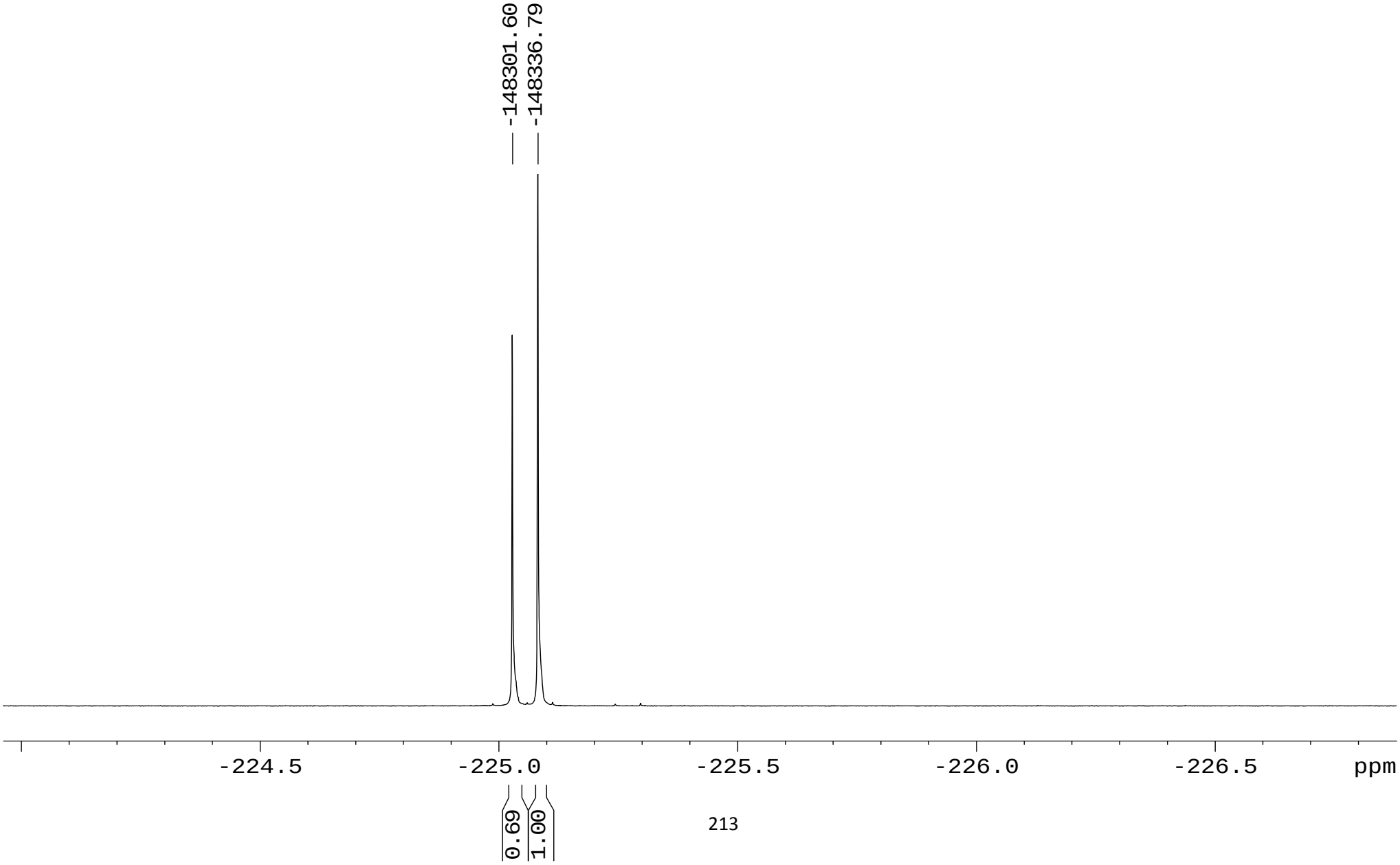

^{1}H NMR of *N*-(2-Hydroxybenzyl)-*N*-methyl-4-phenoxynicotinamide:

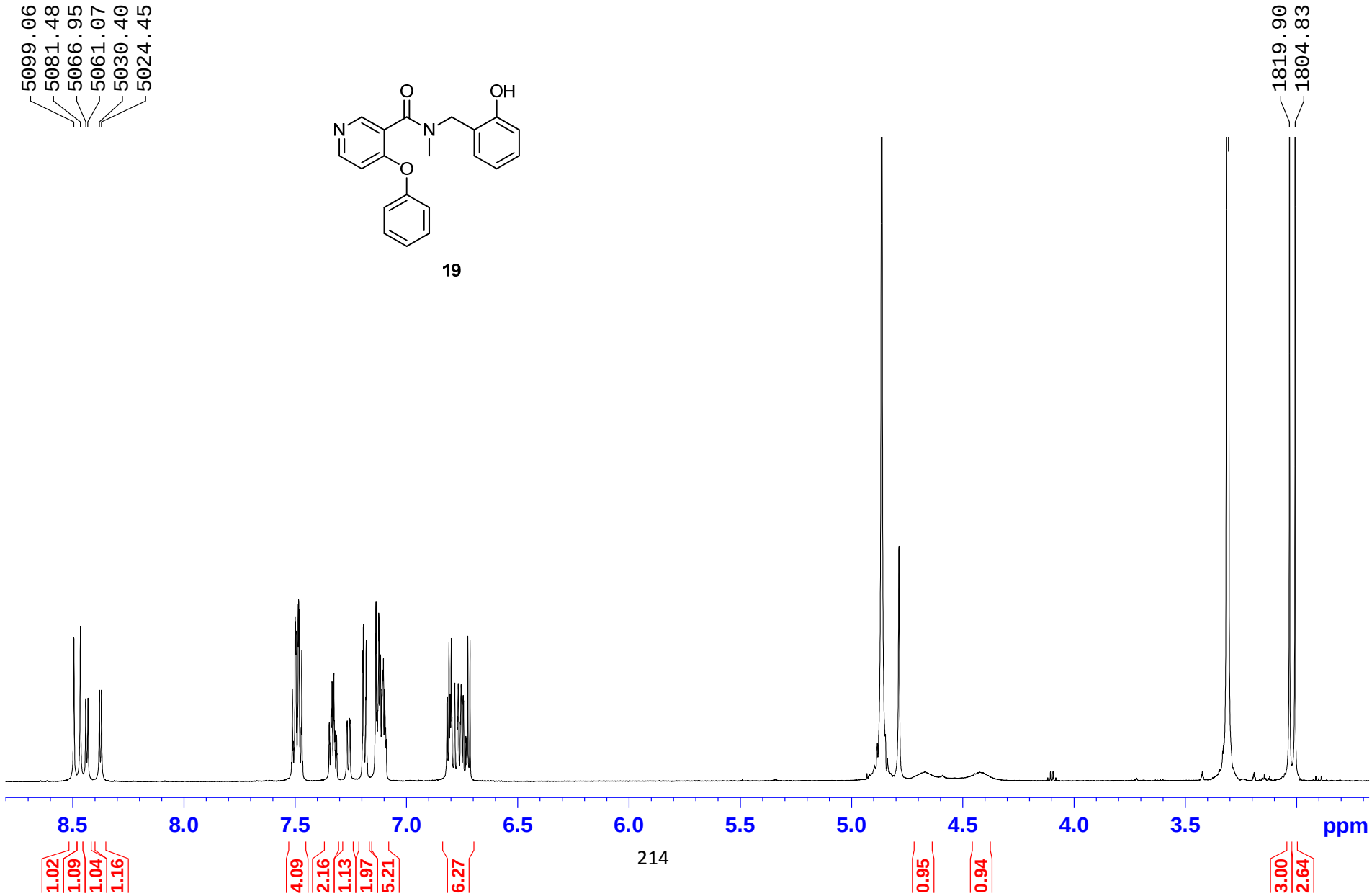

19

^{13}C NMR of *N*-(2-Hydroxybenzyl)-*N*-methyl-4-phenoxynicotinamide:

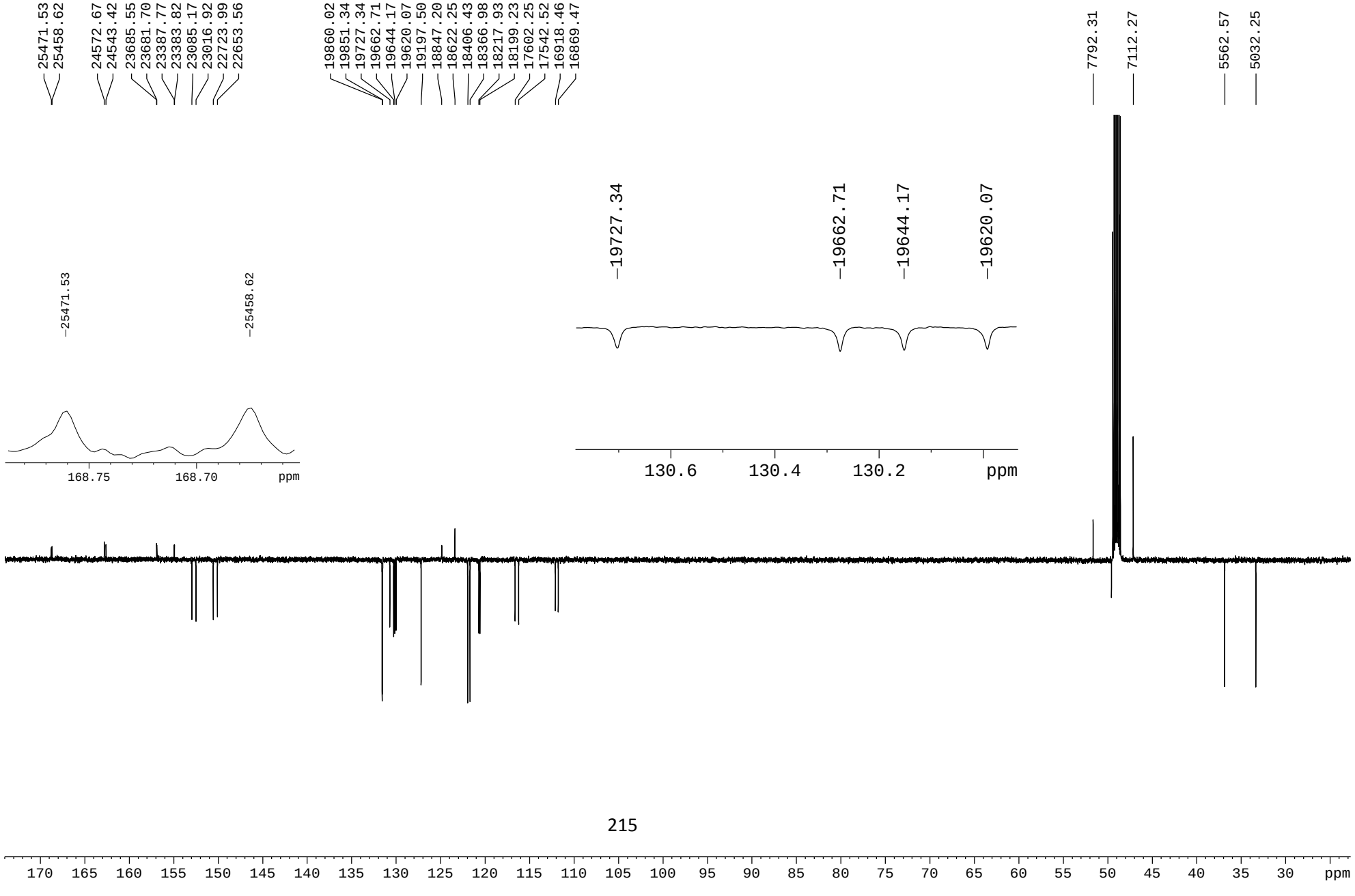

^{1}H NMR of *N*-(2-Hydroxybenzyl)-4-phenoxynicotinamide:

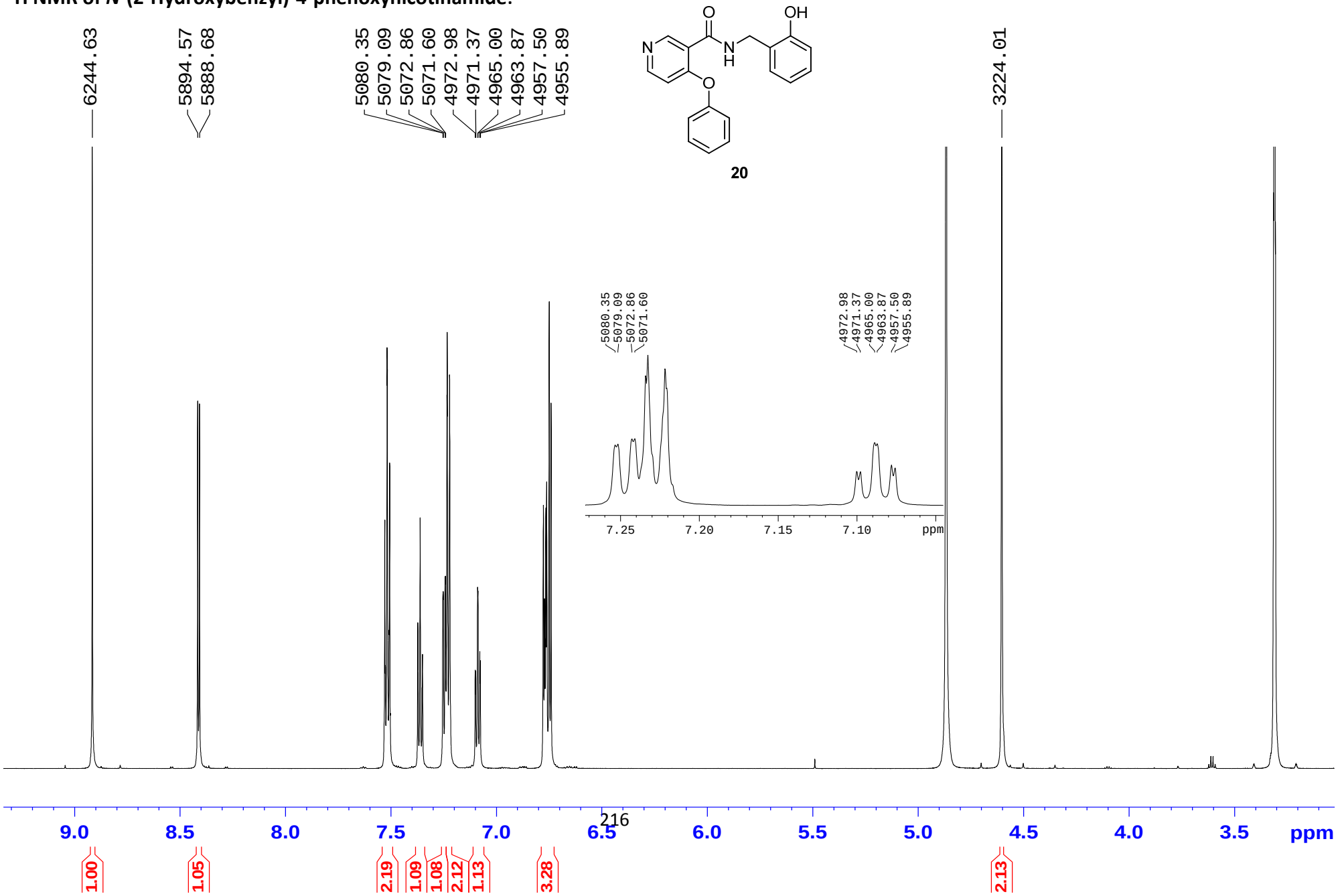

^{13}C NMR of *N*-(2-Hydroxybenzyl)-4-phenoxynicotinamide:

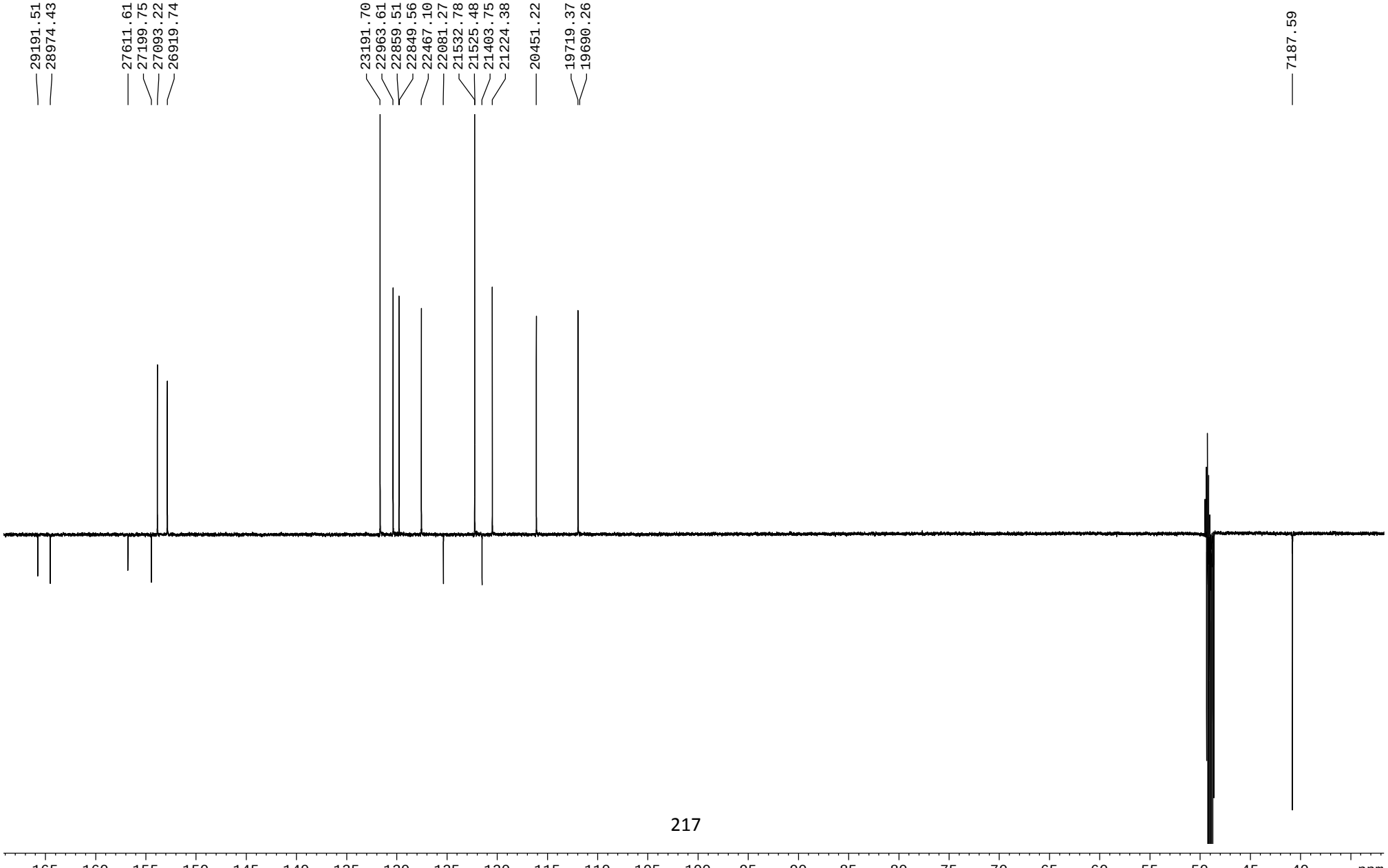

^{1}H NMR of *N*-(2-Methoxybenzyl)-*N*-methyl-4-phenoxynicotinamide:

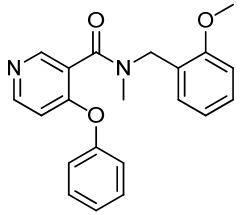

7

^{13}C NMR of *N*-(2-Methoxybenzyl)-*N*-methyl-4-phenoxynicotinamide:

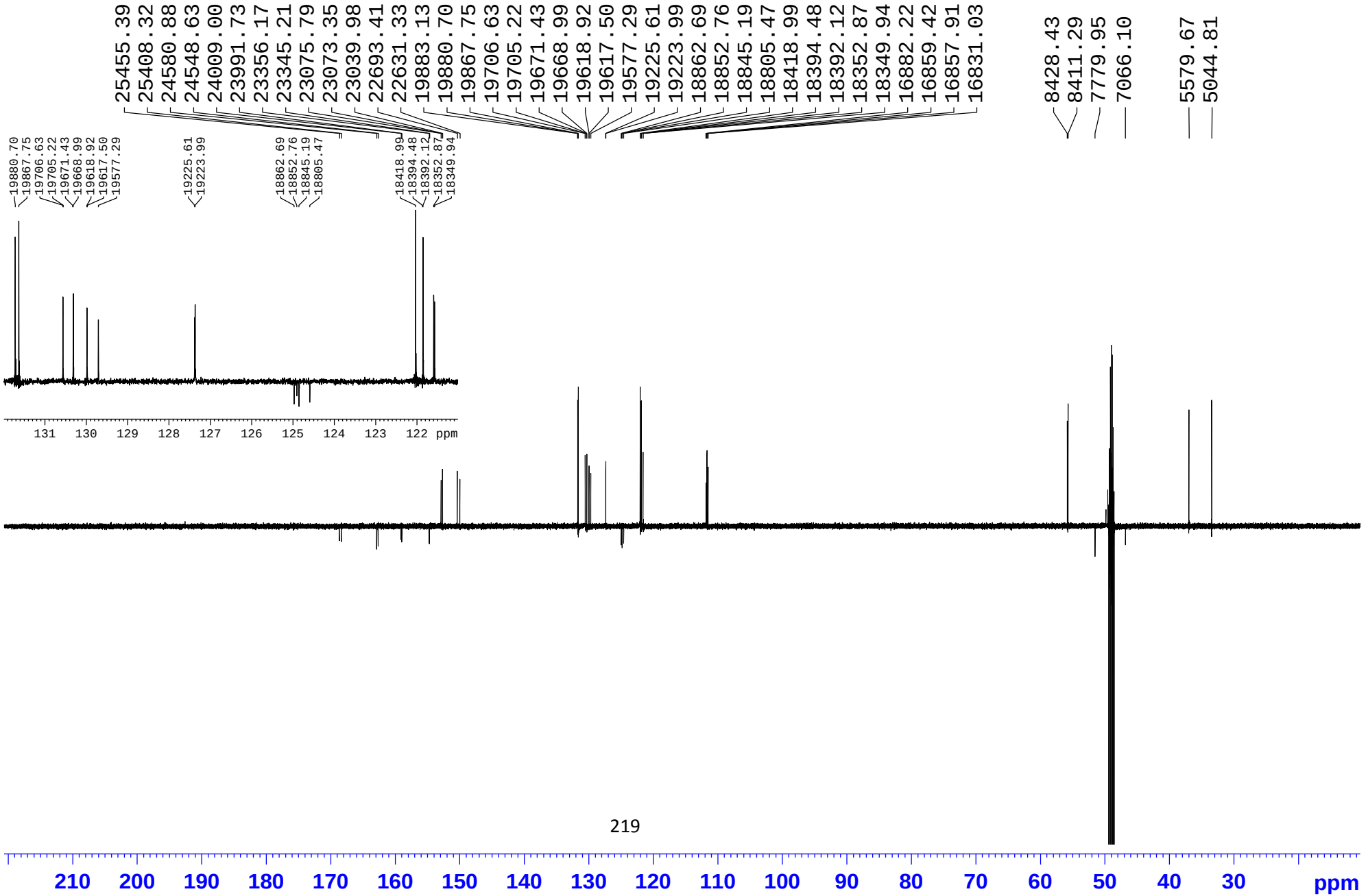

^{1}H NMR of *N*-(2-(2-Fluoroethoxy)benzyl)-*N*-methyl-4-phenoxynicotinamide:

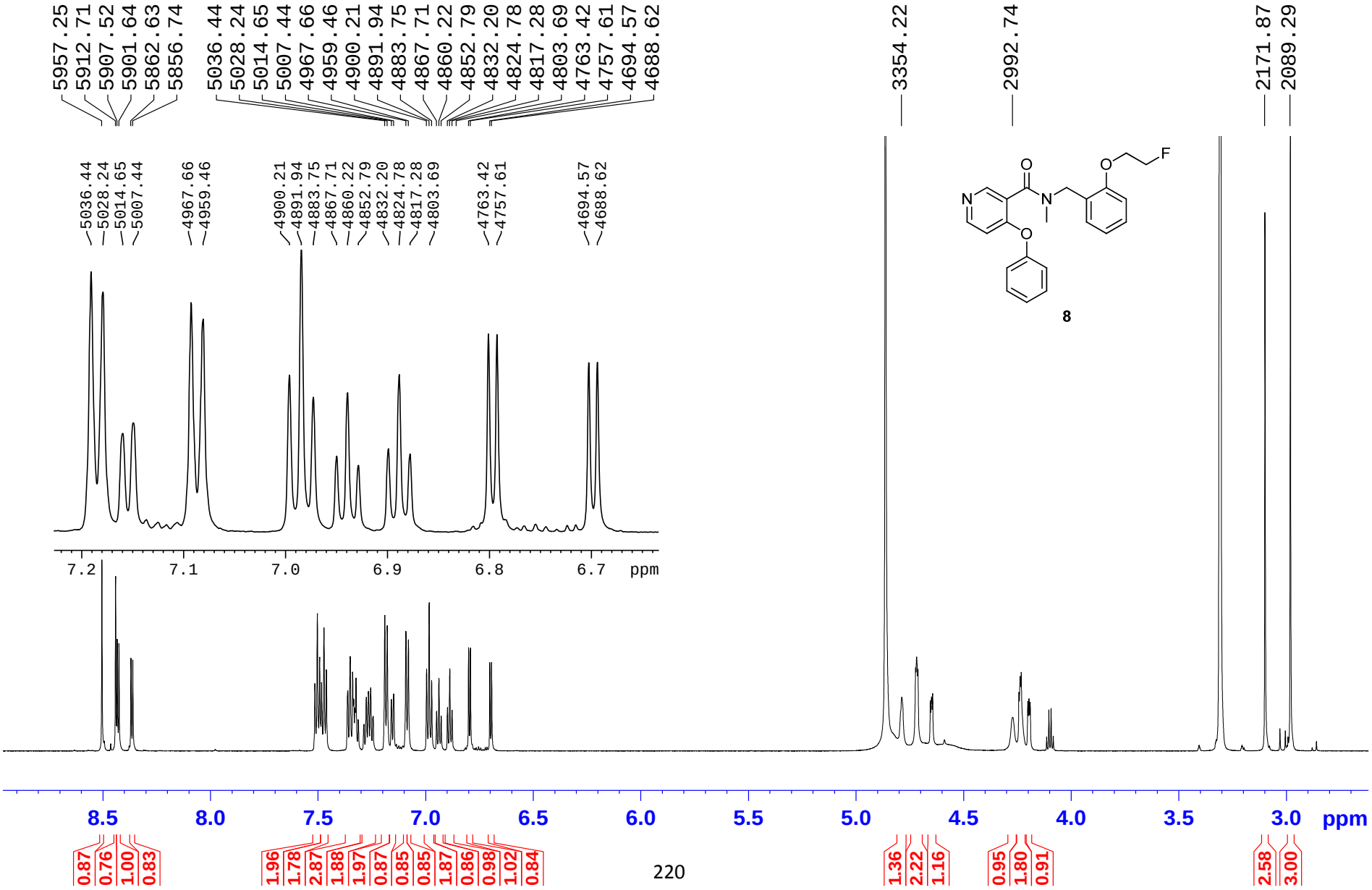

8

^{13}C NMR of *N*-(2-(2-Fluoroethoxy)benzyl)-*N*-methyl-4-phenoxynicotinamide:

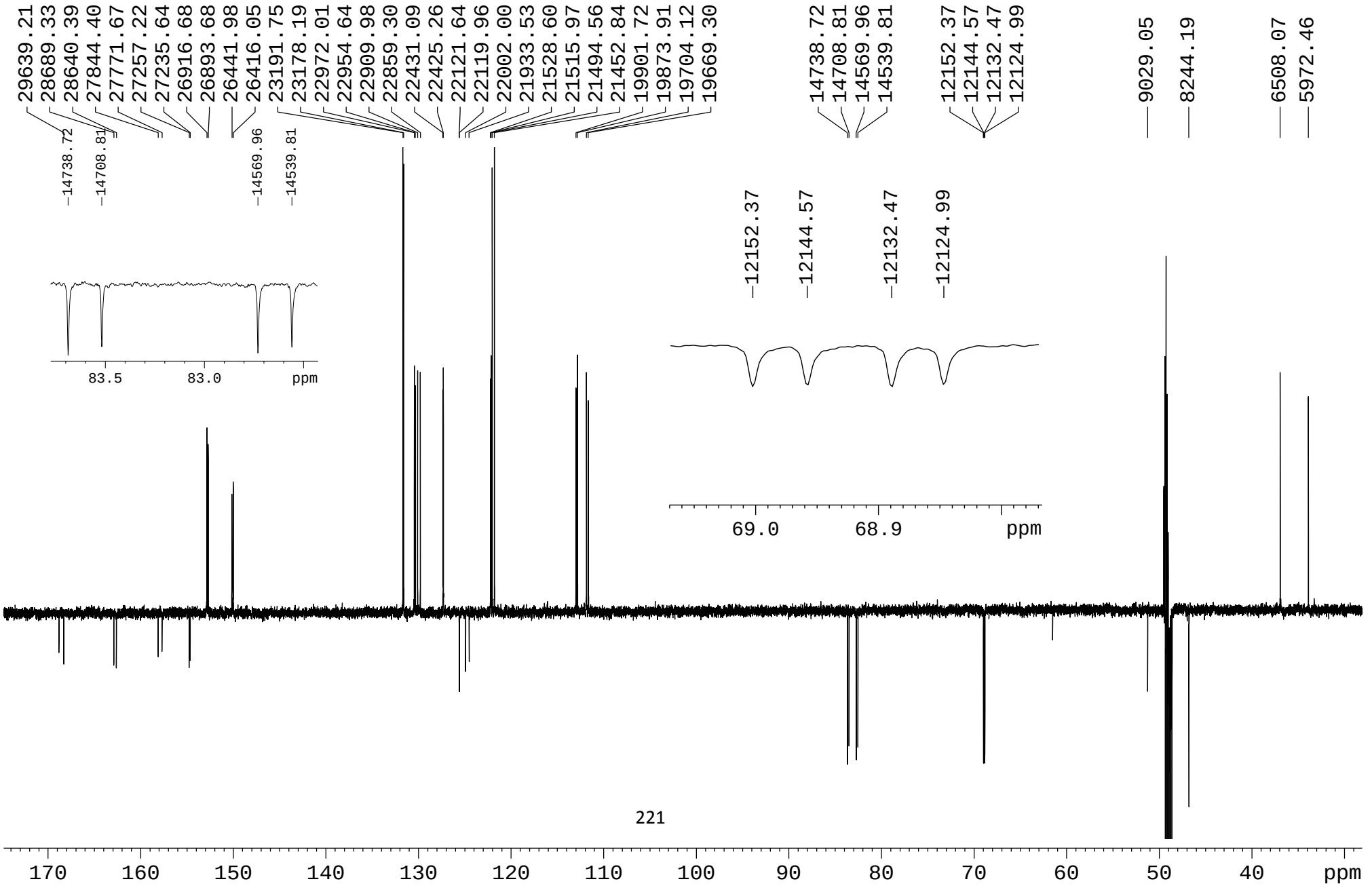

^{19}F NMR of *N*-(2-(2-Fluoroethoxy)benzyl)-*N*-methyl-4-phenoxynicotinamide:

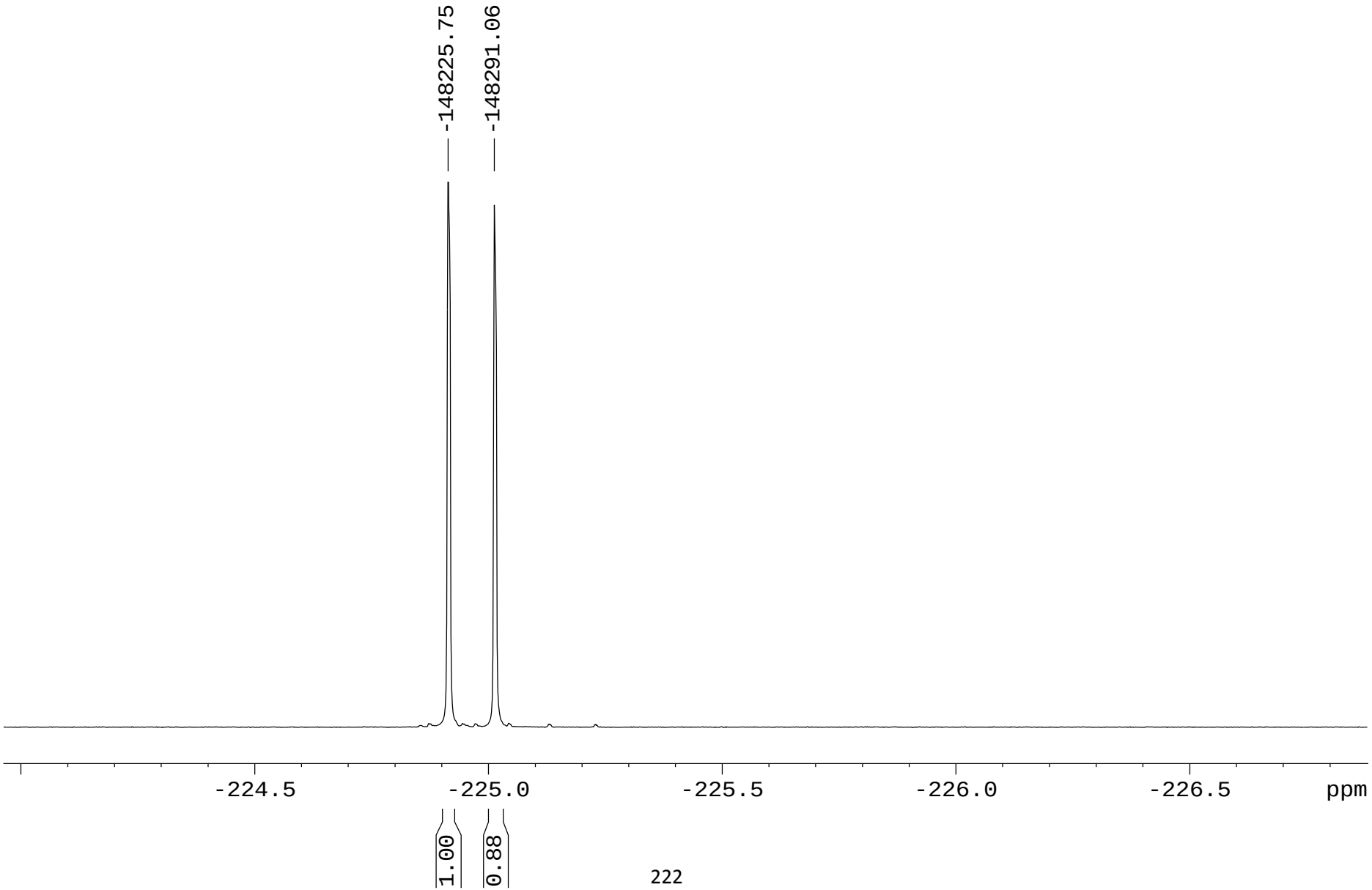

^{1}H NMR of *N*-(2-(2-Fluoroethoxy)benzyl)-4-phenoxynicotinamide:

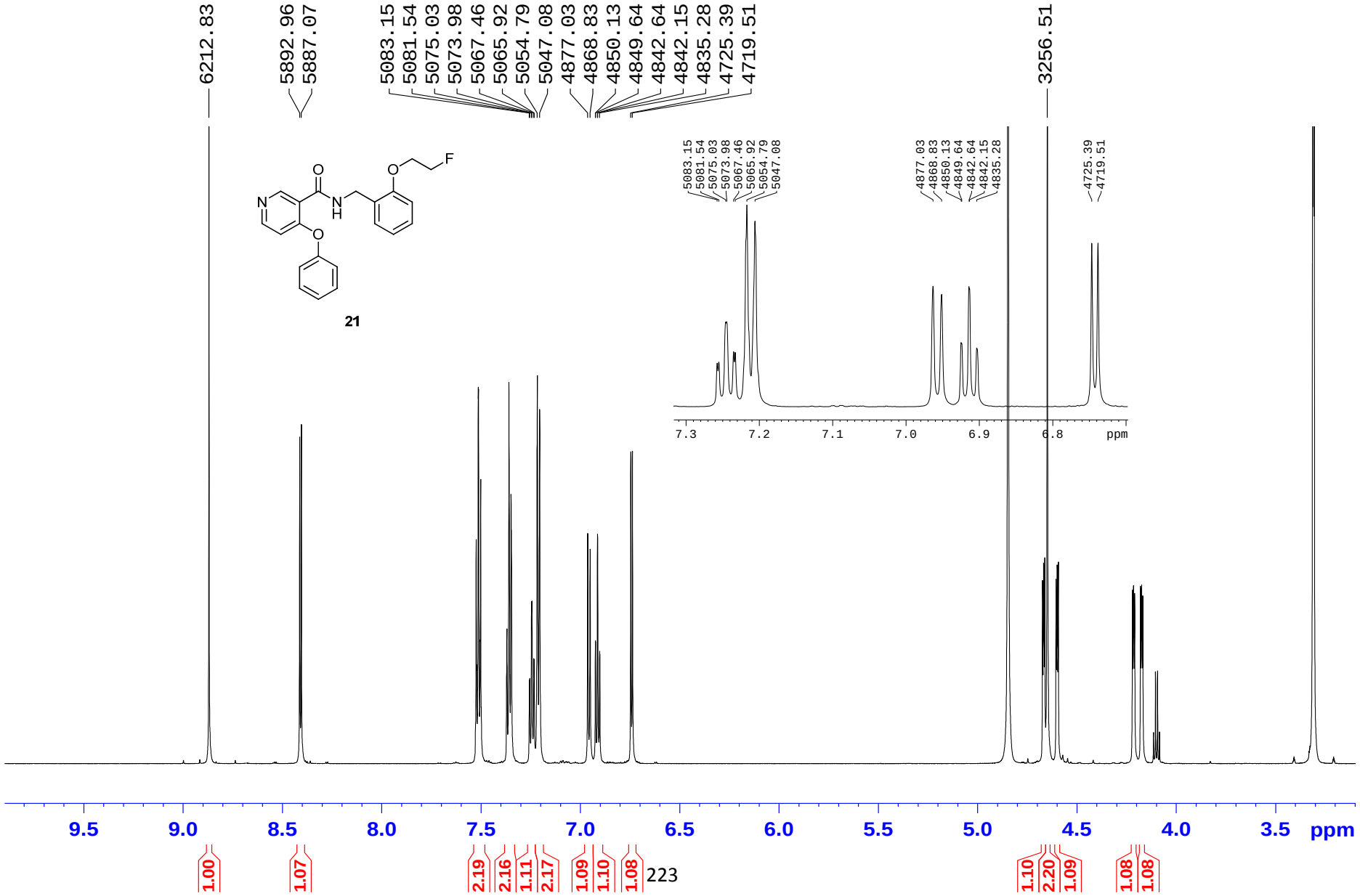

^{13}C NMR of *N*-(2-(2-Fluoroethoxy)benzyl)-4-phenoxynicotinamide:

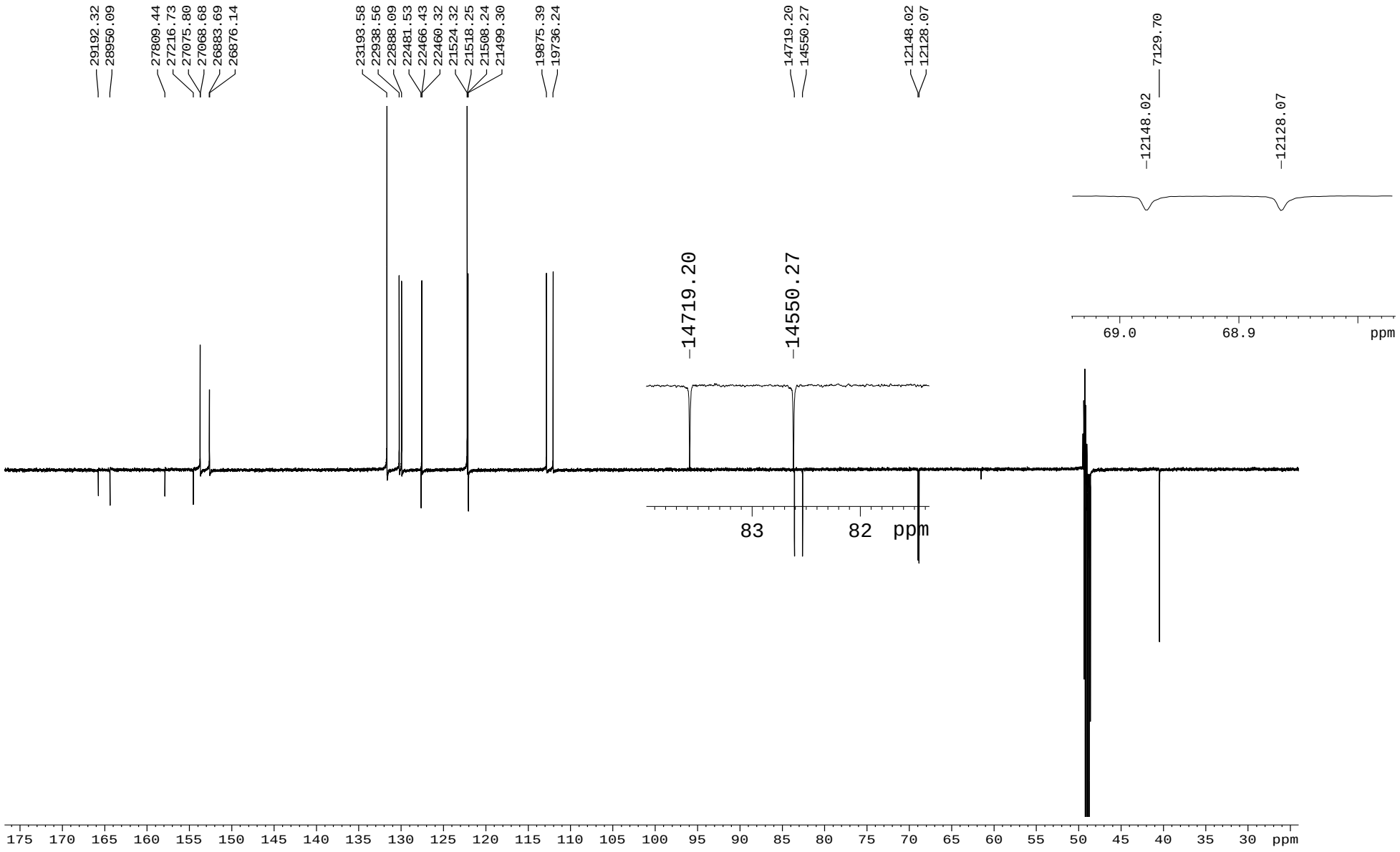

^{19}F NMR of *N*-(2-(2-Fluoroethoxy)benzyl)-4-phenoxynicotinamide:

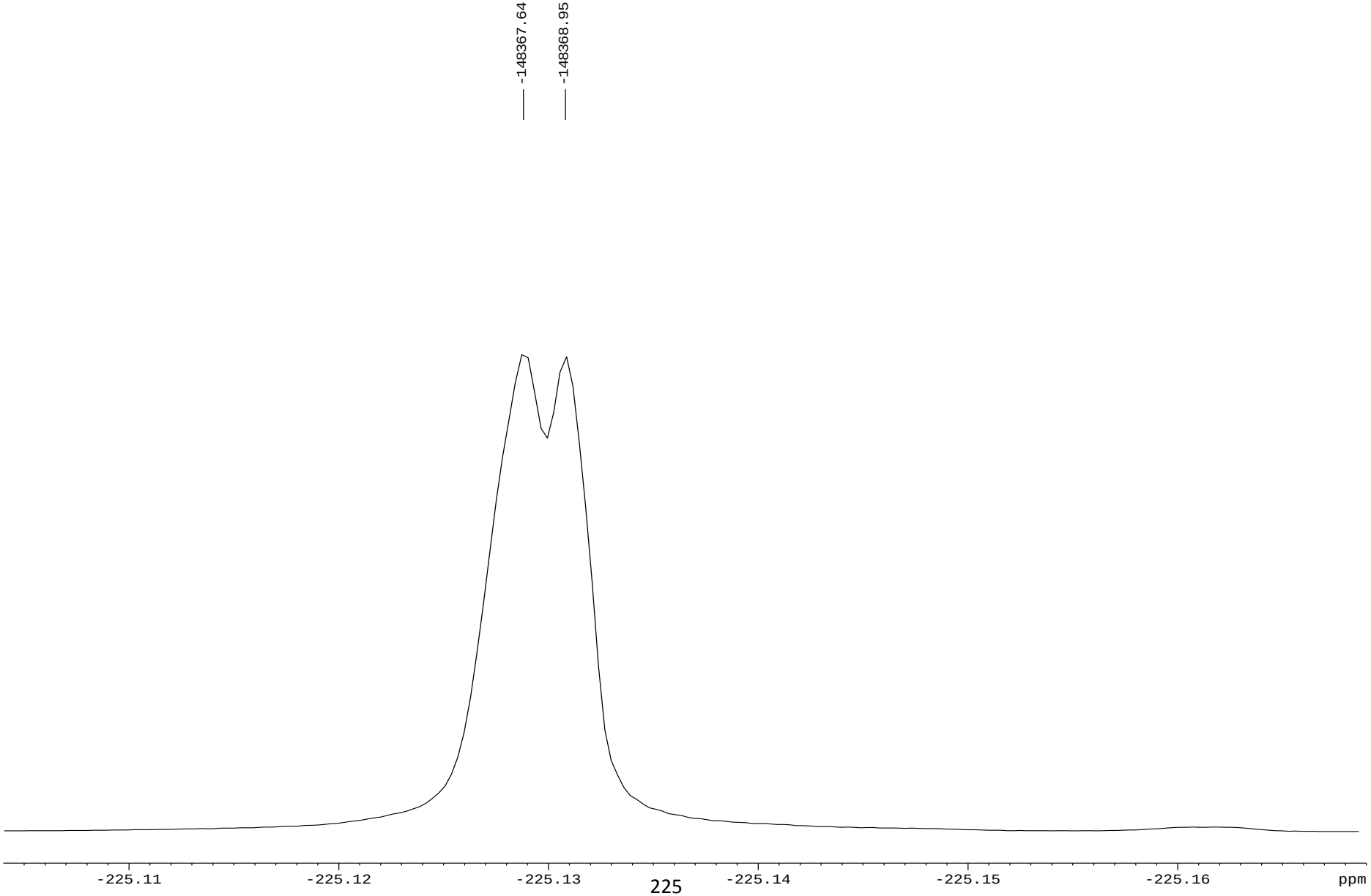

^{1}H NMR of *N*-(-2-Tosylethoxybenzyl)-*N*-methyl-4-phenoxynicotinamide:

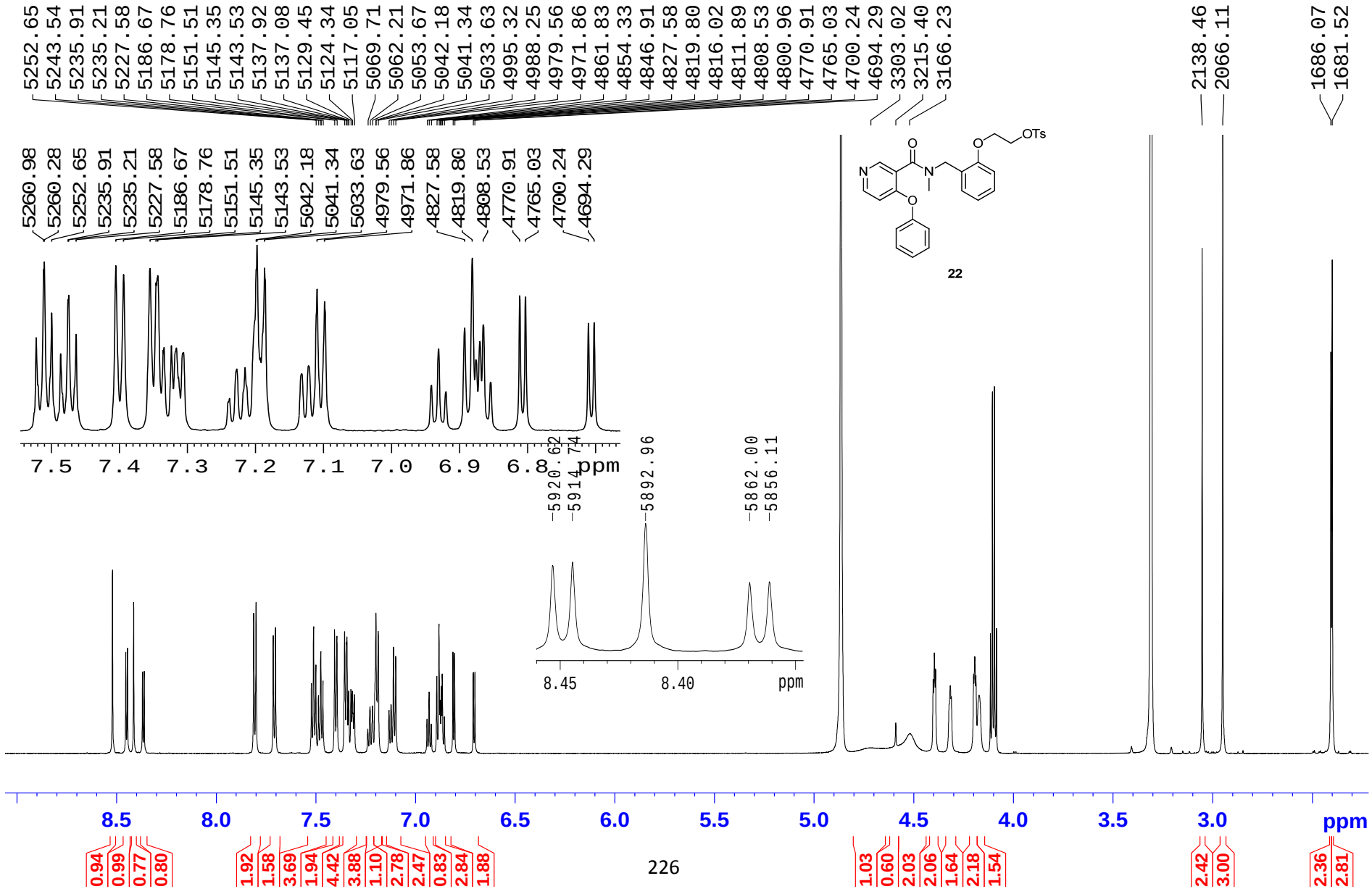

^{13}C NMR of *N*-(-2-Tosylethoxybenzyl)-*N*-methyl-4-phenoxynicotinamide:

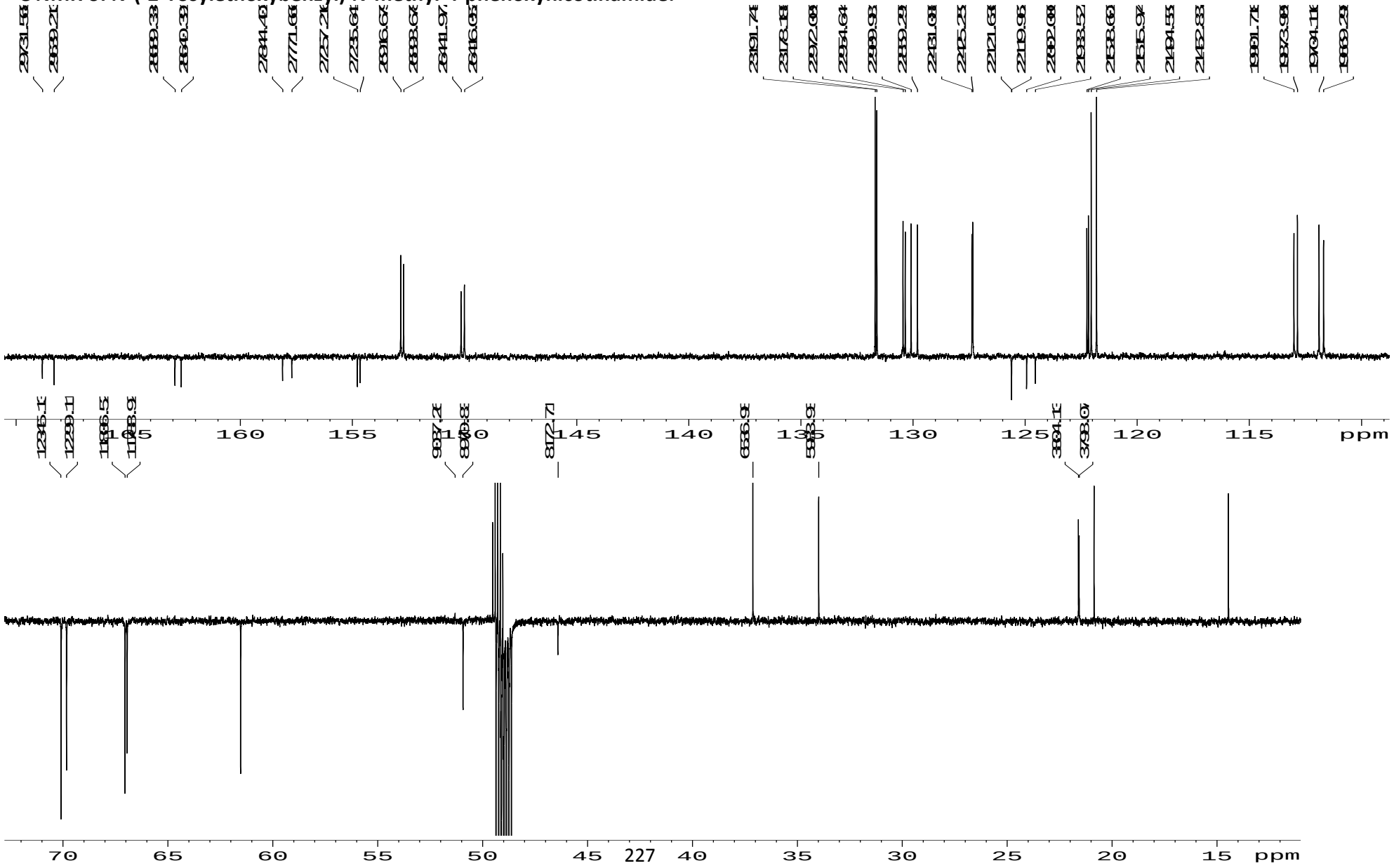

^{1}H NMR of *N*-(2-(2-Tosylethoxy)benzyl)-4-phenoxynicotinamide:

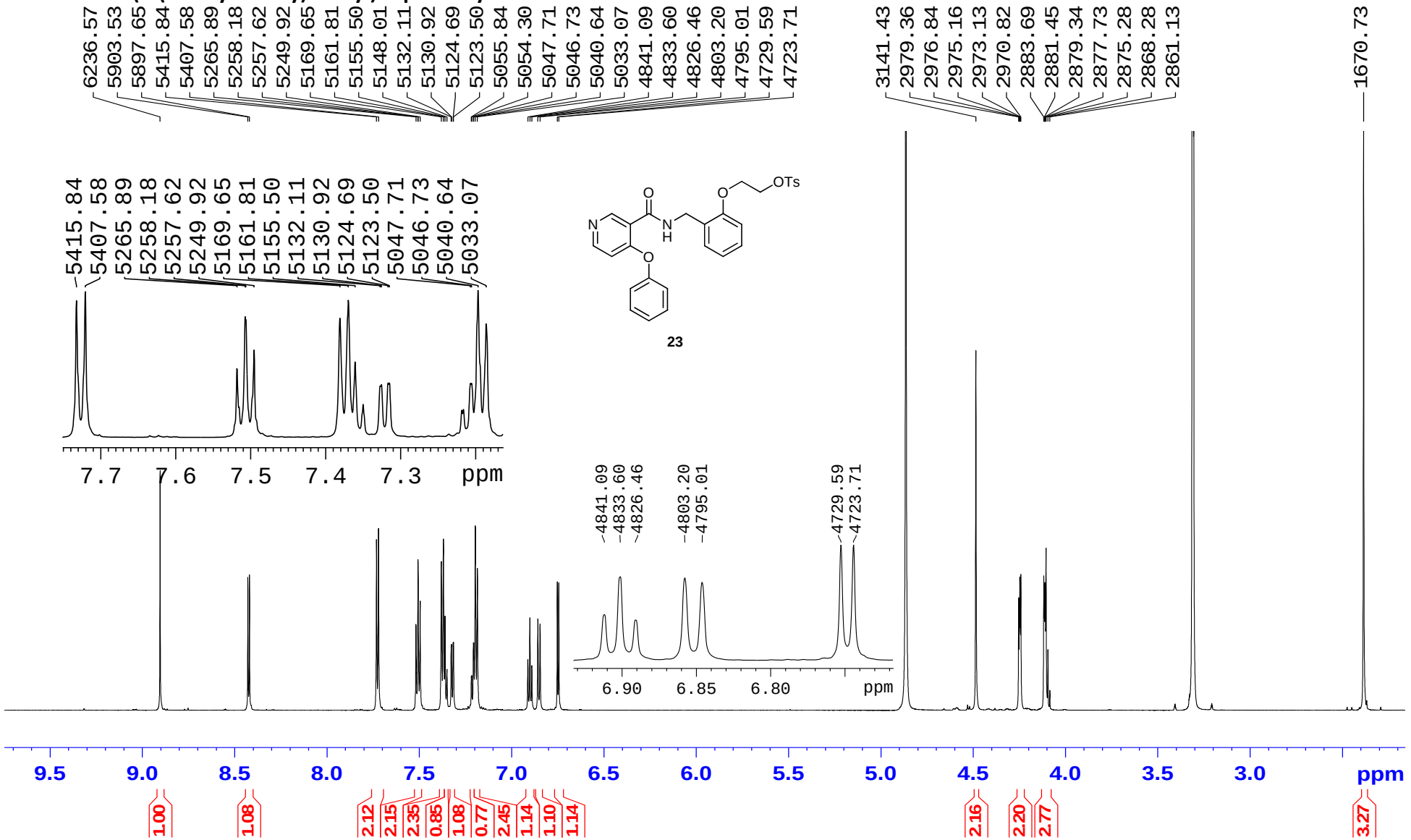

^{13}C NMR of *N*-(2-(2-Tosylethoxy)benzyl)-4-phenoxynicotinamide:

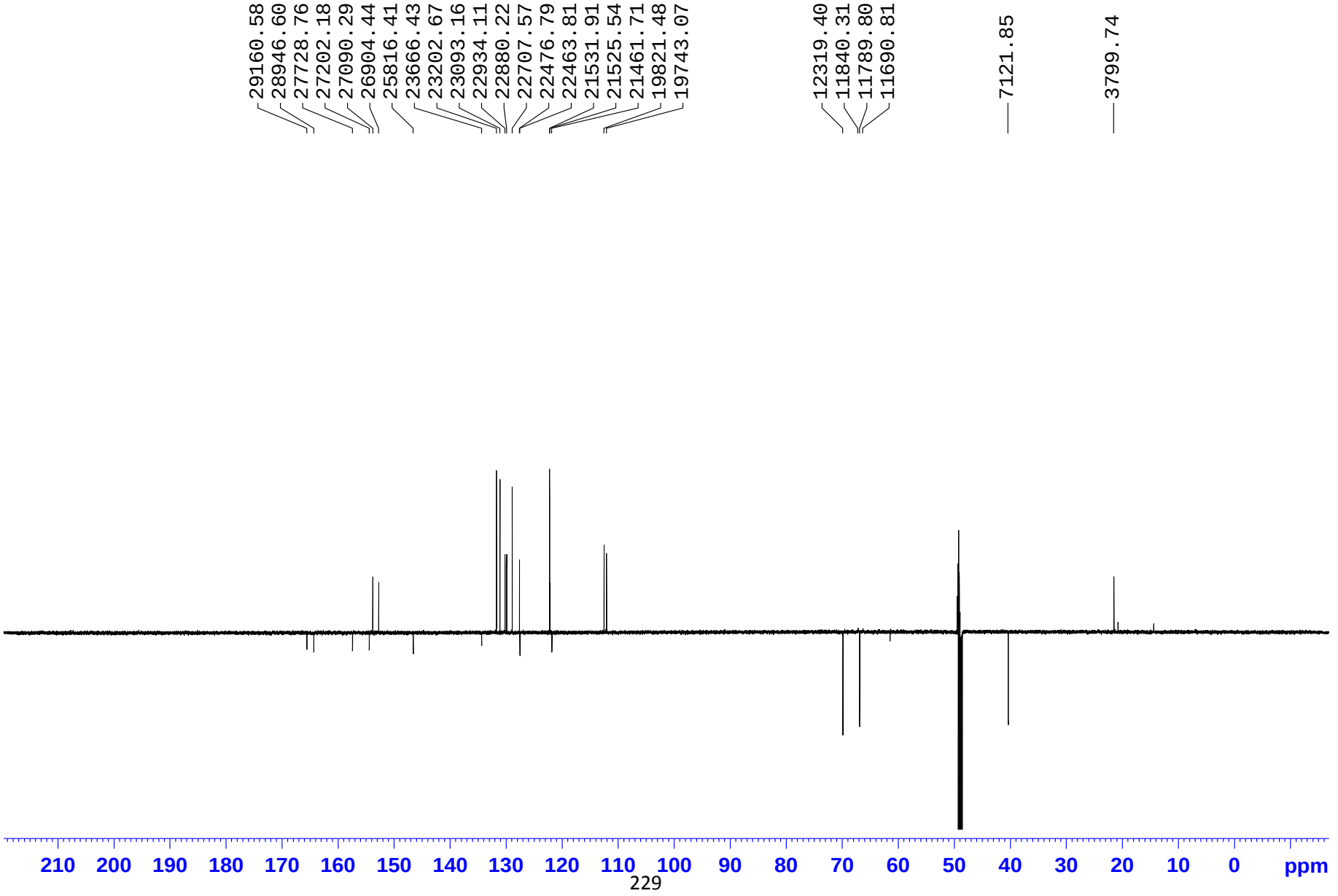

^{1}H NMR of (±)-*N*-(*sec*-Butyl)-4-phenoxynicotinamide:

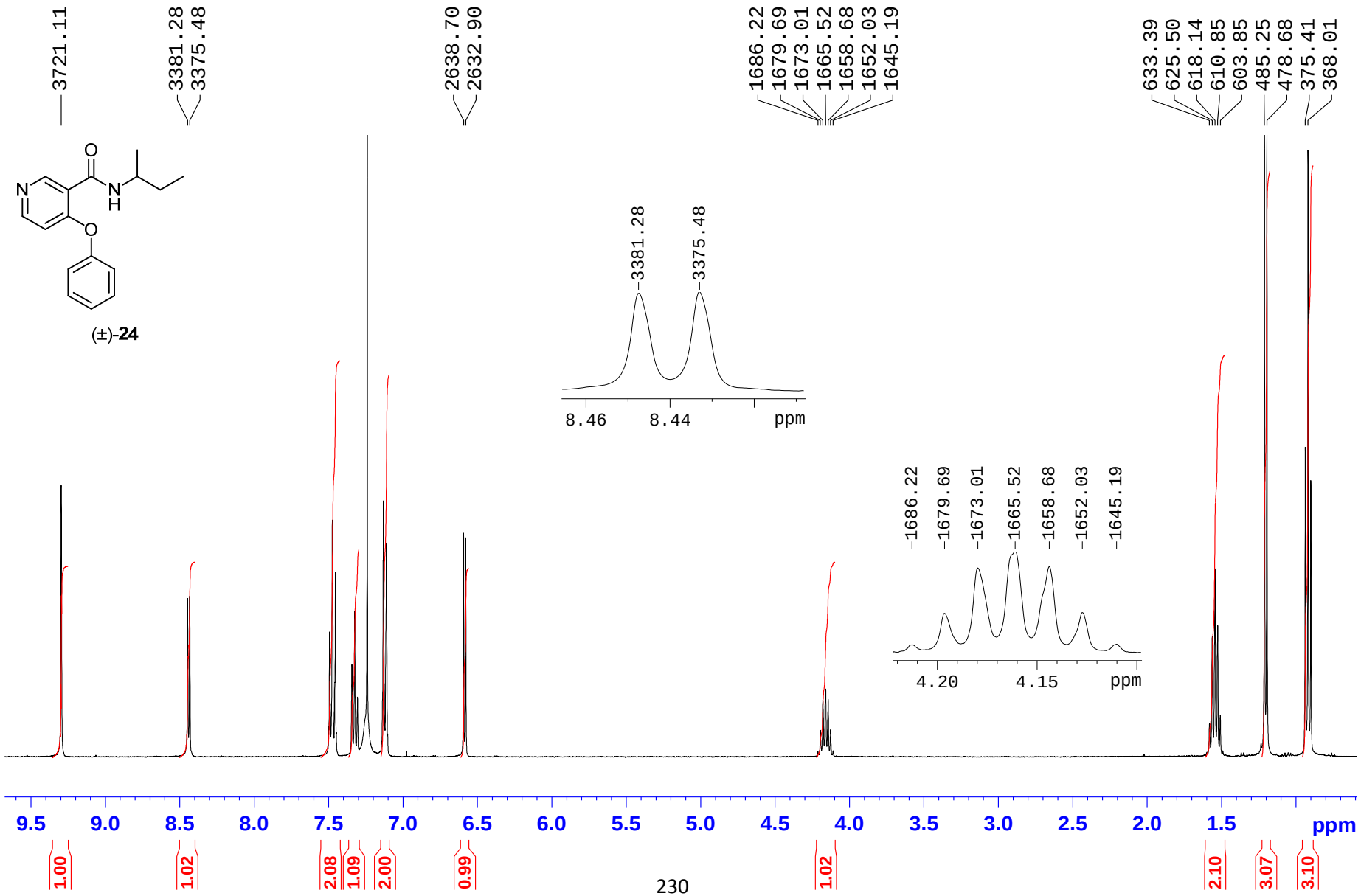

^{13}C NMR of (±)-*N*-(*sec*-Butyl)-4-phenoxynicotinamide:

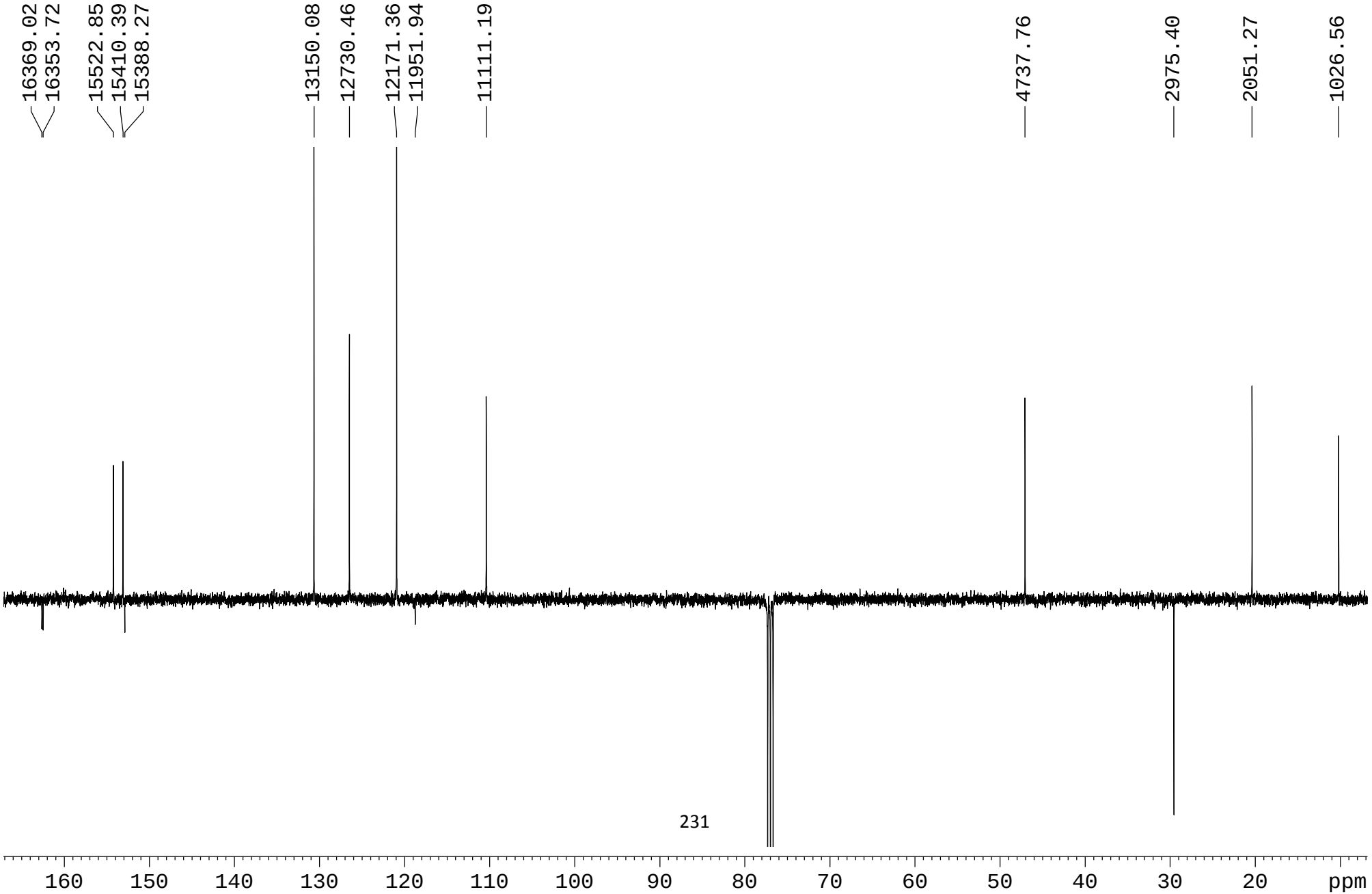

^{1}H NMR of (±)-*N*-*sec*-Butyl-*N*-methyl-4-phenoxynicotinamide:

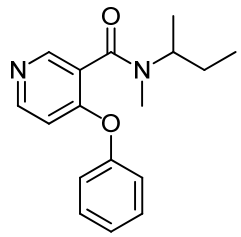

(±)-**9**

^{13}C NMR of (±)-*N*-*sec*-Butyl-*N*-methyl-4-phenoxynicotinamide:

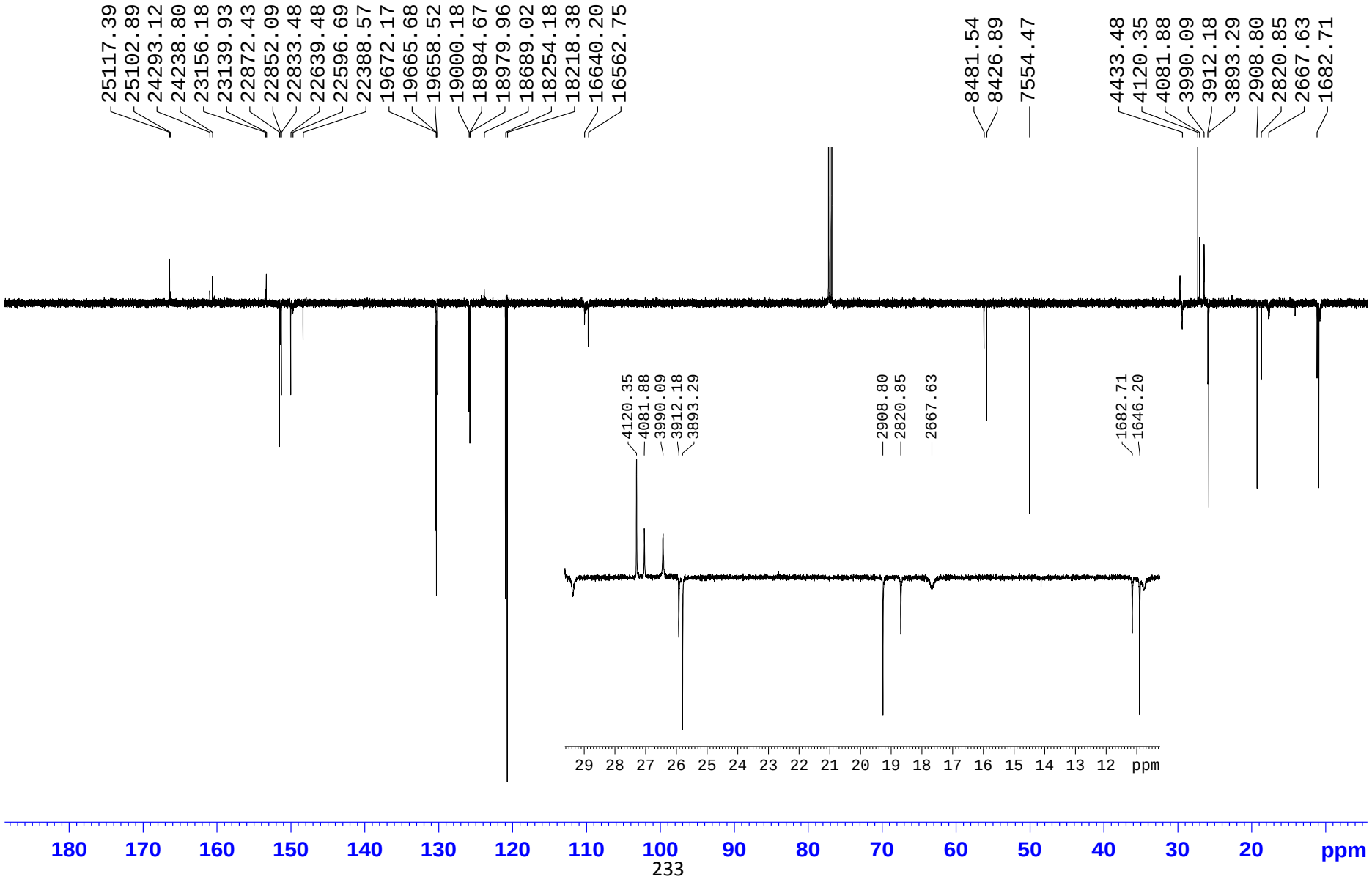

^{1}H NMR of Methyl 1-(2-chloropyridin-3-yl)isoquinoline-3-carboxylate:

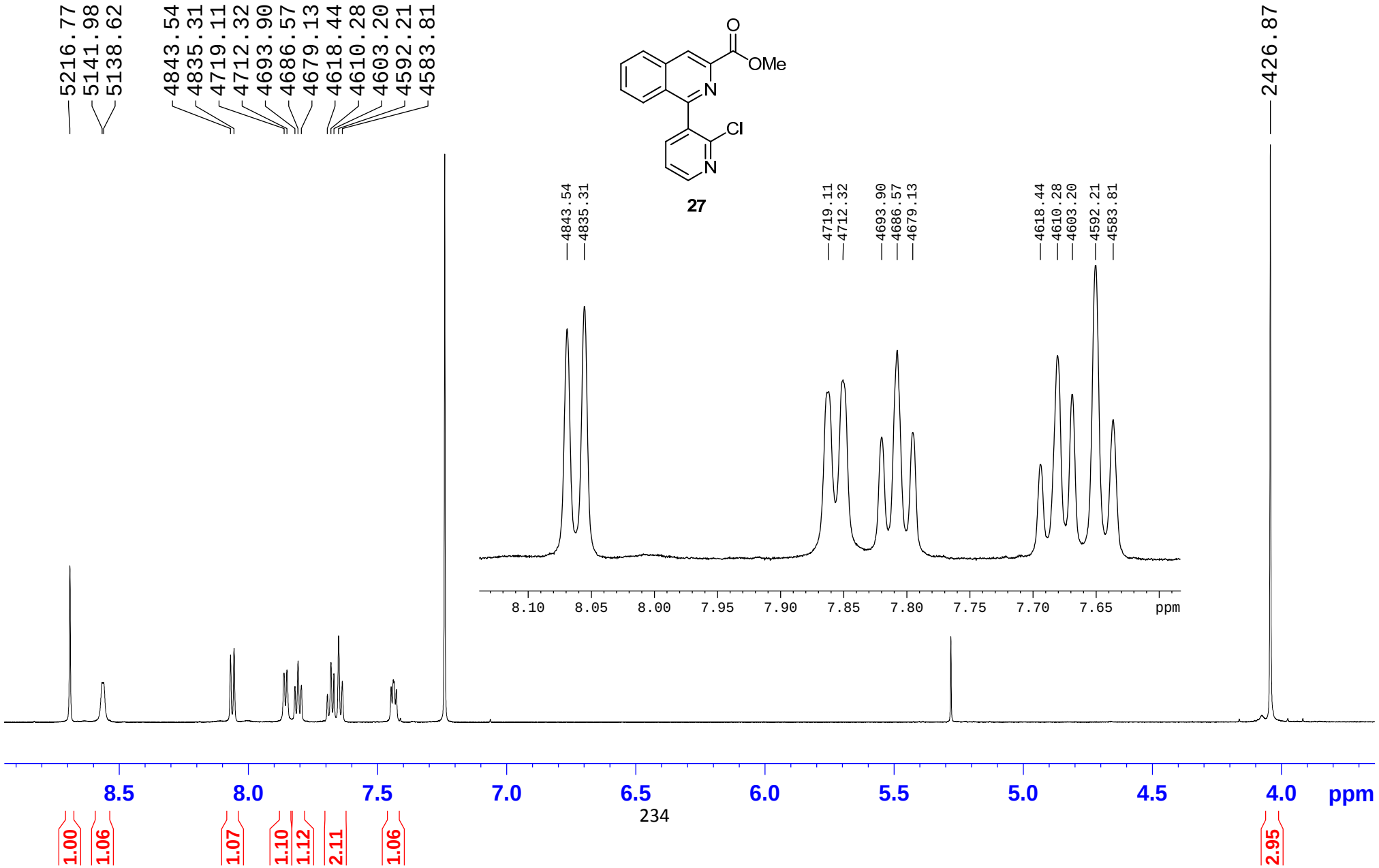

^{13}C NMR of Methyl 1-(2-chloropyridin-3-yl)isoquinoline-3-carboxylate:

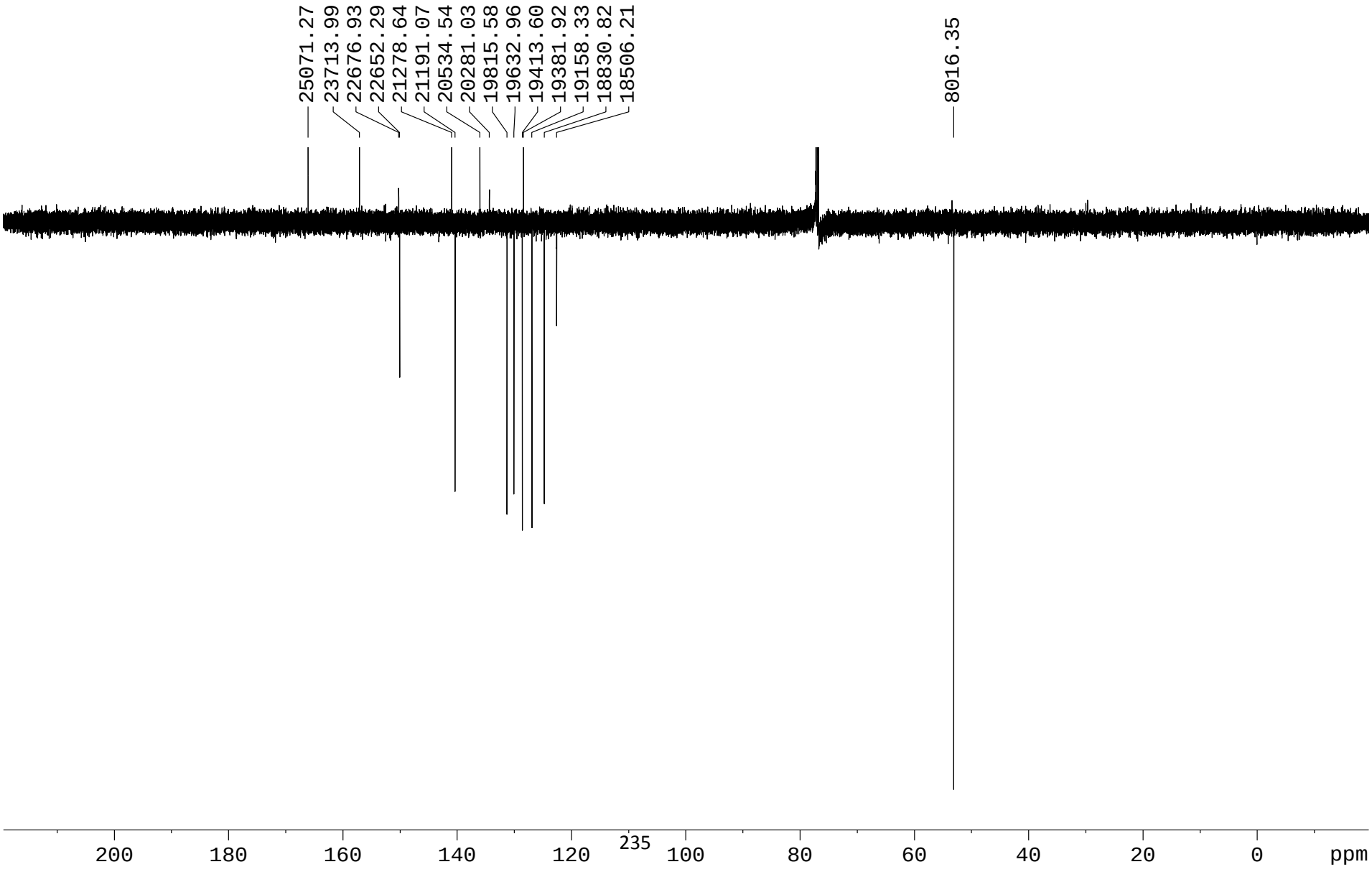

^{1}H NMR of 1-(2-Chloropyridin-3-yl)isoquinoline-3-carboxylic acid:

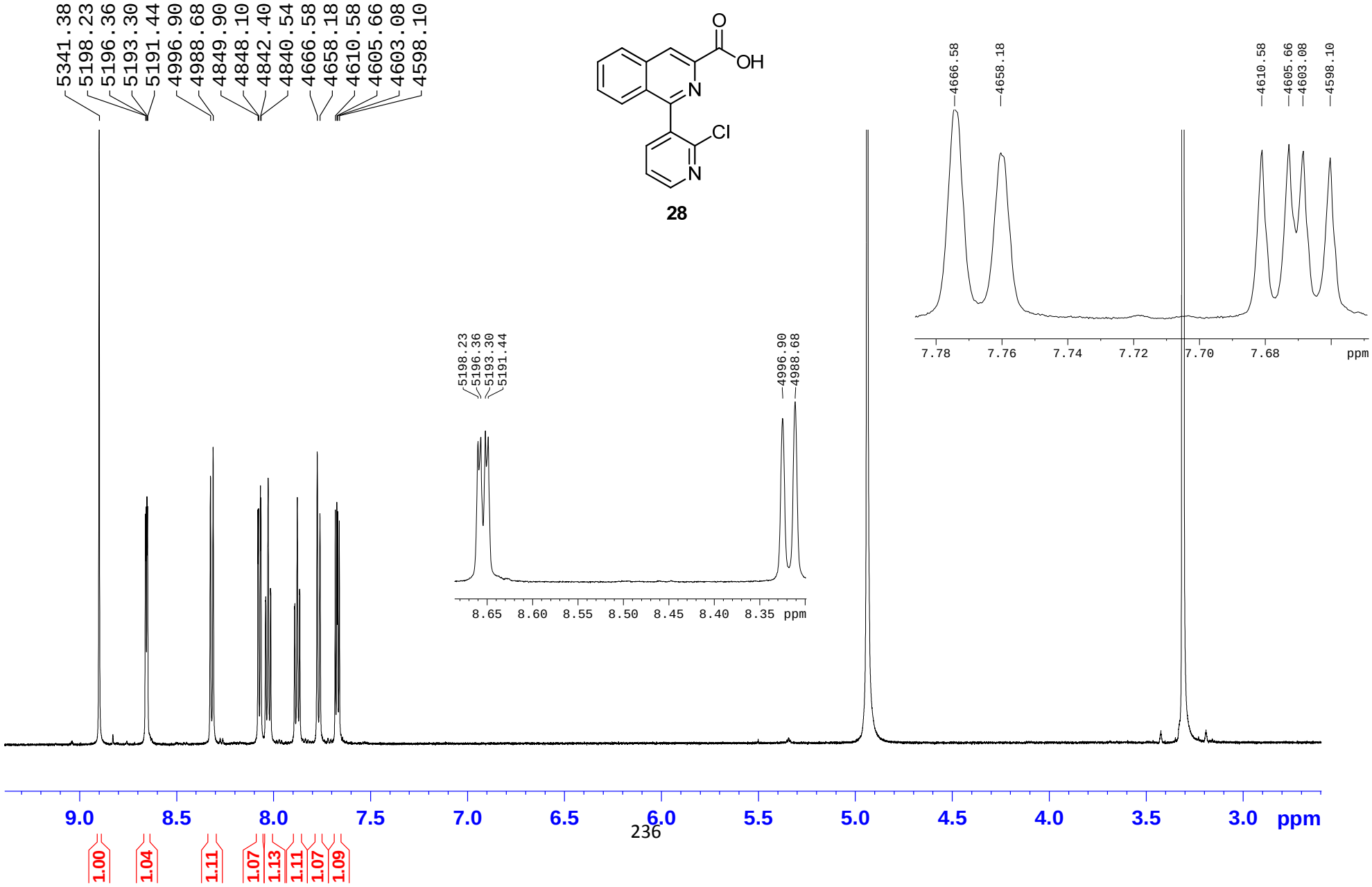

^{13}C NMR of 1-(2-Chloropyridin-3-yl)isoquinoline-3-carboxylic acid:

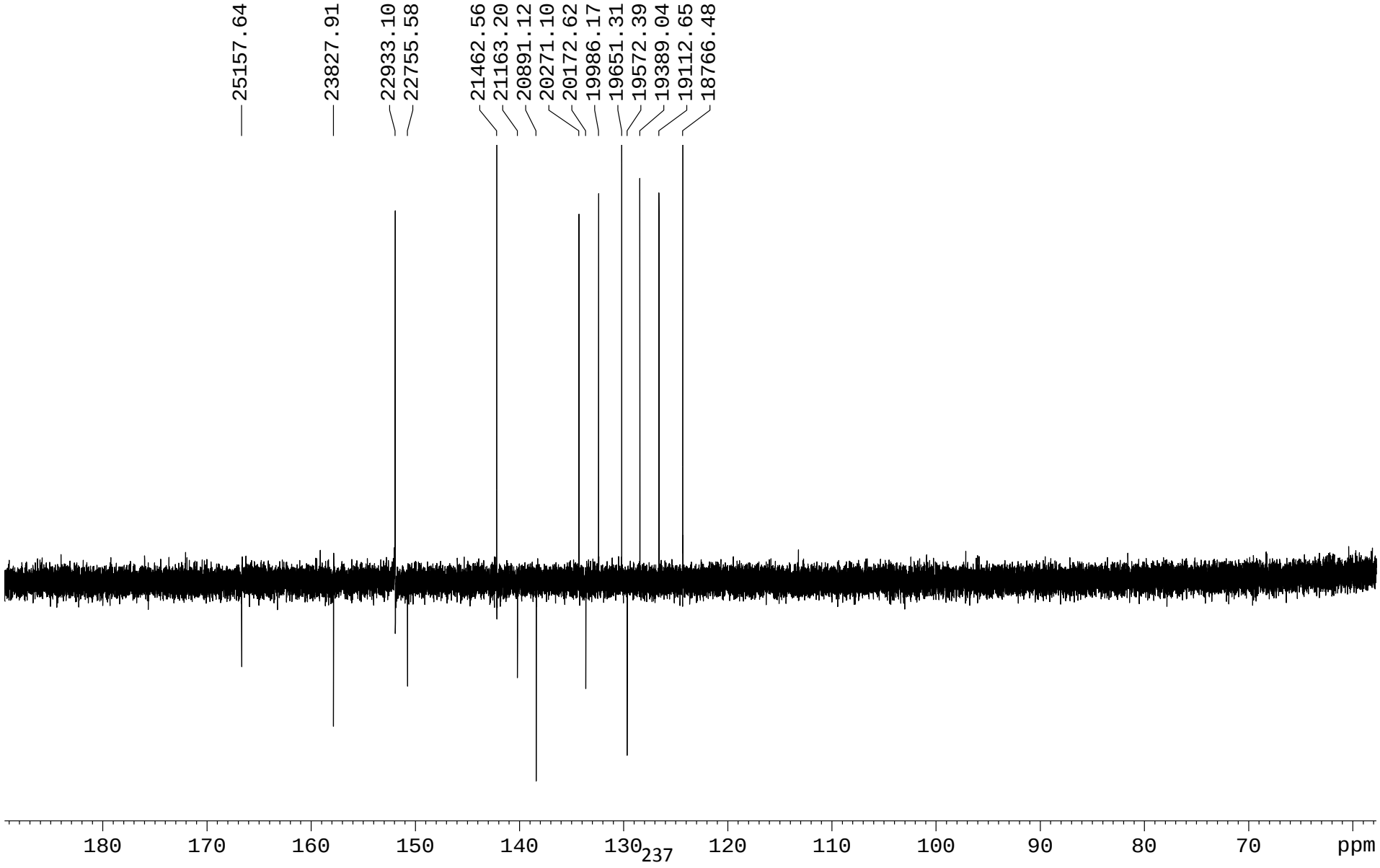

^{1}H NMR of (–)-(*R*)-*N*-(*sec*-Butyl)-1-(2-chloropyridin-3-yl)isoquinoline-3-carboxyamide:

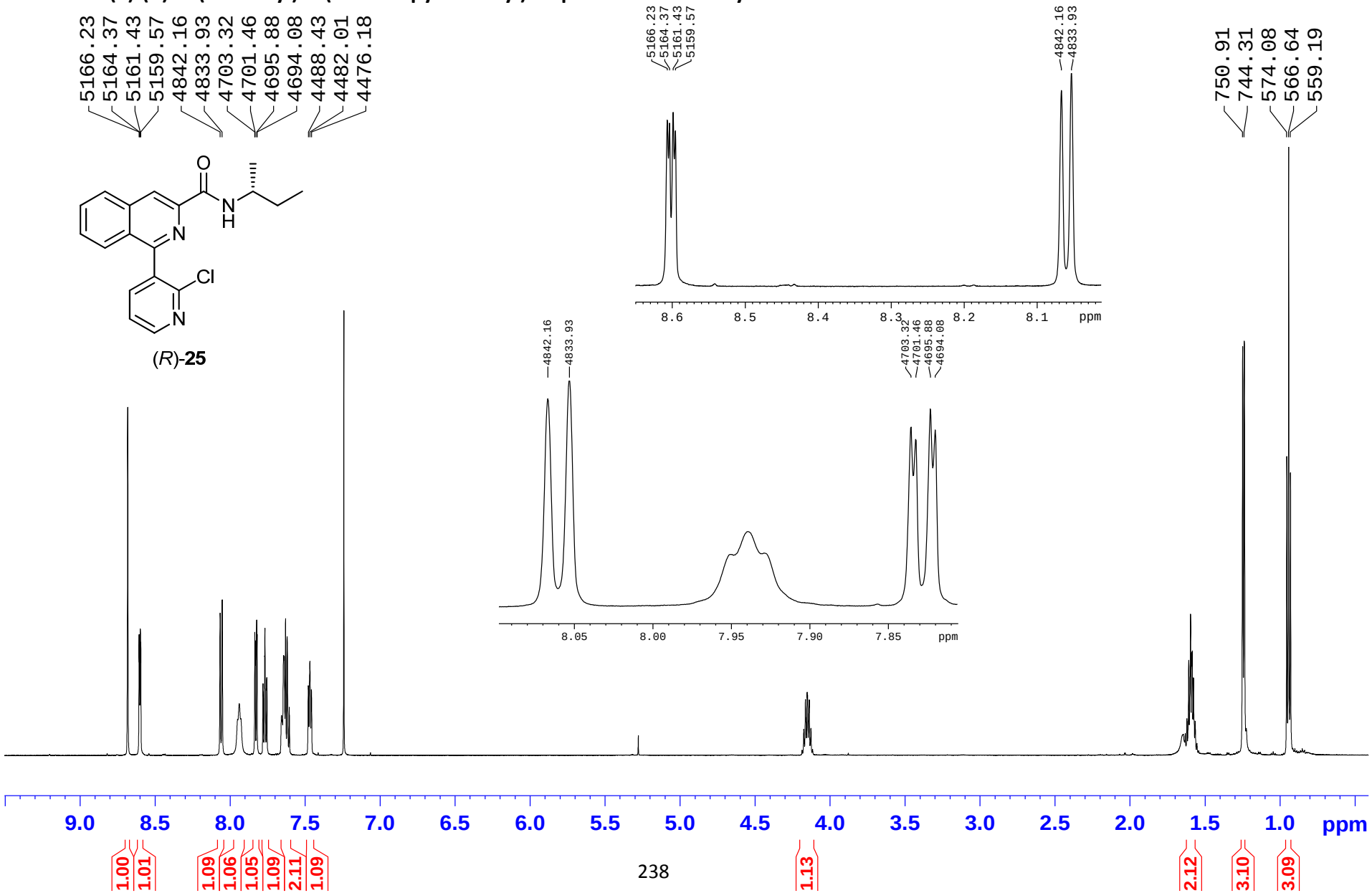

^{13}C NMR of (–)-(*R*)-*N*-(*sec*-Butyl)-1-(2-chloropyridin-3-yl)isoquinoline-3-carboxyamide:

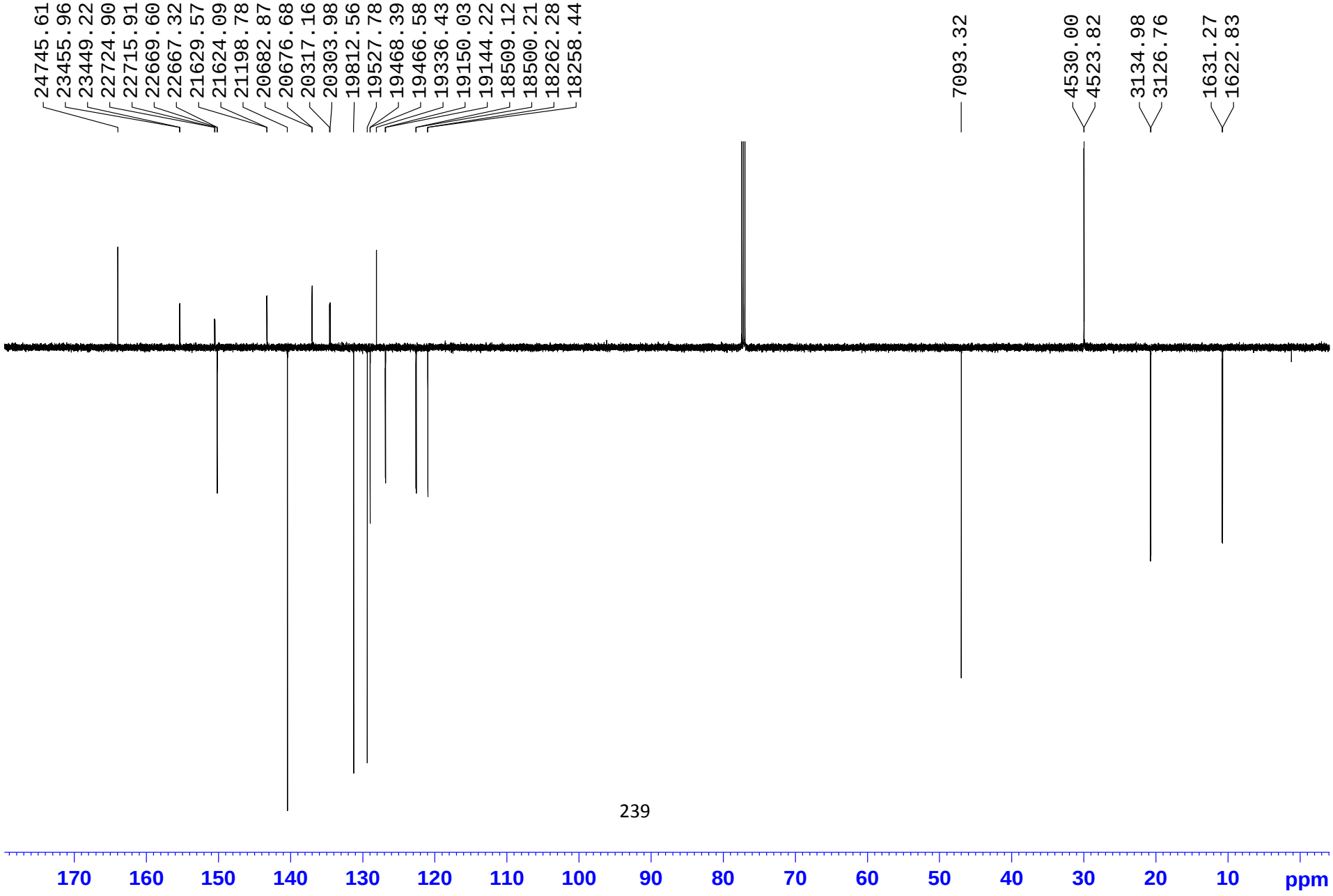

^{1}H NMR of (*R*)-*N*-(*sec*-butyl)-1-(2-chloropyridin-3-yl)-*N*-methylisoquinoline-3-carboxamide:

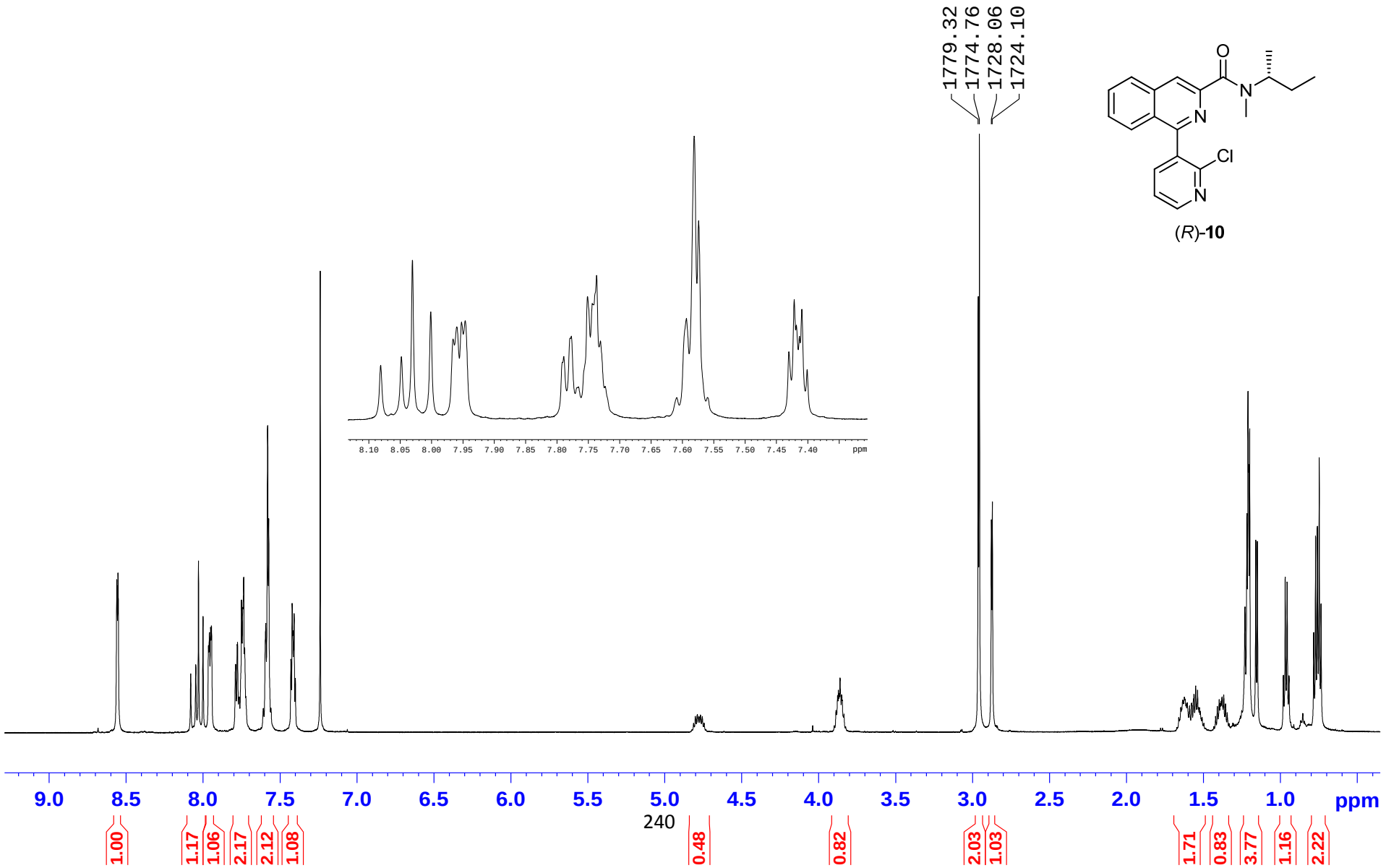

^{13}C NMR of (*R*)-*N*-(*sec*-Butyl)-1-(2-chloropyridin-3-yl)-*N*-methylisoquinoline-3-carboxamide:

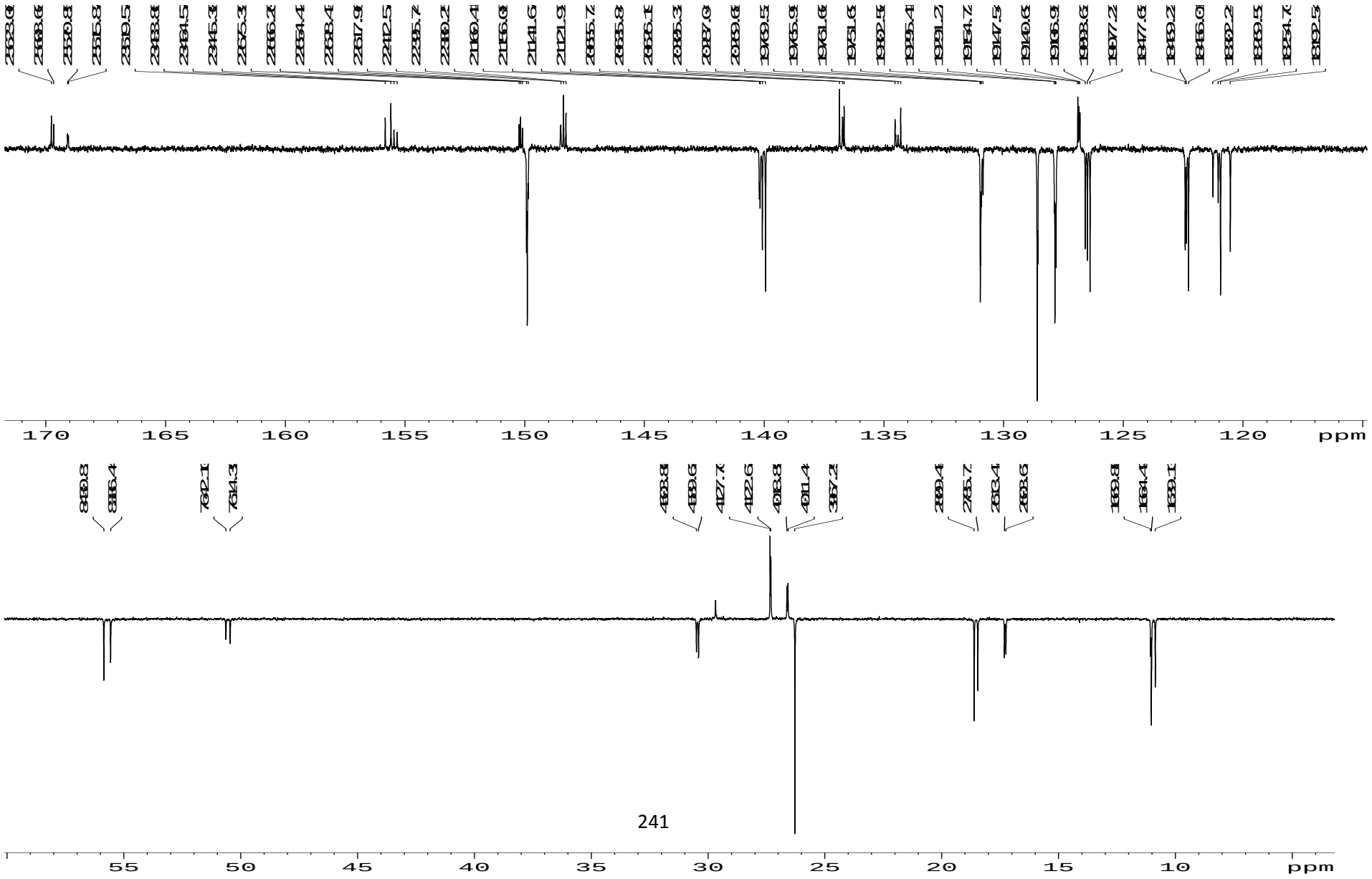

12.2. Purity of target compounds – HPLC chromatograms

HPLC spectra were recorded to determine the purities of the target compounds, using the same system as described in the main text.

Compound 6

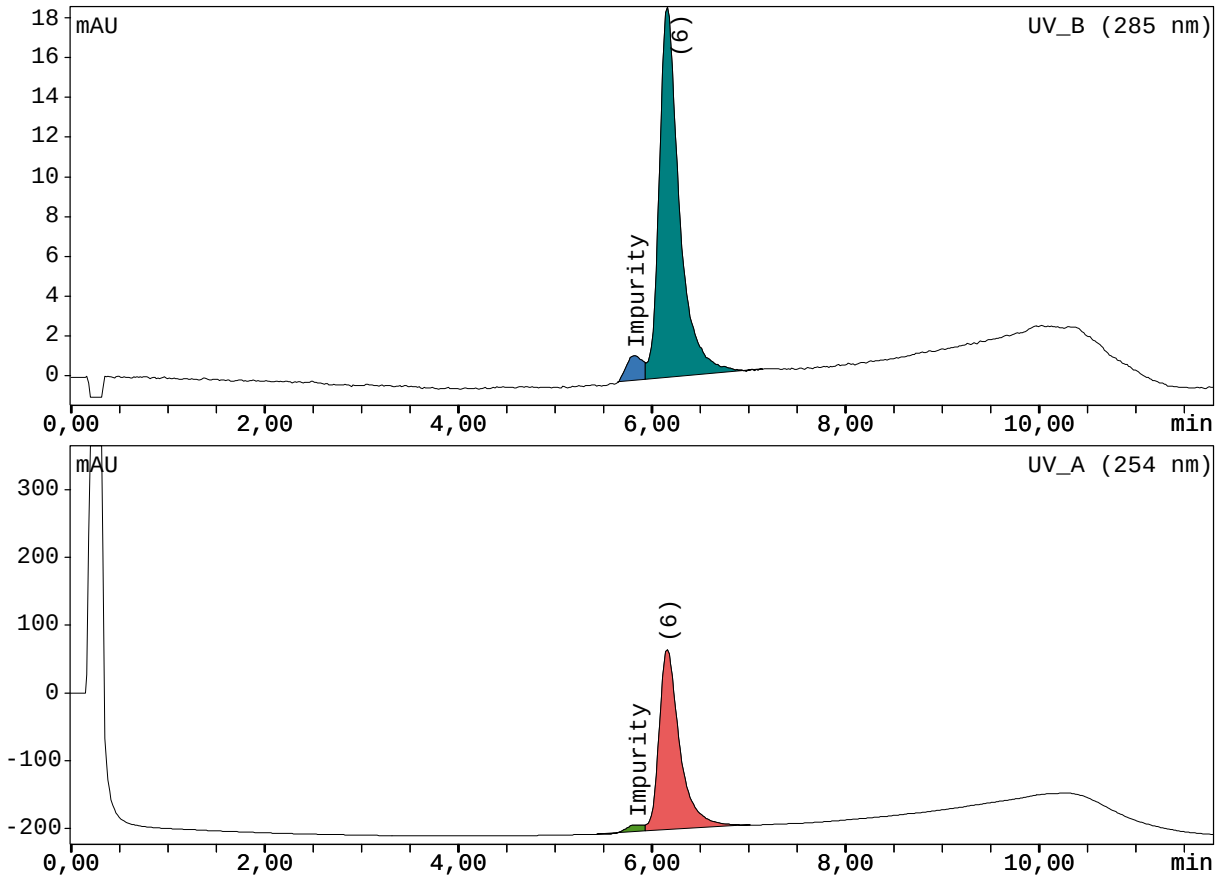

Integration UV_A (254 nm)

Substance	R/T (min)	Area (mAU*min)	%Area %
Impurity	5,85	111,414	2,72
Compound 6	6,17	3991,049	97,28
Total		4102,463	100,00

Integration UV_B (285 nm)

Substance	R/T min	Area mAU*min	%Area %
Impurity	5,83	13,9595	4,90

Compound 6	6,17	270,8431	95,10
Total		284,8026	100,00

Compound 16

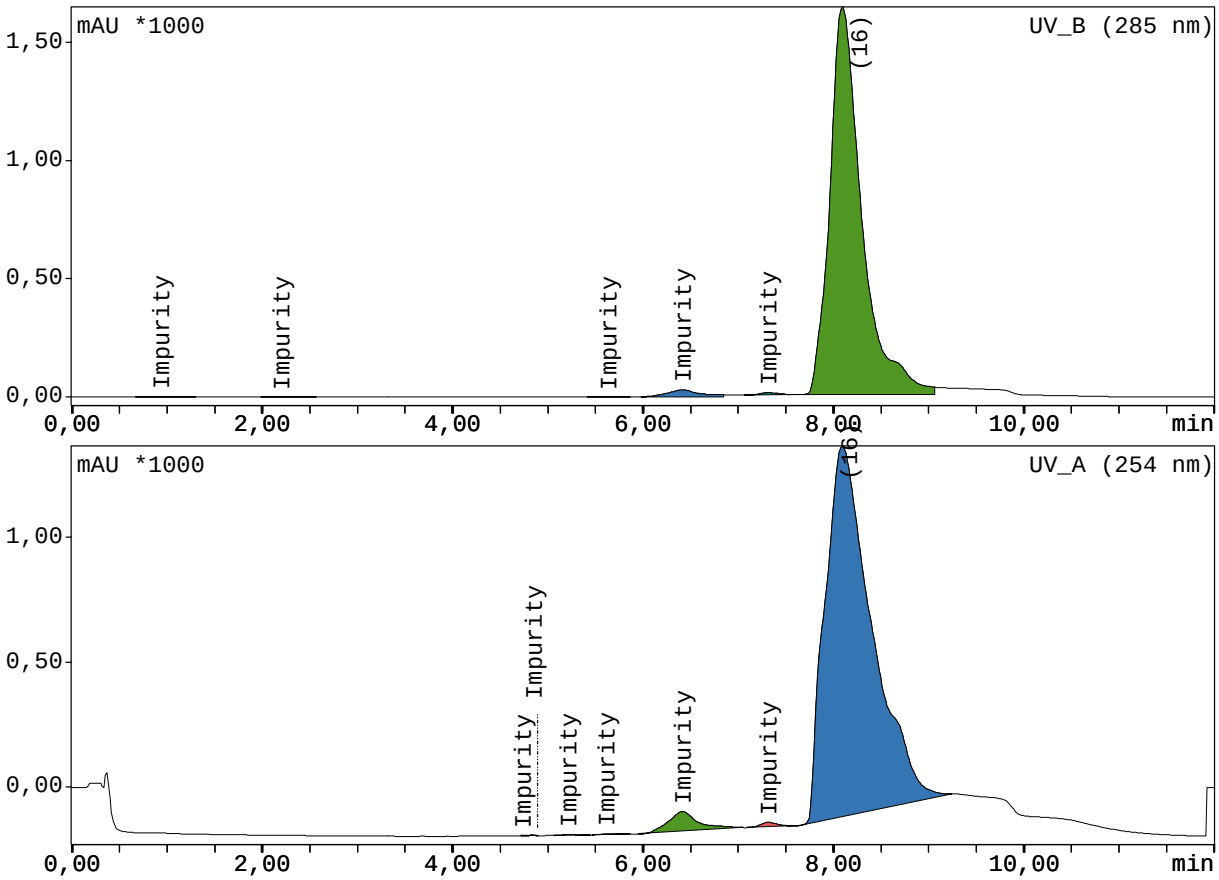

Integration UV_A (254 nm)

Substance	R/T (min)	Area (mAU*min)	%Area
Impurity	4,73	0,47	0,00
Impurity	4,85	8,21	0,02
Impurity	5,22	23,63	0,05
Impurity	5,62	23,61	0,05
Impurity	6,42	1699,92	3,25
Impurity	7,32	199,35	0,38
Compound 16	8,10	50420,21	96,27
Total		52375,40	100

Integration UV_B (285 nm)

Substance	R/T	Area	%Area

	(min)	(mAU*min)	
Impurity	0,93	17,07	0,04
Impurity	2,20	3,47	0,01
Impurity	5,63	4,54	0,01
Impurity	6,42	714,26	1,82
Impurity	7,32	129,52	0,33
Compound 16	8,10	38301,22	97,78
Total		39170,08	100,00

Compound 7

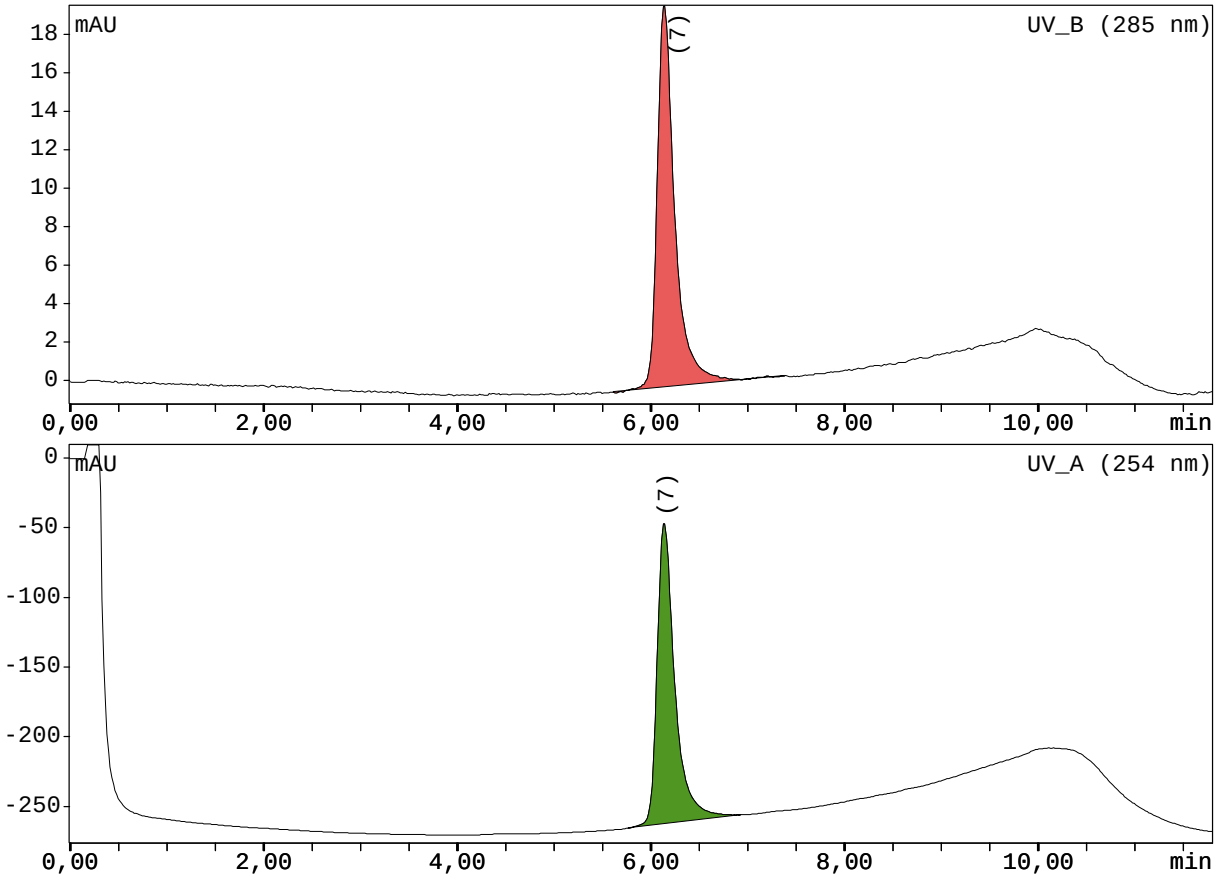

Integration UV_A (254 nm)

Substance	R/T (min)	Area (mAU*min)	% Area
Compound 7	6,15	2756,937	100,00

Total	2756,937	100,00

Integration UV_B (285 nm)

Substance	R/T (min)	Area (mAU*min)	%Area
Compound 7	6,15	252,8145	100,00
		252,8145	100,00

Compound 19

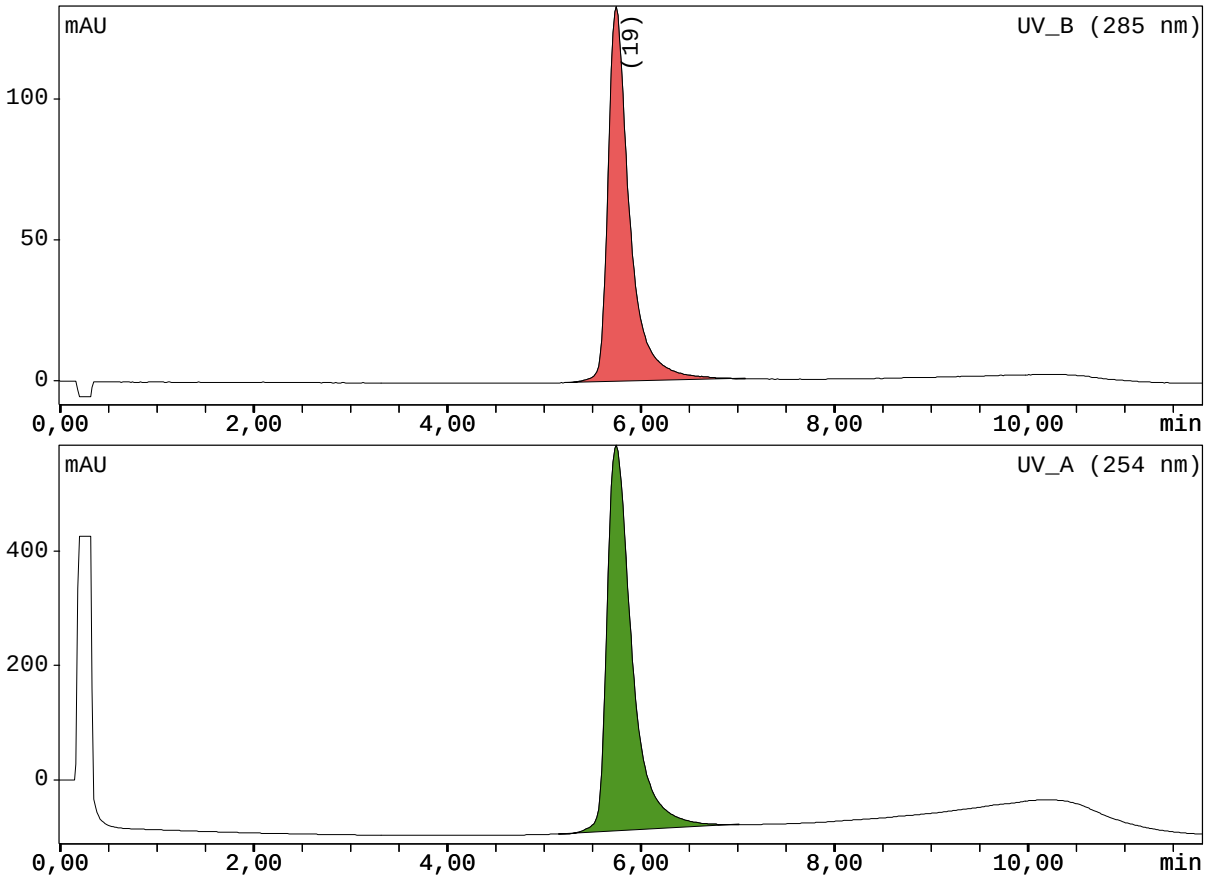

Integration UV_A (254 nm)

Substance	R/T (min)	Area (mAU*min)	%Area
Compound 19	5,75	12149,40	100,00
Total		12149,40	100,00

Integration UV_B (285 nm)

Substance	R/T (min)	Area (mAU*min)	%Area
(19)	5,75	2069,215	100,00
Sum in ROI		2069,215	100,00

Compound 8

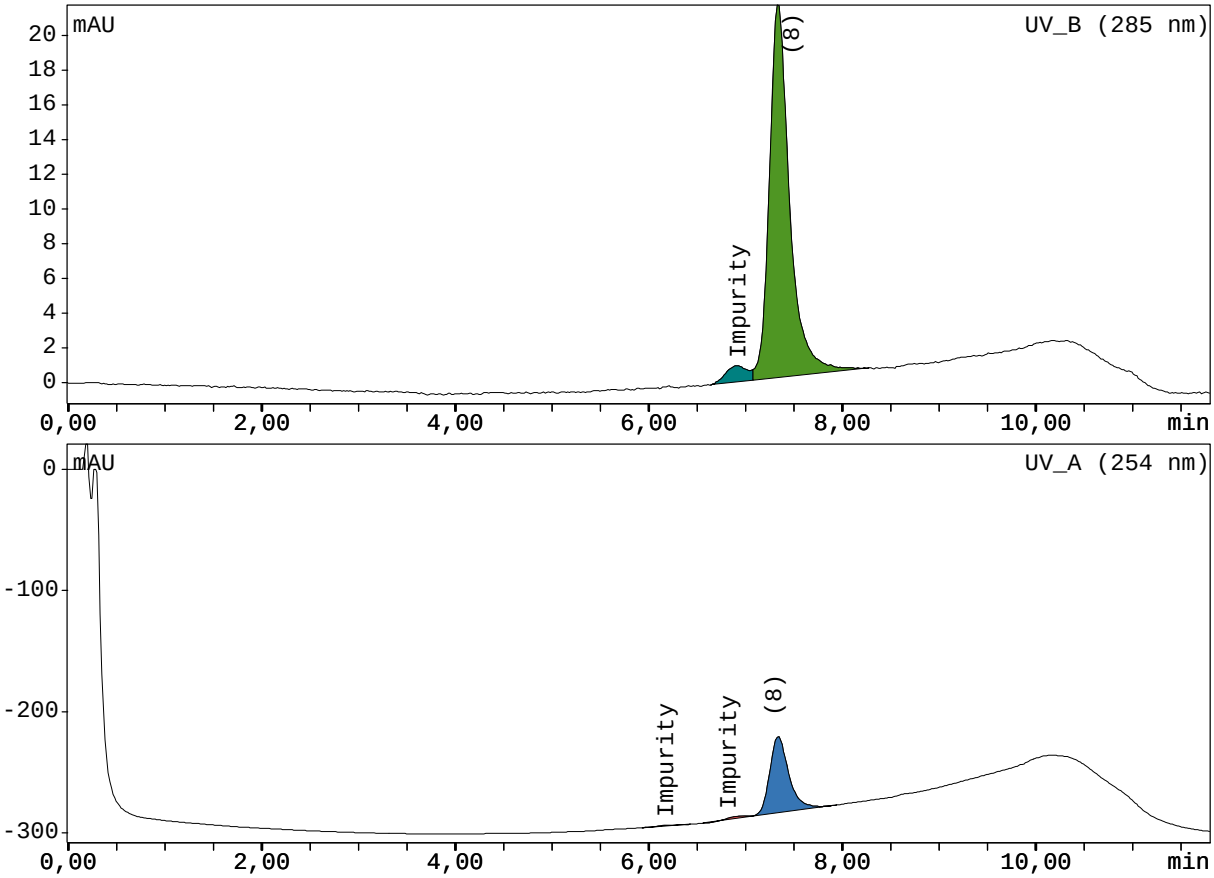

Integration UV_A (254 nm)

Substance	R/T (min)	Area (mAU*min)	%Area
Impurity	6,17	5,4334	0,61
Impurity	6,82	21,8117	2,45
Compound 8	7,35	863,2060	96,94
Total		890,4511	100,00

Integration UV_B (285 nm)

Substance	R/T (min)	Area (mAU*min)	%Area
Impurity	6,92	14,3356	4,37
Compound 8	7,35	314,0560	95,63

Total		328,3916	100,00

Compound 9

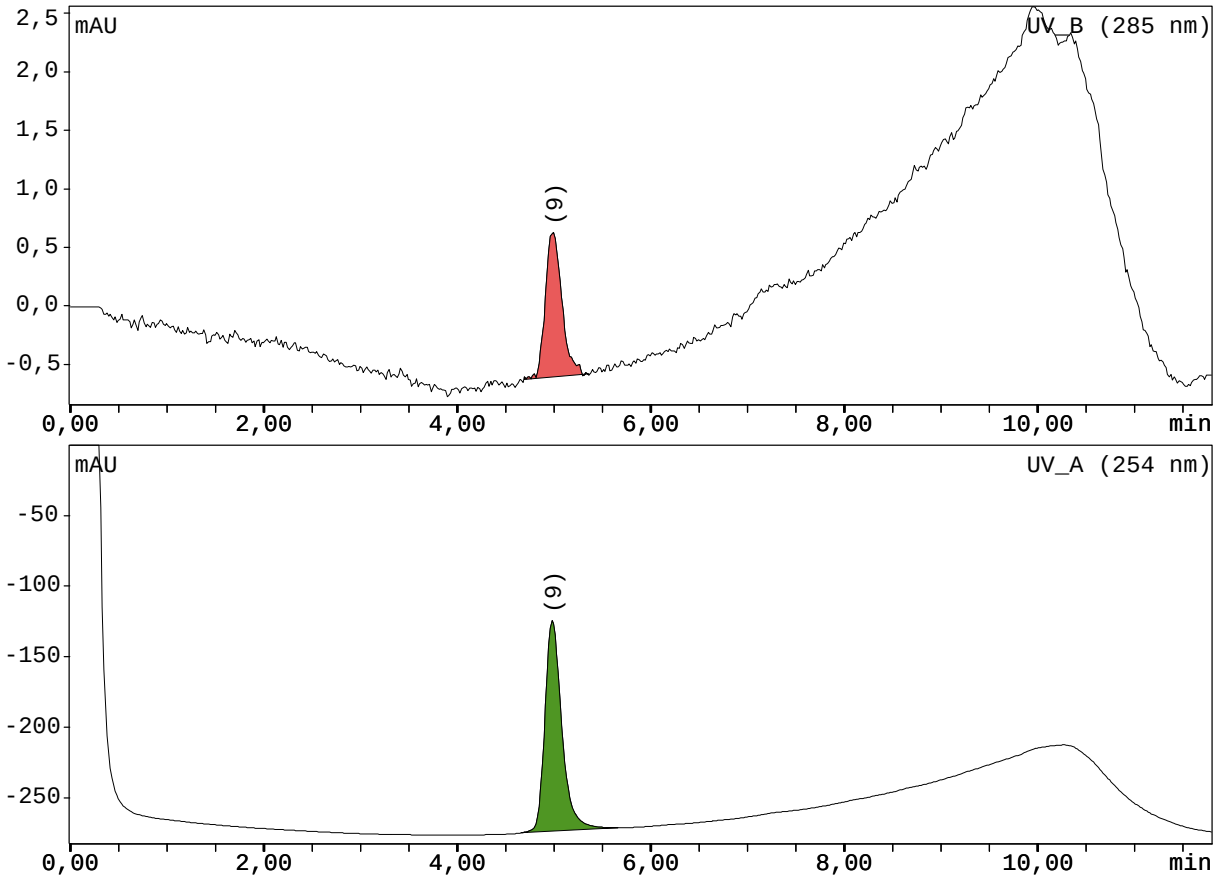

Integration UV_A (254 nm)

Substance	R/T (min)	Area (mAU*min)	%Area
Compound 9	4,98	1809,169	100,00
Total		1809,169	100,00

Integration UV_B (285 nm)

Substance	R/T (min)	Area (mAU*min)	%Area
Compound 9	5,00	14,71786	100,00
Total		14,71786	100,00

Compound 24

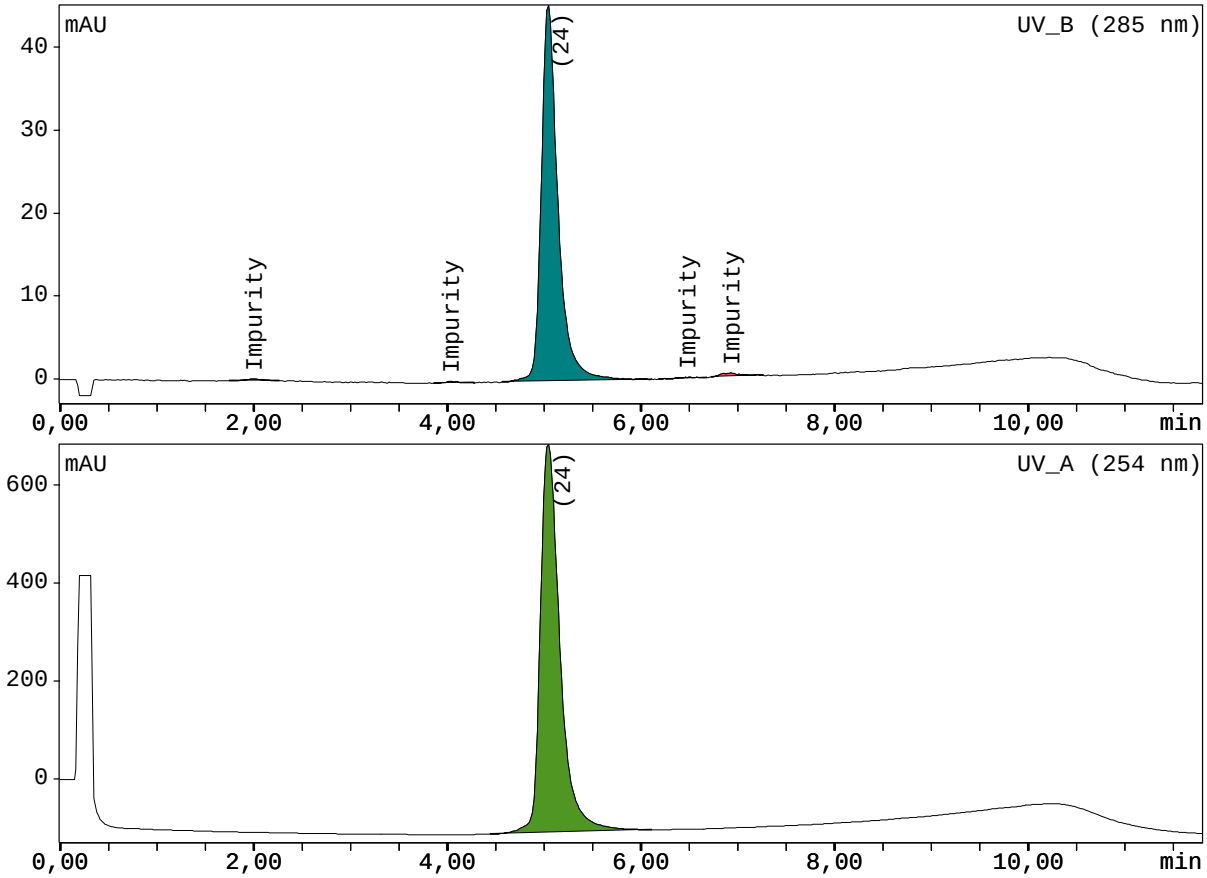

Integration UV_A (254 nm)

Substance	R/T (min)	Area (mAU*min)	%Area
Compound 24	5,05	11162,88	100,00
Total		11162,88	100,00

Integration UV_B (285 nm)

Substance	R/T (min)	Area (mAU*min)	%Area
Impurity	2,00	2,7418	0,49
Impurity	4,03	1,7919	0,32
Compund 24	5,05	544,6148	97,80
Impurity	6,48	1,3353	0,24

Impurity	6,93	6,3609	1,14
Total		556,8447	100,00

Compound 10

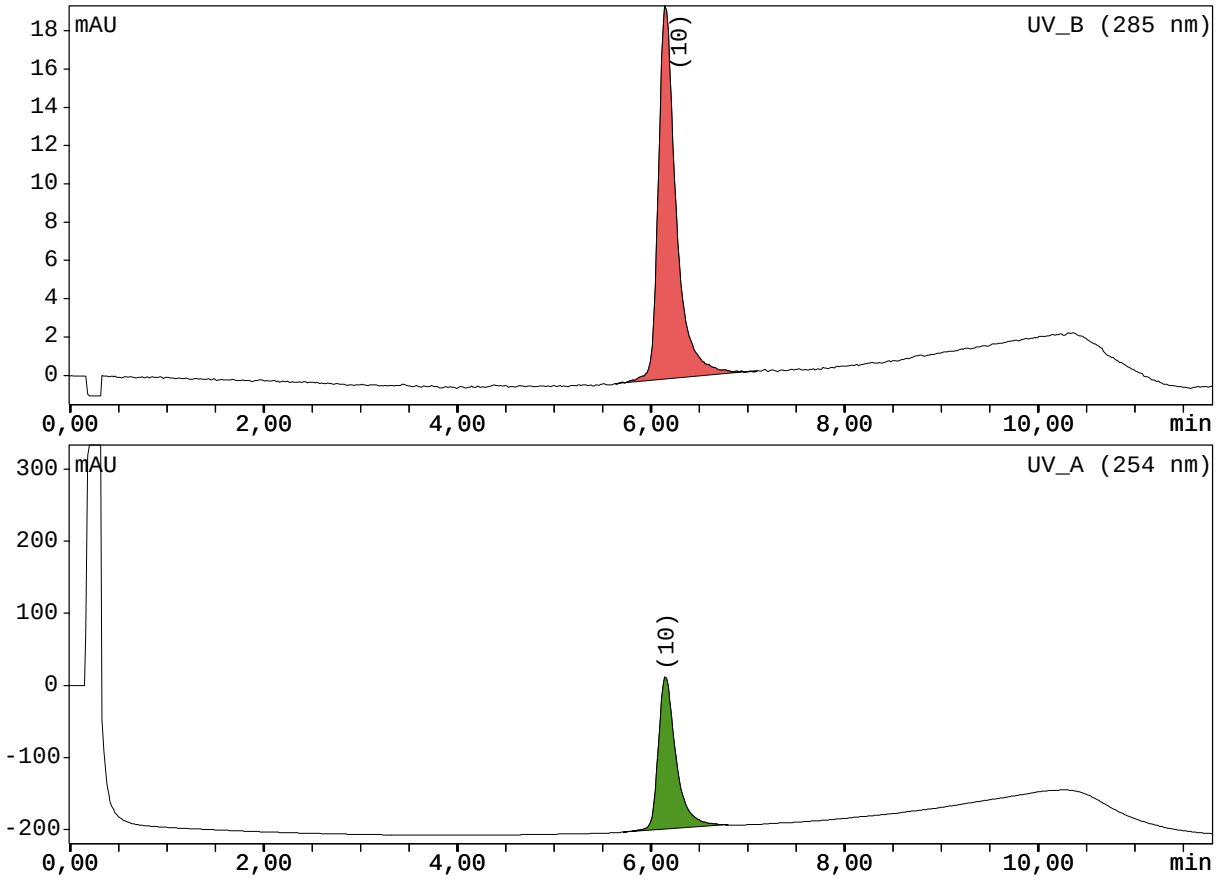

Integration UV_A (254 nm)

Substance	R/T min	Area mAU*min	%Area
Compound 10	6,15	2686,844	100,00
Total		2686,844	100,00

Integration UV_B (285 nm)

Substance	R/T min	Area mAU*min	%Area
Compound 10	6,15	250,4426	100,00
Total		250,4426	100,00

Compound 25

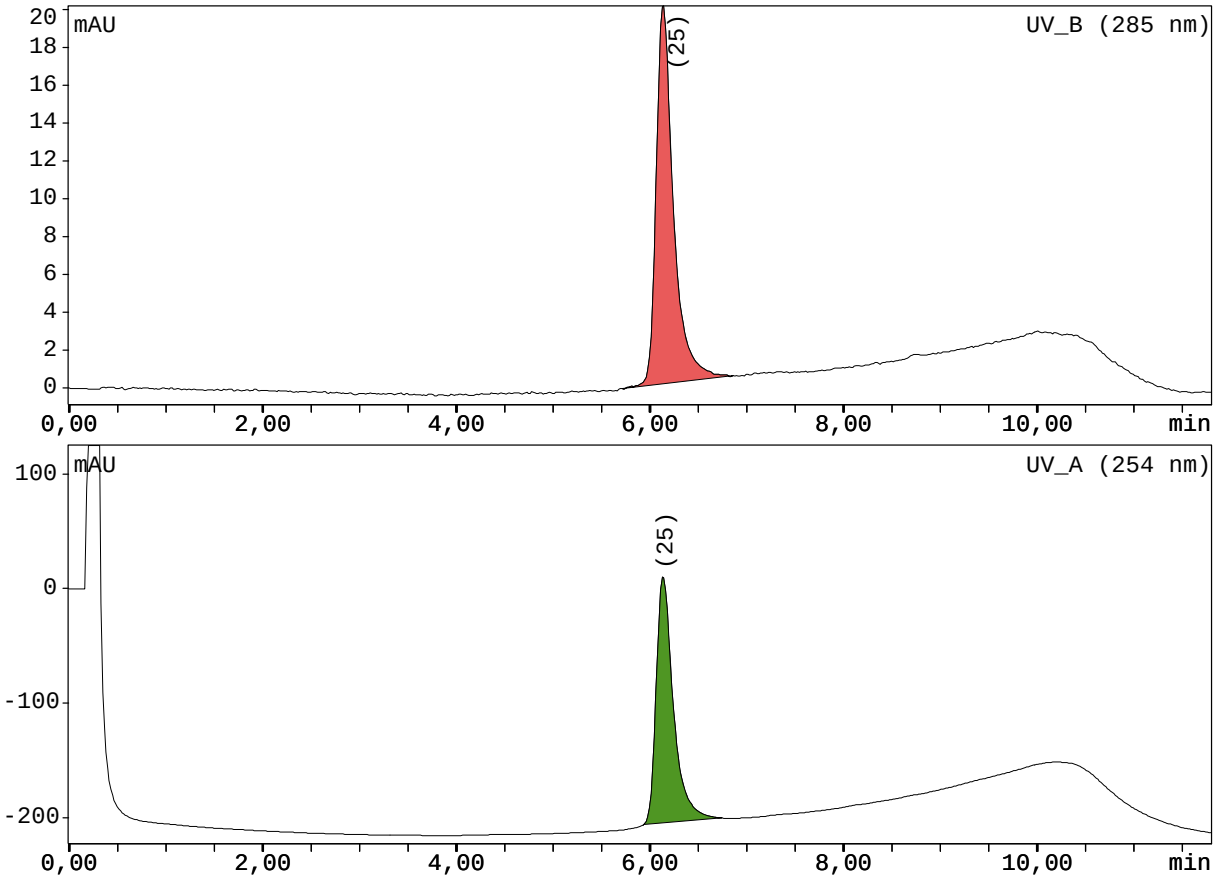

Integration UV_A (254 nm)

Substance	R/T min	Area mAU*min	%Area
Compound 25	6,15	2643,279	100,00
Total		2643,279	100,00

Integration UV_B (285 nm)

Substance	R/T min	Area mAU*min	%Area
Compound 25	6,15	248,0498	100,00
Total		248,0498	100,00

Blank

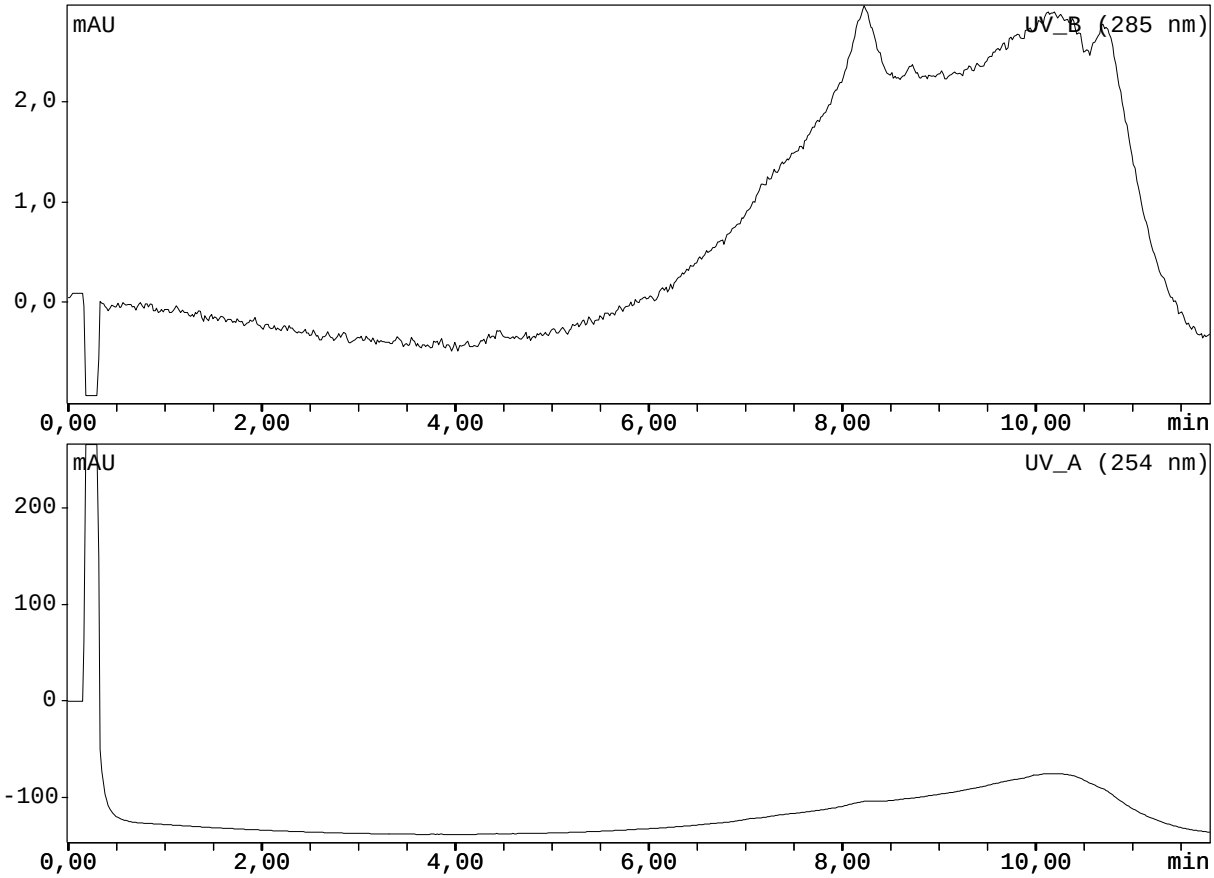

13. References

1. Council of Europe. Radiopharmaceutical preparations. In: Europäisches Arzneibuch (European Pharmacopoeia) (8th ed), Verlag Österreich GmbH, Vienna, Austria, pp 995 (2008).

2. Giri R, Goodell JR, Xing C, *et al.* Synthesis and cancer cell cytotoxicity of substituted xanthenes. *Bioorg. Med. Chem.* 18(4), 1456–1463 (2010).

3. Zou Q, Duan H, Ning M, *et al.* 4-Benzofuranyloxynicotinamide derivatives are novel potent and orally available TGR5 agonists. *Eur J Med Chem*. 82, 1–15 (2014).

4. Duan H, Ning M, Chen X, *et al.* Design, Synthesis, and Antidiabetic Activity of 4-Phenoxynicotinamide and 4-Phenoxypyrimidine-5-carboxamide Derivatives as Potent and Orally Efficacious TGR5 Agonists. *J. Med. Chem.* 55(23), 10475–10489 (2012).

5. Villani FJ, Mann TA, Wefer EA, *et al.* Benzopyranopyridine derivatives. 1. Aminoalkyl derivatives of the azaxanthenes as bronchodilating agents. *J. Med. Chem*. 18(1), 1-8 (2002).

6. Andreu R, C. Ronda J. Synthesis of 3,4-Dihydro-2H-1,3-benzoxazines by Condensation of 2-Hydroxyaldehydes and Primary Amines: Application to the Synthesis of Hydroxy-Substituted and Deuterium-Labeled Compounds. *Synthetic Communications*. 38, 2316–2329 (2008).

7. Ayedi MA, Le Bigot Y, Ammar H, Abid S, El Gharbi R, Delmas M. Synthesis of primary amines by one-pot reductive amination of aldehydes. *Synthetic Communications*. 43(6), 2127–2133 (2013).

8. Tucker SC, Brown JM, Oakes J, Thornthwaite D. Resolution and coupling of 1-(2'-hydroxy-1'-naphthyl)isoquinolines. *Tetrahedron*. 57(13), 2545–2554 (2001).

9. Larsen P, Ulin J, Dahlstrøm K, Jensen M. Synthesis of [^{11}C]iodomethane by iodination of [^{11}C]methane. *Applied Radiation and Isotopes*. 48(2), 153–157 (1997).

10. Jewett DM. A simple synthesis of [^{11}C]methyl triflate. *Int J Rad Appl Instrum A*. 43(11), 1383–1385 (1992).

11. Nics L, Steiner B, Klebermass E-M, *et al.* Speed matters to raise molar radioactivity: Fast HPLC shortens the quality control of C-11 PET-tracers. *Nucl. Med. Biol.* 57, 28–33 (2018).

12. Berroterán-Infante N, Balber T, Fürlinger P, *et al.* [^{18}F]FEPPA: Improved Automated Radiosynthesis, Binding Affinity, and Preliminary in Vitro Evaluation in Colorectal Cancer. *ACS Med. Chem. Lett.* 9(3), 177–181 (2018).

13. Owen DRJ, Gunn RN, Rabiner EA, *et al.* Mixed-Affinity Binding in Humans with 18-kDa Translocator Protein Ligands. *J Nucl Med*. 52(1), 24–32 (2011).

14. Owen DR, Yeo AJ, Gunn RN, *et al.* An 18-kDa Translocator Protein (TSPO) Polymorphism Explains Differences in Binding Affinity of the PET Radioligand PBR28. *J Cereb Blood Flow Metab*. 32(1), 1–5 (2012).

15. Yung-Chi C, Prusoff WH. Relationship between the inhibition constant (KI) and the concentration of inhibitor which causes 50 per cent inhibition (I50) of an enzymatic reaction. *Biochemical Pharmacology*. 22(23), 3099–3108 (1973).

16. Vraka C, Nics L, Wagner K-H, Hacker M, Wadsak W, Mitterhauser M. LogP, a yesterday's value? *Nuclear Medicine and Biology*. 50(Supplement C), 1–10 (2017).

17. Donovan SF, Pescatore MC. Method for measuring the logarithm of the octanol–water partition coefficient by using short octadecyl–poly(vinyl alcohol) high-performance liquid chromatography columns. *Journal of Chromatography A*. 952(1), 47–61 (2002).

18. Lockhart A, Davis B, Matthews JC, *et al.* The peripheral benzodiazepine receptor ligand PK11195 binds with high affinity to the acute phase reactant alpha1-acid glycoprotein: implications for the use of the ligand as a CNS inflammatory marker. *Nucl. Med. Biol.* 30(2), 199–206 (2003).

3. (*R*)-[^{18}F]NEBIFQUINIDE: A TALE OF A NEW THIRD GENERATION TRANSLOCATOR PROTEIN PET TRACER

Neydher Berroterán-Infante, [‡,a,b] *Thomas Kalina,* [‡,c] *Lukas Fetty,* [a] *Victoria Janisch,* [a] *Ramona Velasco,*[c] *Chrysoula Vraka,* [a] *Marcus Hacker,* [a] *Alexander R. Haug,* [a] *Katharina Pallitsch,* [*,c] *Wolfgang Wadsak,* [†,*,a,b,d] *and Markus Mitterhauser.* [†,a,e]

[a]Division of Nuclear Medicine, Department of Biomedical Imaging and Image-guided Therapy, Medical University of Vienna, Währinger Gürtel 18-20, 1090 Vienna, Austria.

[b]Institute of Inorganic Chemistry, Faculty of Chemistry, University of Vienna, Währinger Straße 42, 1090 Vienna, Austria.

[c]Institute of Organic Chemistry, Faculty of Chemistry, University of Vienna, Währinger Straße 38, 1090 Vienna, Austria.

[d]Center for Biomarker Research, CBmed, Stiftingtalstraße 5, 8010 Graz, Austria.

[e]Ludwig Boltzmann Institute Applied Diagnostics, Währinger Gürtel 18-20, 1090 Vienna, Austria.

SUPPORTING INFORMATION

Table of Contents

Compound characterization and Results

Purity of compounds – HPLC chromatograms

HPLC spectra were recorded to determine the purity of the target compound and precursor, using the same system as described in the main text.

Compound (*R*)-[^{18}F]**6b**

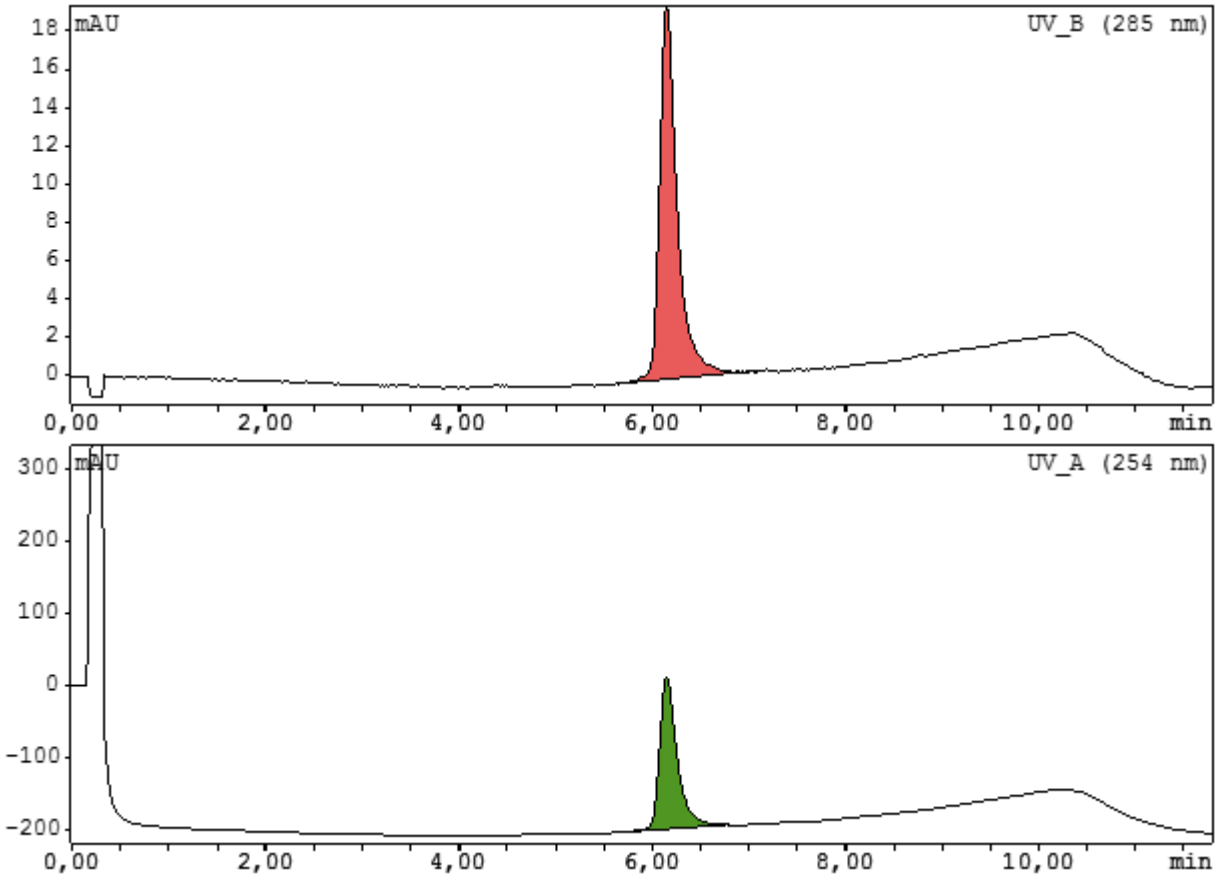

Integration UV_A (254 nm)

Substance	R/T min	Area mAU*min	%Area
Compound (*R*)-6b	6,22	2475,892	100,00
Total		2475,892	100,00

Integration UV_B (285 nm)

Substance	R/T min	Area mAU*min	%Area
Compound (*R*)-6b	6,22	251,3397	100,00
Total		251,3397	100,00

Blank

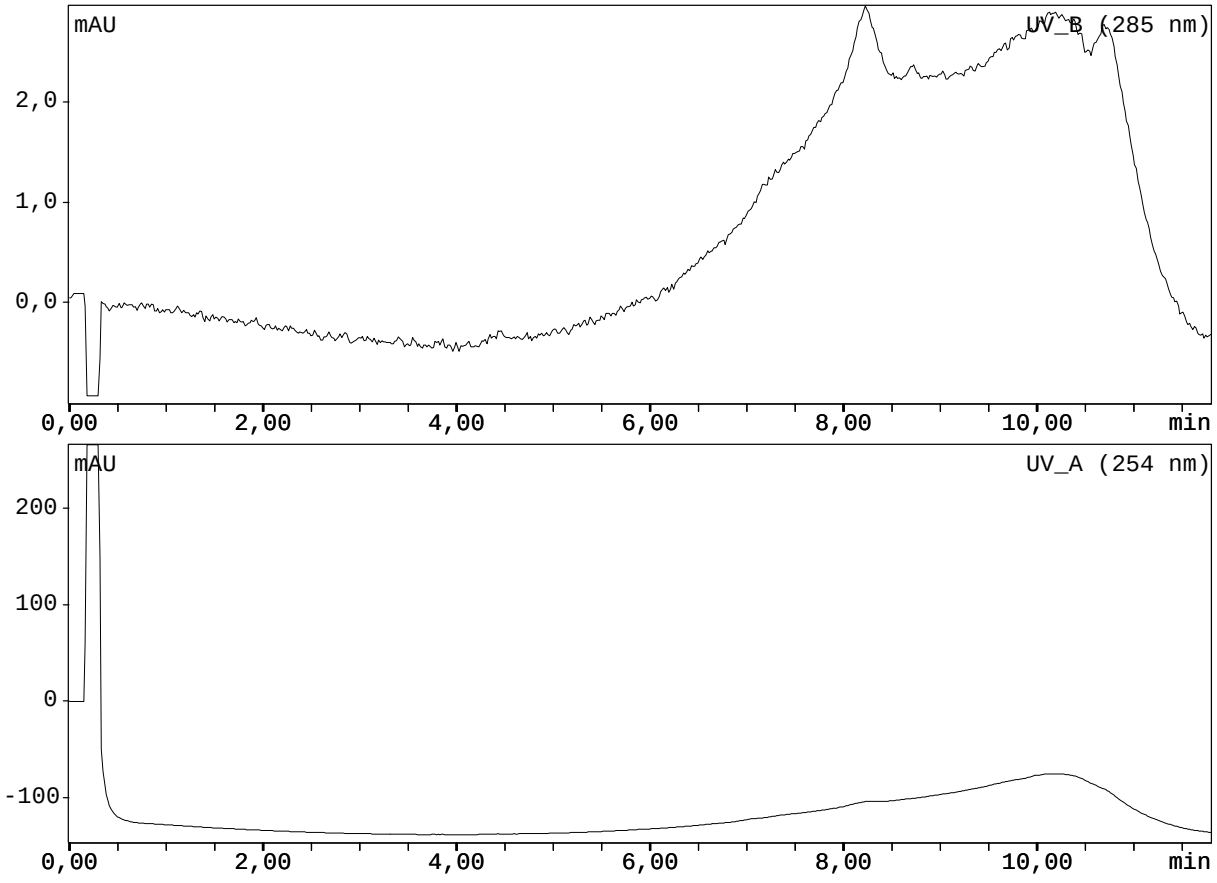

NMR spectra of the compounds

^{1}H, ^{13}C and ^{19}F NMR spectra of all newly synthetized compounds are available as additional material. All assignments, solvents and measuring frequencies are given in the synthetic chemistry section of the supporting information (1.5.1). The first spectrum shown in each series is the full ^{1}H NMR spectrum. Expansions are depicted where they were regarded as necessary. Then the ^{13}C NMR spectrum, followed by the ^{19}F NMR, is depicted in the same manner. The x-axes are in ppm, while the peak labels are in Hz for all given spectra. Structures are always given on top of the full 1H NMR spectrum. Integrals are denoted below the x-axes where they are regarded as necessary and the integration range is marked. The numbering of compounds is in accordance with the numbering of substances in the main text. All ^{13}C NMR spectra were recorded j-modulated.

[1]H NMR of Methyl 1-(2-fluoropyridin-3-yl)isoquinoline-3-carboxylate (8b):

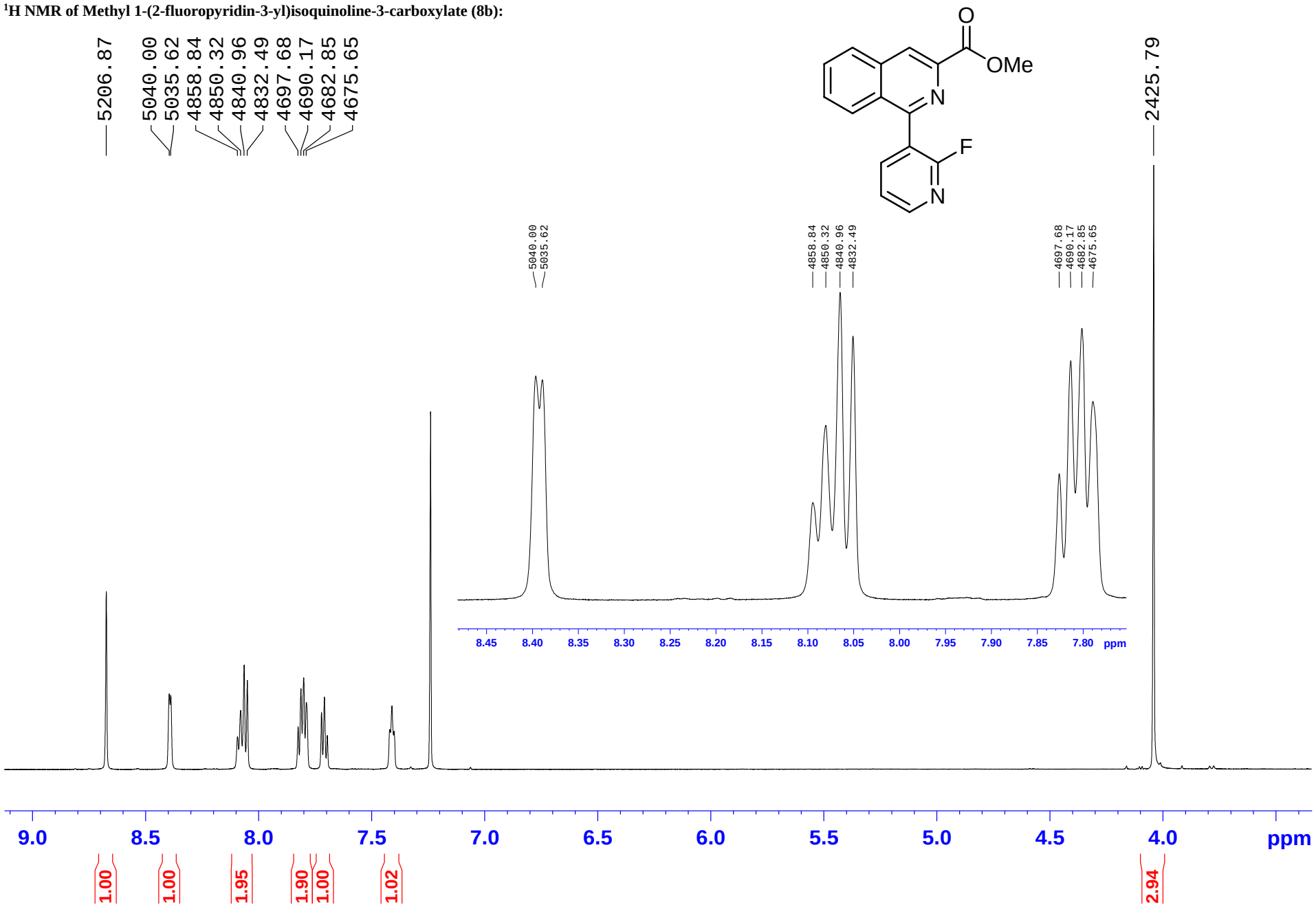

^{13}C NMR of Methyl 1-(2-fluoropyridin-3-yl)isoquinoline-3-carboxylate (8b):

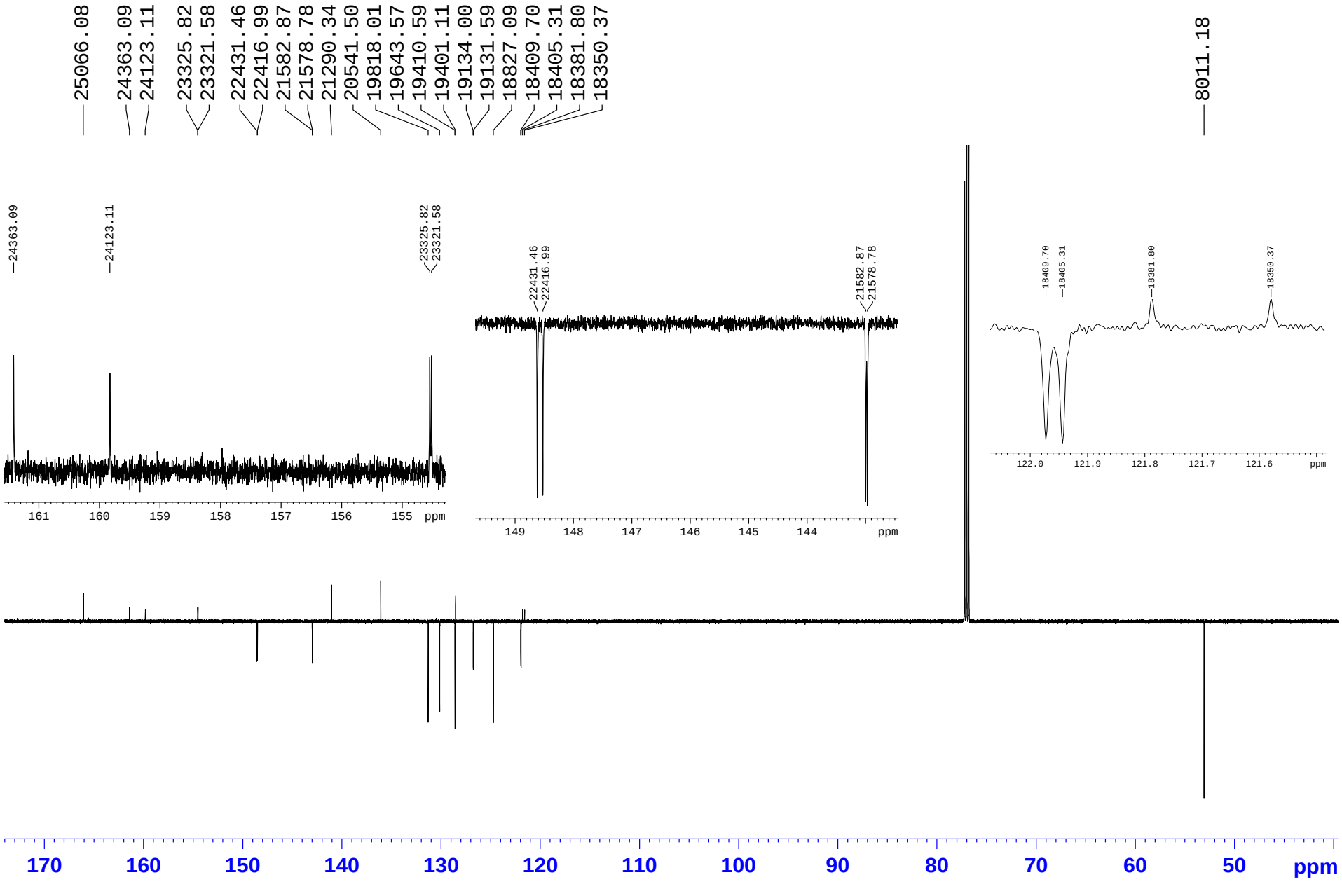

^{19}F NMR of Methyl 1-(2-fluoropyridin-3-yl)isoquinoline-3-carboxylate (8b):

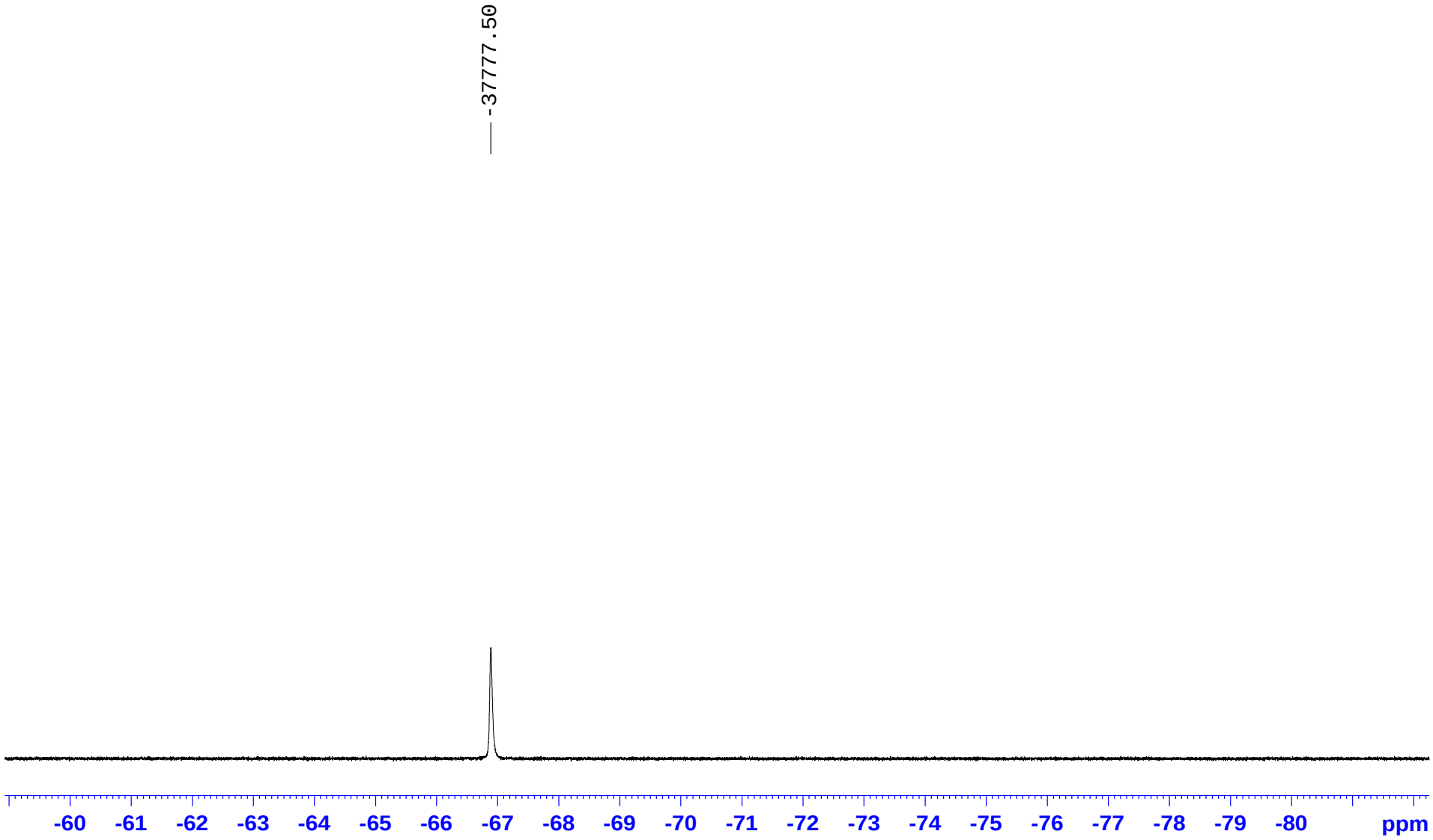

[1]H NMR of 1-(2-Fluoropyridin-3-yl)isoquinoline-3-carboxylic acid (9b):

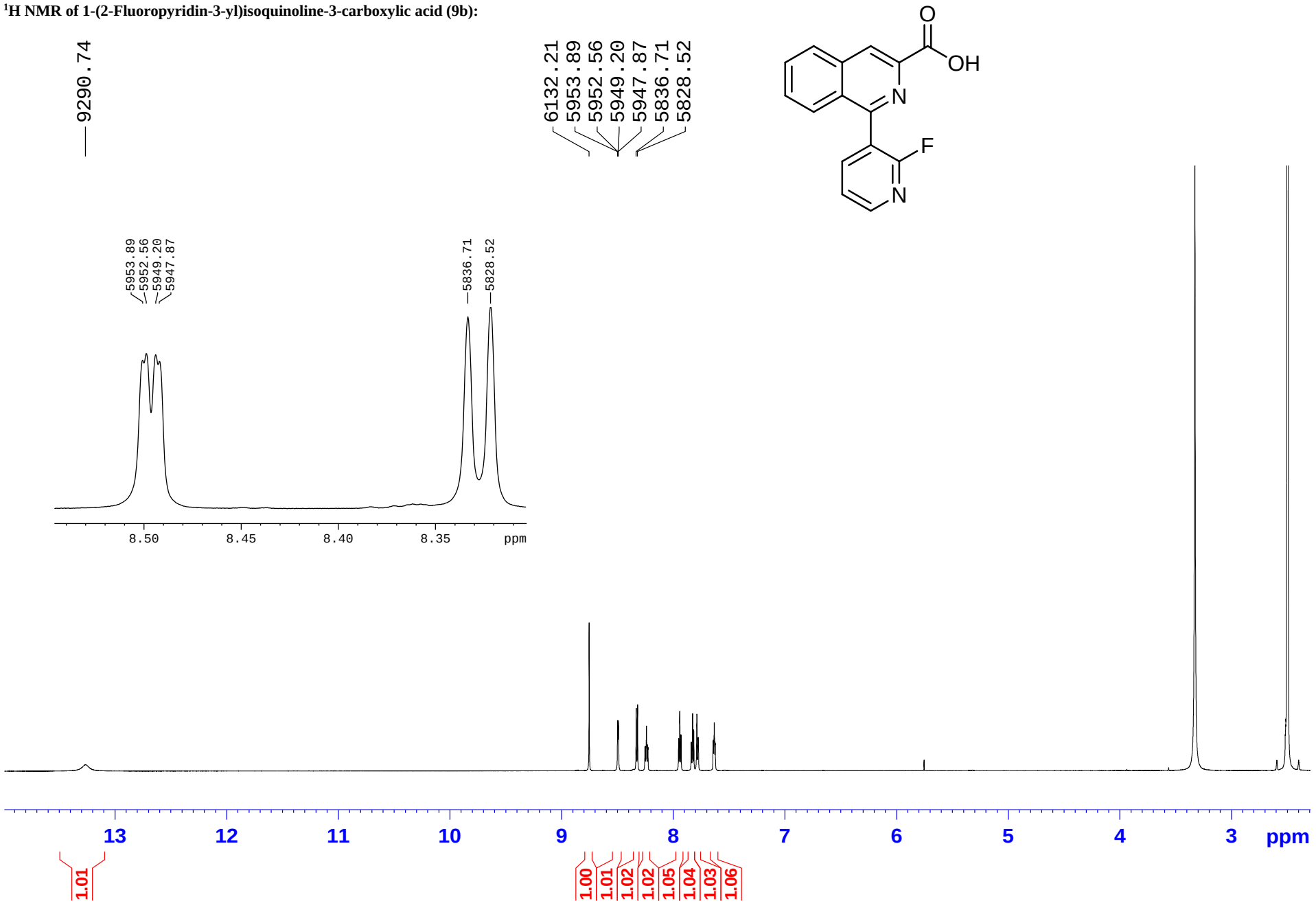

^{13}C NMR of 1-(2-Fluoropyridin-3-yl)isoquinoline-3-carboxylic acid (9b):

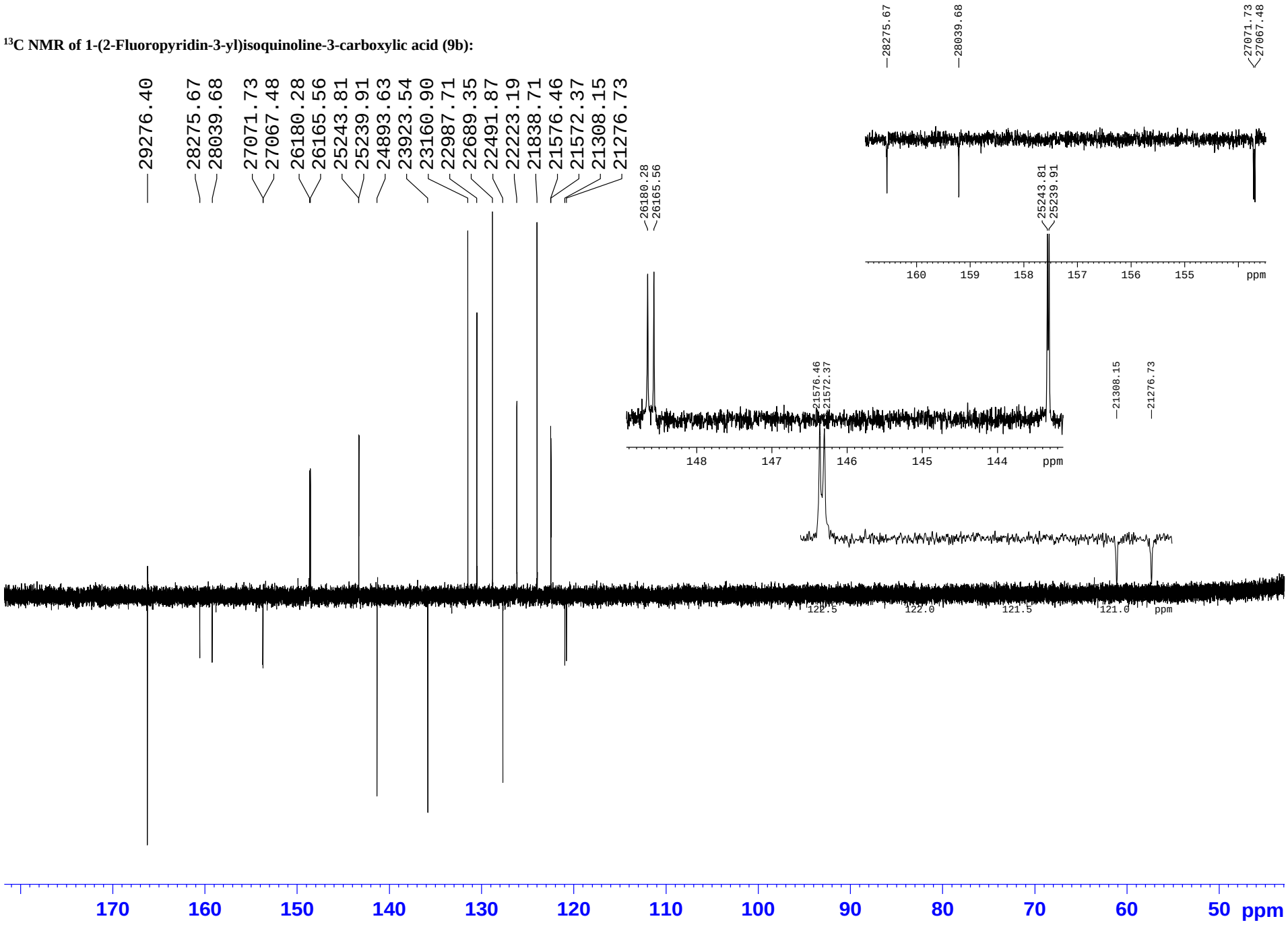

^{19}F NMR of 1-(2-Fluoropyridin-3-yl)isoquinoline-3-carboxylic acid (9b):

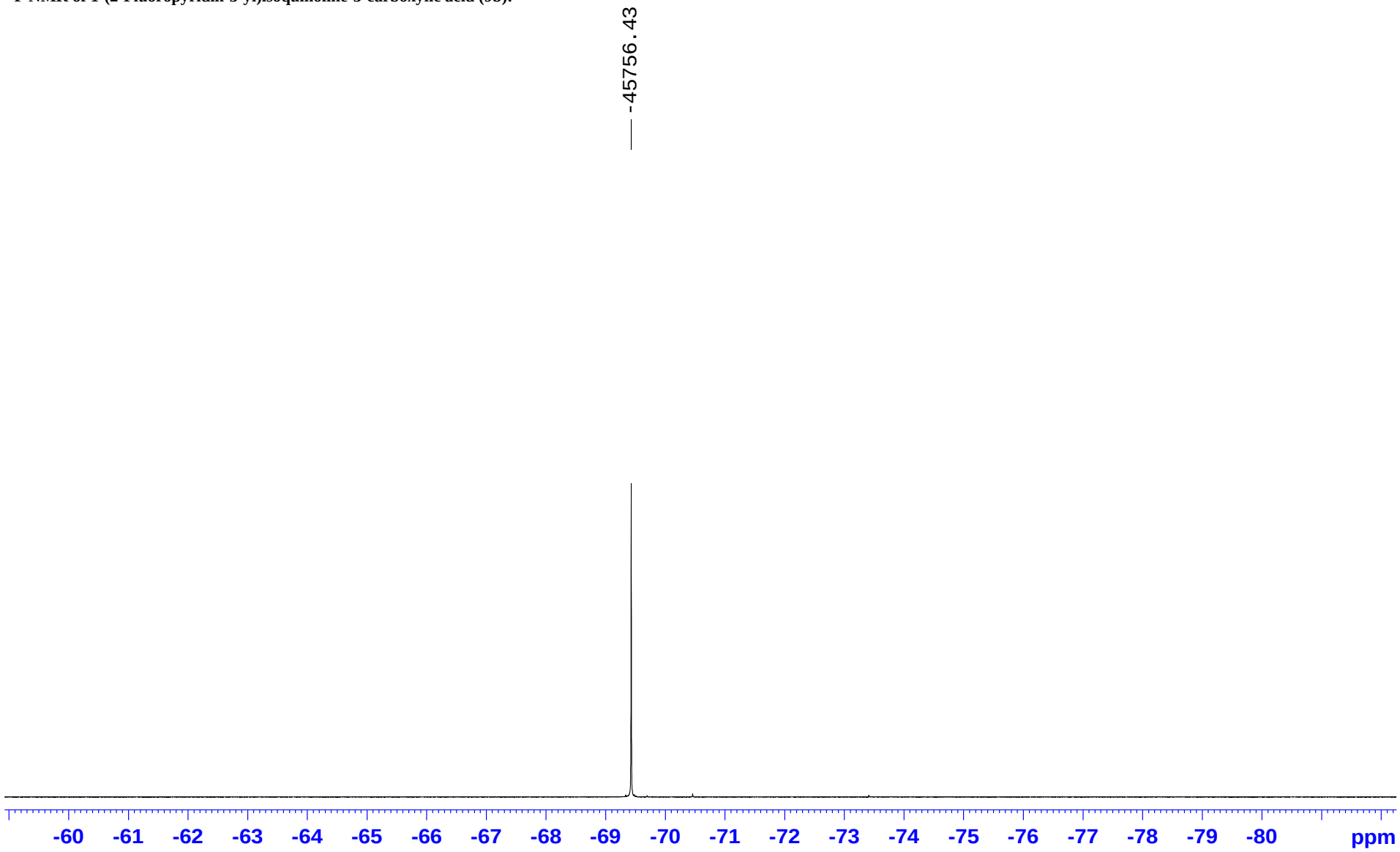

^{1}H NMR of (–)-(*R*)-*N*-(*sec*-butyl)-1-(2-fluoropyridin-3-yl)isoquinoline-3-carboxyamide (10b):

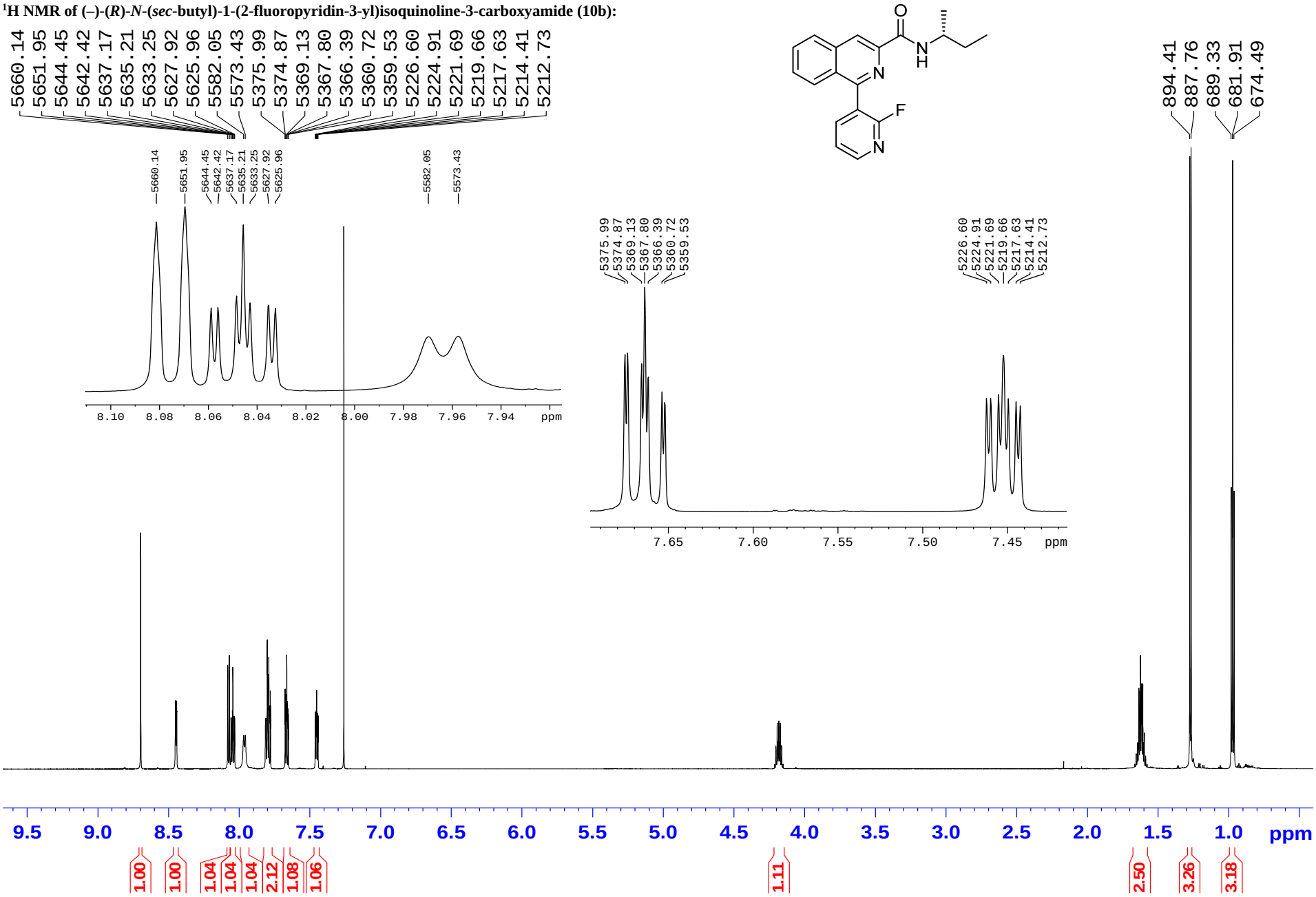

^{13}C NMR of (–)-(*R*)-*N*-(*sec*-butyl)-1-(2-fluoropyridin-3-yl)isoquinoline-3-carboxyamide (10b):

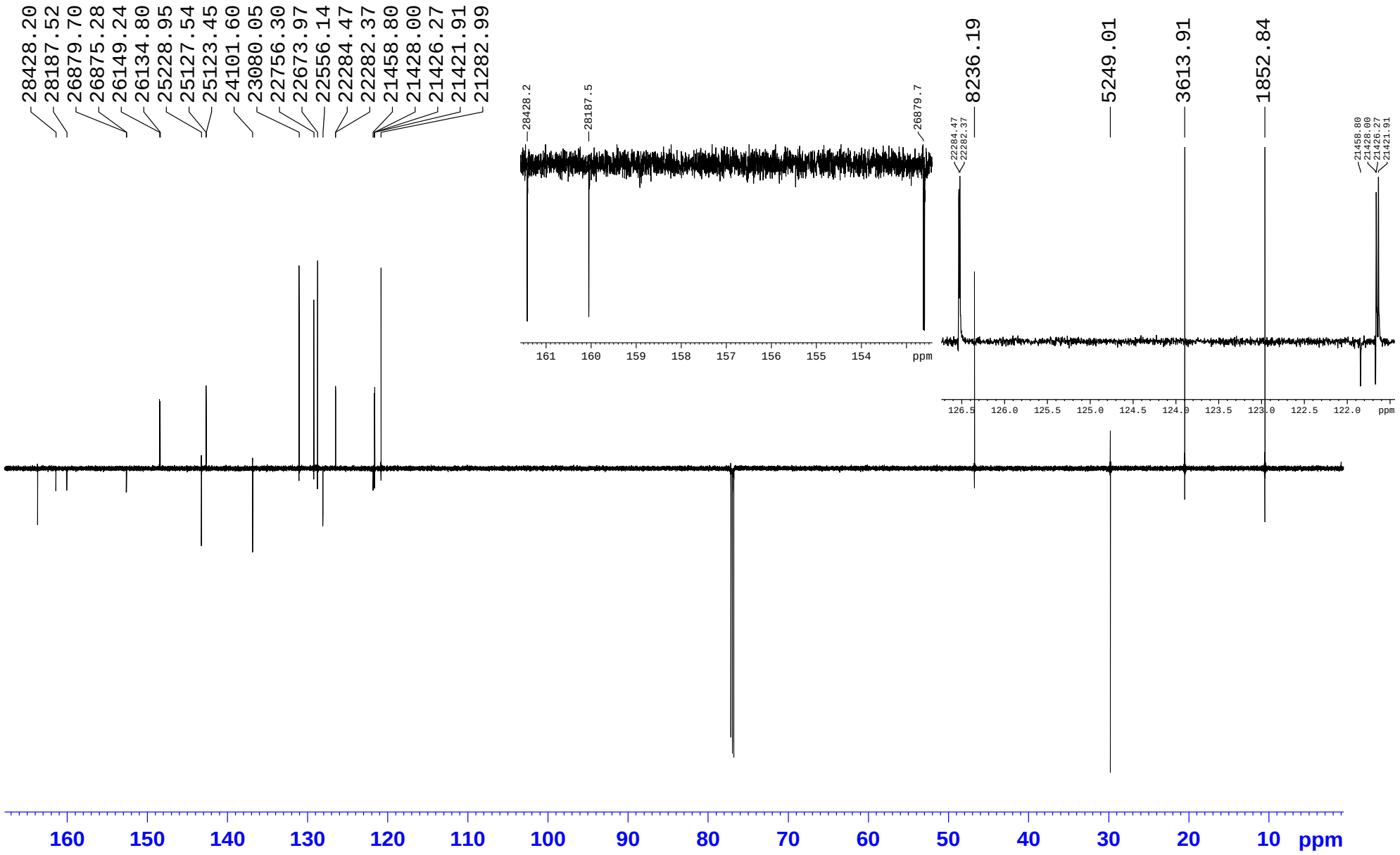

^{19}F NMR of (–)-(*R*)-*N*-(*sec*-butyl)-1-(2-fluoropyridin-3-yl)isoquinoline-3-carboxyamide (10b):

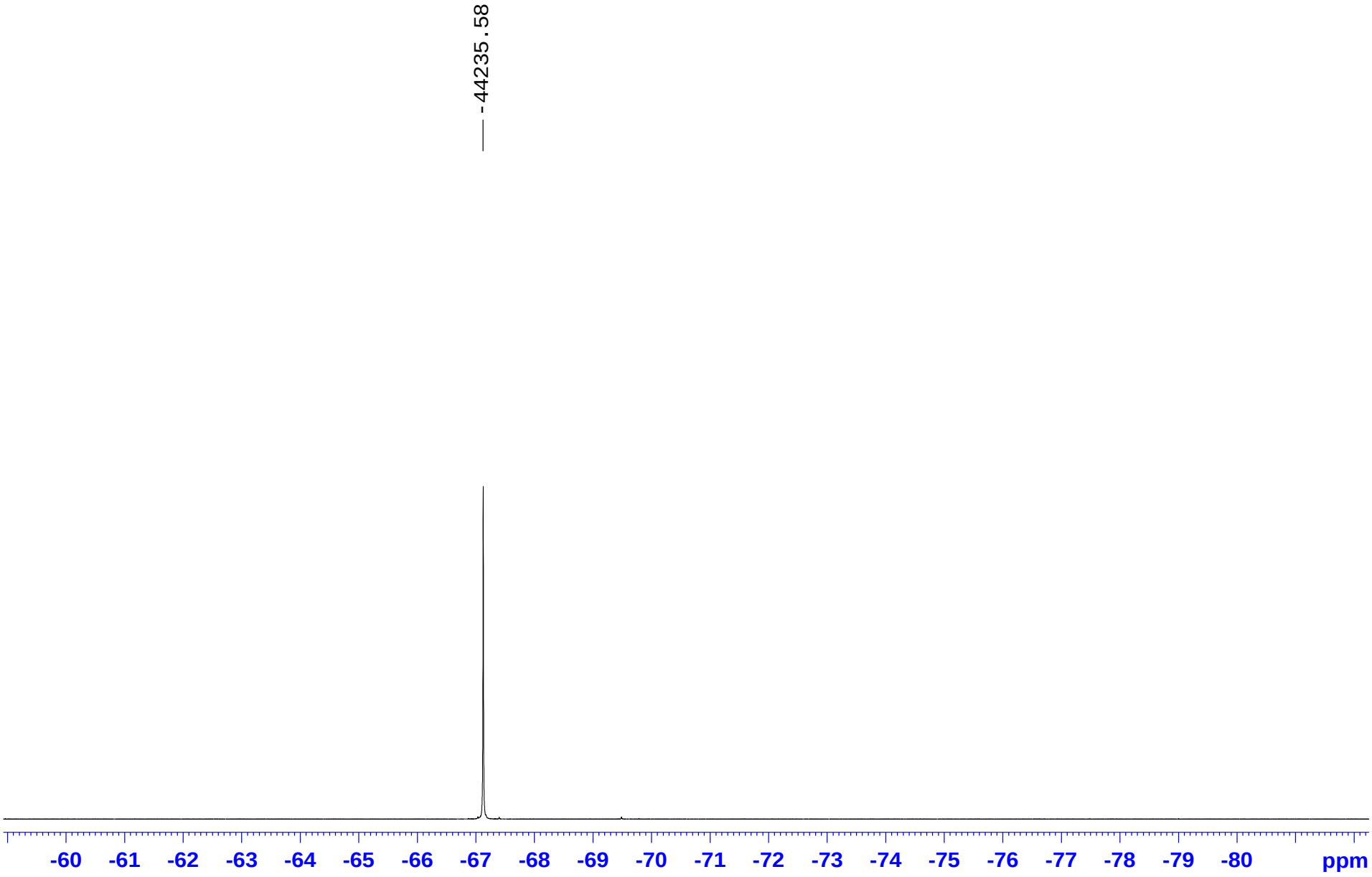

^{1}H NMR of (*R*)-*N*-(*sec*-butyl)-1-(2-fluoropyridin-3-yl)-*N*-methylisoquinoline-3-carboxamide (6b):

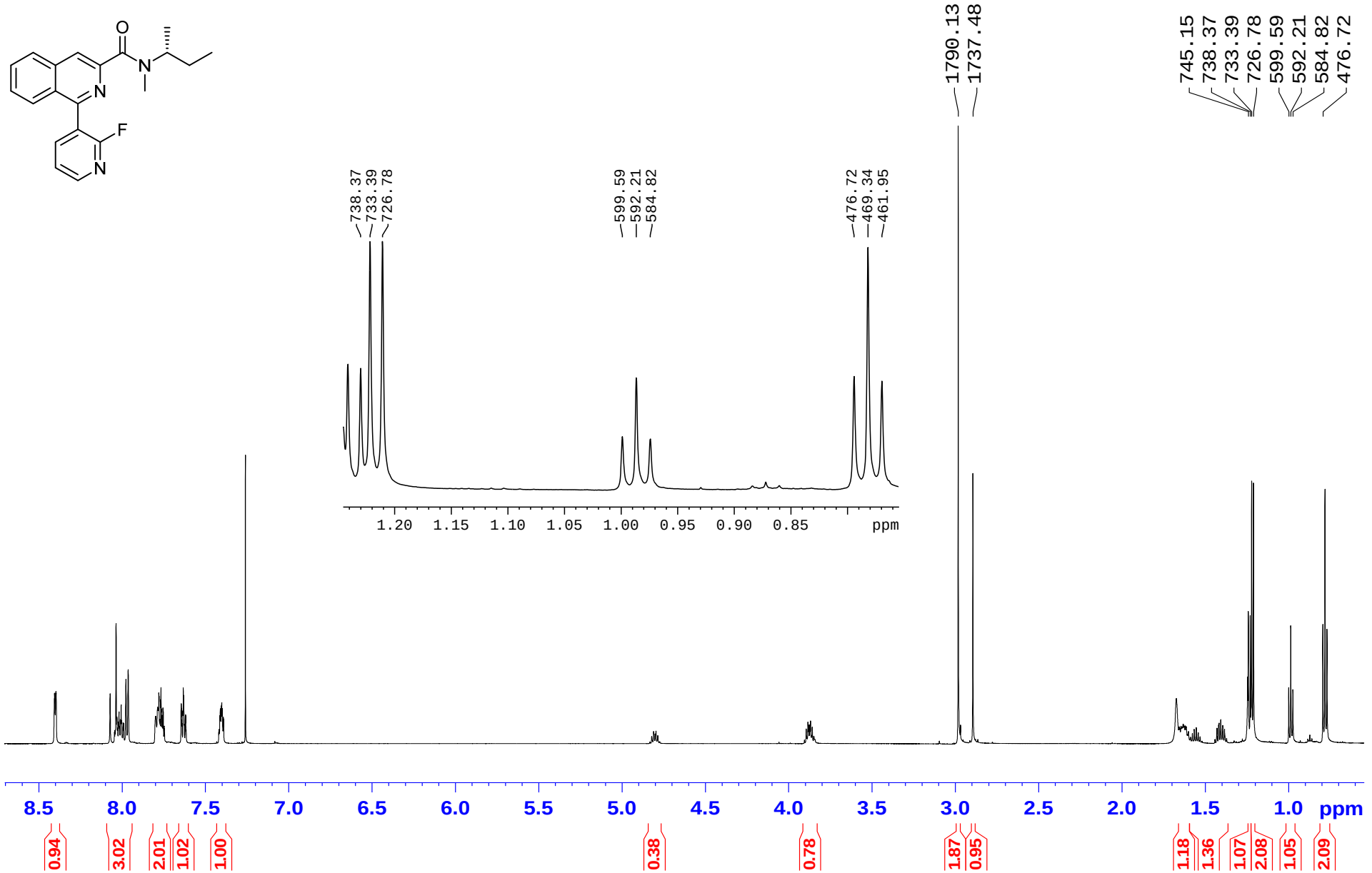

^{13}C NMR of (*R*)-*N*-(*sec*-butyl)-1-(2-fluoropyridin-3-yl)-*N*-methylisoquinoline-3-carboxamide (6b):

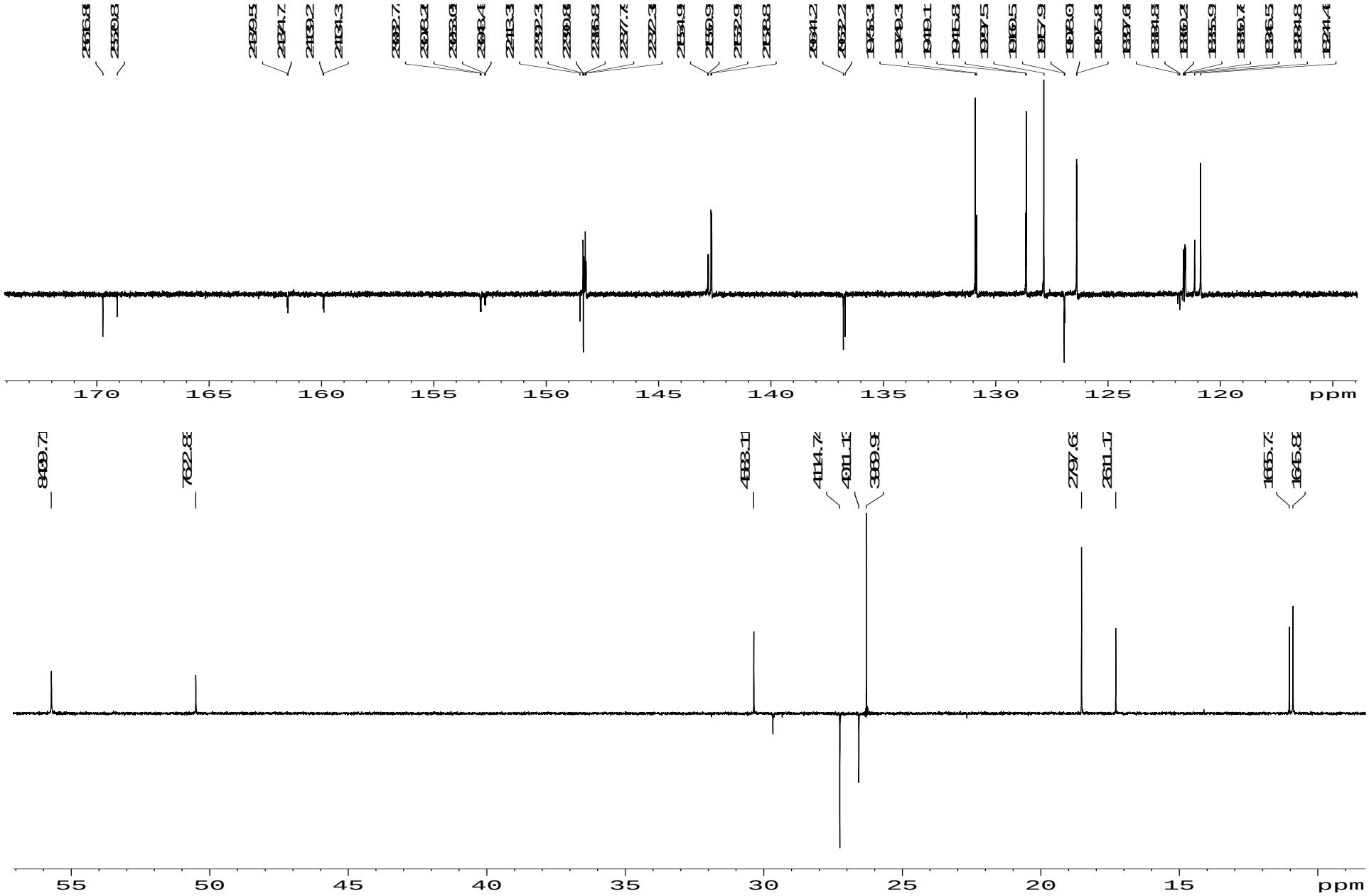

^{19}F NMR of (*R*)-*N*-(*sec*-butyl)-1-(2-fluoropyridin-3-yl)-*N*-methylisoquinoline-3-carboxamide (6b):

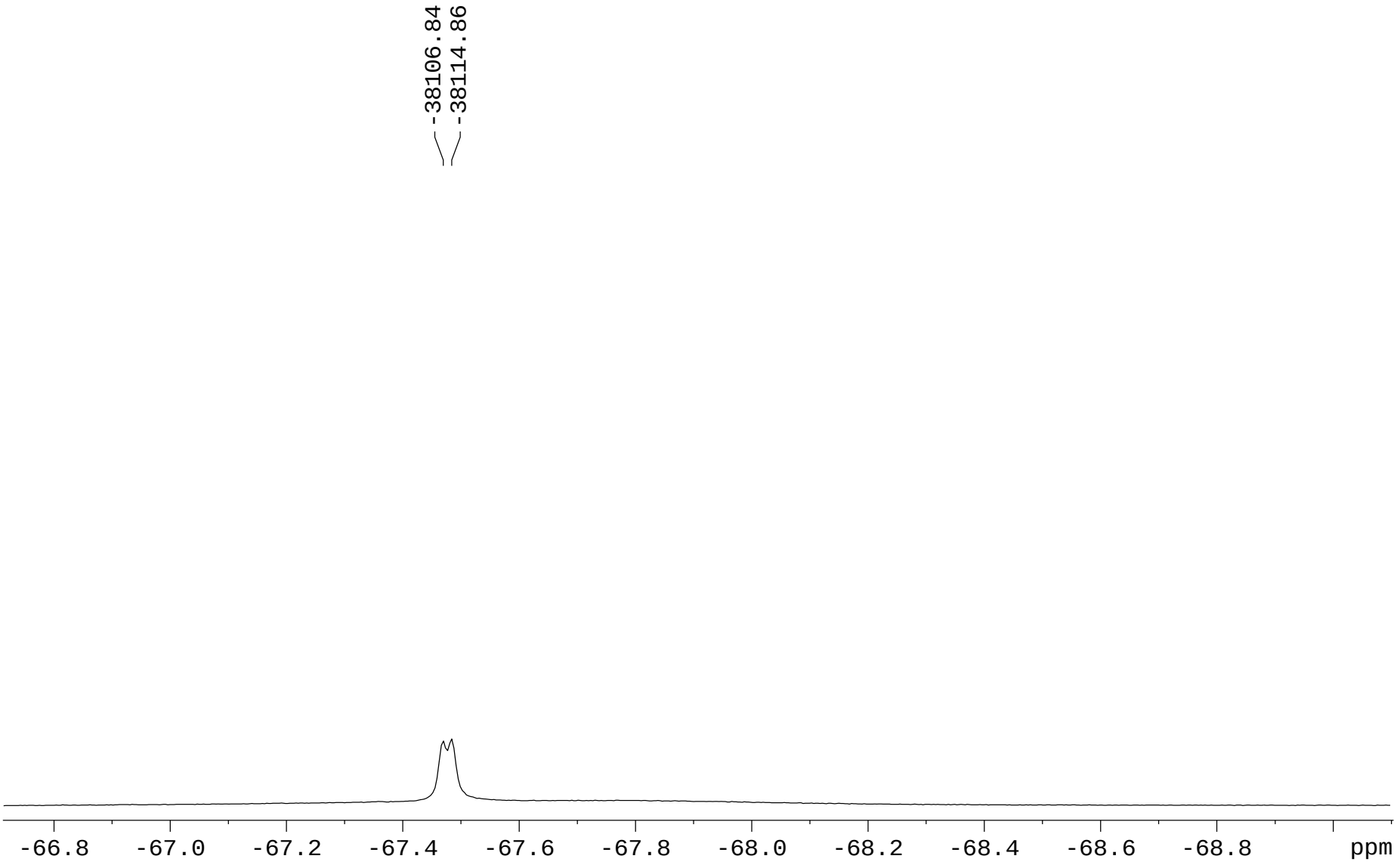

Radiochemistry

Evaluation of reaction conditions

A summary of obtained RCCs using conventional heating is shown in Figures 1 (conventional heating) and 2 (microwave heating) for each reaction parameter tested: solvent, fluorinating agent, precursor concentration, temperature and time.

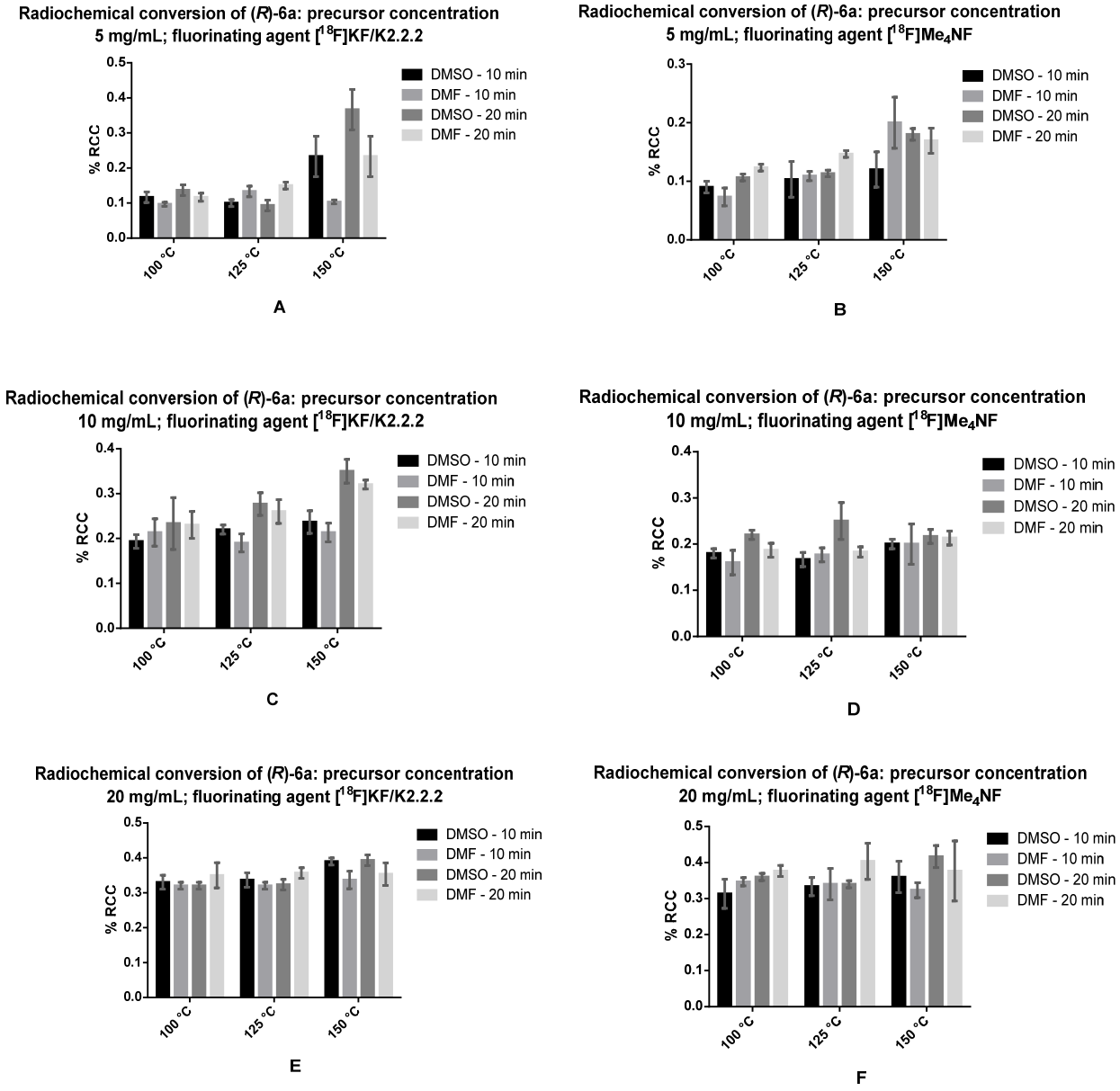

Figure 1. Evaluation of different reaction parameters for the radiolabeling of (*R*)-**6a** under conventional heating (n=3).

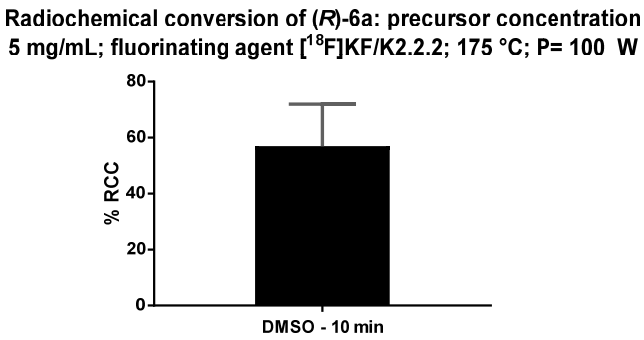

Figure 2. RCC for the tested reaction parameters for the radiolabeling of (*R*)-**6a** under microwave heating (n=3).

Ex vivo evaluation

The emergence of a more hydrophilic radio-metabolite was observed in all analyzed organs (lung, liver and brain) as shown in Figure 2.

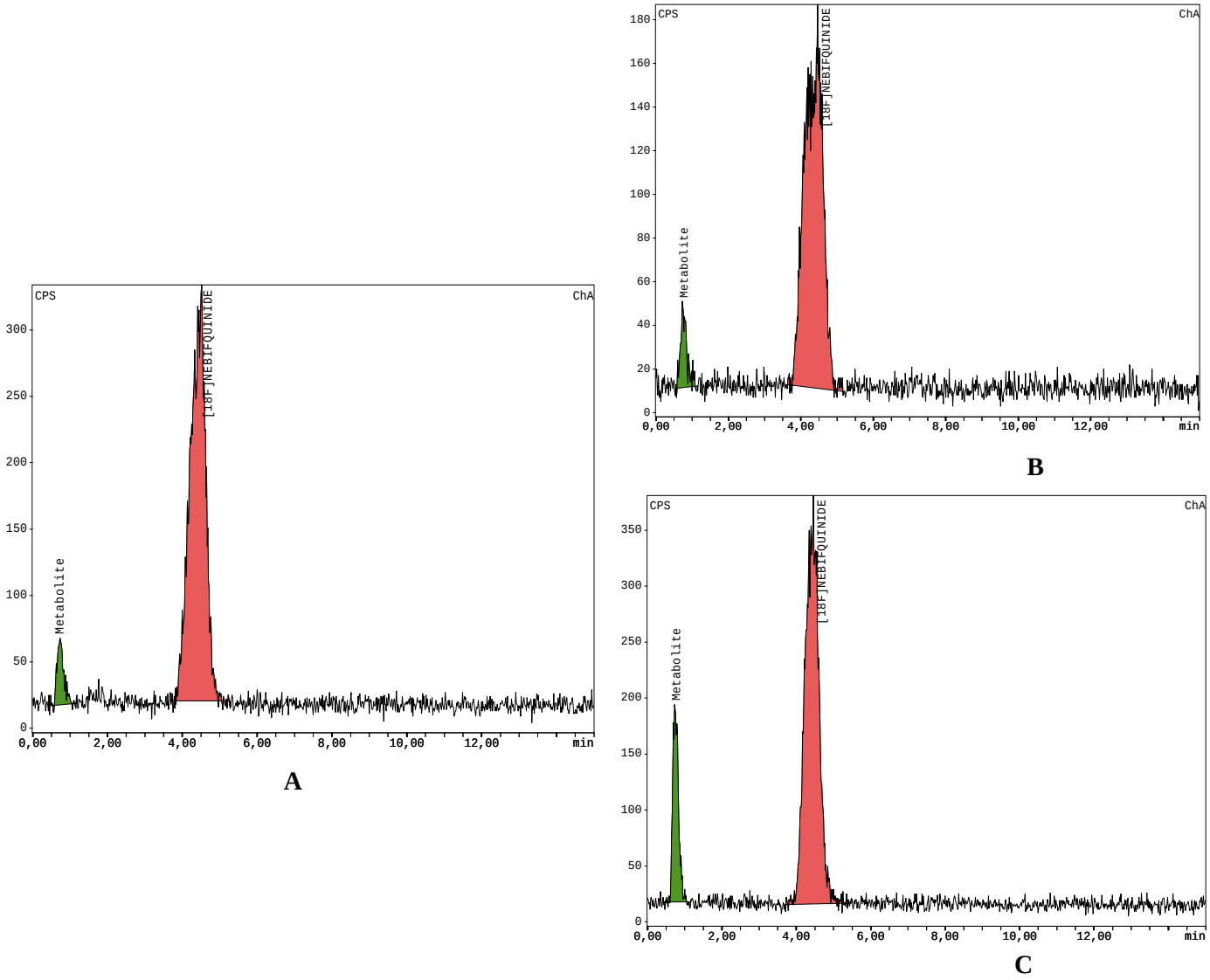

Figure 2. Radio-HPLC chromatograms of liver (A), lung (B) and brain (C) homogenates.

References

[1] Berroterán-Infante, N.; Balber, T.; Fürlinger, P.; Bergmann, M.; Lanzenberger, R.; Hacker, M.; Mitterhauser, M.; Wadsak, W. *ACS Med. Chem. Lett.* **2018**, *9*, 177.

[2] Owen, D. R. J.; Gunn, R. N.; Rabiner, E. A.; Bennacef, I.; Fujita, M.; W. C. Kreisl, R. B. Innis, V. W. Pike, R. Reynolds, P. M. Matthews, et al., *J. Nucl. Med.* **2011**, *52*, 24.

[3] D. R. Owen, A. J. Yeo, R. N. Gunn, K. Song, G. Wadsworth, A. Lewis, C. Rhodes, D. J. Pulford, I. Bennacef, C. A. Parker, et al., *J. Cereb. Blood Flow Metab.* **2012**, *32*, 1.

[4] C. Yung-Chi, W. H. Prusoff, *Biochemical Pharmacology* **1973**, *22*, 3099.

[5] S. F. Donovan, M. C. Pescatore, *J. Chromatogr. A* **2002**, *952*, 47.

[6] C. Vraka, L. Nics, K.-H. Wagner, M. Hacker, W. Wadsak, M. Mitterhauser, *Nucl. Med. Biol.* **2017**, *50*, 1.

[7] A. Lockhart, B. Davis, J. C. Matthews, H. Rahmoune, G. Hong, A. Gee, D. Earnshaw, J. Brown, *Nucl. Med. Biol.* **2003**, *30*, 199.

[8] C. Rami-Mark, N. Eberherr, N. Berroterán-Infante, T. Vanicek, L. Nics, R. Lanzenberger, M. Hacker, W. Wadsak, M. Mitterhauser, *Nucl. Med. Biol.* **2016**, *43*, 490.

Author Contributions

N.B.-I. designed parts of the research, performed all radiosyntheses and preclinical *in vitro* and *ex vivo* experiments; analyzed data and wrote the manuscript; T.K. designed parts of the research, conducted the synthesis of precursor and reference standard, analyzed data and wrote the manuscript, L.F. processed the *in vivo* PET imaging data; V.J. contributed to radiosynthesis optimization; R.V. contributed to synthesis of precursor and reference standard; C.V. contributed to log*P* determinations, M.H., and A.R.H. designed parts of the research and proofread the manuscript; K.P. designed parts of the research, supervised all the chemical syntheses and proofread the manuscript; W.W. conceived and supervised all the radiosyntheses and proofread the manuscript; M.M conceived and supervised the preclinical evaluation and proofread the manuscript. All authors have given approval to the final version of the manuscript.